Improving the Accessibility of Transition Metal Mediated Radical Polymerization

Arkadios Marathianos

A thesis submitted in partial fulfilment of the requirements of the degree of

Doctor of Philosophy in Chemistry

Department of Chemistry

University of Warwick

August 2021

This Ph.D. thesis is dedicated to my parents.

Στους γονείς μου

για ό,τι μου έχουν προσφέρει

Table of Contents

List of Schemes

List of Figures

List of Tables

Abbreviations

^{1}H NMR	Proton Nuclear magnetic resonance
AFCT	Addition-Fragmentation Chain Transfer
AI	Active Ingredient
AIBN	Azobisisobutyronitrile
ARGET	Activator Regenerated by Electron Transfer
ATRP	Atom Transfer Radical Polymerization
BMA	Butyl methacrylate
BzA	Benzyl Acrylate
CCT	Catalytic Chain Transfer
CCTP	Catalytic Chain Transfer Polymerization
CF	Continuous Flow
CLRP	Controlled/Living Radical Polymerization
CMC	Critical micelle concentration
Co	Cobalt
CoBF	bis[(difluoroboryl)dimethylglyoximato]cobalt(II)
CRP	Controlled Radical Polymerization
C_s or C_T	Chain transfer constant
CTA	Chain Transfer Agent
Cu	Copper
CYNT	Cyantraniliprole
Đ	dispersity
DBiB	Dodecyl bromoisobutyrate
DCTB	*trans*-2-[3-(4-*tert*-butylphenyl)-2-methyl-2-propyldene] malononitrile
DLS	Dynamic light scattering
DMF	Dimethylformamide
DMSO	Dimethyl sulfoxide
DP_n	Degree of polymerization
DRI	Differential refractive index
DSA	Drop Shape Analyzer
DSC	Differential scanning calorimetry

EA	Ethyl Acrylate
eATRP	Electrochemically mediated ATRP
EBiB	Ethyl α-bromoisobutyrate
***f* or I_{eff}**	Initiator efficiency
Fe	Iron
FEG	Field emission Electron Gun
FRP	Free Radical Polymerization
GMMA	Glycerol monomethacrylate
GPC	Gel permeation chromatography
GRAS	Generally Regarded As Safe
H_2O_2	Hydrogen peroxide
HEMA	Hydroxyethyl methacrylate
HMTETA	1,1,4,7,10,10- hexamethyl triethylenetetramine
HPLC	High Performance Liquid Chromatography
I	iodine
ICAR	Initiators for Continuous Activator Regeneration
ISET	Inner-sphere electron transfer
IUPAC	International Union of Pure and Applied Chemistry
k_i	Rate constant of initiation
k_p	Rate constant of propagation
KPS	Potassium persulfate
k_t	Rate constant of termination
L	Ligand
LD	Laser Diffraction
LD_{50}	Median Lethal Dose
LS	Dual Angle Light Scatter
MAA	Methacrylic acid
MALDI-ToF-MS	Matrix Assisted Laser Dissociation/Ionization-Time of Flight-Mass Spectrometry
Me_6Tren	Tris[2-(dimethylamino) ethyl]amine
MeOH	Methanol
MM	Macromonomer
MMA	Methyl methacrylate

M_n	Number average molecular weight
MW	Molecular weight
MWD	Molecular Weight Distribution
***n*-BA**	*n*-Butyl Acrylate
NiPAm	N-isopropyl acrylamide
NMP	Nitroxide-Mediated Polymerization
NVP	N-vinyl-pyrrolidone
OEOMA	Oligo(ethyleneoxide) methylether methacrylate
OM	Optical Microscopy
OSET	Outer-sphere electron transfer
PBS	Phosphate buffer solution
PE	Polyethylene
PEGA	Poly(ethylene glycol) methyl ether
PEG-Me	Poly(ethylene glycol) monomethyl ether
PET	Photoinduced Electron Transfer
PLP	Pulsed-Laser Polymerization
pMA	Poly(methyl acrylate)
PMDETA	*N*,*N*,*N*′,*N*″,*N*″-pentamethyldiethylenetriamine
ppm	Part per million
PRE	Persistent Radical Effect
PSD	Particle Size Distribution
pSSNa	Poly(sodium 4-styrenesulfonate)
PVC	Polyvinylchloride
RAFT	Reversible Addition-Fragmentation chain transfer Polymerization
RBF	Round Bottom Flask
RDRP	Reversible Deactivation Radical Polymerization
REACH	Registration, Evaluation, Authorization and Restriction of Chemicals
Ru	Ruthenium
RyRs	Ryanodine Receptors
SARA	Supplemental Activator and Reducing Agent
SDS	Sodium dodecyl sulfate

SEC	Size exclusion chromatography
SEM	Scanning electron microscopy
SET-LRP	Single Electron Transfer-Living Radical Polymerization
SFT	Surface Tension
SLS	Static light scattering
St	Styrene
***t*-BMA**	*tert*-Butyl Methacrylate
TFEA	Trifluoroethyl Acrylate
T_g	Glass transition temperature
TGA	Thermogravimetric analysis
THF	Tetrahydrofuran
TMEDA	Tetramethyl ethylenediamine
UV	Ultraviolet
UV-Vis	Ultraviolet-Visible
V-65	2,2'-Azobis(2,4-dimethylvaleronitrile)
VA	Vinyl acetate
VA-044	2,2'-Azobis[2-(2-imidazolin-2-yl)propane]dihydrochloride
VOC	Volatile organic content
VS	Viscometry
Zn	Zinc

Acknowledgements

First and foremost, I would like to thank my supervisor, Professor David Haddleton, for allowing me the opportunity to pursue a Ph.D. in his group. I am grateful for working under his supervision in an environment that always promotes creativity and scientific freedom. Dave is a great scientist and an even greater person who truly cares about his students; not only for their personal development as scientists but also as individuals. He has a solution for everything, regardless of the difficulty and he always challenges his students to find their way to overcome any kind of problem. One of the most admirable aspects of Dave is his "Just do it" attitude.

Secondly, I would like to express my sincere gratitude to Dr. Evelina Liarou. Without her support this journey would have not been completed. Evelina is the person who can make me find inspiration and motivation out of nowhere, through her passion about Chemistry and her love about Science in general. She is a unique person who enjoys helping her colleagues and a person who can think, discuss and carry out a project in "high-speed mode".

Next, I would like to thank Dr. Alan Wemyss for his support during all these years. Alan has introduced me in the field of CCTP and since the first day he was there to offer his guidance and to help me with any issue I had. He proved to be a great friend and a great neighbor (for about $2^{1/2}$ years)!

I would like to thank my industrial supervisors Dr. Annette Christie, Dr. Chris Lindsay and Dr. Pauline Phillips for the opportunity to work with them and for being so patient and helpful with me.

I would also like to thank past and present members of the Haddleton group. Firstly I want to thank my good friends Dr. James Town and Dr. Dan Lester for their support and advice, as well as for the productive discussions and the pints we enjoyed together. I want to thank past members of the group: Dr. Nikolaos Engelis, Dr. Glen Jones and Dr. Richard Whitfield for their help during my first year in the group. I would like to thank Asst. Prof. Athina Anastasaki for the discussions we had. Finally, it was my pleasure to work with many people including Paul, Ahmed, Joe, Atty, Rachel, Cansu, Rike, Ellis, Congkai, Yongguang and Matthew.

Finally, this work would not be possible without the support of my parents, to whom this thesis is dedicated.

Declaration

The work performed in this thesis was carried out in the Department of Chemistry, University of Warwick between October 2017 and August 2021. Unless otherwise stated below, it is the work of the author and has not been submitted in whole or in part for any degree at this or any other university.

In chapter 2, the synthesis of pGMMA macromonomer was performed by Dr Alan Wemyss and the synthesis of latexes (pS, pBMA and pMMA) stabilized by SDS by Dr Ataulla Shegiwal. SEM imaging was performed by Dr Evelina Liarou. SLS analysis was made by Dr Joe Jones, as well as the development of linear regression model.

The synthesis and the characterization of CoBF was carried out by Dr Ataulla Shegiwal and Dr Chris Abi Saleh. The IR analysis of CoBF was made by the author of this thesis.

In Chapter 3, the initial experiments for the determination of C_T were carried out in collaboration with Dr Alan Wemyss. MALDI-ToF-MS experiments and analysis was made by Dr James Town. SEM images were taken by Dr Evelina Liarou.

In Chapter 4, MALDI-ToF-MS was carried out by Dr Evelina Liarou.

In Chapter 5, the synthesis of pMA_{50} using dodecyl 2-bromoisobutyrate as initiator, as well as the synthesis of $pMMA_{50}$ using methyl α-bromo phenylacetate as initiator were carried out by Dr J. Grace and Ellis Hancox. The MALDI-ToF-MS experiments were carried out by Dr Evelina Liarou.

The content has not previously been published, except as detailed in the publications listed below:

1. Marathianos, A.; Liarou, E.; Anastasaki, A.; Whitfield, R.; Laurel, M.; Wemyss, A. M.; Haddleton, D. M. Photo-Induced Copper-RDRP in Continuous Flow without External Deoxygenation. *Polymer Chemistry* **2019,** *10* (32), 4402-4406.
2. Marathianos, A.; Liarou, E.; Hancox, E.; Grace, J. L.; Lester, D. W.; Haddleton, D. M. Dihydrolevoglucosenone (Cyrene™) as a Bio-Renewable Solvent for Cu(0)Wire-Mediated Reversible Deactivation Radical Polymerization (RDRP) without External Deoxygenation. *Green Chemistry* **2020,** *22* (17), 5833-5837.

3. Marathianos, A.; Wemyss, A. M.; Liarou, E.; Jones, J. R.; Shegiwal, A.; Town, J. S.; Lester, D. W.; Li, Y.; Haddleton, D. M. Controlling the Particle Size in Surfactant-Free Latexes from Ω-Propenyl Oligomers Obtained through Catalytic Chain Transfer Polymerization. *ACS Applied Polymer Materials* **2021,** *3* (6), 3185-3196.

Date:

Arkadios Marathianos

Abstract

This PhD thesis aims to bring new perspectives on the field of Transition Metal Catalyzed Polymerization methods, by investigating alternative synthetic approaches for the generation of various polymers, many of which having high prospect for industrially related use. For this purpose, two distinctive transition metal catalyzed polymerization methods, namely Catalytic Chain Transfer Polymerization (CCTP) and Copper-mediated Reversible Deactivation Radical Polymerization (Cu-RDRP) were examined under various conditions, and used for the generation of polymers which either have compelling applications or are well-defined. For simplicity, this thesis can be divided into two parts; the first part focuses on the use of CCTP in combination with surfactant-free emulsion polymerizations (Chapter 2 and Chapter 3). The second part which focuses on Cu-RDRP, aims to examine the limits of this controlled radical polymerization method under the simultaneous introduction of oxygen tolerance and either continuous flow chemistry or the use of a bio-renewable solvent (Chapter 4 and Chapter 5).

Initially, the ability of CCTP-derived methacrylic macromonomers to act as stabilizers in surfactant-free emulsion polymerizations was investigated (Chapter 2). Although these macromonomers are highly versatile, studies on their behaviour as stabilizers in emulsion processes had been limited. In Chapter 2, ionic and non-ionic CCTP-synthesized oligomers were compared with a conventionally used surfactant (SDS) for their stabilizing effect on surfactant-free emulsion polymerization of hydrophobic monomers. The effect of the stabilizers (ionic vs non-ionic vs low molar mass surfactants) on the properties of the final product was examined and with the alliance of different characterization methods, a statistical method explaining the particle size variations due to the hydrophobic monomer selection was created.

In Chapter 3, the potential use of this type of macromonomers in industrial applications (e.g. in agrochemical industry) was examined. Specifically, amphiphilic macromonomers obtained through CCTP with varying acid content, were used for the development of stable aqueous dispersions of an active ingredient (AI), namely cyantraniliprole (CYNT). Upon finding the optimum conditions for sufficient CYNT dispersion, the direct application of polymeric coating around the CYNT particles was

investigated. For this purpose, surfactant-free emulsion polymerization of a monomer mixture under starved-feed conditions was carried out in the presence of the CYNT dispersion. Finally, the release profile of cyantraniliprole in aqueous media was investigated.

The second part of this dissertation was focused on a different type of Transition Metal Catalyzed Polymerization, namely Cu-RDRP. In this part of the thesis (Chapter 4 and Chapter 5), the limits of this versatile controlled radical polymerization process were examined under various conditions. Specifically, in Chapter 4, the photoinduced Cu-mediated polymerization of different acrylates in a continuous flow reactor was investigated without conventional deoxygenation, hence providing a simplification of the existing continuous flow approaches. Upon optimization, well-defined poly(acrylates) were synthesized with a range of molar masses and low dispersity values. Importantly, although in continuous flow and in the presence of air/oxygen, the synthesized polymers exhibited high end-group fidelity, as confirmed through efficient post polymerization modification. The oxygen tolerant nature of Cu-RDRP was further examined in Chapter 5, this time in batch and with the use of a bio-renewable solvent (CyreneTM), along with the use of very low catalyst loadings. Well-defined polymers with good macromolecular characteristics were obtained, providing an environmentally-friendly alternative synthetic way.

Chapter 1: *Introduction to Radical Polymerizations*

1.1 Polymer History: The Early Years

During the last two centuries new families of materials, known as polymers have been discovered and not only challenged the classical materials but have also made possible the realization of new products which have contributed to extend the range of activities of mankind. The term "polymeric" was first introduced in 1833 by the Swedish chemist J. J. Berzelius,[1] who considered that a polymer was a type of isomeric form in which the relative number of atoms is equal, but the absolute number is unequal (for example benzene, C_6H_6 to be a polymer of acetylene, C_2H_2).[2] However, by this definition, the use of the term alone does not ensure that the product described is a long-chained macromolecular species and other indicators must be utilized to determine the true nature of the molecules (*i.e.* organic versus inorganic), their relative sizes, their structures or their ability to interconvert.

Over time, the term polymer evolved and in 1920 the German chemist H. Staudinger introduced the term *macromolecule*,[3] which led to the modern concept of polymers. A macromolecule is a molecule of high relative molecular mass, the structure of which essentially comprises the multiple repetition of units derived, actually or conceptually, from molecules of low relative molecular mass.[4] A polymer is a substance consisting of very large molecules, or macromolecules, composed of many repeating units. [5]

Although placing the existence and use of polymers in history is rather impossible, the use of polymers is dated thousands of years ago.[6] Flax fabrics were used in pre-dynastic Egypt (3800 BC) and in Neolithic lake dwellings in Switzerland. References to hemp and ramie (fibers cultivated in temperate latitudes) occur in Chinese writings (2800 BC) and in early Sanskrit literature. The culture of silk began

in 2640 BC in China, while wool from sheep was employed for clothing at least 5,000 years ago in Mesopotamia.

Around 1,600 BC the Mayans made rubber balls by coagulation of the latex obtained from rubber trees, *Castilla elastica*. Such trees, like *Heveea Brasiliensis*, are found in the southern equatorial region and mainly were called "Cau-uchu" or "weeping wood" in South America. The lack of satisfactory solvent delayed the progress of rubber utilization until 1823, when Macintosh patented the use of coal tar. Faraday showed in 1826 that natural rubber was a hydrocarbon of empirical formula (C_5H_8) and Williams gave the name isoprene to the volatile liquid obtained by destructive distillation of natural rubber. In 1839 Goodyear found that heating rubber with sulphur and white lead gave it far superior properties, a process to become known as vulcanization, termed by Brockeden.[6]

The first thermoplastic material was known as celluloid (1860s) and it was based on the addition of camphor to nitrocellulose,[6] while the first synthetic thermoset polymer, known as Bakelite, was obtained in 1907 by Baekeland through the polycondensation of phenol with formaldehyde.[7] Poly(vinyl chloride) (PVC) has been discovered the late part of 19th century by Baumann, although it was not commercialized until the 1920s, when Ostramislenski patented flexible film cast from a solution containing PVC and a plasticizer.[8] The high pressure polymerization of ethylene (PE) was accidentally discovered by Gibson and Fawcett and commercialized in 1939,[9] and nowadays it is the most common synthetic polymeric material with an estimated production of over 80 million tonnes per annum. Another significant achievement was the discovery of Nylon 6,6 by Carothers and Du Pont company.[10] Carothers published his theory of polycondensation and compared it with polyaddition in 1929. His initial studies on aliphatic polyesters were done and results were published before discovering the aliphatic polyamide with higher melting point. Nylon 6,6, made from a diamine and diacid, each with six carbons, was commercialized before 1940 and continues until today.[11]

Nowadays, polymers are found everywhere in everyday life; materials utilized ranging from nylon (clothing) and polystyrene (plastic cutlery, cups, etc.) to PVC (pipes, window panels and credit cards), polyethylene (packaging and bottles) and polypropylene (textiles). "Smart" materials have also been developed, like Kevlar in

bullet proof vests, Teflon in non-stick frying pans[12] and Lycra found in elastic clothing.[12-14] A plethora of other materials that are not limited to hard or rigid structures are used in biological applications, such as tissue engineering, drug delivery and diagnostics.[15-17]

1.2 Polymerization Classification

Polymers were firstly classified by Carothers in 1929, as mentioned above, on condensation and addition polymers. This classification was based on the compositional difference between the polymer and the monomer(s) from which it was synthesized.[18] A polymer is classified as a condensation polymer if its synthesis involves the elimination of small molecules, or it contains functional groups as part of the polymer chain, or its repeating unit lacks certain atoms that are present in the monomer to which it can be degraded. If any of these requirements are not fulfilled, the polymer is classified as addition polymer.[18] An additional distinction between polymers was introduced by Flory, in 1953, which was based on the polymerization mechanism and not on polymer structures. Consequently, the modern terminology distinguishes polymerizations into step-growth and chain growth processes (**Table 1-1**).[19]

Table 1-1. Step-Growth versus Chain-Growth Polymerization (adapted from reference 20).

	Step-Growth	**Chain-Growth**
Reactions	One reaction is responsible for polymer formation.	Initiation, propagation, and termination reactions have different rates and mechanisms
Polymer Growth	Any two molecular species present can react; slow, random growth takes place..	The growth reaction takes place by the addition of one unit at a time to the active end of the polymer chain
Polymer Molecular Weight	Molecular weight rises steadily throughout the reaction. High conversion is required for high molecular weight polymer.	High molecular weight polymer is formed immediately
Monomer Concentration During Polymerization	Monomer disappears in the early stages of the polymerization. Less than 1 mol % of the original monomer remaining when the average polymer chain contains only ~100 monomer units.	Monomer concentration decreases steadily throughout the reaction.
Composition of the Polymerization Reaction	A relatively broad, calculable distribution of molecular species are present throughout the course of the polymerization	Mixture contains only monomer, high molecular weight polymer and only about 10^{-8} part of growing chains.*

*This is true shortly after initiation and at the end of the polymerization (except for the growing chain concentration) since 100% conversion of monomer usually is not achieved.

In the first case, step-growth polymerization proceeds by the stepwise reaction between the functional groups of any of the different-sized species present in the reaction system at very slow rates. Moreover, the initiation, propagation and termination steps are meaningless in step-growth polymerization. The molecular weight of the polymer increases steadily, while high molecular weight polymers require high conversions.[19, 20] The average degree of polymerization ($\bar{X}_n$) in step-growth polymerization is described by *Carothers equation*; $\bar{X}_n = \frac{1}{1-p}$, where p is the monomer fraction converted.[21] On the other hand, chain-growth polymerization has distinct steps with different rates and mechanisms. Chain-growth polymerization requires an initiation step, in which an initiator produces an initiator species R^* with a reactive centre (free radical, cation or anion). Subsequently, polymerization occurs by the propagation of the reactive centre by additions of large numbers of monomer molecules in a chain reaction, where the reactive centre is regenerated by each monomer molecule that being added to reactive centre. The step of propagation proceeds until the reactive centre is destroyed by one or more of possible termination reactions.[18, 19, 22] A widely used chain-growth process is Free-Radical Polymerization (FRP).

1.3 Free-Radical Polymerization

Free radical polymerization (FRP) is the most commonly used technique for the production of materials used in our life due to its high versatility and low cost.[23] Experimentally, FRP exhibits relative tolerance to impurities, moisture, air and it is compatible with various solvents and monomers.[24] The polymers are formed by successive addition of a radical to a monomer, usually containing a vinyl group. The mechanism of FRP was described by Flory in 1937 and includes three steps as conceived by Staudinger and Frost; chain initiation, chain propagation and chain termination. [25]

The first step, initiation, consists of two events. Initially, generation of free radicals ($R^{\bullet}$) from initiator molecules, usually from the dissociation of initiating species (I) either through heat or light, where k_d is the rate of constant for the initiator dissociation (**Equation 1.1**). Subsequently, the addition of one of these radicals to a

monomer produces a chain-initiating radical M$^{\bullet}$, where k_i is the rate constant for the initiation step (**Equation 1.2**).

$$I_2 \xrightarrow{k_d} 2R^{\bullet} \qquad (1.1)$$

$$R^{\bullet} + M \xrightarrow{k_i} M^{\bullet} \qquad (1.2)$$

The amount of initiating radicals that undergo the reaction in **Equation 1.2** is described by the initiator efficiency, *f*, defined as the fraction of radicals formed in the primary step of initiator decomposition, which are successful in initiating polymerization. The highest value of $f = 1$ is achieved when all radicals undergo addition to monomer. However *f* is usually less than unity due to wastage of initiator. An important reaction which can affect the initiator efficiency is the chain transfer to initiator, which is caused by the attack of propagating radicals on the initiator, resulting in its decomposition. This reaction does not change the concentration of propagating radicals during polymerization, since a newly formed radical will initiate a new polymer chain. However, an initiator molecule is decomposed without increasing the number of propagating radicals, thus lowering *f*.[18]

Radicals formed in the primary step of initiator decomposition could undergo side reactions to form stable products instead of initiating polymerization. Initially, radicals formed by the decomposition of the initiator are surrounded by a cage consisting of solvent and/or monomer molecules. The radicals of initiator in this cage could undergo reactions (recombination, reaction with each other or with monomer) or may diffuse apart. Reactions of initiator-derived radicals in the solvent cage that form stable products, decrease the *f*, because these products are not able to contribute to chain initiation. The rate constants for radical-radical reactions are higher than the rate constants for radical addition to monomer in the solvent cage, thus increasing the probability that they will occur and reduce *f*. Once they diffuse out of the solvent cage the reaction with monomer occurs predominately in preference to other reactions (due to higher monomer concentration).[18]

Furthermore, *f* depends on the conditions applied to a reaction. Increasing the viscosity of a reaction will decrease *f*, as the lifetimes of radicals in the solvent cage are increased leading to more radical-radical reactions in the solvent cage. In some

cases f varies with solvent as a result of reactions between solvent and radicals before the latter can initiate polymerization. Finally, f for any particular initiator may vary for different monomers due to different rates of radical addition to the different monomers.

Initiator efficiency can be evaluated experimentally by several methods.[18] Measurement of the polymer number-average molecular weight allows the determination of f by comparison of the number of radicals produced with the number of polymer molecules obtained. Another method involves the determination of the number of initiator fragments in the polymer by direct analysis of the polymer end groups. Radical scavengers has also been used for the determination of initiator efficiency. A fourth method is the dead-end polymerization technique, which allows the simultaneous determination of f and the rate of dissociation (k_d).

The initiation process is followed by propagation, where the free radical at the end of the polymer chain reacts with a monomer resulting in the formation of a new radical but larger by one monomer unit. The process of chain growth takes place at rapid rates and is described by **Equation 1.3**, with k_p being the rate constant of propagation with values within the range of 10^2-10^4 L mol^{-1} s^{-1}.

$$M^{\bullet} + nM \xrightarrow{k_p} M_n^{\bullet} \qquad (1.3)$$

Eventually, the propagating polymer chain loses its radical activity and undergoes termination, typically by chain transfer or radical destruction events by either combination or disproportionation.[18] Combination is the process which involves two radicals coupling, leading to the formation of a "dead" polymer chain, with a chain length equal to the sum of the two terminated propagating radical chains. Alternatively, cessation of the propagating radical growth can occur through disproportionation, which involves transfer of a hydrogen atom to give one saturated and one unsaturated "dead" polymer chains. The termination events have rate constants (k_{tc} and k_{td} for combination and disproportionation, respectively), which are kinetically equivalent and both have the same rate equation. In general terms, the termination events can be described in **Equation 1.4** with k_t being the combined rate constant of termination.[26]

$$M_n^{\bullet} + M_m^{\bullet} \xrightarrow{k_t} M_n^{=} + M_m^{H} \text{ or } M_{n+m} \quad (1.4)$$

The rate of polymerization can be defined as the rate of consumption of monomer. Based on this, the rate of polymerization is equal to the rate of initiation (R_i) added to the rate of propagation (R_p), **Equations 1.2 &1.3**. Comparing the actual amounts of monomer consumed by these two reactions it becomes clear that propagation is a much more significant source of monomer depletion and hence the overall rate of polymerization can be described by **Equation 1.5**.

$$\frac{-d[M]}{dt} = R_p = k_p[M^{\bullet}][M] \qquad (1.5)$$

However, **Equation 1.5** can be problematic as it is difficult to experimentally determine the concentration of radicals, $[M^{\bullet}]$ in a reaction (typically on the order of 10^{-8} molar). Thus, a number of assumptions have been applied to the system. Applying a steady state approximation to the concentration of radicals in a polymerization gives a constant value and is used to simplify the equation. As a result, the rate of initiation and termination are effectively equal. The rate of termination is shown in **Equation 1.6**. this expression can be rearranged to give **Equation 1.7**, which can subsequently be substituted into **Equation 1.5** to give **Equation 1.8**.

$$R_t = 2\, k_t\, [M^{\bullet}]^2 \qquad (1.6)$$

$$[M^{\bullet}] = \left(\frac{R_i}{2\, k_t}\right)^{1/2} \qquad (1.7)$$

$$R_p = k_p\, [M] \left(\frac{R_i}{2\, k_t}\right)^{1/2} \qquad (1.8)$$

Addition of an initiating radical to monomer is much faster than homolysis of the initiator, hence the dissociation of the initiator is the rate determining step. Taking a rate expression for the initiation including the initiator efficiency, *f*, and substituting into **Equation 1.8** yields **Equation 1.9**.

$$R_p = k_p\, [M] \left(\frac{f\, k_d[I]}{2\, k_t}\right)^{1/2} \qquad (1.9)$$

The final factor to consider within free radical polymerization is the very common side reaction called chain transfer,[27] which is a method of termination of a

polymer chain, but results in the formation of a new radical. Then, this radical has the ability to reinitiate the polymerization without changing the overall number of radicals in the system. Chain transfer can occur with monomer, initiator or solvent, leading to a lower average molecular weight within the polymerization mixture, or to polymer which can result in branching and higher molecular weights. The effect of chain transfer on the polymerization rate is dependent on whether the rate of reinitiaton (k_a) is comparable to that of the original propagating radical. In **Table 1-2** the main possible situations that may be encountered affecting the R_p and the degree of polymerization (DP_n).

Table 1-2. Effect of chain transfer on R_p and DP_n.[18]

$k_p : k_t$	$k_a : k_p$	Resulting Chain Transfer	Effect on R_p	Effect on DP_n
$k_p >> k_t$	$k_a \sim k_p$	Normal chain transfer	None	Decrease
$k_p << k_t$	$k_a \sim k_p$	Telomerization	None	Large decrease
$k_p >> k_t$	$k_a < k_p$	Retardation	Decrease	Decrease
$k_p << k_t$	$k_a < k_p$	Degradative chain transfer	Large decrease	Large decrease

Catalytic chain transfer polymerization (CCTP) has been developed as a technique, where certain low spin cobalt(II) complexes are used as chain transfer agents (CTAs) so to generate low molecular weight polymers in free radical processes.[28-31] The effectiveness of a CTA is determined by its chain transfer constant (C_s), **Equation 1.10**, which is a ratio of rate of chain transfer (k_{tr}) compared to the rate of propagation (k_p).[32-36]

$$M_n^{\bullet} + CTA \xrightarrow{k_{tr}} M_n + CTA^{\bullet} \quad , C_s = \frac{k_{tr}}{k_p} \qquad (1.10)$$

Although FRP is a widely applied polymerization technique with extended use in industry, it still suffers from significant disadvantages, the most important being the lack of control over the molecular weight and the architecture of the resulting polymers.

1.4 Emulsion Polymerization

Apart from homogeneous media, a polymerization may also take place in heterogeneous media, a system which consists of two phases, insoluble in each other. Emulsion polymerization is a well-established process providing most of the polymeric materials synthesized by industry – it is reported that 40-50 % of all free radical polymerizations performed in industrial scale are in emulsion.[18, 37, 38] Especially, the production of latex materials produced free radically by emulsion polymerization for various applications, depending on the colloidal and physicochemical properties of the obtained polymer latex.[39-42] The two phases in emulsion polymerization are the aqueous phase, also referred to as the "continuous" phase and the organic, known as "dispersed". Reaction may be carried out *via* various operating modes, such as batch, semi-batch or continuous system and the reagents required are water, (usually) water soluble initiators (for instance potassium persulfate, KPS), monomers of low water solubility (like styrene) and low molar mass amphiphilic molecules (like sodium dodecyl sulfate, SDS), known as surfactants.[43-48] Surfactants are dissolved in water until the critical micelle concentration (CMC) is reached and are used to prevent coagulation of the latex particles, as well as to provide the conditions for sufficient colloidal stability.[43]

There are three phases in an emulsion polymerization mixture before the reaction starts. The continuous phase, consisting of the water-soluble initiator and in very small quantities, molecularly dissolved surfactant and monomer. The dispersed phase contains monomer droplets (1-10 μm), which remain in suspension due to agitation and to the adsorption of molecules of surfactant. Droplets contain the largest amount of monomer present in the system. Also part of the dispersed phase are the monomer-swollen micelles (5-10 nm). The use of water as solvent makes the whole system inexpensive, relatively odorless and non-flammable. The high heat capacity of the water facilitates temperature regulation and guarantees efficient heat transfer. Moreover, the low volatile organic content (VOC) makes the method environmentally friendly. High conversions and low viscosity of the produced latex, independently of the molecular weight of the polymer are other important benefits by the use of this technique.

However, emulsion polymerization has also a few drawbacks, the main being the unavoidable presence of additives (surfactants) and the difficulties of water removal if required at the end of polymerization.[28, 49]

1.4.1 Emulsion polymerization processes and sequence of events

As mentioned above there are three types of emulsion polymerization processes. In batch emulsion polymerization all ingredients are present in the reaction vessel from the beginning. Polymerization starts when the initiator is activated, usually by the application of heat. In a semi-continuous process (also called semi-batch), one or more reagents (*e.g.* monomer) are fed into the reaction vessel throughout the polymerization. Finally, in a continuous emulsion polymerization, the components of the reaction system are continuously fed and removed from the vessel. Due to this particularity, special types of reactors are required for this process.

Emulsion polymerizations are also classified according to the way of polymer particle formation. An emulsion polymerization might start in a system where there are no formed *loci* of polymerization (particles). In this case, the process is called "*ab initio*" emulsion polymerization and particle formation (nucleation) needs to take place at an early stage of the process. In contrast, in seeded emulsion polymerization, the *loci* of polymerization have previously been formed in a separate process.

An *ab initio* emulsion polymerization is divided into three stages. The first stage, also known as *Interval 1*, is defined as the period during which particles are formed. There are three mechanisms for particle nucleation and the one that dominates is usually decided by the conditions. Nevertheless, the first event is common and is the formation of oligomeric radicals *via* the decomposition of the water-soluble initiator and the subsequent addition of the primary radicals to molecules of monomer. The oligomeric radicals may reach two critical degrees of polymerization, usually represented as z or j (for z-mers or j-mers respectively, with $z < j$). Beyond the formation of z-mers and j-mers, the three nucleation mechanisms differentiate from each other.

In *micellar nucleation*, *z*-mers enter the existing monomer-swollen micelles, thus continuing polymerization due to the molecules of monomer, already present there.[50, 51] Micelles that do not absorb a *z*-mer are subsequently ceased, releasing their monomeric content to the system, while their molecules of surfactant get absorbed by newly-formed particles, offering supplementary stability. Micellar nucleation stops when all micelles are consumed either by becoming particles or by having ceased. It should be noted that as the number of micelles is much higher than that of monomer droplets, oligomeric radicals almost entirely enter the first ones. Micellar nucleation takes place when CMC is exceeded.

Homogeneous nucleation occurs when oligomeric radicals keep on propagating until becoming *j*-mers.[47, 52] At that point, chains collapse and become particles while still retaining their active chain end. Subsequently, the newly-shaped particles adsorb molecules of surfactant in order to secure their stability as well as molecules of monomer as to continue chain growth. *Coagulative nucleation* is similar to homogeneous nucleation.[53] In this case, primary particles coagulate forming particle aggregates. The latter are colloidally stable and able of absorbing molecules of monomer in order to propagate. A further mechanism is *droplet nucleation*, which occurs when a *z*-mer enters a monomer droplet.[47, 54-56] This type of nucleation is considered unlikely in emulsion polymerization, however it is the dominant mechanism in mini-emulsion polymerization, where ideally each monomer droplet becomes a particle. By the end of *Interval 1*, monomer conversion is about 10% (**Figure 1-1**) and it is considered that the number of particles formed does not change until the end of the polymerization reaction.[43, 44]

Interval 2 is considered the stage of particle growth and is oriented between 10 and 40 % conversion, **Figure 1-1**.[43-45, 57] During this stage, monomer droplets act as monomer reservoirs, containing molecules that reach the latex particles (where polymerization takes place) *via* diffusion through the continuous phase. During *Interval 2*, the monomer concentration in the particle ($[M]_p$) as well as the number of particles per unit of volume (N_p) and the average number of radicals per particle ($\overline{n}$) are considered to be constant, thus resulting in a constant rate of polymerization . It should be noted that the rate of monomer diffusion through the aqueous phase exceeds

the rate of polymerization and as a result, there is sufficient amount of monomer entering the particles in order to maintain propagation.

In *Interval 3*, the rate of polymerization decreases due to the fact that monomer droplets are exhausted. As a result, polymerization continues only with the molecules of monomer still present in the particles or the few dissolved in the continuous phase. The number of particles is also considered to remain constant during this stage.

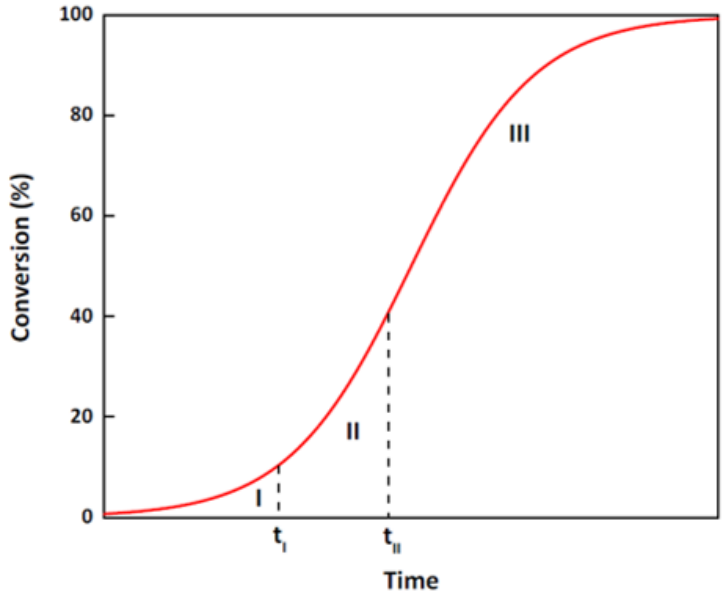

Figure 1-1. Schematic representation of the variation of conversion with time for an emulsion polymerization system. t_I and t_{II} are the completion times for intervals I and II respectively.

1.5 Transition Metal-mediated Living Radical Polymerization

The use of transition metals as catalyst-deriving species has found application in various polymerization processes, like controlled/living radical polymerization[58] and late transition metal mediated polymerization.[59] Depending on the desired polymers, and therefore on the polymerization process/mechanism, numerous transition metals (and subsequently their complexes) have been used as catalytic species, including Nickel (Ni), Titanium (Ti), Palladium (Pd), Iron (Fe), Ruthenium (Ru), Cobalt (Co) and Copper (Cu). In particular the last decades have witnessed tremendous advances in the discovery and application of transition metal catalysts. Arguably, the introduction of Ziegler-Natta catalysts (*e.g.* $TiCl_4$) in the mid-1950s,[60,

[61] revolutionized the synthesis of polyolefins and led to a Nobel Prize in 1963. In the late 1950s, the use of Molybdenum (Mo), Ruthenium (Ru), Wolfram (W) and Rhenium (Re) allowed for the ring-opening of cyclic olefins, thus introducing the Ring-Opening Metathesis Polymerization (ROMP).[62] Among other advances, in 1995 the use of low valent Ruthenium (Ru^{II}) and Copper (Cu^{I}) complexes were reported by Sawamoto[63] and Matyjaszewski[64] respectively, as excellent catalyst sources for the so called Transition Metal Mediated-Living Radical Polymerization (TMM-LRP).

The catalytic systems based on ruthenium have been extensively studied in order to enhance the required catalytic aspects for a living radical polymerization. Therefore, a variety of ruthenium catalysts have been developed *via* ligand design, including anionic ligands, like halogens, conjugated carbanions and phenoxy anions, as well as neutral, such as phosphines, amines, cymene and carbenes.[58, 65] Apart from ruthenium, iron complexes have been used for metal-catalyzed living radical polymerization, offering cheaper, safer and more environmentally friendly systems.[66] A dimeric Fe(I) carbonyl cyclopentadienyl complex was used for the controlled polymerization of vinyl acetate (VAc),[67] overcoming the issues of the instability of the non-conjugating and highly reactive VAc radical and the frequent chain transfer. Nickel catalysts have also been developed and their characteristics in living radical polymerization are similar to Fe(II) family, however they are sensitive to polar functional groups.[65] Other metal complexes have also been reported to control the activation and deactivation for initiating and growing radicals under suitable equilibrium, including osmium, rhenium, molybdenum, titanium, chromium, manganese, cobalt, nickel, rhodium, palladium, etc.[68]

An ideal catalyst in living radical polymerization allows the synthesis of well-defined polymers with narrow molecular weight distributions and high end-functionality throughout the polymerization, even with very low amounts of the catalyst. The choice of the metal complex is most of the times dependent on the purpose of the final product, such as iron-based catalysts for bioapplications due to the biocompatibility of iron. Moreover, the choice of ligand has been shown to be crucial, as it can influence the catalytic activity of the complex. For instance, copper complexes with nitrogen-based ligands were six orders of magnitude more efficient than complexes with phosphorous-, sulfur- or oxygen-based ligands.[69]

Since the area of transition metal-catalyzed polymerizations is vast and covers the whole field of polymers, this work will focus on two polymerization methods (*i.e.* Catalytic Chain Transfer Polymerization and Copper-mediated Reversible Deactivation Radical Polymerization) that use cobalt and copper complexes, respectively.

1.6 Catalytic Chain Transfer Polymerization (CCTP)

Catalytic chain transfer polymerization (CCTP) is an efficient and versatile technique for the synthesis of low molecular weight functional polymers/oligomers in free radical polymerization (FRP).[29, 30, 70, 71] The technique is based on the use of certain low spin Co(II) complexes which catalyze the chain transfer of hydrogen to monomer reaction[32, 72, 73] and also provides a high level of vinyl ω-end group functionality.[74, 75] Due to their high chain transfer constants, Co(II) complexes are efficient in low concentrations (ppm to monomer). The effectiveness of the catalysts, and the fact that radical addition to the vinyl end group of CCTP macromonomers forms adducts that readily undergo β-scission, allow them to function as addition-fragmentation chain transfer agents (CTAs) and render CCTP extensively applicable in industry.[76]

1.6.1 Brief history of CCTP catalysts and their evolution

CCTP was discovered in the USSR in the mid-1970s, when Smirnov and Marchenko were investigating cobalt porphyrins (**Figure 1-2, (1)**) catalysts for the redox decomposition of peroxy initiators for radical polymerisation.[70] The observation that some Co(II) complexes appeared to inhibit FRP of methyl methacrylate (MMA) lead to further investigation. Thus, further studies from Gridnev,[77-80] DuPont,[81, 82] O'Driscoll,[83, 84] the Glidden Paint company[85-87] and ICI/Zeneca[88, 89] have led to a significant understanding of the catalytic process and to the very active cobaloxime catalysts being developed (**Figure 1-2, (2, 3)**).

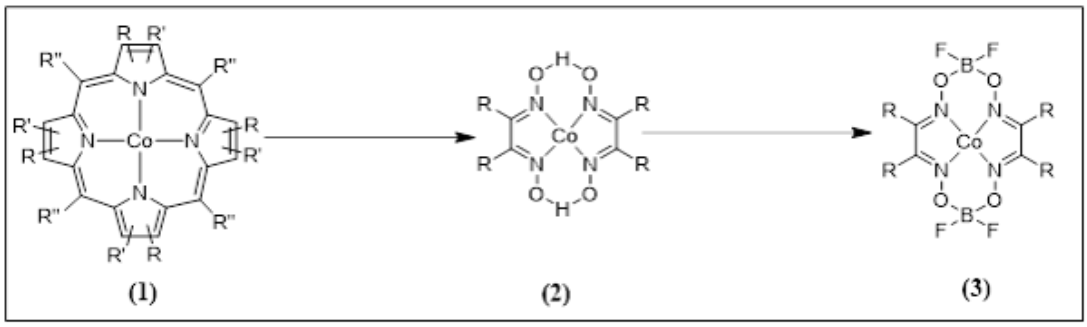

Figure 1-2. The evolution of CCT agents

In general, the most effective CCT agents are low-spin cobalt$^{(II)}$ complexes with octahedral geometry derived from a square planar ligand with two axial sites. Co(II) is a $3d^7$ electron system and can exist as either low- or high- spin (*i.e.* one or three unpaired electrons **Figure 1-3)**), so the choice of the correct ligand to give a low-spin complex becomes an important aspect of catalyst design for a CCT agent. Co(II) porphyrin (**1**) complexes showed relatively high activity,[28] however, are highly colored, only soluble in water, relatively expensive and much less active than the cobaloximes and were soon replaced by cobaloximes (**2**)[86, 87]. Cobaloximes show much higher activity ($C_s > 2 \times 10^4$) than their porphyrin analogues and are less expensive, however, they are very sensitive to hydrolysis and oxidation. The addition of a BF_2 bridging group between the axial oxygen atoms led to the development of BF_2 bridged catalysts (**3**) overcoming these disadvantages and increasing their stability towards acid and low pH as well as their activity ($C_s > 4 \times 10^4$). BF_2 bridged catalysts are typically handled as solid, even in aerobic conditions, but in solution are still sensitive to acid hydrolysis and oxidation by peroxides and other oxygen-centered radicals , but lesser than catalyst **2**.[28] The sensitivity to oxidation can be further enhanced by introduction of alkylated Co(III) derivative of (**3**), which will dissociate into the active Co(II) catalyst and an alkyl radical.[28, 32, 73, 78, 90]

Therefore, the most common used catalysts at present are the derivatives of catalyst (**3**), where the substitute R can be tailored based on desired solubility and activity. This work will mostly focus on bis[(difluoroboryl)dimethylglyoximato] cobalt(II) often, denoted as CoBF, where the four R ¼ substituents are methyl groups. The CoBF catalyst is exceptionally stable due to the boron-bridging groups that impart hydrolytic stability, allowing its use at low pH and at elevated temperatures.[31, 71, 90]

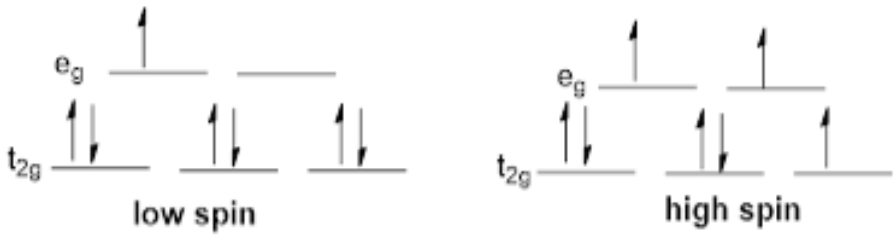

Figure 1- 3. d-electron configurations of d^7 Co(II) in low spin (left) and high spin (right).

1.6.2 Determination of catalytic activity of CTA

The activity of a CTA is given by the chain transfer constant (C_s), as discussed previously.[34-36] Conventional chain transfer agents (for example mercaptans) have C_s values on the order of magnitude of 1-10 for methacrylates, whereas cobaloximes such as CoBF, typically have C_s values in the region of 10^4 for methyl methacrylate, as they do not consumed within the reaction.

The C_s value can be calculated experimentally a series of polymerizations undertaken with various ratios of CTA to monomer, including one reaction without CTA as control. The polymerization reactions have to be stopped at low conversion (in general < 5-10 %) in order to avoid changes in monomer concentration and to minimize termination events. Subsequently, using the Mayo equation (**Equation 1-11)**, a Mayo plot can be constructed, by utilizing the ratio of the degree of polymerization in the presence (DP_n) and absence (DP_{n0}) of CTA ([CTA] and [M] are the concentrations of CTA and monomer respectively).

$$\frac{1}{DP_n} = \frac{1}{DP_{\mathrm{n0}}} + C_s \frac{[CTA]}{[M]} \qquad (1.11)$$

1.6.3 Mechanism of CCTP

Considering the mechanism of CCTP, its catalytic nature was proved when the regenerated cobalt(II) porphyrin has been isolated following polymerization.[71] Three distinct mechanisms have been proposed and are outlined in **Figure 1-4**, of which the most widely accepted involves reinitiaton mediated by a Co(III) hydride ([Co(III)]-H). Mechanism (**1**) is unlikely to occur, as the monomer does not directly participate in the hydrogen abstraction step, indicating that the methacrylate does not abstract an

H atom.[31, 91] The mechanism (**2**) suggests that the rate of CCT is dependent on monomer concentration, an assumption which has also been disproved.[92] In the case of mechanism (**3**) all the experimental evidence suggest that cobaloxime-mediated CCT proceeds *via* a two-step radical process in which the Co(II) complex first abstracts a hydrogen atom from the growing radical leading to a Co(III)-H complex and a vinyl terminated macromonomer. The Co(III)-H complex then reacts with a monomer molecule giving back the original Co(II) complex. The chain transfer process continues until total consumption of the monomer and results in the length of the polymer chain being dependent on the amount of CCT agent. Higher amount of CCT agent present in the reaction mixture lead to more chain transfer reactions and

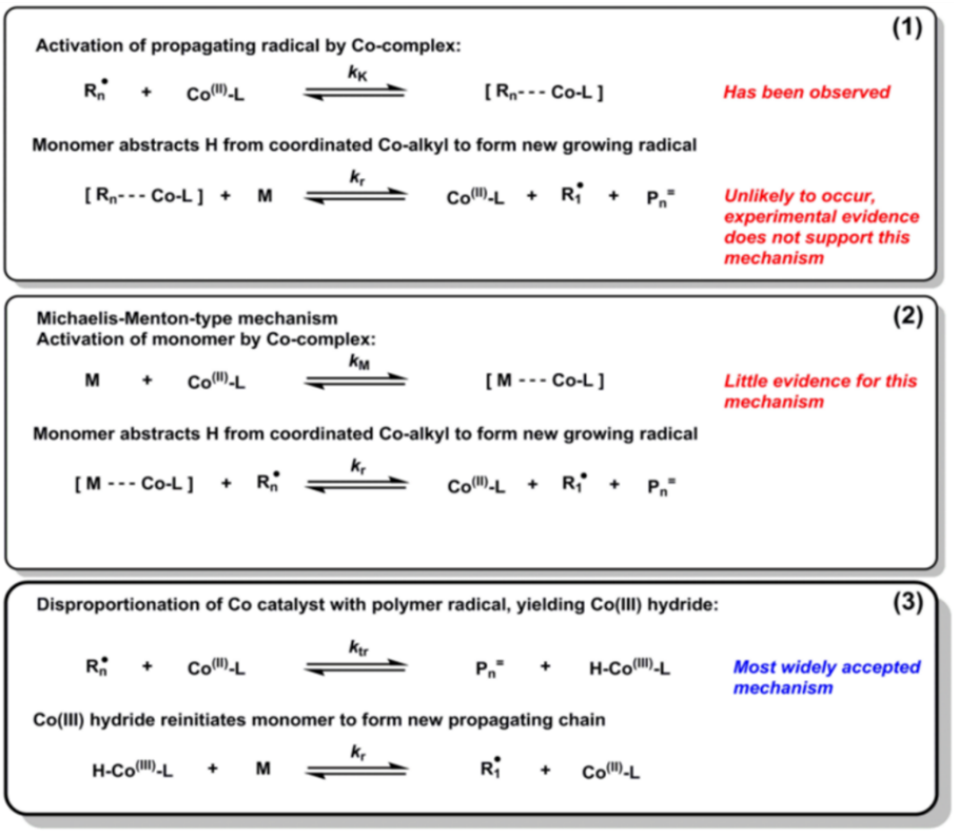

Figure 1-4. Proposed mechanisms for CCTP. R_n and R_1 are the polymeric and monomeric radicals, M is the monomer, Co(II)-L is the cobalt chelate CCTA and $P_n^=$ is a polymer with an unsaturated chain end.[29]

consequently lower molecular weight. This mechanism has investigated in detail and can be summarized in **Figure 1-5**.[29, 30, 32, 70-73, 78, 80, 83, 84, 91-97]

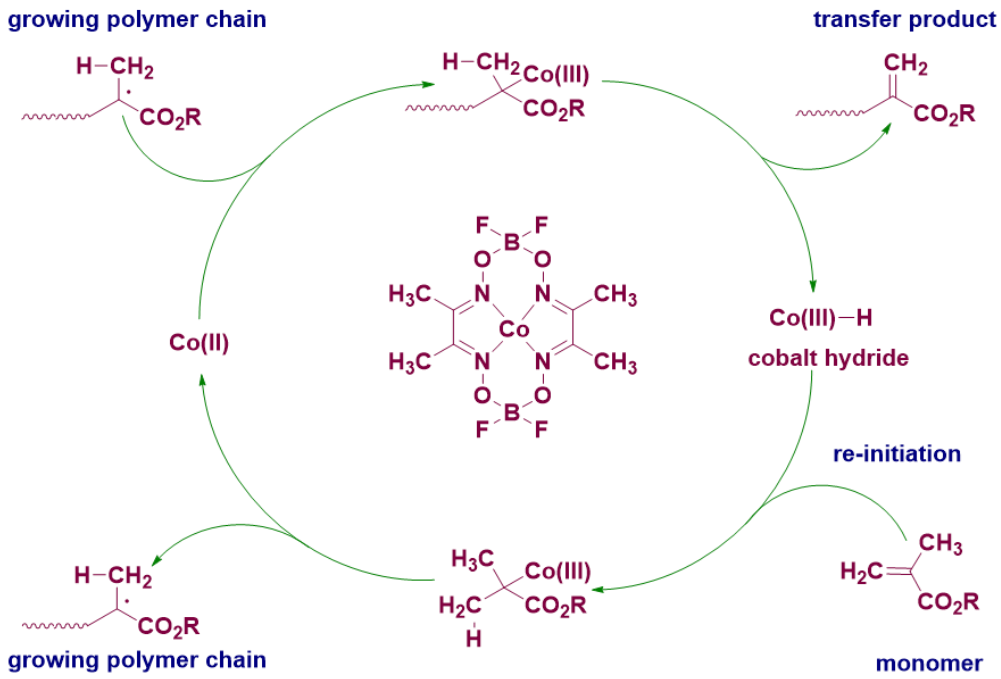

Figure 1-5. Most widely accepted mechanism for CCTP of methacrylates.

1.6.4 Monomer selection

A wide range of monomers can be efficiently polymerized in the presence of the catalytic chain transfer agents. Monomers containing an α-methyl group form tertiary propagating radicals (*e.g.* methacrylates) providing high chain transfer efficiency.[98] An H-atom easily abstracted by the CCTA complex yielding in a labile Co(III)-C bond and allows the formation of a Co(III)-H complex and a vinyl terminated polymer chain. On the other hand, monomers that do not have an α-methyl group, such as acrylates, form secondary propagating radicals and the hydrogen abstraction takes place from the backbone, resulting in the formation of relatively stable Co(III)-C bond. This results in the temporary removal of the catalyst from the cycle, reducing the chain transfer constant.[72, 78] **Figure 1-6** illustrates the expected results for active and less active CCTP monomers.

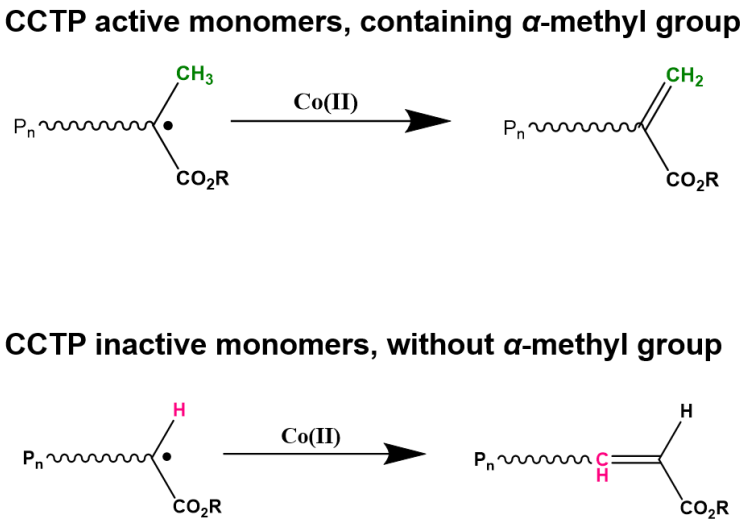

Figure 1-6. General monomer properties for CCT active and less active monomers.

It should be noted that styrene is an exception among the monomers without α-methyl group but forms a relatively stable internal double bond as it is relatively active, despite the absence of an H-atom that can be easily abstracted. Moreover, the rate of CCTP of styrene has been demonstrated to be UV-light dependent; the rate of CCT in dark was less than 500, however it increases to a maximum of C_s = 5,000 under UV irradiation.[28, 32] This is probably attributed to the homolysis of the Co(III)-C bond (formed by addition of styrene radical to the Co(II)) during UV irradiation. In addition, C_s is also found to be dependent on the concentration of initiator, as it decreases with higher initiator concentration.[32]

A variety of methacrylic monomers with different functionalities have been shown to polymerize well under CCT conditions. Among those, monomers with reactive functionality, capable for post-polymerization modification such as allyl methacrylate,[99] monomers with interesting functionality like sugar-monomers[100, 101] or monomers carrying reactive functional groups, such as carboxylic acids.[102] The ability of these polymers exhibiting reactive and tolerant functional groups, combined with terminal vinyl groups have been exploited as macromonomers as well as post-polymerization modifications. These vinyl terminated products of CCTP will be often referred to as macromonomers in this thesis. Macromonomers can be used further in polymerization involving the synthesis of graft, hyper-branched polymers and other unique polymeric morphologies. In the case of hyper-branched polymers synthesised from bifunctional or multifunctional methacrylate monomers, significant number of

vinyl end group functionality remains which can be exploited for further polymerization.[31, 103, 104] The most common form of post polymerization functionalization technique in CCTP involves the addition of functional thiols to the olefinic bonds, commonly termed as thiolene additions.[99-105]

To conclude, a successful CCTP requires a monomer capable to undergo CCTP as describe previously, an appropriate organocobalt complex such as cobaloxime, a solvent that is able to solubilize and to stabilize the catalyst and a free radical initiator which should not generate oxygen centered radicals (i.e. potassium persulfate) as these species deactivate the CCT catalysts. For the same reason, oxygen-free conditions are required.

1.6.5 Application of CCTP macromonomers

In addition to the industrial application of CCTP for the control of MW polymers in FRP systems, bulk products manufactured by CCTP have a plethora of applications, especially in products where aesthetics are important such as the automotive industry. Although CCTP derived products require further modification, there are many applications where they are deployed directly.[106, 107] For example, in electrophotographic toners, where CCT catalyst is directly utilized in emulsion systems along with suspensions of black or colored pigments improving their stability (in comparison with those attained with thiol chain transfer reagents), which subsequently are precipitated to obtain toners with narrow particle size.[28, 32]

In the automotive industry, functional monomers are used in the production of low volatile organic compounds (VOC) with high solids coating, like hydroxyethyl methacrylate (HEMA).[108, 109] The multiple hydroxyl groups on the macromonomer (copolymers containing HEMA) crosslink with trimethyl orthoformate and hexamethylene diisocyanate trimers, forming products with excellent flow ability; cure of these products provide good weatherability and adhesion after the application of coating.[108, 110-112]

The use of CCTP derived oligomers as CTA is another useful application. For example, the use of hydroxyethyl methacrylate dimer in MMA polymerization results in α,ω-telechelic polymer.[109] Telechelic polymers from radical chain polymerization have a broad range of uses in polymer chemistry, such as initiators, iniferters,

functional CTAs (telomers) and are used in incorporation of cleavable weak link along polymer chains.[113, 114] Other commonly used dimers for similar applications are methacrylic acid, ethyl methacrylate, methacrylonitrile and α-methyl styrene.[32, 34, 115, 116]

1.6.6 CCTP in emulsion

The first report about performing CCTP in a dispersed system was introduced about ten years after the initial discovery.[117] When performing CCTP in emulsion, the key difference is the lower catalyst efficiency compared to an equivalent solution process.[118-120] This is demonstrated by the higher molecular weight observed for a specific catalyst to monomer ratio. The presence of the catalyst at the loci of polymerization is a prerequisite for efficient control over the molecular weight. However, most of the widely used cobaloximes possess some solubility in both the continuous and the dispersed phase.[120-122] As a result, these catalysts partition between the two phases. The extent of partitioning depends on the monomer hydrophobicity and the structure of the cobaloxime complex. It is expressed by the partition coefficient, shown in **Equation 1-12**, where $[Co]_{disp}$ is the catalyst concentration in the dispersed phase while $[Co]_{aq}$ is the corresponding value for the continuous phase.

$$m_{Co} = \frac{[Co]_{disp}}{[Co]_{aq}} \qquad (1.12)$$

Generally, the partition coefficient increases when the hydrophobicity of the R-group of the complex increases or the hydrophilicity of the monomer increases. Data reported for the partition coefficient of several monomers indicate that a considerable amount of catalyst may reside to the aqueous phase.[28] Consequently, the concentration of catalyst at the loci of polymerization (particles) is significantly lower than the overall concentration of catalyst in the system. When extremely hydrophobic cobaloximes are employed, transfer limitations may occur. For example, CoPhBF is insoluble in water thus, the necessary mass transport to polymer particles cannot take place *via* the continuous phase. In this case, mass transport is considered to occur through collisions between polymer particles.[123] Moreover, in dispersed media, cobaloximes still demonstrate the same sensitivity towards oxygen and (peroxide) radicals.[30, 32, 80, 98] In

order to circumvent these drawbacks, the application of oxygen-free conditions as well as the avoidance of peroxy initiators are suggested.

1.7 Controlled/Living Radical Polymerization

Living polymerization was first observed during 1920s by Ziegler and Bahr.[124] Early approaches had been made during 1940s, such as the polymerization of sarcosine carbonic anhydride by Waley and Watson,[125] however the concept of living polymerization was pioneered by Szwarc in the 1950s with his work on the anionic polymerization of styrene,[126] and later expanded to include a range of vinyl monomers with electron withdrawing substituents, which can stabilize the negative charge through delocalization, including styrene derivatives and (meth)acrylates.[127]

Living polymerization is considered as a type of chain growth polymerization, which proceeds without chain-breaking reactions, namely the active centers are unable to undergo chain transfer or termination reactions.[128] The main characteristic is that the initiation is faster than propagation with each molecule of initiator initiating one polymer chain; all polymer chains grow simultaneously and at the same rate. As a result, the DP_n is directly linked to the concentration of initiator at t_0 and the amount of monomer consumed. The negligible presence of chain transfer and chain termination allows for specific molecular weights to be targeted, as well as retention of activity after full monomer conversion. This retention of the carbanion at the chain end make possible the synthesis of well-defined block copolymers and other complex macromolecular architectures, by sequential addition of a second monomer aliquot in the reaction vessel.

However, living anionic polymerizations are highly sensitive to impurities such as moisture (H_2O), oxygen (O_2) and carbon dioxide (CO_2), thus high vacuum techniques (anaerobic conditions) and highly purified reagents are required. Furthermore, high temperatures and solvents able to undergo chain transfer should be avoided. Nowadays, the production of high quality polymers (block copolymers, predetermined narrow molecular weight distributions or ease of functionalization of the terminated chain end) is a distinctive feature of living polymerizations, however, the commercialization of these processes can be hindered by the demanding experimental conditions required.

Living radical polymerizations can be achieved by minimizing normal bimolecular termination and prolonging the lifetime of living polymer chains through the introduction of dormant states for the propagating species. This is accomplished through reversible termination or reversible transfer (**Scheme 1-1)**.[18]

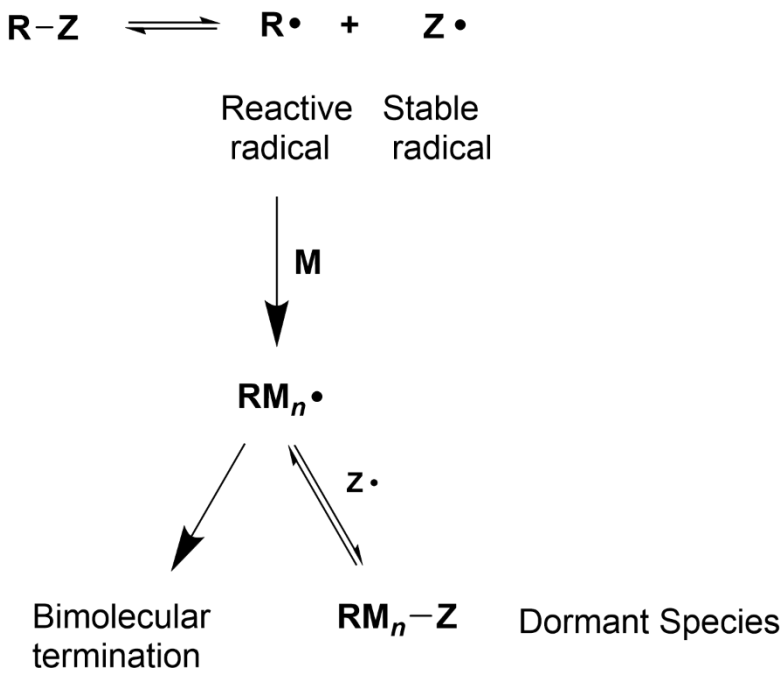

Scheme 1-1. Living radical polymerization process with reversible termination.

1.8 Reversible Deactivation Radical Polymerization

Reversible deactivation radical polymerization (RDRP) describes a family of techniques sharing a common characteristic, which is a dynamic equilibrium between free radical propagating species and dormant species.[129, 130] The equilibrium can be achieved either *via* the reversible deactivation of the propagating radical to form the dormant species, or through degenerate transfer between the propagating radicals and the dormant species. The term Controlled/Living Radical Polymerization (CLRP) has also been used to describe these processes, however, RDRPs proceed *via* a radical intermediate and therefore radical-radical termination is inevitable to some extent.[131] In addition, there is high possibility of side reactions related to chain transfer to solvent or monomer and as such, the RDRPs deviate from the definition of livingness as proposed by Szwarc. Based on this, the International Union of Pure and Applied Chemistry (IUPAC) suggested that the term *living* should be avoided for RDRP

systems, despite these systems exhibit a proximity to living polymerization reactions.[132]

The aim of these techniques is to eliminate chain breaking reactions, reserve the same probability of each chain in order to yield polymers with narrow molecular weight distributions (dispersity) and a number average molecular weight directly correlated with the ratio between monomer and initiator.[131] Three main techniques have emerged as the most viable RDRP approaches including nitroxide-mediated polymerization (NMP),[133, 134] reversible addition-fragmentation chain transfer (RAFT)[135, 136] polymerization and transition metal-mediated approaches (*e.g.* atom transfer radical polymerization, ATRP)[63, 137].

1.8.1 Nitroxide-Mediated Polymerization

Nitroxide-mediated polymerization is historically the first example of RDRP, developed at CSIRO by Solomon, Rizzardo and Cacioli in the 1980s,[138] who describe a method for controlled-growth radical polymerization. More specifically, by heating an alkoxyamine with methyl acrylate in bulk at 80 ^{o}C, oligomers of pMA were occurred with monomer inserted into every alkoxyamine, however, due to the additional stability of the inserted products, no further reaction was illustrated. By increasing the temperature to 120 ^{o}C, reversible dissociation occurred, resulting in a successful polymerization in 90 minutes. The development of methods to stabilize radical polymerization and probe the chemistry of its initiation included radical trapping and the use of nitroxides. Nitroxides have the ability to (selectively) scavenge carbon-centered radicals and are able to act as inhibitors for radical polymerization.[139] In order to study the initiation in styrene polymerization, Georges *et al.* use 2,2,6,6-tetramethylpiperidinyl-1-oxy (TEMPO) as the nitroxide and benzoyl peroxide as the initiator.[140] Further studies led to the development of a number of new alkoxyamines (**Scheme 1-2**), like those developed by Tordo and coworkers (TIPNO and SG1).[141, 142] Among the conclusions that followed these studies it was suggested that the alkoxyamines were thermally labile at higher temperatures and collectively, this observations led to the development of NMP.[143-145]

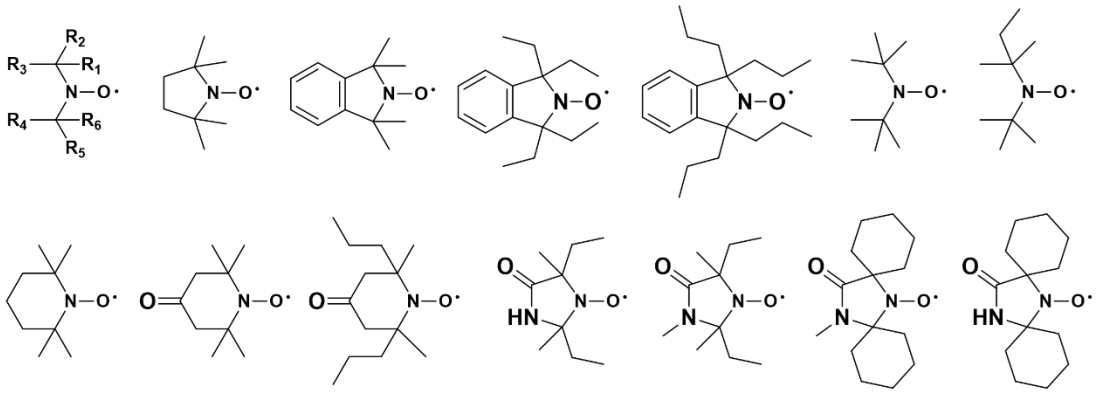

Scheme 1-2. Different nitroxides used in NMP.

Although NMP was firstly applicable only to styrenic monomers,[140] the development of nitroxides and alkoxyamines gave access to more monomer families including acrylates,[146] acrylamides,[147] acrylonitrile[142] and 1,3-dienes.[148] In the case of methacrylates, NMP was not successful due to the disproportionation reaction between TEMPO and the growing radical[149, 150] or the high activation – deactivation constant when TIPNO or SG1 were used.[151] Only copolymerizations with large amounts of styrene were possible, however the dispersity was increased when higher amounts of methacrylates were used.[152, 153] Charleux *et al* reported for the first time the successful NMP (using SG1) of methyl methacrylate at 90 ^{o}C, in the presence of small amounts of styrene.[154]

Regarding the mechanism in NMP, the control is dominated by the equilibrium between dormant species (the nitroxide is covalently bound to the polymer chain-end) and active species, $P_n^{\bullet}$ (the nitroxide is homolytically cleaved to generate a propagating radical at the polymer chain-end), (**Scheme 1-3**). The activation/deactivation constant K is determined by k_d and k_c ($K = k_d/k_c$).[145, 155, 156] Moreover, the concentration of $P_n^{\bullet}$ should be low to minimize side reactions and the exchange between the dormant and active species needs to be much faster than propagation and termination, so as the polymer chains to grow simultaneously.[157]

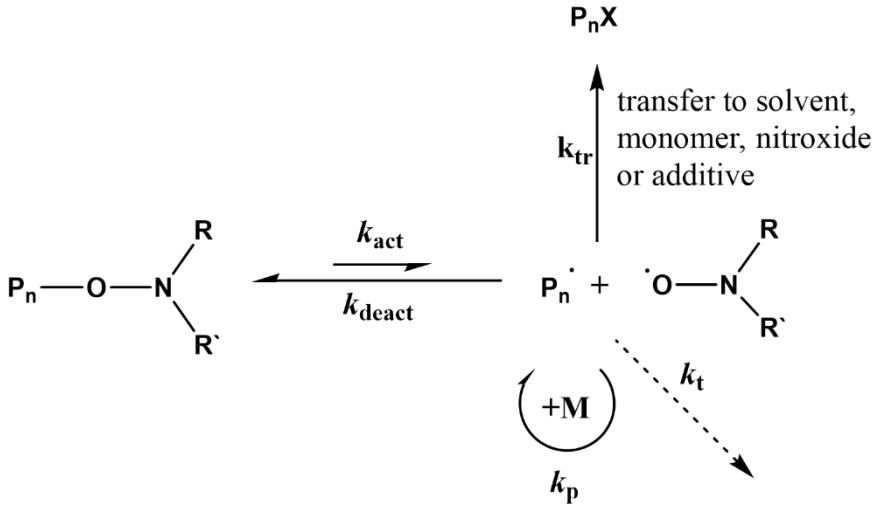

Scheme 1-3. Proposed mechanism of NMP.

NMP provides control over the macromolecular characteristics of the obtained polymers, however termination events are possible to occur, like transfer to monomer[158] or to the nitroxide,[159] resulting in the generation of P_nX species, where X is the fragment of the transfer agent.[156]

1.8.2 Reversible Addition-Fragmentation Chain Transfer Polymerization

One of the most well-studied RDRP techniques is RAFT, reversible addition-fragmentation chain transfer polymerization, which was first reported in 1998 by Chiefari *et al.* at CSIRO,[135] which represented a step-change in the field of CLRP. The mechanism in this system (**Scheme 1-4**) is based on the equilibrium between active and dormant chains, achieved by degenerative transfer.[157] Initially, generation of an initiator-derived primary radical is obtained through thermal dissociation of a conventional radical initiator (*e.g.* AIBN), which subsequently initiate a polymer chain, $P_n^{\bullet}$. These can add to the CTA, also known as RAFT agent (thiocarbonylthio compounds, RSC(Z)=S, are the most commonly used),[160-162] to give a radical intermediate. Fragmentation can then occur to form a thiocarbonylthio compound and a new radical, $R_n^{\bullet}$. In the next step, the new radical reacts with a monomer unit leading to the formation of a propagating radical, $P_m^{\bullet}$. The reversible transfer of the thiocarbonylthio group or any other functional chain-end group between the dormant

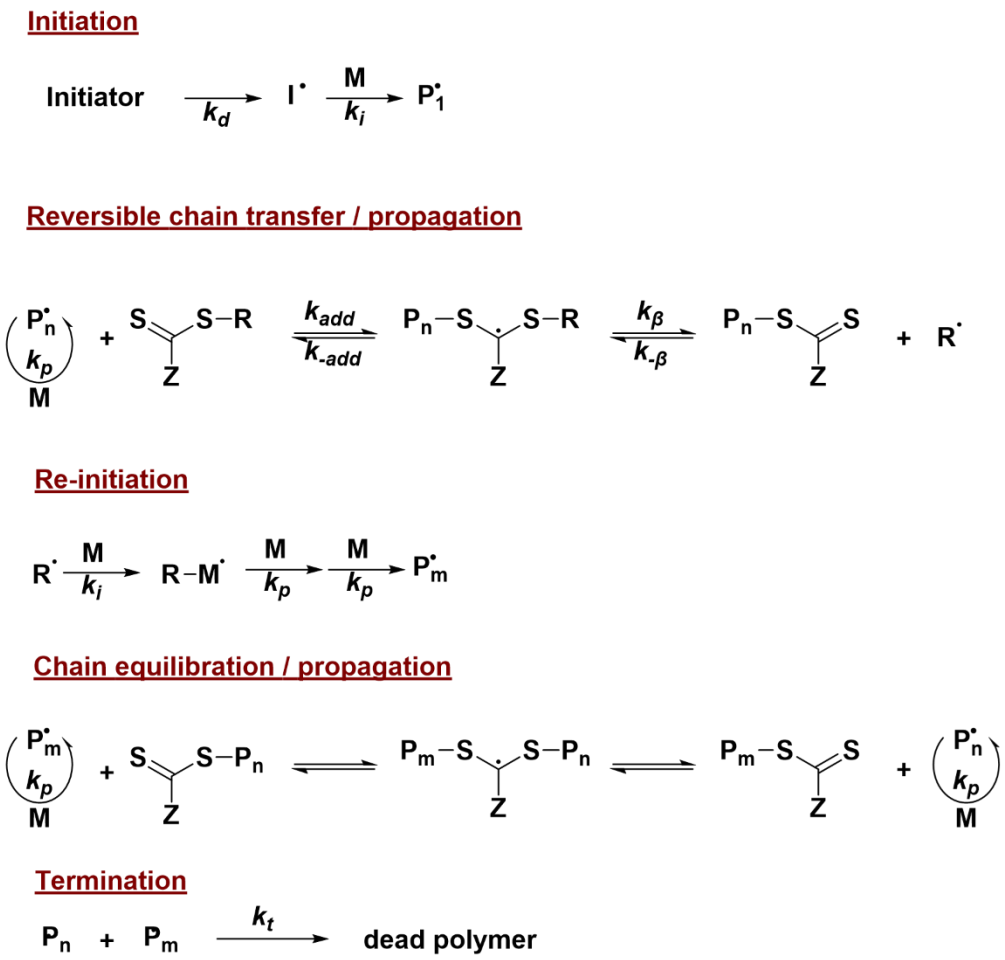

Scheme 1-4. Proposed mechanism of RAFT.

chains and the propagating radicals is the key characteristic of the RAFT process.

In a successful RAFT process, the rate of addition/fragmentation is higher than the rate of propagation leading to similar degree of polymerization for all the chains. One of the most distinct differences between RAFT and other RDRPs (*e.g.* ATRP or NMP) is that a bimolecular termination event does not lead to loss of the chain end, with the number of end-functionalized chains remaining the same even upon, conventional for other RDRPs, termination events.[136]

The usefulness of the RAFT process lies in the fact that it can be applied to most monomers which are able to undergo conventional FRP, such as (meth)acrylates, (meth)acrylamides, styrenics,[163] vinyl esters[164, 165] and vinyl amides[166, 167]. Poly(vinyl acetate) and poly(*N*-vinyl pyrrolidone) (NVP) in particular have proven a challenge to synthesize using other CRP methods,[168, 169] however RAFT is probably the most

efficient method for the synthesis of "difficult" monomers, including both activated (*i.e.* (meth)acrylic) and less activated (*i.e.* vinyl acetate, N-vinyl pyrrolidone) ones.[170] A characteristic example is polyethylene which, although until recently was rather challenging to obtain through RAFT. D'Agosto and Monteil investigated the RAFT polymerization of ethylene with the use of xanthates as controlling agents.[171] One of the drawbacks of RAFT is that typically the CTA used in this process has to be tailored to the desired monomer (often by altering the Z group) which requires extra synthetic steps. In addition, since most of the polymer chains will be capped with the conventionally sulfur-containing CTA, this often imparts a yellow or pink colour which may be undesirable depending on the intended use. However, the latter can be addressed with the use of sulfur-free RAFT,[172] where macromonomers obtained *via* CCTP can be used as chain transfer agents. Although their chain transfer constant is lower than the conventional sulfur-containing CTAs, it can be increased under specific conditions, for instance by monomer feeding.[173, 174]

1.8.3 Atom Transfer Radical Polymerization

In ATRP, a redox-active metal halide/ligand complex (Mt_m X/L, with Mt being the metal at *m* oxidation state and L being the ligand) activates (k_{act}) an alkyl halide (P_n-X) *via* reversible homolytic bond cleavage, resulting in Mt^{m+1} X_2/L and a $P_n^{\bullet}$ radical, which leads to chain growth (**Scheme 1-5**). The deactivator, namely the transition metal complex in the higher oxidation state, reversibly reacts (k_{deact}) with the propagating radical ($P_n^{\bullet}$) to regenerate the dormant species and the activator. This equilibrium heavily favors the side of the dormant chains, thus the radical concentration is kept low, limiting the termination reactions and providing control over the polymerization.[175-178] Furthermore, the retention of the terminal halide groups on the polymer allows for continuous reinitiaton, thus making this a pseudo- living system. In general, ATRP is restricted to monomers which contain an electron withdrawing substituent, adjacent to the vinyl group, which is able to stabilize the resulting radical, including (meth)acrylates, styrenics and (meth)acrylamides.

In all RDRP methods eventually occur termination events to some extent. However, at the initial stages of the polymerization there is a small presence of termination, which results in slight excess of deactivating species, shifting the equilibrium towards the dormant species. This will decrease the rate of polymerization

and will suppress the rate of termination; ultimately will lead to better control over the molecular weight distributions. This self-regulating ability of the technique is known as persistent radical effect (PRE)[155, 179, 180] and firstly introduced by Otsu and coworkers.[181] There are many factors that synergistically contribute to a controlled ATRP process by shifting the equilibrium, including among others the structure of the ligand and therefore the nature and stability of the catalyst,[182-187] the initiator[188-191] and the reaction medium.[192, 193]

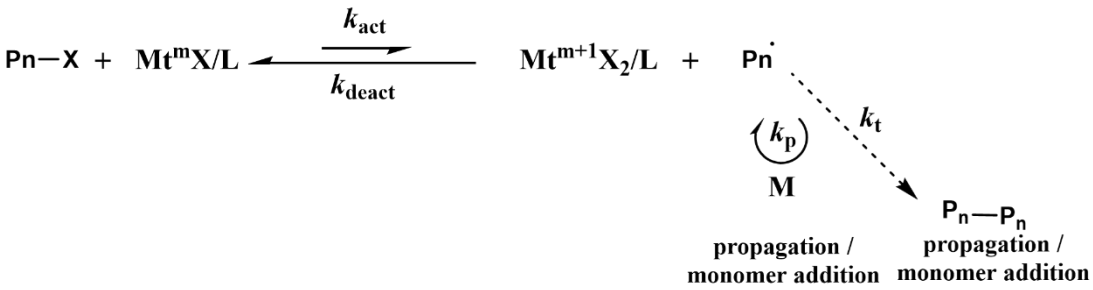

Scheme 1-5. Simplified ATRP activation/deactivation equilibrium.[129]

For the RDRPs which are catalyzed by copper (Cu), there are two mechanistic pathways described in the literature; outer-sphere electron transfer (OSET) and inner-sphere electron transfer process (ISET).[194, 195] The traditional ATRP is considered to follow the ISET process where a transition metal complex in the lower oxidation state (most often Cu(I)/L), activates an alkyl halide, through an energetically favored ISET process, to generate a radical and the transition metal complex in a higher oxidation state (*i.e.* Cu(II)/L). Subsequently, the generated radical can propagate with monomer before reacting with the higher oxidation state complex to return to the alkyl halide.[196]

Alternative approaches to conventional ATRP have been introduced mainly by Matyjaszewski and colleagues, including Activator Regenerated by Electron Transfer (ARGET-ATRP)[197] and Initiators for Continuous Activator Regeneration (ICAR-ATRP),[198] in order to minimize the transition metal loadings. ARGET-ATRP has been considered a "greener" approach to conventional ATRP with the utilization of ppm of the catalyst and in the presence of a suitable reducing agent[199] (*i.e.* tin(II) 2-ethylhexanoate ($Sn(EH)_2$),[200] glucose,[201, 202] ascorbic acid,[203]). In the ARGET process, the reducing agent is employed to (re)generate the active catalyst from the, accumulated *via* termination events, deactivating species.[200] In the ICAR-ATRP, low loadings of the metal catalyst are as previously used and thus, in order to avoid the

activator's consumption through termination events, a free-radical source (e.g. AIBN) is employed to regenerate the activator.[197]

1.8.4 Single Electron Transfer-Living Radical Polymerization

The concept of SET-LRP (or Cu(0)-mediated RDRP) was initially introduced by Percec and co-workers in 2002[204] and attracted more attention in 2006, when the "*ultrafast synthesis of ultrahigh molecular weight polymers*" at ambient temperature or below from functional monomers containing electron withdrawing groups such as acrylates and methacrylates was reported.[205] Polar solvents, such as H_2O, dimethyl sulfoxide (DMSO), alcohols and ionic liquids were reported to encourage the rapid disproportionation of CuBr into Cu(0) and $CuBr_2$ species in the presence of ligands that promote disproportionation (*e.g.* tris[2-(dimethylamino) ethyl]amine (Me_6-Tren), *N*,*N*,*N'*,*N''*,*N''*-pentamethyldiethylenetriamine (PMDETA) *etc.*). The initial activation step was proposed to occur *via* Cu(0), either in the form of copper wire or copper powder, *via* single electron transfer (SET) to the electron acceptor alkyl halide. Without any purification step the synthesis of high molecular weight polymers (M_n ~ 1,400,000 g.mol^{-1}) was demonstrated in less than 3 h.

According to the proposed mechanism Cu(0) (or "nascent" Cu(0) particles) is the major activator of alkyl halides[138, 206, 207] and CuBr is "inactive" under "SET-LRP conditions" (polar solvents and *N*-containing ligands) due to rapid or even instantaneous disproportionation into Cu(0) and $CuBr_2$.[208, 209] The activation step is proposed to occur *via* an outer sphere electron transfer process (OSET) through the formation and decomposition of a radical anion intermediate (**Scheme 1-6**).

Cu(0), either in the form of powder or wire, is a very efficient method for polymer synthesis when organic solvents are employed. For applications where water is the required solvent, the polymerization of acrylates has proved to be compatible with the copper wire system, resulting in full conversion within 6 h and low dispersities.[210] An excess of external $CuBr_2$ is required to provide good control over the MWDs in most cases.

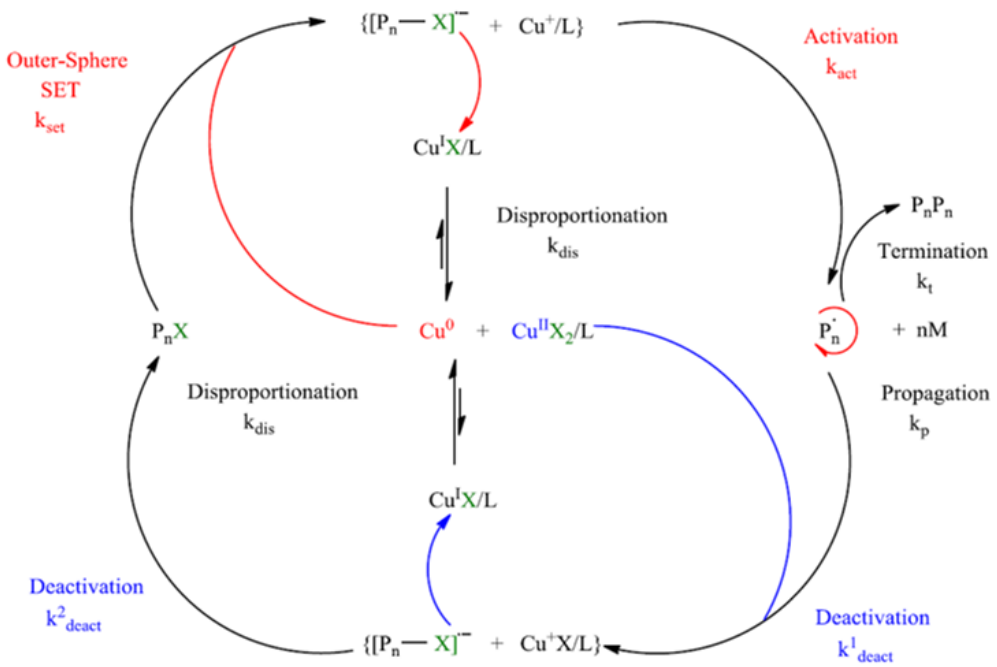

Scheme 1-6. Proposed mechanism for the SET-LRP.[206]

Conversely, transition metal-mediated polymerization of acrylamide monomers proved to be problematic, either due to lack of control or the necessity to use high ratio of Cu(II) salts to achieve efficient deactivation and therefore good control.[211, 212] However, in 2013, Haddleton and colleagues demonstrated a novel method for conducting Cu(0)-mediated RDRP in water, by exploiting full disproportionation of Cu(I) in water in the presence of the aliphatic tertiary amine Me_6Tren.[213] Specifically, the key-step for a controlled Cu(0)-RDRP in water was to allow for full disproportionation of Cu(I) prior to addition of monomer and initiator. Thus, upon completion of the pre-disproportionation reaction where nascent Cu(0) and Cu(II) are generated, the addition of monomer and initiator followed, and within 15 minutes well-defined polyacrylamides, as well as hydrophilic polyacrylates were synthesized.

The advantageous nature of this platform lies on the mild reaction conditions, which include low or ambient temperature and the fast polymerization rates. Apart from the polymerization of acrylamides in water, other more complex aqueous media, such as blood serum,[214] alcoholic beverages[215] and ionic liquids,[216] were employed for the Cu(0)-RDRP of NiPAm, resulting in successful disproportionation of Cu(I) (and thus, *in-situ* generation of highly active Cu(0)). Finally, even in complex media, control over the macromolecular characteristics of the obtained polymers was

achieved, with low dispersities, high chain-end fidelity and high monomer conversions. It should be noted that although the Cu(0)-RDRP platform is considered as a robust and versatile system, exhibits some limitations which lie on the fact that less activated monomers such as vinyl pyrrolidone (VP) and vinyl acetate (VA) are incompatible with the technique, while further development is required for the polymerization of styrene, methacrylates and methacrylamides.[205]

1.8.5 Cu(0)-Mediated RDRP: Mechanistic controversies

The use of Cu(0) has provided many advantages in the implementation of Cu-RDRP including milder conditions, shorter reaction times and the simple removal of Cu-species when Cu(0)-wire is used.[130] However, some controversies have been arisen regarding the mechanistic profile of Cu-RDRP. The main debate is between two models that the same polymerization reagents are used; the supplemental activator and reducing agent (SARA)-ATRP and SET-LRP.[195] The first model, SARA-ATRP, follows the same rationale as conventional ATRP, where the main species responsible

Scheme 1-7. (top) The mechanism of SARA ATRP, (bottom) the mechanism of SET-LRP. Bold arrows indicate major reactions, whereas solid arrows indicate supplemental or contributing reactions and dashed arrows indicate minor reactions that can be neglected from the mechanism. Cu^0 , Cu^I X/L and $Cu^{II}X_2$/L represent a Cu^0 , Cu^I and Cu^{II} species without particular speciation.[195]

for deactivation being Cu(II) and for activation Cu(I), while Cu(0) acts as supplemental activator of alkyl halides and as a reducing agent for Cu(II). Moreover, the kinetic contribution of disproportionation is negligible, whilst comproportionation has a predominant role. Conversely, in the SET-LRP approach, the disproportionation of Cu(I) towards Cu(0) and Cu(II) has a predominant role with Cu(0) being the main active species, **Scheme 1-7**.[201]

1.8.6 Photoinduced Cu-Mediated RDRP

The development of RDRP techniques has proved to be one of the key strategies for the synthesis of polymers with diverse properties, well-defined macromolecular characteristics and a wide range of functionality.[148, 217-221] One of the most challenging tasks in the field has been the "on demand" regulation of RDRP techniques, namely the achievement of spatiotemporal control over the polymerization. Based on this, researchers developed the utilization of external stimuli including light, electrochemical approaches with applied voltage or mechanical processes in order to render the equilibrium between active and dormant species tunable.[222, 223]

The use of light combines several advantages since it is widely available, non-invasive and environmentally benign, thus is considered to be one of the most prominent among the external stimuli available.[222] Apart from the ability to switch "on" and "off" the polymerization, light allows further and more precise control over the reaction rate by modifying the intensity of irradiation. Oster and Yang were the first to employ light as an external stimulus for the polymerization of vinyl monomers in 1968.[224] Subsequently, three main strategies have been developed employing light for the activation of the monomer,[225, 226] initiator (also known as photo-initiators)[227-230] or catalyst.[231-234] Despite the strategy employed, the field of photo-polymerization encompass a wide range of applications (*e.g.* photoresist materials,[235] photolithography,[236] printing plates,[237] dental filling materials,[238] *etc.*) and thus attracts more and more scientific interest.

In particular, the direct activation of the catalyst through light irradiation has been the focus of many investigations that are based on RDRP and Cu-RDRP. Hawker and colleagues, utilizing visible light and a photoactive iridium complex (fac-

[Ir(ppy)$_3$](ppy = 2-pyridylphenyl), reported the synthesis of well-defined PMMA with spatiotemporal control.[231, 239] Their investigation was based on the ability of the Ir-based catalyst to absorb light and form excited Ir^{III*} species that can reduce the alkyl bromide initiator, leading to the generation of initiating radicals. The Ir^{IV} produced can subsequently oxidize the active radical chain-end leading to the formation of dormant species, and this process, upon addition of a photon can be repeated. The same Ir-catalyst was employed by Boyer and colleagues who pioneered on the development of photoinduced electron transfer (PET)-RAFT.[240-242] Apart from Ir-based catalysts, different metal-based catalysts have also been developed; Cu,[182, 243, 244] cobalt (Co),[245-247] zinc (Zn),[248-250] ruthenium (Ru),[240, 251] iron (Fe)[252, 253] and iodine (I),[254] and even metal-free systems have been reported to provide control over the produced polymers.[255, 256]

Copper, particularly in the form of Cu(II), donor ligand complexes, has been known to participate in photoredox reactions upon UV-irradiation.[257] The concept of photoinduced Cu-mediated polymerization was first developed by Yagci and colleagues,[258] who reported on the photo(co)polymerization of methacrylates. They used Cu(II) in order to photo-generate Cu(I) *in-situ*, in the presence of *N,N,N′,N″,N″*-pentamethyldiethylenetriamine (PMDETA). The polymerization, although having been conducted in bulk, showed a linear increase of the molecular weight with increasing conversion, and the ability of the system to undergo copolymerization was illustrated by a chain extension. As proposed by Yagci and colleagues, the initial step included the *in-situ* generation of the Cu(I)X/L activator from the Cu(II) species which subsequently reacted with the initiator P_n-X to form an active radical $P_n^{\cdot}$, which in turn could propagate with monomer addition (M), terminate and undergo deactivation through reaction with Cu(II)X_2/L, leading to Cu(I)X/L and a halogen-terminated polymer chain (**Scheme 1-8**).

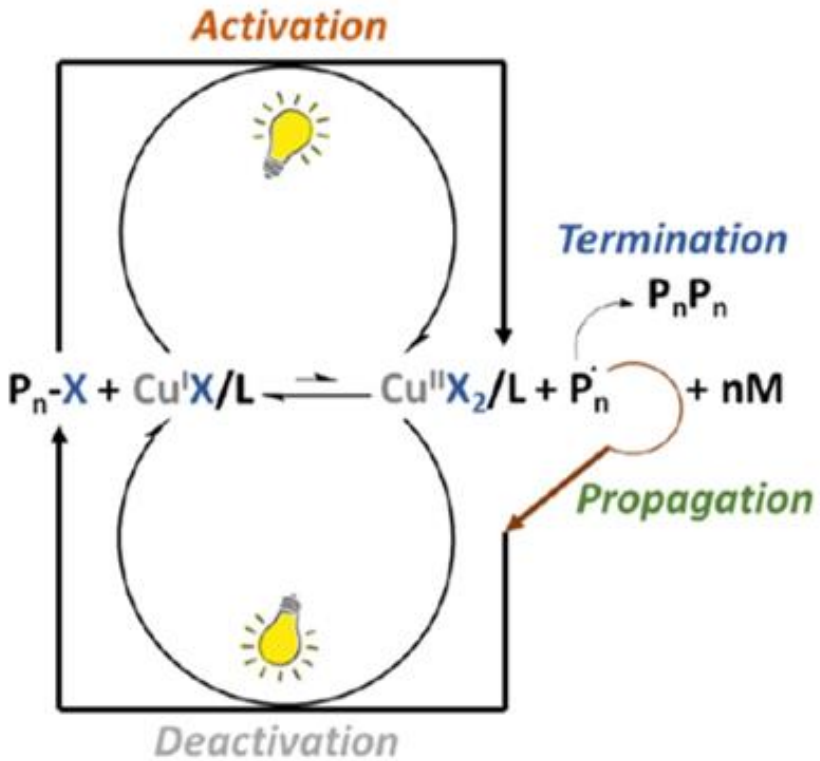

Scheme 1-8. Graphical illustration of the mechanism of photoinduced controlled radical polymerization as reported by Yagci and colleagues.[258]

Konkolewicz, Matyjaszewski and coworkers reported the use of visible light and sunlight for the photoinduced ATRP of (meth)acrylic monomers, where Cu(II)Br_2/TPMA complexes with low ppm of Cu catalyst were used under mild light sources (sunlight, blue and violet LEDs) to generate well-defined polymers and block copolymers.[259] The proposed mechanism of photoinduced ATRP was based on the homolytic cleavage of the Cu(II)X/L complex in the excited state to form the Cu(I)/L activator and a halogen radical responsible for the initiation of the polymerization. The system exhibited "on demand" control by switching the light source "on" and "off".[259]

A further important contribution on the photoinduced Cu-RDRP approach was reported in 2014 by Haddleton and colleagues, where Cu(II)Br_2 and the aliphatic tertiary amine Me_6Tren along with UV irradiation (λ_{max} ~ 365 nm) were used for the photoinduced Cu-RDRP of acrylates.[243] With this approach, the polymerization rates were significantly faster (quantitative conversions were obtained in less than 2 hours) compared to the previous approaches and, notably, temporal control was also demonstrated, as well as controlled molecular weights, low dispersity values and high

end-group fidelity. Further studies by the Haddleton group were reported including the photopolymerization of various acrylates (hydrophilic, hydrophobic and functionalized) in different organic solvents[260] and the synthesis of one-pot multiblock copolymers.[261] Moreover, the addition of sodium halides (NaBr) enhanced the control over the polymerization in water and as a result, water-soluble acrylates were successfully polymerized under UV-irradiation and in the presence of the $Cu(II)Br_2/Me_6Tren$ complex.[262] Notably, high end-group fidelity was maintained allowing for *in-situ* chain extensions in water, while the polymerization exhibited high temporal control, as depicted by the "on-off" experiments.

1.8.6.1 Photoinduced Cu-Mediated RDRP: Mechanistic Aspects

Several approaches have been made to unravel the mechanism of the photoinduced RDRP systems. In their first study, Haddleton and colleagues reported that an excess of the ligand Me_6Tren relative to $Cu(II)Br_2$ is required to maintain excellent control over the polymerization of acrylates.[243] UV–Vis spectroscopy was applied to follow the polymerization and monitor the effect of UV-irradiation on the components of the polymerization over time. Based on their findings, they proposed that the photoexcitation of free Me_6Tren is responsible for the C-Br bond homolysis, which occurs through an outer-sphere single-electron transfer (OSET) when the alkyl halide initiator is present. This C-Br scission is followed by the formation of an initiating radical, a Me_6Tren-based radical cation and its analogous bromide, Br^-, counterion, with the initiating radical mediating the propagation. When monomer is present, propagation occurs while the deactivating species $Cu(II)Br_2/Me_6Tren$ maintains the control over the polymerization (**Scheme 1-9**).

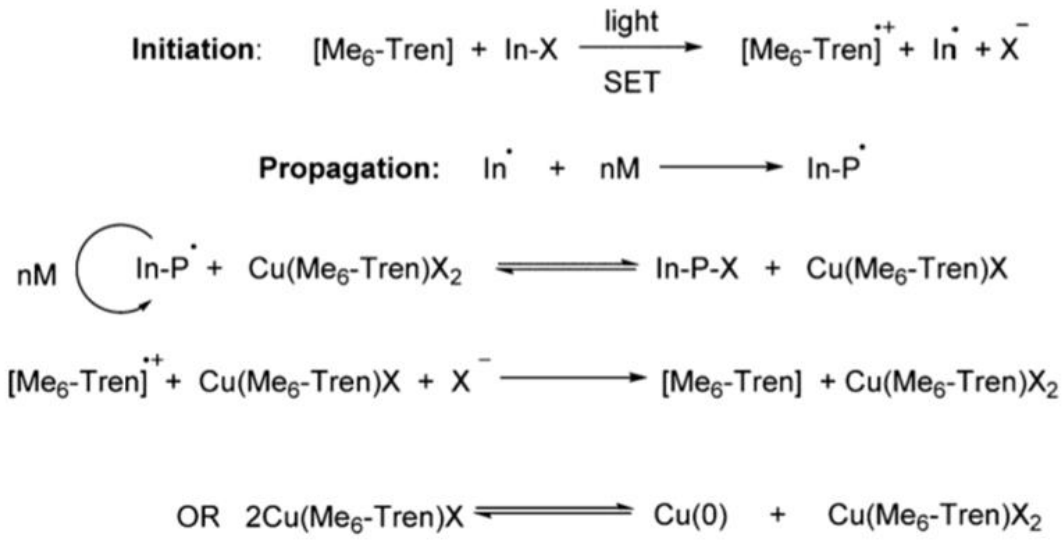

Scheme 1-9. Proposed mechanism for the Cu(II)Br_2/Me_6Tren-mediated photoinduced RDRP.[243]

Another investigation on the initiation mechanism of photoinduced RDRP by Barner-Kowollik, Haddleton and colleagues includes the use of pulsed-laser polymerization (PLP) and high resolution mass spectrometry, highlighting the important role of the ligand (which acts as a reducing agent).[263] Upon UV-irradiation, scission of the initiator's C-Br bond occurs which subsequently provides radicals that can propagate and also react with Cu(II) species **(Scheme 1-10)**. Moreover, an electron transfer reaction takes place between the photoexcited ligand and Cu(II) complexes leading to the generation of Cu(I) species. Finally, they proposed that the Cu(II) complex absorbs a photon to result in an excited state and this is subsequently quenched by free ligand present, generating the analogous Cu(I) complex and the ligand radical cation.

More recently, Liarou, Haddleton and co-workers investigated the effect of UV-irradiation on Cu(II)-based complexes, when different aliphatic amines are used as ligands.[182] Several characterization techniques were applied in order to provide insights into the catalyst behavior upon photo-irradiation. The excited-state dynamics, the electrochemical behavior of the Cu(II)/Cu(I) redox couples and the detection of

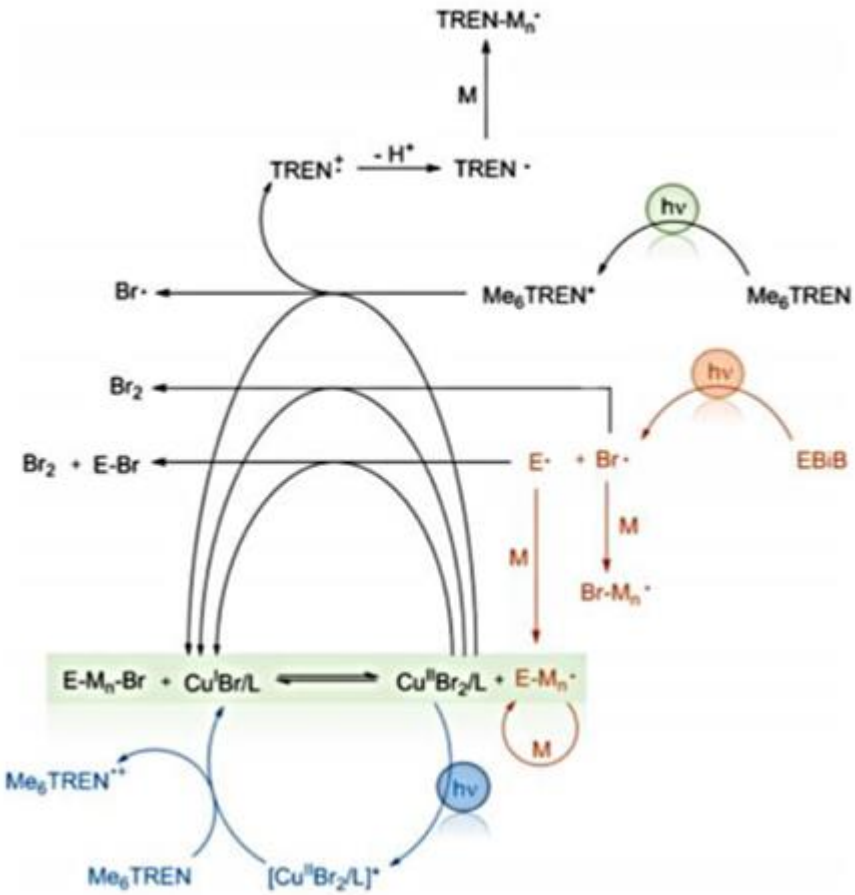

Scheme 1-10. Proposed mechanism of photoinduced RDRP as reported by Kowollik, Haddleton and colleagues.[263]

different species upon complexation of the ligand to the metal center (before and after UV-irradiation) were examined. It was found that, after the use of Me_6Tren, similarly good control over the polymerization was achieved when the tridentate PMDETA was used, while when the linear tetradentate 1,1,4,7,10,10- hexamethyl triethylenetetramine (HMTETA) and the bidentate tetramethyl ethylenediamine (TMEDA) were used, poor control over the molecular weights and dispersity values was seen. These observations for the polymerizations where HMETA- and TMEDA-based complexes were used, were attributed to restricted mobility of those complexes, which leads to inability of the complex to abstract the halogen atom from the alkyl halide initiator.

1.9 O_2-Tolerant Controlled Radical Polymerizations

Although the interest in CRP techniques has increased over the last 25 years due to their versatility (various conditions, different media and scales and functional groups), since the early beginning of their development, stringent anaerobic conditions were required in order to avoid contamination from oxygen, air or moisture. Furthermore, the integrity and precision of materials synthesized through these techniques can be compromised by oxygen moieties during the polymerization, as oxygen can irreversibly react with reaction components (*e.g.* initiator, catalyst, etc.) leading to terminated polymer chains and/or cessation of the polymerization.[264]

1.9.1 Radical Polymerizations and Oxygen

Oxygen can act as inhibitor in radical polymerizations, however aerial oxygen has been used as initiator for the synthesis of low-density polyethylene, and as was demonstrated in 1980s, it could act both as initiator and inhibitor when high temperatures (160-170 ºC) and high pressure was applied. In other cases, oxygen can participate in redox reactions to generate initiating radicals for the polymerization of vinyl monomers in the presence of ascorbic acid and transition metal salts[265] and has been essential for the production of hydrogen peroxides in photosensitized polymerizations.[266]

Several studies have been made in order to investigate the generation of peroxides during the radical polymerization of vinyl monomers in the presence of oxygen. Mayo *et al.* hypothesized that a copolymerization-type reaction takes place between oxygen and monomer, with the latter reacting thousand times faster with oxygen that with itself when the concentration of the two is equal in the reaction.[267, 268] In a further study by Decker and Jenkins, an induction period was observed in homopolymerization of acrylates in the presence of air, since no polymerization takes place until all of the dissolved oxygen gets consumed into peroxide.[269]

Although the effect of oxygen on a radical polymerization, an thus the observed induction period, are dependent on many factors including temperature and pressure, as well as the diffusion coefficient of oxygen in different media,[270] early reports tried to correlate induction period with experimental variables (*i.e.* monomer

(M), initiator (A) and O_2 concentration).[271] As a result of these studies, reaction models were proposed and are illustrated in **Scheme 1-11**, however alterations from the existing RDRP systems are expected, since different and more sophisticated mechanistic pathways have been proposed for the various radical polymerization platforms.

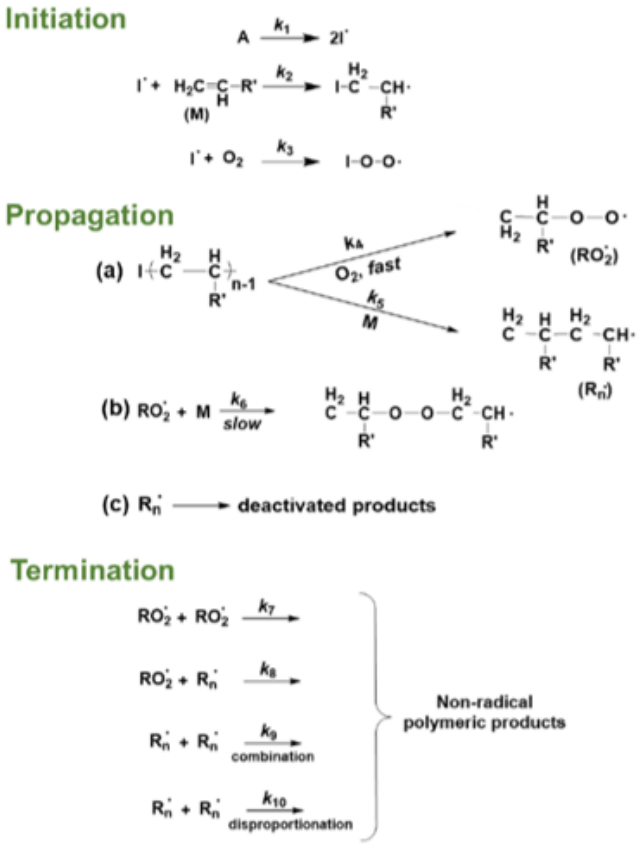

Scheme 1-11. The generation of peroxides during the radical polymerization of vinyl monomers, upon reaction of the generated radical with oxygen.

1.9.2 O_2-Tolerant Cu-RDRP

1.9.2.1 O_2-Tolerance through extrinsic reducing agents

The implementation of (SARA/ARGET) ATRP in the presence of oxygen was first reported by Matyjaszewski in 1998 who demonstrated that the oxygen present in a sealed vessel could be scrubbed *via* oxidation of Cu(I) into Cu(II).[272] This process led to accumulation of the Cu(II) deactivator, necessitating the addition of a reducing agent (Cu(0) powder in this case) in order to regenerate the active Cu(I) species. Although for the sealed reactions an induction period and slower polymerization rate

were observed, the obtained polymers exhibited controlled molecular weight and dispersity at high conversions, as well as high end-group fidelity which allowed for block copolymerizations.[273] Notably, the open-to-air reactions did not result in polymerization.

In a so-called oxygen tolerant Cu-RDRP system, the removal of oxygen is synergistically dependent on all the components including the initiator, the catalyst system which involves the copper species and the ligand, even the monomer and the solvent.[274-277] However, in some Cu-RDRP platforms the need for external reducing agents is necessary for a successful polymerization when no deoxygenation is applied. There have been reports about the ability of oxygen to initiate the polymerization in the presence of a suitable Cu-complex, yielding polymers with low dispersity values but uncontrolled molecular weights.[278] Hence, reducing agents that could regenerate the deactivator leading to control over the molecular weights were employed, with these approaches being known as either Activator Generated by Electron Transfer (AGET-) ATRP, or Activator ReGenerated by Electron Transfer (ARGET) ATRP (when low ppm of the catalyst are used).[200, 202]

1.9.2.2 O_2-Tolerance through enzyme deoxygenation

The concept of enzyme deoxygenation was, as mentioned earlier, initially used in order to avoid O_2-inhibition in free radical polymerization.[279, 280] The successful implementation of GOx inspired researchers to introduce the same concept in RAFT and subsequently in Cu-RDRP, in order to replace conventional deoxygenation and expand the scope of Cu-RDRP towards lower volumes which would facilitate the implementation of these systems on bio-approaches. Matyjaszewski and colleagues, recently (2018) utilized GOx along with sodium pyruvate for the ICAR-ATRP of oligo(ethylene oxide) methylether methacrylate ($OEOMA_{500}$).[281] In this system, GOx catalyzed the oxidation of glucose into d-glucono-1,5-lactone and hydrogen peroxide (H_2O_2), with the latter being removed by the sacrificial substrate sodium pyruvate, in order to avoid the generation of new chains by H_2O_2. Their initial study was subsequently followed by the application of GOx for the deoxygenation of ARGET, ICAR, photo- and electrochemically mediated ATRP (eATRP), in mini-emulsion and emulsion, with low ppm of catalyst.[282] Furthermore, the same group reported on the

synthesis of (DNA- and BSA-) bioconjugates through ICAR-ATRP, in which continuous air supply was applied.[283] In this case, GOx was used for the conversion of β-D-glucose and oxygen into gluconate and H_2O_2, with the latter being used along with acetylacetonate as substrate for horseradish peroxidase which, in turn, supplies the system with radicals. The reaction of the generated radicals with the monomer, led to carbon-based radicals which could reduce Cu(II) into Cu(I), providing the active catalyst species for ICAR-ATRP following the described biocatalytic cascade. (**Scheme 1-12**).

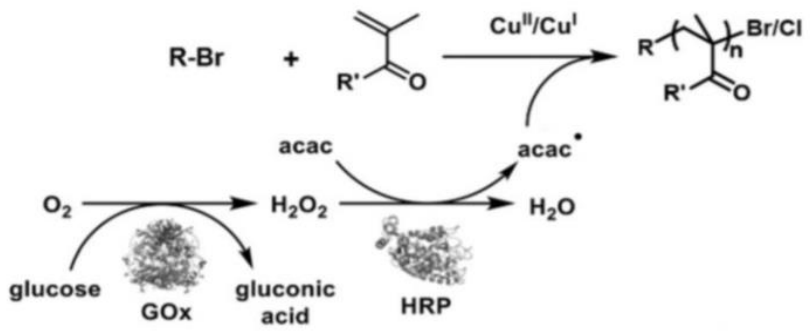

Scheme 1-12. The biocatalytic cascade which starts from the GOx-catalyzed oxidation of glucose and ultimately leads to the generation of polymers in the presence of constant air supply.[283]

1.9.2.3 O_2-Tolerance through headspace elimination

In 2018, Liarou, Haddleton *et al.*, reported on the Cu(0)-RDRP of (meth)acrylates, styrene and acrylamides in organic and aqueous media, without any type of external deoxygenation or addition of extrinsic reducing agents.[276] By eliminating the headspace and up-filling the vessel with the reaction solution, the concentration of gaseous oxygen was significantly reduced, whilst the solution reaction still containing the dissolved oxygen included in the polymerization components. The application of an oxygen probe for the *in-situ* monitoring oxygen concentration in the polymerization solution showed that the all the components synergistically contributed to full oxygen consumption after 4 minutes of the start of the reaction. Furthermore, the O_2-reducing ability of each component was examined individually, leading to the conclusion that the initiator (ethyl α-bromoisobutyrate, EBiB), the Cu(0)-wire and the complex (Cu(II)Br_2/Me_6Tren) could individually lead to oxygen consumption when combined with the monomer (methyl acrylate, MA) and

the solvent (DMSO), but the combination of all was the key-step to fast and full oxygen consumption, **Figure 1-7**. Although polymerization without headspace had very small induction period, the reactions conducted in bigger vessels had longer induction periods, analogous to the extent of headspace. Finally, the no-headspace polymerization exhibited controlled molecular weights and low dispersity values at quantitative conversions, for a range of monomers. Even in vessels with small headspace, the end-group fidelity was high, leading to *in-situ* chain extensions.

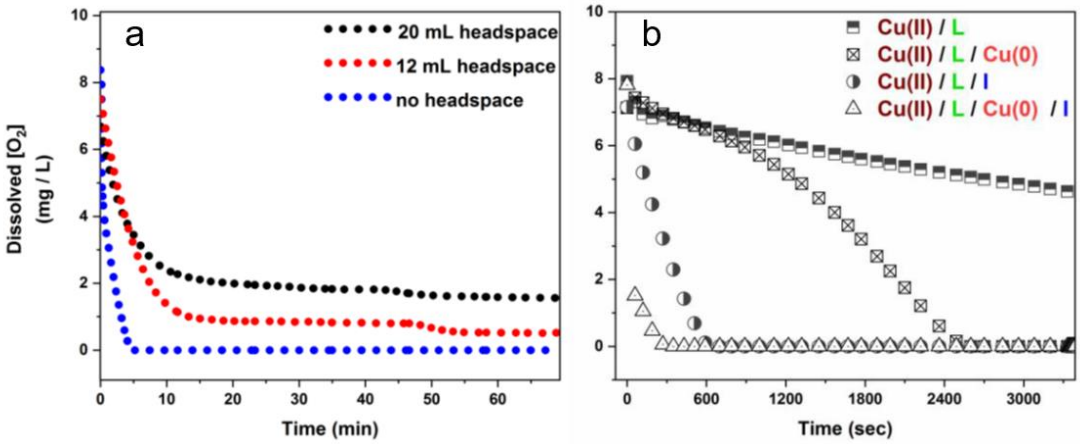

Figure 1-7. Line graphs illustrating a) the effect of the headspace and b) the effects of Cu(0) wire, EBiB (I), and Me6Tren (L) on the evolution of the dissolved oxygen concentration during polymerization.

More recently, the same group reported that instantaneous self-deoxygenation occurs in the SET-LRP of various monomers in aqueous media (**Scheme 1-13**).[284] They reported that disproportionation of Cu(I)/Me_6Tren in water towards Cu(II) and highly reactive Cu(0), led to O_2-free reaction environments within the first seconds of the reaction, even when the reaction took place in the open-air. By leveraging this significantly fast O_2-reducing activity of the disproportionation reaction, well-defined water-soluble polymers with very narrow dispersity were attained in a few minutes or less. Importantly, this methodology provides the ability to prepare block copolymers *via* sequential monomer addition with little evidence for chain termination over the lifetime of the polymerization and allows for the synthesis of star-shaped polymers with the use of multi-functional initiators. By using a range of characterization tools they gave insights into this "*self-deoxygenating*" platform and they were able to identify the species that participate in the oxygen consumption, as well as the species generated upon exposure of the solution to O_2-rich environments.

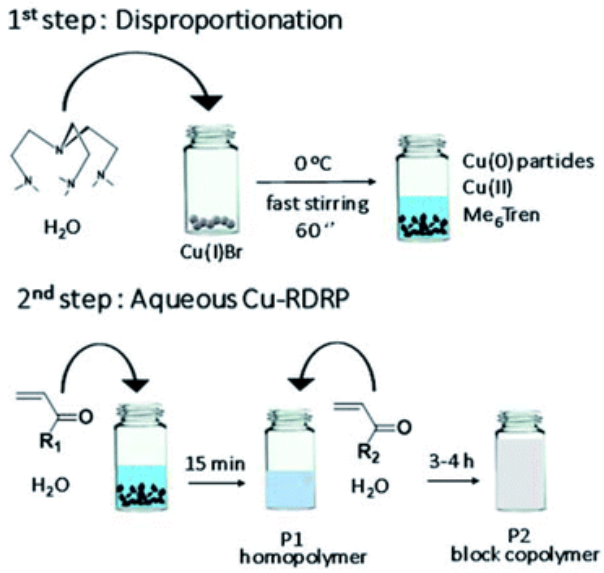

Scheme 1-13. Schematic representation of the *self-deoxygenating* aqueous Cu-RDRP of acrylamides employing the pre-disproportionation of Cu(I)Br/Me_6Tren.

1.9.2.4 O_2-Tolerance in Photoinduced Cu-RDRP

External control over the Cu-RDRP dynamic equilibrium can be achieved through many stimuli including electrochemical and light. Light in particular has proved to be highly advantageous since it offers excellent regulation of the active/dormant species ratio and apart from that, it is a benign and versatile stimulus. The non-deoxygenated photoinduced ATRP was studied by Mosnacek and colleagues. In their studies, irradiation at $\lambda > 350$ nm and Cu(II)Br_2/TPMA as the catalyst complex were employed for the photoinduced ATRP of methyl methacrylate (MMA). It was shown that the photopolymerization exhibited and induction period which was only shortened when 4-fold excess of TPMA with respect to copper was used.[285] In the mechanistic pathway that was proposed, the Cu(II)Br_2/ligand complex undergoes photochemical reduction upon photo-irradiation, leading to the active Cu(I)Br/ligand species. The latter can either undergo oxidation in the presence of oxygen to form Cu(II)Br(O_2), or activate the alkyl halide initiator, leading to the formation of radicals. Furthermore, it was speculated that the free amine ligand could also participate in oxygen consumption. The photoinduced ATRP equilibrium is reached when full oxygen consumption has occurred (**Figure 1-8**). In a subsequent report by the same group, the effect of light intensity, ligand and the oxygen concentration were also investigated, showing that the evolution of a non-deoxygenated photoinduced ATRP

is dependent on many parameters in order to reach good control over the macromolecular characteristics of the synthesized polymers.[286]

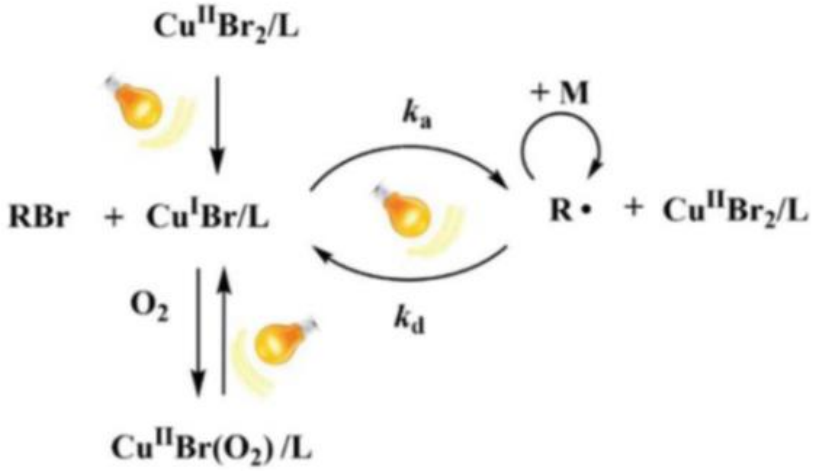

Figure 1-8. Simplified mechanism of photoinduced ATRP in the presence of oxygen, as proposed by Mosnacek and colleagues.[285]

In 2019, Liarou, Haddleton and co-workers demonstrated the photoinduced Cu-RDRP of various hydrophobic, hydrophilic and semi-fluorinated (meth)acrylates in ultralow volumes (as low as 5 μL), without applying any type of extrinsic deoxygenation.[275] The online monitoring of the dissolved O_2 concentration, which was conducted through an oxygen probe, showed that the generation of sufficient amounts of active copper species was the requirement for efficient O_2-consumption, with the synergy of all the components leading to oxygen-free solutions as fast as 4 minutes. This approach was compatible with very low volumes (5-200 μL), as well as higher scales (*i.e.* 0.5 L).

1.10 References

1. Jensen, W. B., The Origin of the Polymer Concept. *J. Chem. Educ.* **2008,** *85* (5), 624.

2. Rasmussen, S. C., Introduction. In *Acetylene and Its Polymers: 150+ Years of History*, Rasmussen, S. C., Ed. Springer International Publishing: Cham, **2018**; pp 1-19.

3. H. Staudinger, Über Polymerisation. *Ber. Dtsch. Chem. Ges. (A B Ser.)* **1920,** (53), 1073–1085.

4. IUPAC Compendium of Chemical Terminology, 2nd Ed. (the "Gold Book") **1997**. https://doi.org/10.1351%2Fgoldbook.M03667.

5. IUPAC Compendium of Chemical Terminology, 2nd Ed., the "Gold Book", **1997**. https://doi.org/10.1351%2Fgoldbook.P04735.

6. Feldman, D., Polymer History. *Des. Monomers Polym.* **2008,** *11* (1), 1-15.

7. Seymour, R. B., Polymers Are Everywhere. *J. Chem. Educ.* **1988,** *65* (4), 327.

8. Seymour, R. B., Pioneers in Polymer Science. **1989**; pp. 81–91.

9. Russel, G. A., *Chemistry, Society, and Environment. A New History of British Chemical Industry*. Royal Society of Chemistry, Cambridge: **2000.**

10. Carothers, W. H. Linear Polyamides and Their Production, US2130523A. **1938**.

11. Ober, C. K., Archer, L., Rodriguez, F., & Cohen, F. , *Principles of Polymer Systems (5th Ed.). CRC Press.* . **2003**.

12. Armand, C. Polytetrafluoroethylene Coated Cooking Utensils, US3008601A. **1961**.

13. Hicks, E. M.; Ultee, A. J.; Drougas, J., Spandex Elastic Fibers. *Science* **1965,** *147* (3656), 373.

14. Lee, Y. S.; Wetzel, E. D.; Wagner, N. J., The Ballistic Impact Characteristics of Kevlar® Woven Fabrics Impregnated with a Colloidal Shear Thickening Fluid. *J. Mater. Sci.* **2003,** *38* (13), 2825-2833.

15. Allen, T. M.; Cullis, P. R., Drug Delivery Systems: Entering the Mainstream. *Science* **2004,** *303* (5665), 1818.

16. Cho, K.; Wang, X.; Nie, S.; Chen, Z.; Shin, D. M., Therapeutic Nanoparticles for Drug Delivery in Cancer. *Clin. Cancer Res.* **2008,** *14* (5), 1310.

17. Farokhzad, O. C.; Langer, R., Nanomedicine: Developing Smarter Therapeutic and Diagnostic Modalities. *Adv. Drug Delivery Rev.* **2006,** *58* (14), 1456-1459.

18. Odian, G., *Principles of Polymerization*. 4th ed.; Wiley:: **2004**

19. P. J. Flory, Principles of Polymer Chemistry, Cornell Univ. Press, Ithaca, New York, **1953**.

20. Stille, J. K., Step-Growth Polymerization. *J. Chem. Educ.* **1981,** *58* (11), 862.

21. Carothers, W. H., Polymers and Polyfunctionality. *J.Chem.Soc., Faraday trans* **1936,** *32* (0), 39-49.

22. Penczek, S.; Moad, G., Glossary of Terms Related to Kinetics, Thermodynamics, and Mechanisms of Polymerization (Iupac Recommendations 2008). *Pure Appl. Chem.* **2008,** *80* (10), 2163-2193.

23. M. F. Cunningham, R. H., In Handbook of Radical Polymerization. John Wiley & Sons, Inc.: **2003**; pp 333-359.

24. K. Matyjaszewski and T. P. Davis, E., Handbook of Radical Polymerization. John Wiley & Sons, Inc: Hoboken, NJ, USA, , **2002**.

25. Flory, P. J., The Mechanism of Vinyl Polymerizations1. *J. Am. Chem. Soc.* **1937,** *59* (2), 241-253.

26. Nicholson, J. W., *In the Chemistry of Polymers*. Royal Society of Chemistry, Cambridge: **2006**.

27. J. Chiefari, E. R., *Handbook of Radical Polymerization*. **2002**.

28. Heuts, J. P. A.; Smeets, N. M. B., Catalytic Chain Transfer and Its Derived Macromonomers. *Polym. Chem.* **2011,** *2* (11), 2407-2423.

29. Davis, T. P.; Kukulj, D.; Haddleton, D. M.; Maloney, D. R., Cobalt-Mediated Free-Radical Polymerization of Acrylic Monomers. *Trends Polym. Sci.* **1995,** *3* (11), 365-373.

30. Heuts, J. P. A.; Roberts, G. E.; Biasutti, J. D., Catalytic Chain Transfer Polymerization: An Overview. *Aust. J. Chem.* **2002,** *55* (7), 381-398.

31. Slavin, S.; McEwan, K.; Haddleton, D. M., 3.09 - Cobalt-Catalyzed Chain Transfer Polymerization: A Review. In *Polymer Science: A Comprehensive Reference*, Matyjaszewski, K.; Möller, M., Eds. Elsevier: Amsterdam, **2012**; pp 249-275.

32. Gridnev, A. A.; Ittel, S. D., Catalytic Chain Transfer in Free-Radical Polymerizations. *Chem. Rev.* **2001,** *101* (12), 3611-3660.

33. Haddleton, D. M.; Maloney, D. R.; Suddaby, K. G.; Muir, A. V. G.; Richards, S. N., Catalytic Chain Transfer Polymerisation (CCTP) of Methyl Methacrylate: Effect of Catalyst Structure and Reaction Conditions on Chain Transfer Coefficient. *Macromol. Symp.* **1996,** *111* (1), 37-46.

34. Moad, C. L.; Moad, G.; Rizzardo, E.; Thang, S. H., Chain Transfer Activity of ω-Unsaturated Methyl Methacrylate Oligomers. *Macromolecules* **1996,** *29* (24), 7717-7726.

35. Mayo, F. R., Chain Transfer in the Polymerization of Styrene: The Reaction of Solvents with Free Radicals1. *J. Am. Chem. Soc.* **1943,** *65* (12), 2324-2329.

36. Davis, P. T.; Zammit, D. M.;J. P.A. Heuts,; Moody, K., A Novel Route to the Preparation of Aldehyde End-Functionalised Oligomers Via Catalytic Chain Transfer Polymerisation. *Chem. Commun.* **1998,** (21), 2383-2384.

37. Warson, H., Emulsion Polymerization, a Mechanistic Approach. R. G. Gilbert. Academic Press, London, 1995. pp. XVIII + 362, Price £55.00. ISBN 0-12-283060-1. *Polym. Int.* **1996,** *41* (3), 352-352.

38. Lovell, P. A.; El-Aasser, M. S., *Emulsion Polymerization and Emulsion Polymers*. J. Wiley: New York, **1997**.

39. Dong, Y.; Argaiz, M.; He, B.; Tomovska, R.; Sun, T.; Martín-Fabiani, I., Zinc Oxide Superstructures in Colloidal Polymer Nanocomposite Films: Enhanced Antibacterial Activity through Slow Drying. *ACS Appl. Polym. Mater.* **2020,** *2* (2), 626-635.

40. Fulmer, P. A.; Wynne, J. H., Development of Broad-Spectrum Antimicrobial Latex Paint Surfaces Employing Active Amphiphilic Compounds. *ACS Appl. Mater. Interfaces* **2011,** *3* (8), 2878-2884.

41. Mulqueen, P., Recent Advances in Agrochemical Formulation. *Adv. Colloid Interface Sci.* **2003,** *106* (1), 83-107.

42. Wang, T.; Canetta, E.; Weerakkody, T. G.; Keddie, J. L.; Rivas, U., pH Dependence of the Properties of Waterborne Pressure-Sensitive Adhesives Containing Acrylic Acid. *ACS Appl. Mater. Interfaces* **2009,** *1* (3), 631-639.

43. Chern, C. S., Emulsion Polymerization Mechanisms and Kinetics. *Prog. Polym. Sci.* **2006,** *31* (5), 443-486.

44. Thickett, S. C.; Gilbert, R. G., Emulsion Polymerization: State of the Art in Kinetics and Mechanisms. *Polymer* **2007,** *48* (24), 6965-6991.

45. Asua, J. M., Emulsion Polymerization: From Fundamental Mechanisms to Process Developments. *J. Macromol. Sci. Part A: Polym. Chem.* **2004,** *42* (5), 1025-1041.

46. Dhoot, S. N.; Freeman, B. D.; Stewart, M. E., Barrier Polymers. In *Encyclopedia of Polymer Science and Technology*, **2002**.

47. Hansen, F. K.; Ugelstad, J., Particle Nucleation in Emulsion Polymerization. I. A Theory for Homogeneous Nucleation. *J. Macromol. Sci.: Polym. Chem. Ed.* **1978,** *16* (8), 1953-1979.

48. Chern, C.-S.; Chang, H.-T., Particle Nucleation and Growth Mechanisms in Miniemulsion Polymerization of Styrene. *Polym. Int.* **2002,** *51* (12), 1428-1438.

49. Young, R. J.; Lovell, P. A., *Introduction to Polymers*. CRC Press: Boca Ratón, FL, **2011**.

50. De Bruyn, H.; Miller, C. M.; Bassett, D. R.; Gilbert, R. G., Emulsion Polymerization of Vinyl Neo-Decanoate, a "Water-Insoluble" Monomer. *Macromolecules* **2002,** *35* (22), 8371-8377.

51. Dong, Y.; Sundberg, D. C., Radical Entry in Emulsion Polymerization: Estimation of the Critical Length of Entry Radicals Via a Simple Lattice Model. *Macromolecules* **2002,** *35* (21), 8185-8190.

52. Fitch, R. M.; Prenosil, M. B.; Sprick, K. J., The Mechanism of Particle Formation in Polymer Hydrosols. I. Kinetics of Aqueous Polymerization of Methyl Methacrylate. *J. Macromol. Sci. Part C: Polym. Symp.* **1969,** *27* (1), 95-118.

53. Feeney, P. J.; Napper, D. H.; Gilbert, R. G., Coagulative Nucleation and Particle Size Distributions in Emulsion Polymerization. *Macromolecules* **1984,** *17* (12), 2520-2529.

54. Hansen, F. K.; Ugelstad, J., Particle Nucleation in Emulsion Polymerization. II. Nucleation in Emulsifier-Free Systems Investigated by Seed Polymerization. *J. Macromol. Sci.: Polym. Chem. Ed.* **1979,** *17* (10), 3033-3045.

55. Fitch, R. M.; Tsai, C. H. In *Particle Formation in Polymer Colloids, III: Prediction of the Number of Particles by a Homogeneous Nucleation Theory*, Polymer Colloids, Boston, MA, 1971//; Fitch, R. M., Ed. Springer US: Boston, MA, **1971**; pp 73-102.

56. Abdollahi, M., Effect of Carboxylic Acid Monomer Type on Particle Nucleation and Growth in Emulsifier-Free Emulsion Copolymerization of Styrene-Carboxylic Acid Monomer. *Polym. J.* **2007,** *39* (8), 802-812.

57. Feldman, D., Emulsion Polymers and Emulsion Polymerization, D. R. Bassett and and A. E. Hamielec, Eds., American Chemical Society, Washington, Dc, 1981, 605 pp. No Price Given. *J. Macromol. Sci.: Polym. Lett. Ed.* **1982,** *20* (5), 279-279.

58. Ouchi, M.; Terashima, T.; Sawamoto, M., Transition Metal-Catalyzed Living Radical Polymerization: Toward Perfection in Catalysis and Precision Polymer Synthesis. *Chem. Rev.* **2009,** *109* (11), 4963-5050.

59. Guo, L.; Liu, W.; Chen, C., Late Transition Metal Catalyzed A-Olefin Polymerization and Copolymerization with Polar Monomers. *Materials Chemistry Frontiers* **2017,** *1* (12), 2487-2494.

60. Natta, G.; Pino, P.; Corradini, P.; Danusso, F.; Mantica, E.; Mazzanti, G.; Moraglio, G., Crystalline High Polymers of α-Olefins. *J. Am. Chem. Soc.* **1955,** *77* (6), 1708-1710.

61. K. Ziegler, E. Holzkamp, H. Breil and H. Martin, Polymerisation Von Äthylen Und Anderen Olefinen. *Angew. Chem.* **1955,** *67* (16).

62. Schrock, R. R.; DePue, R. T.; Feldman, J.; Schaverien, C. J.; Dewan, J. C.; Liu, A. H., Preparation and Reactivity of Several Alkylidene Complexes of the Type W(CHR')(N-2,6-C6H3-Iso-Pr2)(or)2 and Related Tungstacyclobutane Complexes. Controlling Metathesis Activity through the Choice of Alkoxide Ligand. *J. Am. Chem. Soc.* **1988,** *110* (5), 1423-1435.

63. Kato, M.; Kamigaito, M.; Sawamoto, M.; Higashimura, T., Polymerization of Methyl Methacrylate with the Carbon Tetrachloride/Dichlorotris-(Triphenylphosphine)Ruthenium(II)/Methylaluminum Bis(2,6-Di-Tert-Butylphenoxide) Initiating System: Possibility of Living Radical Polymerization. *Macromolecules* **1995,** *28* (5), 1721-1723.

64. Wang, J.-S.; Matyjaszewski, K., Controlled/"Living" Radical Polymerization. Atom Transfer Radical Polymerization in the Presence of Transition-Metal Complexes. *J. Am. Chem. Soc.* **1995,** *117* (20), 5614-5615.

65. Ouchi, M.; Terashima, T.; Sawamoto, M., Precision Control of Radical Polymerization Via Transition Metal Catalysis: From Dormant Species to Designed Catalysts for Precision Functional Polymers. *Accounts of Chemical Research* **2008,** *41* (9), 1120-1132.

66. Kamigaito, M.; Onishi, I.; Kimura, S.; Kotani, Y.; Sawamoto, M., A Highly Active Fe(I) Catalyst for Radical Polymerisation and Taming the Polymerisation with Iodine. *Chem. Commun.* **2002,** (22), 2694-2695.

67. Wakioka, M.; Baek, K.-Y.; Ando, T.; Kamigaito, M.; Sawamoto, M., Possibility of Living Radical Polymerization of Vinyl Acetate Catalyzed by Iron(I) Complex. *Macromolecules* **2002,** *35* (2), 330-333.

68. di Lena, F.; Matyjaszewski, K., Transition Metal Catalysts for Controlled Radical Polymerization. *Prog. Polym. Sci.* **2010,** *35* (8), 959-1021.

69. Tang, W.; Matyjaszewski, K., Effect of Ligand Structure on Activation Rate Constants in ATRP. *Macromolecules* **2006,** *39* (15), 4953-4959.

70. Gridnev, A., The 25th Anniversary of Catalytic Chain Transfer. *J. Macromol. Sci. Part A: Polym. Chem.* **2000,** *38* (10), 1753-1766.

71. Enikolopyan, N. S.; Smirnov, B. R.; Ponomarev, G. V.; Belgovskii, I. M., Catalyzed Chain Transfer to Monomer in Free Radical Polymerization. *J. Macromol. Sci.: Polym. Chem. Ed.* **1981,** *19* (4), 879-889.

72. Smirnov, B.R., Morozova, I. S., Marchenko, A. P., Markevich, M. A., Pushchaeva, L. M and Enikolopyan, N. S. *Dokl. Akad. Nauk SSSR* **1980,** (253), 891.

73. Smirnov, B. R.; Plotnikov, V. D.; Ozerkovskii, B. V.; Roshchupkin, V. P.; Yenikolopyan, N. S., Catalysis of Chain Transfer and Oligometer Structure in Radical Polymerization of Styrene in the Presence of Cobalt Complexes of Porphyrins. *Polym. Sci. U.S.S.R.* **1981,** *23* (11), 2807-2816.

74. Anastasaki, A.; Waldron, C.; Nikolaou, V.; Wilson, P.; McHale, R.; Smith, T.; Haddleton, D. M., Polymerization of Long Chain [Meth]Acrylates by Cu(0)-Mediated and Catalytic Chain Transfer Polymerisation (CCTP): High Fidelity End Group Incorporation and Modification. *Polym. Chem.* **2013,** *4* (15), 4113-4119.

75. Maloney, D. R.; Hunt, K. H.; Lloyd, P. M.; Muir, A. V. G.; Richards, S. N.; Derrick, P. J.; Haddleton, D. M., Polymethylmethacrylate End-Group Analysis by Matrix-Assisted Laser Desorption Ionisation Time-of-Flight Mass Spectrometry (MALDI-ToF-MS). *J. Chem. Soc., Chem. Commun.* **1995,** (5), 561-562.

76. Darmon, M. J., Berge, C. T., Antonelli, J. A. US Pat., 5362826 **1993**.

77. Gridnev, A. A., Belgovskii, P. M., Enikolopyan, N. S. *Vysokomol. Soedin., Ser. B* **1986** (28), 85.

78. Gridnev, A. A., Features of the Radical Polymerization of Styrene and Methacrylates in the Presence of Cobalt-Oximes. *Polym. Sci. U.S.S.R.* **1989,** *31* (10), 2369-2376.

79. Nokel, A. Y., Gridnev, A. A., Mironov, A. F., *Izvestia Vissh. Uchebn.Zaved., Khim. Khim. Teknol.* **1990,** (33), 57.

80. Gridnev, A. A., Radical Polymerization of Methyl Methacrylate in the Presence of Cobaloximes and Benzoyl Peroxide. *Polym. J.* **1992,** *24* (7), 613-623.

81. A. H. Janowicz, L. R. Melby. US Pat., 4680352. **1987**.

82. Janowicz, A. H. US Pat., 4694054. **1987**.

83. Burczyk, A. F.; O'Driscoll, K. F.; Rempel, G. L., Cobaloxime as a Catalytic Chain Transfer Agent. *J. Macromol. Sci.: Polym. Chem. Ed.* **1984,** *22* (11), 3255-3262.

84. Sanayei, R. A.; O'Driscoll, K. F., Catalytic Chain-Transfer in Polymerization of Methyl Methacrylate. I. Chain-Length Dependence of Chain-Transfer Coefficient. *J. Macromol. Sci.: Part A - Chem.* **1989,** *26* (8), 1137-1149.

85. G. M. Carlson and Abbey, K. J. Us Pat., 4526945. **1985**.

86. J. C. Lin and Abbey, K. J. Us Pat., 4680354. 1987.

87. Abbey, K. J.; Trumbo, D. L.; Carlson, G. M.; Masola, M. J.; Zander, R. A., Synthesis and Copolymerization Behavior of Methacrylate Dimers. *J. Macromol. Sci. Part A: Polym. Chem.* **1993,** *31* (13), 3417-3424.

88. Haddleton, D. M., Muir, A. V. G. and Leeming, S. W. WO Pat., 95/ 17435. **1995**.

89. Muir, A. V. G., Lawson, J. R. and Haddleton, D. M. WO Pat., 95/ 27737. **1995**.

90. Smirnov, B. R.; Marchenko, A. P.; Korolev, G. V.; Bel'govskii, I. M.; Yenikolopyan, N. S., Kinetic Study of Catalysis of the Chain Transfer Reaction to Monomer in the Radical Polymerization of Methyl Methacrylate. *Polym. Sci. U.S.S.R.* **1981,** *23* (5), 1158-1168.

91. Heuts, J. P. A.; Forster, D. J.; Davis, T. P., The Role of Monomer in the Chain Transfer Reaction in Cobaloxime-Mediated Free-Radical Polymerization. *Macromol. Rapid Commun.* **1999,** *20* (6), 299-302.

92. Mironychev, V. Y.; Mogilevich, M. M.; Smirnov, B. R.; Shapiro, Y. Y.; Golikov, I. V., The Effect of the Size of the Alkyl Substituent on the Catalysis of Chain Transfer to Monomer in Radical Polymerization of N-Alkyl Methacrylates. *Polym. Sci. U.S.S.R.* **1986,** *28* (9), 2103-2107.

93. Karmilova, L. V.; Ponomarev, G. V.; Smirnov, B. R.; Bel'govskii, I. M., Metalloporphyrins as Catalysts of Chain Transfer in Radical Polymerisation and Stereoselective Oxidation. *Russ. Chem. Rev.* **1984,** *53* (2), 132-139.

94. Davis, T. P.; Haddleton, D. M.; Richards, S. N., Controlled Polymerization of Acrylates and Methacrylates1. *J. Macromol. Sci. Part C* **1994,** *34* (2), 243-324.

95. Pierik, S. C. J.; Vollmerhaus, R.; van Herk, A. M.; German, A. L., Shining a Light on Catalytic Chain Transfer. *Macromol. Symp.* **2002,** *182* (1), 43-52.

96. Roberts, G. E.; Davis, T. P.; Heuts, J. P. A.; Russell, G. T., Viscosity Effects in Cobaloxime-Mediated Catalytic Chain-Transfer Polymerization of Methacrylates. *J. Macromol. Sci. Part A: Polym. Chem.* **2002,** *40* (6), 782-792.

97. Heuts, J. P. A.; Forster, D. J.; Davis, T. P., Mechanistic Aspects of Catalytic Chain Transfer Polymerization. In *Transition Metal Catalysis in*

Macromolecular Design, American Chemical Society: **2000**; Vol. 760, pp 254-272.

98. Morrison, D. A.; Davis, T. P.; Heuts, J. P. A.; Messerle, B.; Gridnev, A. A., Free Radical Polymerization with Catalytic Chain Transfer: Using NMR to Probe the Strength of the Cobalt–Carbon Bond in Small Molecule Model Reactions. *J. Macromol. Sci. Part A: Polym. Chem.* **2006,** *44* (21), 6171-6189.

99. Slavin, S.; Khoshdel, E.; Haddleton, D. M., Biological Surface Modification by 'Thiol-Ene' Addition of Polymers Synthesised by Catalytic Chain Transfer Polymerisation (CCTP). *Polym. Chem.* **2012,** *3* (6), 1461-1466.

100. Zhang, Q.; Slavin, S.; Jones, M. W.; Haddleton, A. J.; Haddleton, D. M., Terminal Functional Glycopolymers Via a Combination of Catalytic Chain Transfer Polymerisation (CCTP) Followed by Three Consecutive Click Reactions. *Polym. Chem.* **2012,** *3* (4), 1016-1023.

101. McEwan, K. A.; Slavin, S.; Tunnah, E.; Haddleton, D. M., Dual-Functional Materials Via CCTP and Selective Orthogonal Thiol-Michael Addition/Epoxide Ring Opening Reactions. *Polym. Chem.* **2013,** *4* (8), 2608-2614.

102. Haddleton, D. M.; Depaquis, E.; Kelly, E. J.; Kukulj, D.; Morsley, S. R.; Bon, S. A. F.; Eason, M. D.; Steward, A. G., Cobalt-Mediated Catalytic Chain-Transfer Polymerization (CCTP) in Water and Water/Alcohol Solution. *J. Macromol. Sci. Part A: Polym. Chem.* **2001,** *39* (14), 2378-2384.

103. Smeets, N. M. B., Amphiphilic Hyperbranched Polymers from the Copolymerization of a Vinyl and Divinyl Monomer: The Potential of Catalytic Chain Transfer Polymerization. *Eur. Polym. J.* **2013,** *49* (9), 2528-2544.

104. McEwan, K. A.; Haddleton, D. M., Combining Catalytic Chain Transfer Polymerisation (CCTP) and Thio-Michael Addition: Enabling the Synthesis of Peripherally Functionalised Branched Polymers. *Polym. Chem.* **2011,** *2* (9), 1992-1999.

105. Li, G.-Z.; Randev, R. K.; Soeriyadi, A. H.; Rees, G.; Boyer, C.; Tong, Z.; Davis, T. P.; Becer, C. R.; Haddleton, D. M., Investigation into Thiol-(Meth)Acrylate Michael Addition Reactions Using Amine and Phosphine Catalysts. *Polym. Chem.* **2010,** *1* (8), 1196-1204.

106. Cacioli, P.; Hawthorne, D. G.; Laslett, R. L.; Rizzardo, E.; Solomon, D. H., Copolymerization of ω-Unsaturated Oligo(Methyl Methacrylate): New Macromonomers. *J. Macromol. Sci.: Part A - Chem.* **1986,** *23* (7), 839-852.

107. Shegiwal, A.; Wemyss, A. M.; Liarou, E.; Town, J.; Patias, G.; Atkins, C. J.; Marathianos, A.; Lester, D. W.; Efstathiou, S.; Haddleton, D. M., Polymerisable Surfactants for Polymethacrylates Using Catalytic Chain Transfer Polymerisation (CCTP) Combined with Sulfur Free-Raft in Emulsion Polymerisation. *Eur. Polym. J.* **2020,** *125*, 109491.

108. Adamsons, K.; Blackman, G.; Gregorovich, B.; Lin, L.; Matheson, R., Oligomers in the Evolution of Automotive Clearcoats: Mechanical Performance Testing as a Function of Exposure. *Prog. Org. Coat.* **1998,** *34* (1), 64-74.

109. Haddleton, D. M.; Topping, C.; Hastings, J. J.; Suddaby, K. G., α,ω-Dihydroxy Telechelic Poly(Methyl Methacrylate) Via B-Scission (Radical Addition-Fragmentation) Chain Transfer Polymerisation by Macromonomer

Chain Transfer Agents, as Prepared by Catalytic Chain Transfer Polymerisation. *Macromol. Chem. Phys.* **1996,** *197* (9), 3027-3042.

110. Ravve, A., Physical Properties and Physical Chemistry of Polymers. In *Principles of Polymer Chemistry*, Ravve, A., Ed. Springer New York: New York, NY, **2012**; pp 17-67.

111. Fukuhara, D.; Sundberg, D., Latex Produced with Carboxylic Acid Comonomer for Waterborne Coatings: Particle Morphology Variations with Changing Ph. *JCT Res.* **2005,** *2* (7), 509-516.

112. Guan, Z., Control of Polymer Topology through Transition-Metal Catalysis: Synthesis of Hyperbranched Polymers by Cobalt-Mediated Free Radical Polymerization. *J. Am. Chem. Soc.* **2002,** *124* (20), 5616-5617.

113. Haddleton, D. M.; Topping, C.; Kukulj, D.; Irvine, D., α,ω -Dicarboxyl Telechelic Poly(Methyl Methacrylate) Via Radical Addition-Fragmentation Polymerization. *Polymer* **1998,** *39* (14), 3119-3128.

114. Haddleton, D. M.; Maloney, D. R.; Suddaby, K. G., Competition between B-Scission of Macromonomer-Ended Radicals and Chain Transfer to Cobalt(II) in Catalytic Chain Transfer Polymerization (CCTP). *Macromolecules* **1996,** *29* (1), 481-483.

115. Yamada, B.; Tagashira, S.; Aoki, S., Preparation of Polymers with Substituted Allyl End Group Using Dimer of A-Methylvinyl Monomer as Addition Fragmentation Chain Transfer Agent at High Temperatures. *J. Macromol. Sci. Part A: Polym. Chem.* **1994,** *32* (14), 2745-2754.

116. Trumbo, D. L.; Abbey, K. J.; Carlson, G. M., Synthesis and Copolymerization of 2,2-Dimethyl-4-Methylene Glutaric Anhydride. *J. Macromol. Sci. Part C: Polym. Lett.* **1987,** *25* (5), 229-232.

117. Janowicz, A. H. Bimetallic Catalytic Chain Transfer Agents for Molecular Weight Control in Free Radical Polymerization. US4746713A, **1987**.

118. Haddleton, D. M.; Morsley, D. R.; O'Donnell, J. P.; Richards, S. N., The Effect of Feed Conditions in the Emulsion Catalytic Chain Transfer Polymerization of Alkyl Methacrylates. *J. Macromol. Sci. Part A: Polym. Chem.* **1999,** *37* (18), 3549-3557.

119. Smeets, N. M. B.; Heuts, J. P. A.; Meuldijk, J.; Cunningham, M. F.; Van Herk, A. M., The Effect of Co(II)-Mediated Catalytic Chain Transfer on the Emulsion Polymerization Kinetics of Methyl Methacrylate. *J. Macromol. Sci. Part A: Polym. Chem.* **2009,** *47* (19), 5078-5089.

120. Kukulj, D.; Davis, T. P.; Suddaby, K. G.; Haddleton, D. M.; Gilbert, R. G., Catalytic Chain Transfer for Molecular Weight Control in the Emulsion Homo- and Copolymerizations of Methyl Methacrylate and Butyl Methacrylate. *J. Macromol. Sci. Part A: Polym. Chem.* **1997,** *35* (5), 859-878.

121. Suddaby, K. G.; Haddleton, D. M.; Hastings, J. J.; Richards, S. N.; O'Donnell, J. P., Catalytic Chain Transfer for Molecular Weight Control in the Emulsion Polymerization of Methyl Methacrylate and Methyl Methacrylate−Styrene. *Macromolecules* **1996,** *29* (25), 8083-8091.

122. Bon, S. A. F.; Morsley, D. R.; Waterson, J.; Haddleton, D. M.; Lees, M. R.; Horne, T., Advances in Catalytic Chain Transfer Polymerisation Mediated by Cobaloximes. *Macromol. Symp.* **2001,** *165* (1), 29-42.

123. Smeets, N. M. B.; Jansen, T. G. T.; van Herk, A. M.; Meuldijk, J.; Heuts, J. P. A., Mass Transport by Collisions in Emulsion Polymerization: Why It Is Possible to Use Very Hydrophobic Catalysts for Efficient Molecular Weight Control. *Polym. Chem.* **2011,** *2* (8), 1830-1836.

124. Ziegler, K.; Bähr, K., Über Den Vermutlichen Mechanismus Der Polymerisationen Durch Alkalimetalle (Vorläufige Mitteilung). *Ber. Dtsch. Chem. Ges. (A B Ser.)* **1928,** *61* (2), 253-263.

125. Waley, S. G.; Watson, J.; Wilson, A. H., The Kinetics of the Polymerization of Sarcosine Carbonic Anhydride. *Proc. R. Soc. London. Ser A. Math. Phys.l Sci.* **1949,** *199* (1059), 499-517.

126. Szwarc, M., 'Living' Polymers. *Nature* **1956,** *178* (4543), 1168-1169.

127. Baskaran, D., Strategic Developments in Living Anionic Polymerization of Alkyl (Meth)Acrylates. *Prog. Polym. Sci.* **2003,** *28* (4), 521-581.

128. Klumperman, B., Living Radical Polymerization. In *Encyclopedia of Polymer Science and Technology*.

129. Matyjaszewski, K., Atom Transfer Radical Polymerization (ATRP): Current Status and Future Perspectives. *Macromolecules* **2012,** *45* (10), 4015-4039.

130. Anastasaki, A.; Nikolaou, V.; Nurumbetov, G.; Wilson, P.; Kempe, K.; Quinn, J. F.; Davis, T. P.; Whittaker, M. R.; Haddleton, D. M., Cu(0)-Mediated Living Radical Polymerization: A Versatile Tool for Materials Synthesis. *Chem. Rev.* **2016,** *116* (3), 835-877.

131. Quirk, R. P.; Lee, B., Experimental Criteria for Living Polymerizations. *Polym. Int.* **1992,** *27* (4), 359-367.

132. Jenkins, A. D.; Jones, R. G.; Moad, G., Terminology for Reversible-Deactivation Radical Polymerization Previously Called "Controlled" Radical or "Living" Radical Polymerization (IUPAC Recommendations 2010). *Pure Appl. Chem.* **2009,** *82* (2), 483-491.

133. Hawker, C. J.; Bosman, A. W.; Harth, E., New Polymer Synthesis by Nitroxide Mediated Living Radical Polymerizations. *Chem. Rev.* **2001,** *101* (12), 3661-3688.

134. Nicolas, J.; Guillaneuf, Y.; Lefay, C.; Bertin, D.; Gigmes, D.; Charleux, B., Nitroxide-Mediated Polymerization. *Prog. Polym. Sci.* **2013,** *38* (1), 63-235.

135. Chiefari, J.; Chong, Y. K.; Ercole, F.; Krstina, J.; Jeffery, J.; Le, T. P. T.; Mayadunne, R. T. A.; Meijs, G. F.; Moad, C. L.; Moad, G.; Rizzardo, E.; Thang, S. H., Living Free-Radical Polymerization by Reversible Addition−Fragmentation Chain Transfer: The RAFT Process. *Macromolecules* **1998,** *31* (16), 5559-5562.

136. Perrier, S., 50th Anniversary Perspective: RAFT Polymerization—a User Guide. *Macromolecules* **2017,** *50* (19), 7433-7447.

137. Xia, J.; Matyjaszewski, K., Controlled/"Living" Radical Polymerization. Atom Transfer Radical Polymerization Using Multidentate Amine Ligands. *Macromolecules* **1997,** *30* (25), 7697-7700.

138. David H. Solomon, E. R., Paul Cacioli Polymerization Process and Polymers Produced Thereby. US4581429A, **1986**.

139. Moad, G.; Rizzardo, E., Chapter 1 the History of Nitroxide-Mediated Polymerization. In *Nitroxide Mediated Polymerization: From Fundamentals to Applications in Materials Science*, The Royal Society of Chemistry: **2016**; pp 1-44.

140. Georges, M. K.; Veregin, R. P. N.; Kazmaier, P. M.; Hamer, G. K., Narrow Molecular Weight Resins by a Free-Radical Polymerization Process. *Macromolecules* **1993,** *26* (11), 2987-2988.

141. Benoit, D.; Grimaldi, S.; Finet, J. P.; Tordo, P.; Fontanille, M.; Gnanou, Y., Controlled Free - Radical Polymerization in the Presence of a Novel Asymmetric Nitroxyl Radical. *American Chemical Society, Polymer Preprints, Division of Polymer Chemistry* **1997,** *38* (1), 729-730.

142. Benoit, D.; Chaplinski, V.; Braslau, R.; Hawker, C. J., Development of a Universal Alkoxyamine for "Living" Free Radical Polymerizations. *J. Am. Chem. Soc.* **1999,** *121* (16), 3904-3920.

143. Chong, Y. K.; Ercole, F.; Moad, G.; Rizzardo, E.; Thang, S. H.; Anderson, A. G., Imidazolidinone Nitroxide-Mediated Polymerization. *Macromolecules* **1999,** *32* (21), 6895-6903.

144. Goto, A.; Terauchi, T.; Fukuda, T.; Miyamoto, T., Gel Permeation Chromatographic Determination of Activation Rate Constants in Nitroxide-Controlled Free Radical Polymerization, 1. Direct Analysis by Peak Resolution. *Macromol. Rapid Commun.* **1997,** *18* (8), 673-681.

145. Fukuda, T.; Terauchi, T.; Goto, A.; Ohno, K.; Tsujii, Y.; Miyamoto, T.; Kobatake, S.; Yamada, B., Mechanisms and Kinetics of Nitroxide-Controlled Free Radical Polymerization. *Macromolecules* **1996,** *29* (20), 6393-6398.

146. Hlalele, L.; Klumperman, B., In Situ ^{1}H NMR Studies of High-Temperature Nitroxide-Mediated Polymerization of N-Butyl Acrylate. *Macromolecules* **2011,** *44* (18), 7100-7108.

147. Grassl, B.; Clisson, G.; Khoukh, A.; Billon, L., Nitroxide-Mediated Radical Polymerization of Acrylamide in Water Solution. *Eur. Polym. J.* **2008,** *44* (1), 50-58.

148. Benoit, D.; Harth, E.; Fox, P.; Waymouth, R. M.; Hawker, C. J., Accurate Structural Control and Block Formation in the Living Polymerization of 1,3-Dienes by Nitroxide-Mediated Procedures. *Macromolecules* **2000,** *33* (2), 363-370.

149. Burguière, C.; Dourges, M.-A.; Charleux, B.; Vairon, J.-P., Synthesis and Characterization of ω-Unsaturated Poly(Styrene-B-N-Butyl Methacrylate) Block Copolymers Using TEMPO-Mediated Controlled Radical Polymerization. *Macromolecules* **1999,** *32* (12), 3883-3890.

150. Moad, G.; Anderson, A. G.; Ercole, F.; Johnson, C. H. J.; Krstina, J.; Moad, C. L.; Rizzardo, E.; Spurling, T. H.; Thang, S. H., Controlled-Growth Free-Radical Polymerization of Methacrylate Esters: Reversible Chain Transfer Versus Reversible Termination. In *Controlled Radical Polymerization*, American Chemical Society: **1998**; Vol. 685, pp 332-360.

151. Ananchenko, G. S.; Souaille, M.; Fischer, H.; Le Mercier, C.; Tordo, P., Decomposition of Model Alkoxyamines in Simple and Polymerizing Systems. II. Diastereomeric N-(2-Methylpropyl)-N-(1-Diethyl-Phosphono-2,2-Dimethyl-Propyl)-Aminoxyl-Based Compounds. *J. Macromol. Sci. Part A: Polym. Chem.* **2002,** *40* (19), 3264-3283.

152. Hawker, C. J.; Elce, E.; Dao, J.; Volksen, W.; Russell, T. P.; Barclay, G. G., Well-Defined Random Copolymers by a "Living" Free-Radical Polymerization Process. *Macromolecules* **1996,** *29* (7), 2686-2688.

153. Butz, S.; Baethge, H.; Schmidt-Naake, G., Narrow-Polydispersity Polystyrene/Poly[Styrene-Co-(Butyl Methacrylate)] Block Copolymers by an N-Oxyl Mediated Free Radical Polymerization Process. *Macromol. Rapid Commun.* **1997,** *18* (12), 1049-1055.

154. Charleux, B.; Nicolas, J.; Guerret, O., Theoretical Expression of the Average Activation−Deactivation Equilibrium Constant in Controlled/Living Free-Radical Copolymerization Operating Via Reversible Termination. Application to a Strongly Improved Control in Nitroxide-Mediated Polymerization of Methyl Methacrylate. *Macromolecules* **2005,** *38* (13), 5485-5492.

155. Fischer, H., The Persistent Radical Effect: A Principle for Selective Radical Reactions and Living Radical Polymerizations. *Chem. Rev.* **2001,** *101* (12), 3581-3610.

156. Petton, L.; Ciolino, A. E.; Dervaux, B.; Du Prez, F. E., From One-Pot Stabilisation to in Situ Functionalisation in Nitroxide Mediated Polymerisation: An Efficient Extension Towards Atom Transfer Radical Polymerisation. *Polym. Chem.* **2012,** *3* (7), 1867-1878.

157. Goto, A.; Fukuda, T., Kinetics of Living Radical Polymerization. *Prog. Polym. Sci.* **2004,** *29* (4), 329-385.

158. Zetterlund, P. B.; Saka, Y.; McHale, R.; Nakamura, T.; Aldabbagh, F.; Okubo, M., Nitroxide-Mediated Radical Polymerization of Styrene: Experimental Evidence of Chain Transfer to Monomer. *Polymer* **2006,** *47* (23), 7900-7908.

159. Souaille, M.; Fischer, H., Living Free Radical Polymerizations Mediated by the Reversible Combination of Transient Propagating and Persistent Nitroxide Radicals. The Role of Hydroxylamine and Alkene Formation. *Macromolecules* **2001,** *34* (9), 2830-2838.

160. Moad, G.; Rizzardo, E.; Thang, S. H., Living Radical Polymerization by the RAFT Process a Second Update. *Aust. J. Chem.* **2009,** *62* (11), 1402-1472.

161. Hill, M. R.; Carmean, R. N.; Sumerlin, B. S., Expanding the Scope of RAFT Polymerization: Recent Advances and New Horizons. *Macromolecules* **2015,** *48* (16), 5459-5469.

162. Keddie, D. J., A Guide to the Synthesis of Block Copolymers Using Reversible-Addition Fragmentation Chain Transfer (RAFT) Polymerization. *Chem. Soc. Rev.* **2014,** *43* (2), 496-505.

163. Goto, A.; Sato, K.; Tsujii, Y.; Fukuda, T.; Moad, G.; Rizzardo, E.; Thang, S. H., Mechanism and Kinetics of RAFT-Based Living Radical Polymerizations of Styrene and Methyl Methacrylate. *Macromolecules* **2001,** *34* (3), 402-408.

164. Stenzel, M. H.; Cummins, L.; Roberts, G. E.; Davis, T. P.; Vana, P.; Barner-Kowollik, C., Xanthate Mediated Living Polymerization of Vinyl Acetate: A Systematic Variation in MADIX/RAFT Agent Structure. *Macromol. Chem. Phys.* **2003,** *204* (9), 1160-1168.

165. Zhao, F.; Mahdavian, A. R.; Teimouri, M. B.; Daniels, E. S.; Klein, A.; El-Aasser, M. S., RAFT-Mediated Emulsion Polymerization of Vinyl Acetate: A Challenge Towards Producing High Molecular Weight Poly(Vinyl Acetate). *Colloid Polym. Sci.* **2012,** *290* (13), 1247-1255.

166. Mishra, V.; Kumar, R., RAFT Polymerization of N-Vinyl Pyrrolidone Using Prop-2-Ynyl Morpholine-4-Carbodithioate as a New Chain Transfer Agent. *J. Appl. Polym. Sci.* **2012,** *124* (6), 4475-4485.

167. Guinaudeau, A.; Mazières, S.; Wilson, D. J.; Destarac, M., Aqueous RAFT/MADIX polymerisation of N-Vinyl Pyrrolidone at Ambient Temperature. *Polym. Chem.* **2012,** *3* (1), 81-84.

168. Granel, C.; Jérôme, R.; Teyssié, P.; Jasieczek, C. B.; Shooter, A. J.; Haddleton, D. M.; Hastings, J. J.; Gigmes, D.; Grimaldi, S.; Tordo, P.; Greszta, D.; Matyjaszewski, K., Investigation of Methyl Methacrylate and Vinyl Acetate Polymerization Promoted by Al(Ibu)3/2,2‘-Bipyridine and Al(Ibu)3/2,2‘-Bipyridine/Tempo Complexes. *Macromolecules* **1998,** *31* (21), 7133-7141.

169. Lu, X.; Gong, S.; Meng, L.; Li, C.; Yang, S.; Zhang, L., Controllable Synthesis of Poly(N-Vinylpyrrolidone) and Its Block Copolymers by Atom Transfer Radical Polymerization. *Polymer* **2007,** *48* (10), 2835-2842.

170. Benaglia, M.; Chiefari, J.; Chong, Y. K.; Moad, G.; Rizzardo, E.; Thang, S. H., Universal (Switchable) RAFT Agents. *J. Am. Chem. Soc.* **2009,** *131* (20), 6914-6915.

171. Dommanget, C.; D'Agosto, F.; Monteil, V., Polymerization of Ethylene through Reversible Addition–Fragmentation Chain Transfer (RAFT). *Angew. Chem. Int. Ed.* **2014,** *53* (26), 6683-6686.

172. Krstina, J.; Moad, C. L.; Moad, G.; Rizzardo, E.; Berge, C. T.; Fryd, M., A New Form of Controlled Growth Free Radical Polymerization. *Macromol. Symp.* **1996,** *111* (1), 13-23.

173. Marathianos, A.; Wemyss, A. M.; Liarou, E.; Jones, J. R.; Shegiwal, A.; Town, J. S.; Lester, D. W.; Li, Y.; Haddleton, D. M., Controlling the Particle Size in Surfactant-Free Latexes from ω-Propenyl Oligomers Obtained through Catalytic Chain Transfer Polymerization. *ACS Appl. Polym. Mater.* **2021,** *3* (6), 3185-3196.

174. Engelis, N. G.; Anastasaki, A.; Nurumbetov, G.; Truong, N. P.; Nikolaou, V.; Shegiwal, A.; Whittaker, M. R.; Davis, T. P.; Haddleton, D. M., Sequence-

Controlled Methacrylic Multiblock Copolymers Via Sulfur-Free RAFT Emulsion Polymerization. *Nature Chemistry* **2017,** *9* (2), 171-178.

175. Tang, H.; Arulsamy, N.; Radosz, M.; Shen, Y.; Tsarevsky, N. V.; Braunecker, W. A.; Tang, W.; Matyjaszewski, K., Highly Active Copper-Based Catalyst for Atom Transfer Radical Polymerization. *J. Am. Chem. Soc.* **2006,** *128* (50), 16277-16285.

176. Tang, W.; Kwak, Y.; Braunecker, W.; Tsarevsky, N. V.; Coote, M. L.; Matyjaszewski, K., Understanding Atom Transfer Radical Polymerization: Effect of Ligand and Initiator Structures on the Equilibrium Constants. *J. Am. Chem. Soc.* **2008,** *130* (32), 10702-10713.

177. Simula, A.; Nikolaou, V.; Alsubaie, F.; Anastasaki, A.; Haddleton, D. M., The Effect of Ligand, Solvent and Cu(0) Source on the Efficient Polymerization of Polyether Acrylates and Methacrylates in Aqueous and Organic Media. *Polym. Chem.* **2015,** *6* (32), 5940-5950.

178. Alsubaie, F.; Anastasaki, A.; Nikolaou, V.; Simula, A.; Nurumbetov, G.; Wilson, P.; Kempe, K.; Haddleton, D. M., Investigating the Mechanism of Copper(0)-Mediated Living Radical Polymerization in Aqueous Media. *Macromolecules* **2015,** *48* (18), 6421-6432.

179. Fischer, H., The Persistent Radical Effect in Controlled Radical Polymerizations. *J. Macromol. Sci. Part A: Polym. Chem.* **1999,** *37* (13), 1885-1901.

180. Fischer, H., The Persistent Radical Effect in "Living" Radical Polymerization. *Macromolecules* **1997,** *30* (19), 5666-5672.

181. Otsu, T.; Yoshida, M., Role of Initiator-Transfer Agent-Terminator (Iniferter) in Radical Polymerizations: Polymer Design by Organic Disulfides as Iniferters. *Makromol. Chem. Rapid Commun.* **1982,** *3* (2), 127-132.

182. Liarou, E.; Staniforth, M.; Town, J. S.; Marathianos, A.; Grypioti, M.; Li, Y.; Chang, Y.; Efstathiou, S.; Hancox, E.; Wemyss, A. M.; Wilson, P.; Jones, B. A.; Aljuaid, M.; Stavros, V. G.; Haddleton, D. M., UV Irradiation of Cu-Based Complexes with Aliphatic Amine Ligands as Used in Living Radical Polymerization. *Eur. Polym. J.* **2020,** *123*, 109388.

183. Foley, J.; Tyagi, S.; Hathaway, B. J., The Crystal Structure and Electronic Properties of Bis(2,2′-Bipyridyl)-Copper(II) Bis(Hexafluorophosphate). *J. Chem. Soc., Dalton Trans.* **1984,** (1), 1-5.

184. Kickelbick, G.; Pintauer, T.; Matyjaszewski, K., Structural Comparison of CuII Complexes in Atom Transfer Radical Polymerization. *New J. Chem.* **2002,** *26* (4), 462-468.

185. Malkov, A. V.; Baxendale, I. R.; Bella, M.; Langer, V.; Fawcett, J.; Russell, D. R.; Mansfield, D. J.; Valko, M.; Kočovský, P., Synthesis of New Chiral 2,2'-Bipyridyl-Type Ligands, Their Coordination to Molybdenum(0), Copper(II), and Palladium(II), and Application in Asymmetric Allylic Substitution, Allylic Oxidation, and Cyclopropanation. *Organometallics* **2001,** *20* (4), 673-690.

186. Bernhardt, P. V., On the Structure, Electrochemistry, and Spectroscopy of the (N,N‘-Bis(2‘-(Dimethylamino)Ethyl)-N,N‘-Dimethylpropane-1,3-Diamine)Copper(II) Ion. *J. Am. Chem. Soc.* **1997,** *119* (4), 771-774.

187. Haddleton, D. M.; Jasieczek, C. B.; Hannon, M. J.; Shooter, A. J., Atom Transfer Radical Polymerization of Methyl Methacrylate Initiated by Alkyl Bromide and 2-Pyridinecarbaldehyde Imine Copper(I) Complexes. *Macromolecules* **1997,** *30* (7), 2190-2193.

188. Kwak, Y.; Matyjaszewski, K., Effect of Initiator and Ligand Structures on Atrp of Styrene and Methyl Methacrylate Initiated by Alkyl Dithiocarbamate. *Macromolecules* **2008,** *41* (18), 6627-6635.

189. Tang, W.; Matyjaszewski, K., Effects of Initiator Structure on Activation Rate Constants in Atrp. *Macromolecules* **2007,** *40* (6), 1858-1863.

190. Goto, A.; Fukuda, T., Determination of the Activation Rate Constants of Alkyl Halide Initiators for Atom Transfer Radical Polymerization. *Macromol. Rapid Commun.* **1999,** *20* (12), 633-636.

191. Shen, Y.; Zhu, S.; Zeng, F.; Pelton, R., Versatile Initiators for Macromonomer Syntheses of Acrylates, Methacrylates, and Styrene by Atom Transfer Radical Polymerization. *Macromolecules* **2000,** *33* (15), 5399-5404.

192. Anastasaki, A.; Nikolaou, V.; Haddleton, D. M., Cu(0)-Mediated Living Radical Polymerization: Recent Highlights and Applications; a Perspective. *Polym. Chem.* **2016,** *7* (5), 1002-1026.

193. Ribelli, T. G.; Lorandi, F.; Fantin, M.; Matyjaszewski, K., Atom Transfer Radical Polymerization: Billion Times More Active Catalysts and New Initiation Systems. *Macromol. Rapid Commun.* **2019,** *40* (1), 1800616.

194. Lin, C. Y.; Coote, M. L.; Gennaro, A.; Matyjaszewski, K., Ab Initio Evaluation of the Thermodynamic and Electrochemical Properties of Alkyl Halides and Radicals and Their Mechanistic Implications for Atom Transfer Radical Polymerization. *J. Am. Chem. Soc.* **2008,** *130* (38), 12762-12774.

195. Konkolewicz, D.; Wang, Y.; Krys, P.; Zhong, M.; Isse, A. A.; Gennaro, A.; Matyjaszewski, K., SARA ATRP or SET-LRP. End of Controversy? *Polym. Chem.* **2014,** *5* (15), 4396-4417.

196. Konkolewicz, D.; Wang, Y.; Zhong, M.; Krys, P.; Isse, A. A.; Gennaro, A.; Matyjaszewski, K., Reversible-Deactivation Radical Polymerization in the Presence of Metallic Copper. A Critical Assessment of the SARA ATRP and SET-LRP Mechanisms. *Macromolecules* **2013,** *46* (22), 8749-8772.

197. Matyjaszewski, K.; Jakubowski, W.; Min, K.; Tang, W.; Huang, J.; Braunecker, W. A.; Tsarevsky, N. V., Diminishing Catalyst Concentration in Atom Transfer Radical Polymerization with Reducing Agents. *Proc. Natl. Acad. Sci.* **2006,** *103* (42), 15309.

198. Dong, H.; Tang, W.; Matyjaszewski, K., Well-Defined High-Molecular-Weight Polyacrylonitrile Via Activators Regenerated by Electron Transfer Atrp. *Macromolecules* **2007,** *40* (9), 2974-2977.

199. Kwak, Y.; Matyjaszewski, K., ARGET ATRP of Methyl Methacrylate in the Presence of Nitrogen-Based Ligands as Reducing Agents. *Polym. Int.* **2009,** *58* (3), 242-247.

200. Jakubowski, W.; Matyjaszewski, K., Activator Generated by Electron Transfer for Atom Transfer Radical Polymerization. *Macromolecules* **2005,** *38* (10), 4139-4146.

201. de Vries, A.; Klumperman, B.; de Wet-Roos, D.; Sanderson, R. D., The Effect of Reducing Monosaccharides on the Atom Transfer Radical Polymerization of Butyl Methacrylate. *Macromol. Chem. Phys.* **2001,** *202* (9), 1645-1648.

202. Jakubowski, W.; Matyjaszewski, K., Activators Regenerated by Electron Transfer for Atom-Transfer Radical Polymerization of (Meth)Acrylates and Related Block Copolymers. *Angew. Chem. Int. Ed.* **2006,** *45* (27), 4482-4486.

203. Min, K.; Gao, H.; Matyjaszewski, K., Use of Ascorbic Acid as Reducing Agent for Synthesis of Well-Defined Polymers by ARGET ATRP. *Macromolecules* **2007,** *40* (6), 1789-1791.

204. Percec, V.; Popov, A. V.; Ramirez-Castillo, E.; Monteiro, M.; Barboiu, B.; Weichold, O.; Asandei, A. D.; Mitchell, C. M., Aqueous Room Temperature Metal-Catalyzed Living Radical Polymerization of Vinyl Chloride. *J. Am. Chem. Soc.* **2002,** *124* (18), 4940-4941.

205. Percec, V.; Guliashvili, T.; Ladislaw, J. S.; Wistrand, A.; Stjerndahl, A.; Sienkowska, M. J.; Monteiro, M. J.; Sahoo, S., Ultrafast Synthesis of Ultrahigh Molar Mass Polymers by Metal-Catalyzed Living Radical Polymerization of Acrylates, Methacrylates, and Vinyl Chloride Mediated by SET at 25 °C. *J. Am. Chem. Soc.* **2006,** *128* (43), 14156-14165.

206. Lligadas, G.; Rosen, B. M.; Bell, C. A.; Monteiro, M. J.; Percec, V., Effect of Cu(0) Particle Size on the Kinetics of SET-LRP in DMSO and Cu-Mediated Radical Polymerization in MeCN at 25 °C. *Macromolecules* **2008,** *41* (22), 8365-8371.

207. Nguyen, N. H.; Sun, H.-J.; Levere, M. E.; Fleischmann, S.; Percec, V., Where Is Cu(0) Generated by Disproportionation During SET-LRP? *Polym. Chem.* **2013,** *4* (5), 1328-1332.

208. Levere, M. E.; Nguyen, N. H.; Leng, X.; Percec, V., Visualization of the Crucial Step in SET-LRP. *Polym. Chem.* **2013,** *4* (5), 1635-1647.

209. Rosen, B. M.; Jiang, X.; Wilson, C. J.; Nguyen, N. H.; Monteiro, M. J.; Percec, V., The Disproportionation of Cu(I)X Mediated by Ligand and Solvent into Cu(0) and Cu(II)X_2 and Its Implications for SET-LRP. *J. Macromol. Sci. Part A: Polym. Chem.* **2009,** *47* (21), 5606-5628.

210. Nguyen, N. H.; Kulis, J.; Sun, H.-J.; Jia, Z.; van Beusekom, B.; Levere, M. E.; Wilson, D. A.; Monteiro, M. J.; Percec, V., A Comparative Study of the SET-LRP of Oligo(Ethylene Oxide) Methyl Ether Acrylate in DMSO and in H_2O. *Polym. Chem.* **2013,** *4* (1), 144-155.

211. Rademacher, J. T.; Baum, M.; Pallack, M. E.; Brittain, W. J.; Simonsick, W. J., Atom Transfer Radical Polymerization of N,N-Dimethylacrylamide. *Macromolecules* **2000,** *33* (2), 284-288.

212. Millard, P.-E.; Mougin, N. C.; Böker, A.; Müller, A. H. E., Controlling the Fast ATRP of N-Isopropylacrylamide in Water. In *Controlled/Living Radical Polymerization: Progress in ATRP*, American Chemical Society: 2009; Vol. 1023, pp 127-137.

213. Zhang, Q.; Wilson, P.; Li, Z.; McHale, R.; Godfrey, J.; Anastasaki, A.; Waldron, C.; Haddleton, D. M., Aqueous Copper-Mediated Living Polymerization: Exploiting Rapid Disproportionation of CuBr with Me_6tren. *J. Am. Chem. Soc.* **2013,** *135* (19), 7355-7363.

214. Zhang, Q.; Li, Z.; Wilson, P.; Haddleton, D. M., Copper-Mediated Controlled Radical Polymerization under Biological Conditions: SET-LRP in Blood Serum. *Chem. Commun.* **2013,** *49* (59), 6608-6610.

215. Waldron, C.; Zhang, Q.; Li, Z.; Nikolaou, V.; Nurumbetov, G.; Godfrey, J.; McHale, R.; Yilmaz, G.; Randev, R. K.; Girault, M.; McEwan, K.; Haddleton, D. M.; Droesbeke, M.; Haddleton, A. J.; Wilson, P.; Simula, A.; Collins, J.; Lloyd, D. J.; Burns, J. A.; Summers, C.; Houben, C.; Anastasaki, A.; Li, M.; Becer, C. R.; Kiviaho, J. K.; Risangud, N., Absolut "Copper Catalyzation Perfected"; Robust Living Polymerization of NiPAm: Guinness Is Good for SET-LRP. *Polym. Chem.* **2014,** *5* (1), 57-61.

216. Ma, J.; Chen, H.; Zhang, M.; Yu, M., SET-LRP of Acrylonitrile in Ionic Liquids without Any Ligand. *J. Macromol. Sci. Part A: Polym. Chem.* **2012,** *50* (3), 609-613.

217. Soeriyadi, A. H.; Boyer, C.; Nyström, F.; Zetterlund, P. B.; Whittaker, M. R., High-Order Multiblock Copolymers Via Iterative Cu(0)-Mediated Radical Polymerizations (SET-LRP): Toward Biological Precision. *J. Am. Chem. Soc.* **2011,** *133* (29), 11128-11131.

218. Alsubaie, F.; Anastasaki, A.; Wilson, P.; Haddleton, D. M., Sequence-Controlled Multi-Block Copolymerization of Acrylamides Via Aqueous SET-LRP at 0 °C. *Polym. Chem.* **2015,** *6* (3), 406-417.

219. Beyer, V. P.; Kim, J.; Becer, C. R., Synthetic Approaches for Multiblock Copolymers. *Polym. Chem.* **2020,** *11* (7), 1271-1291.

220. Aksakal, R.; Resmini, M.; Becer, C. R., Pentablock Star Shaped Polymers in Less Than 90 Minutes Via Aqueous SET-LRP. *Polym. Chem.* **2016,** *7* (1), 171-175.

221. Marathianos, A.; Liarou, E.; Anastasaki, A.; Whitfield, R.; Laurel, M.; Wemyss, A. M.; Haddleton, D. M., Photo-Induced Copper-RRDP in Continuous Flow without External Deoxygenation. *Polym. Chem.* **2019,** *10* (32), 4402-4406.

222. Leibfarth, F. A.; Mattson, K. M.; Fors, B. P.; Collins, H. A.; Hawker, C. J., External Regulation of Controlled Polymerizations. *Angew. Chem. Int. Ed.* **2013,** *52* (1), 199-210.

223. Chen, M.; Zhong, M.; Johnson, J. A., Light-Controlled Radical Polymerization: Mechanisms, Methods, and Applications. *Chem. Rev.* **2016,** *116* (17), 10167-10211.

224. Oster, G.; Yang, N.-L., Photopolymerization of Vinyl Monomers. *Chem. Rev.* **1968,** *68* (2), 125-151.

225. Tanabe, M.; Manners, I., Photolytic Living Anionic Ring-Opening Polymerization (ROP) of Silicon-Bridged [1]Ferrocenophanes Via an Iron-Cyclopentadienyl Bond Cleavage Mechanism. *J. Am. Chem. Soc.* **2004,** *126* (37), 11434-11435.

226. Tanabe, M.; Vandermeulen, G. W. M.; Chan, W. Y.; Cyr, P. W.; Vanderark, L.; Rider, D. A.; Manners, I., Photocontrolled Living Polymerizations. *Nat. Mater.* **2006,** *5* (6), 467-470.

227. Zheng, X.; Yue, M.; Yang, P.; Li, Q.; Yang, W., Cycloketyl Radical Mediated Living Polymerization. *Polym. Chem.* **2012,** *3* (8), 1982-1986.

228. Dadashi-Silab, S.; Aydogan, C.; Yagci, Y., Shining a Light on an Adaptable Photoinitiator: Advances in Photopolymerizations Initiated by Thioxanthones. *Polym. Chem.* **2015,** *6* (37), 6595-6615.

229. Yagci, Y.; Jockusch, S.; Turro, N. J., Photoinitiated Polymerization: Advances, Challenges, and Opportunities. *Macromolecules* **2010,** *43* (15), 6245-6260.

230. Gong, T.; Adzima, B. J.; Bowman, C. N., A Novel Copper Containing Photoinitiator, Copper(II) Acylphosphinate, and Its Application in Both the Photomediated Cuaac Reaction and in Atom Transfer Radical Polymerization. *Chem. Commun.* **2013,** *49* (72), 7950-7952.

231. Fors, B. P.; Hawker, C. J., Control of a Living Radical Polymerization of Methacrylates by Light. *Angew. Chem. Int. Ed.* **2012,** *51* (35), 8850-8853.

232. Xu, J.; Shanmugam, S.; Duong, H. T.; Boyer, C., Organo-Photocatalysts for Photoinduced Electron Transfer-Reversible Addition–Fragmentation Chain Transfer (PET-RAFT) Polymerization. *Polym. Chem.* **2015,** *6* (31), 5615-5624.

233. Shanmugam, S.; Xu, J.; Boyer, C., Utilizing the Electron Transfer Mechanism of Chlorophyll a under Light for Controlled Radical Polymerization. *Chem. Sci.* **2015,** *6* (2), 1341-1349.

234. Treat, N. J.; Fors, B. P.; Kramer, J. W.; Christianson, M.; Chiu, C.-Y.; Read de Alaniz, J.; Hawker, C. J., Controlled Radical Polymerization of Acrylates Regulated by Visible Light. *ACS Macro Lett.* **2014,** *3* (6), 580-584.

235. Moon, J. H.; Ford, J.; Yang, S., Fabricating Three-Dimensional Polymeric Photonic Structures by Multi-Beam Interference Lithography. *Polym. Adv. Technol.* **2006,** *17* (2), 83-93.

236. Connal, L. A.; Vestberg, R.; Hawker, C. J.; Qiao, G. G., Fabrication of Reversibly Crosslinkable, 3-Dimensionally Conformal Polymeric Microstructures. *Adv. Funct. Mater.* **2008,** *18* (20), 3315-3322.

237. Hiller, J.; Mendelsohn, J. D.; Rubner, M. F., Reversibly Erasable Nanoporous Anti-Reflection Coatings from Polyelectrolyte Multilayers. *Nat. Mater,* **2002,** *1* (1), 59-63.

238. Moszner, N.; Salz, U.; Zimmermann, J., Chemical Aspects of Self-Etching Enamel–Dentin Adhesives: A Systematic Review. *Dent. Mater.* **2005,** *21* (10), 895-910.

239. Poelma, J. E.; Fors, B. P.; Meyers, G. F.; Kramer, J. W.; Hawker, C. J., Fabrication of Complex Three-Dimensional Polymer Brush Nanostructures

through Light-Mediated Living Radical Polymerization. *Angew. Chem. Int. Ed.* **2013,** *52* (27), 6844-6848.

240. Shanmugam, S.; Boyer, C., Stereo-, Temporal and Chemical Control through Photoactivation of Living Radical Polymerization: Synthesis of Block and Gradient Copolymers. *J. Am. Chem. Soc.* **2015,** *137* (31), 9988-9999.

241. Shanmugam, S.; Xu, J.; Boyer, C., Photoinduced Electron Transfer–Reversible Addition–Fragmentation Chain Transfer (PET-RAFT) Polymerization of Vinyl Acetate and N-Vinylpyrrolidinone: Kinetic and Oxygen Tolerance Study. *Macromolecules* **2014,** *47* (15), 4930-4942.

242. Corrigan, N.; Xu, J.; Boyer, C.; Allonas, X., Exploration of the PET-RAFT Initiation Mechanism for Two Commonly Used Photocatalysts. *ChemPhotoChem* **2019,** *3* (11), 1193-1199.

243. Anastasaki, A.; Nikolaou, V.; Zhang, Q.; Burns, J.; Samanta, S. R.; Waldron, C.; Haddleton, A. J.; McHale, R.; Fox, D.; Percec, V.; Wilson, P.; Haddleton, D. M., Copper(II)/Tertiary Amine Synergy in Photoinduced Living Radical Polymerization: Accelerated Synthesis of *ω*-Functional and *α,ω*-Heterofunctional Poly(Acrylates). *J. Am. Chem. Soc.* **2014,** *136* (3), 1141-1149.

244. Tasdelen, M. A.; Uygun, M.; Yagci, Y., Studies on Photoinduced ATRP in the Presence of Photoinitiator. *Macromol. Chem. Phys.* **2011,** *212* (18), 2036-2042.

245. Kermagoret, A.; Wenn, B.; Debuigne, A.; Jérôme, C.; Junkers, T.; Detrembleur, C., Improved Photo-Induced Cobalt-Mediated Radical Polymerization in Continuous Flow Photoreactors. *Polym. Chem.* **2015,** *6* (20), 3847-3857.

246. Zhao, Y.; Yu, M.; Zhang, S.; Liu, Y.; Fu, X., Visible Light Induced Living/Controlled Radical Polymerization of Acrylates Catalyzed by Cobalt Porphyrins. *Macromolecules* **2014,** *47* (18), 6238-6245.

247. Miao, X.; Zhu, W.; Zhang, Z.; Zhang, W.; Zhu, X.; Zhu, J., Photo-Induced Cobalt-Mediated Radical Polymerization of Vinyl Acetate. *Polym. Chem.* **2014,** *5* (2), 551-557.

248. Shanmugam, S.; Xu, J.; Boyer, C., Exploiting Metalloporphyrins for Selective Living Radical Polymerization Tunable over Visible Wavelengths. *J. Am. Chem. Soc.* **2015,** *137* (28), 9174-9185.

249. Gormley, A. J.; Yeow, J.; Ng, G.; Conway, Ó.; Boyer, C.; Chapman, R., An Oxygen-Tolerant PET-RAFT Polymerization for Screening Structure–Activity Relationships. *Angew. Chem. Int. Ed.* **2018,** *57* (6), 1557-1562.

250. Yeow, J.; Shanmugam, S.; Corrigan, N.; Kuchel, R. P.; Xu, J.; Boyer, C., A Polymerization-Induced Self-Assembly Approach to Nanoparticles Loaded with Singlet Oxygen Generators. *Macromolecules* **2016,** *49* (19), 7277-7285.

251. Chen, T.; Xu, Y.; Peng, Z.; Li, A.; Liu, J., Simultaneous Utilization of a Bifunctional Ruthenium Complex as an Efficient Catalyst for RAFT Controlled Photopolymerization and a Sensing Probe for the Facile Fabrication of an ECL Platform. *Polym. Chem.* **2016,** *7* (37), 5880-5887.

252. Bian, C.; Zhou, Y.-N.; Guo, J.-K.; Luo, Z.-H., Photoinduced Fe-Mediated Atom Transfer Radical Polymerization in Aqueous Media. *Polym. Chem.* **2017,** *8* (47), 7360-7368.

253. Pan, X.; Malhotra, N.; Dadashi-Silab, S.; Matyjaszewski, K., A Simplified Fe-Based PhotoATRP Using Only Monomers and Solvent. *Macromol. Rapid Commun.* **2017,** *38* (13), 1600651.

254. Dadashi-Silab, S.; Szczepaniak, G.; Lathwal, S.; Matyjaszewski, K., Iodine-Mediated PhotoATRP in Aqueous Media with Oxygen Tolerance. *Polym. Chem.* **2020,** *11* (4), 843-848.

255. Yilmaz, G.; Yagci, Y., Photoinduced Metal-Free Atom Transfer Radical Polymerizations: State-of-the-Art, Mechanistic Aspects and Applications. *Polym. Chem.* **2018,** *9* (14), 1757-1762.

256. Treat, N. J.; Sprafke, H.; Kramer, J. W.; Clark, P. G.; Barton, B. E.; Read de Alaniz, J.; Fors, B. P.; Hawker, C. J., Metal-Free Atom Transfer Radical Polymerization. *J. Am. Chem. Soc.* **2014,** *136* (45), 16096-16101.

257. Natarajan, P.; Ferraudi, G., Photochemical Properties of Copper(II)-Amino Acid Complexes. *Inorg. Chem.* **1981,** *20* (11), 3708-3712.

258. Tasdelen, M. A.; Uygun, M.; Yagci, Y., Photoinduced Controlled Radical Polymerization. *Macromol. Rapid Commun.* **2011,** *32* (1), 58-62.

259. Konkolewicz, D.; Schröder, K.; Buback, J.; Bernhard, S.; Matyjaszewski, K., Visible Light and Sunlight Photoinduced ATRP with ppm of Cu Catalyst. *ACS Macro Lett.* **2012,** *1* (10), 1219-1223.

260. Anastasaki, A.; Nikolaou, V.; Simula, A.; Godfrey, J.; Li, M.; Nurumbetov, G.; Wilson, P.; Haddleton, D. M., Expanding the Scope of the Photoinduced Living Radical Polymerization of Acrylates in the Presence of $CuBr_2$ and Me_6-Tren. *Macromolecules* **2014,** *47* (12), 3852-3859.

261. Anastasaki, A.; Nikolaou, V.; Pappas, G. S.; Zhang, Q.; Wan, C.; Wilson, P.; Davis, T. P.; Whittaker, M. R.; Haddleton, D. M., Photoinduced Sequence-Control Via One Pot Living Radical Polymerization of Acrylates. *Chem. Sci.* **2014,** *5* (9), 3536-3542.

262. Jones, G. R.; Whitfield, R.; Anastasaki, A.; Haddleton, D. M., Aqueous Copper(II) Photoinduced Polymerization of Acrylates: Low Copper Concentration and the Importance of Sodium Halide Salts. *J. Am. Chem. Soc.* **2016,** *138* (23), 7346-7352.

263. Frick, E.; Anastasaki, A.; Haddleton, D. M.; Barner-Kowollik, C., Enlightening the Mechanism of Copper Mediated PhotoRDRP Via High-Resolution Mass Spectrometry. *J. Am. Chem. Soc.* **2015,** *137* (21), 6889-6896.

264. Bhanu, V. A.; Kishore, K., Role of Oxygen in Polymerization Reactions. *Chem. Rev.* **1991,** *91* (2), 99-117.

265. Reddy, G. G.; Nagabhushanam, T.; Venkata Rao, K.; Santappa, M., Polymerization of Methyl Methacrylate in the Presence of Molecular Oxygen — a Kinetic Study. *Polymer* **1981,** *22* (12), 1692-1698.

266. Delzenne, G.; Toppet, S.; Smets, G., Photopolymerization of Acrylamide. I. Formation of the Initiating Redox System. *J. Polym. Sci.* **1960,** *48* (150), 347-355.

267. Miller, A. A.; Mayo, F. R., Oxidation of Unsaturated Compounds. I. The Oxidation of Styrene1. *J. Am. Chem. Soc.* **1956,** *78* (5), 1017-1023.

268. Mayo, F. R.; Miller, A. A., Oxidation of Unsaturated Compounds. II. Reactions of Styrene Peroxide1. *J. Am. Chem. Soc.* **1956,** *78* (5), 1023-1034.

269. Decker, C.; Jenkins, A. D., Kinetic Approach of Oxygen Inhibition in Ultraviolet- and Laser-Induced Polymerizations. *Macromolecules* **1985,** *18* (6), 1241-1244.

270. Xing, W.; Yin, G.; Zhang, J., *Rotating Electrode Methods and Oxygen Reduction Electrocatalysts*. Elsevier B.V.: **2014**.

271. Garton, A.; George, M. H., Effect of Oxygen on the Polymerization of Vinyl Chloride. I. Kinetic Features. *J. Macromol. Sci.: Polym. Chem. Ed.* **1973,** *11* (9), 2153-2167.

272. Matyjaszewski, K.; Coca, S.; Gaynor, S. G.; Wei, M.; Woodworth, B. E., Controlled Radical Polymerization in the Presence of Oxygen. *Macromolecules* **1998,** *31* (17), 5967-5969.

273. Matyjaszewski, K.; Beers, K. L.; Metzner, Z.; Woodworth, B., Controlled/Living Radical Polymerization in the Undergraduate Laboratories. 2. Using ATRP in Limited Amounts of Air to Prepare Block and Statistical Copolymers of N-Butyl Acrylate and Styrene. *J. Chem. Educ.* **2001,** *78* (4), 547.

274. Yeow, J.; Chapman, R.; Gormley, A. J.; Boyer, C., Up in the Air: Oxygen Tolerance in Controlled/Living Radical Polymerisation. *Chem. Soc. Rev.* **2018,** *47* (12), 4357-4387.

275. Liarou, E.; Anastasaki, A.; Whitfield, R.; Iacono, C. E.; Patias, G.; Engelis, N. G.; Marathianos, A.; Jones, G. R.; Haddleton, D. M., Ultra-Low Volume Oxygen Tolerant Photoinduced Cu-RDRP. *Polym. Chem.* **2019,** *10* (8), 963-971.

276. Liarou, E.; Whitfield, R.; Anastasaki, A.; Engelis, N. G.; Jones, G. R.; Velonia, K.; Haddleton, D. M., Copper-Mediated Polymerization without External Deoxygenation or Oxygen Scavengers. *Angew. Chem. Int. Ed.* **2018,** *57* (29), 8998-9002.

277. Marathianos, A.; Liarou, E.; Hancox, E.; Grace, J. L.; Lester, D. W.; Haddleton, D. M., Dihydrolevoglucosenone (Cyrene™) as a Bio-Renewable Solvent for Cu(0)Wire-Mediated Reversible Deactivation Radical Polymerization (RDRP) without External Deoxygenation. *Green Chem.* **2020,** *22* (17), 5833-5837.

278. Acar, A. E.; Yağci, M. B.; Mathias, L. J., Adventitious Effect of Air in Atom Transfer Radical Polymerization: Air-Induced (Reverse) Atom Transfer Radical Polymerization of Methacrylates in the Absence of an Added Initiator. *Macromolecules* **2000,** *33* (21), 7700-7706.

279. Iwata, H.; Hata, Y.; Matsuda, T.; Ikada, Y., Initiation of Radical Polymerization by Glucose Oxidase Utilizing Dissolved Oxygen. *J. Macromol. Sci. Part A: Polym. Chem.* **1991,** *29* (8), 1217-1218.

280. Oytun, F.; Kahveci, M. U.; Yagci, Y., Sugar Overcomes Oxygen Inhibition in Photoinitiated Free Radical Polymerization. *J. Macromol. Sci. Part A: Polym. Chem.* **2013,** *51* (8), 1685-1689.

281. Enciso, A. E.; Fu, L.; Russell, A. J.; Matyjaszewski, K., A Breathing Atom-Transfer Radical Polymerization: Fully Oxygen-Tolerant Polymerization Inspired by Aerobic Respiration of Cells. *Angew. Chem. Int. Ed.* **2018,** *57* (4), 933-936.

282. Wang, Y.; Fu, L.; Matyjaszewski, K., Enzyme-Deoxygenated Low Parts Per Million Atom Transfer Radical Polymerization in Miniemulsion and Ab Initio Emulsion. *ACS Macro Lett.* **2018,** *7* (11), 1317-1321.

283. Enciso, A. E.; Fu, L.; Lathwal, S.; Olszewski, M.; Wang, Z.; Das, S. R.; Russell, A. J.; Matyjaszewski, K., Biocatalytic "Oxygen-Fueled" Atom Transfer Radical Polymerization. *Angew. Chem. Int. Ed.* **2018,** *57* (49), 16157-16161.

284. Liarou, E.; Han, Y.; Sanchez, A. M.; Walker, M.; Haddleton, D. M., Rapidly Self-Deoxygenating Controlled Radical Polymerization in Water Via in Situ Disproportionation of Cu(I). *Chem. Sci.* **2020,** *11* (20), 5257-5266.

285. Mosnáček, J.; Ilčíková, M., Photochemically Mediated Atom Transfer Radical Polymerization of Methyl Methacrylate Using Ppm Amounts of Catalyst. *Macromolecules* **2012,** *45* (15), 5859-5865.

286. Borská, K.; Moravčíková, D.; Mosnáček, J., Photochemically Induced Atrp of (Meth)Acrylates in the Presence of Air: The Effect of Light Intensity, Ligand, and Oxygen Concentration. *Macromol. Rapid Commun.* **2017,** *38* (13), 1600639.

Chapter 2: *Controlling the particle size in surfactant-free latexes from ω-functional propenyl oligomers obtained through catalytic chain transfer polymerization*

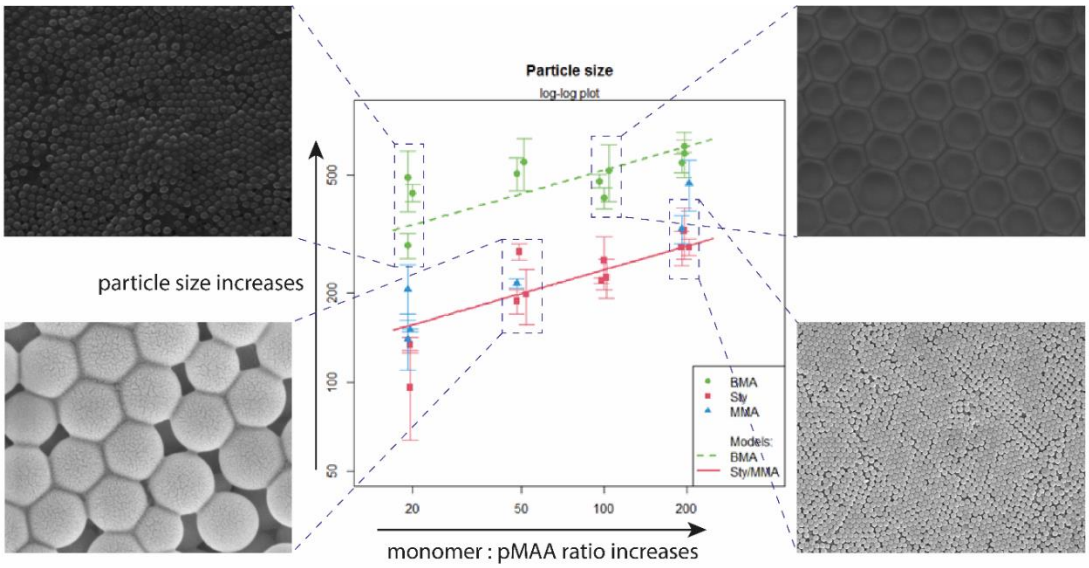

CCTP • surfactant free • colloidal stability • particle size control

The surfactant-free emulsion polymerization of styrene (St), butyl methacrylate (BMA) and methyl methacrylate (MMA) was conducted under starved-feed conditions in the presence of ω-propenyl functional poly(methacrylic acid) (pMAA) oligomers, obtained through catalytic chain transfer polymerization (CCTP), as stabilizer. A range of monomer to oligomer molar ratios were used, which resulted in stable latexes without any sign of coagulation even after standing for more than two years at ambient temperature. Moreover, the effect of substituting pMAA for a non-ionic stabilizer (poly(glycerol monomethacrylate), p(GMMA)) or a low molar mass ionic surfactant (sodium dodecyl sulfate, SDS) on the final properties of the latex was evaluated. Kinetic studies gave insight into the process through which the stabilization occurs, indicating that in the initial stages monomeric radicals react with the oligomer to form amphiphilic copolymers. Subsequently, micelles formed from these

copolymers swell with the additional monomer, which then polymerizes through a free radical mechanism. Thermogravimetric analysis (TGA) showed that the polymers have thermal stability up to 420 °C, whilst differential scanning calorimetry (DSC) revealed copolymer compatibility only at low monomer to oligomer molar ratios. Finally, static and dynamic light scattering techniques (SLS and DLS) and scanning electron microscopy (SEM) were used for the determination of the particle size, particle size distributions, and the development of a linear regression model to summarize the particle size characterization, according to which an increase in monomer to oligomer ratio by a factor of x is associated with a proportional increase in particle volume.

2.1 Introduction

Emulsion polymerization is a well-established process that provides many advantages for the synthesis of latex materials, both in academia and industry.[1, 2] The main characteristic of this process is the formation of a polymer in an aqueous dispersion, which can be used in a range of applications depending on the colloidal and physicochemical properties of the polymer latex.[3-6] Although emulsion polymerization is conventionally applied to free-radical processes, it has also been explored using controlled/living radical polymerization techniques,[7-10] such as atom transfer radical polymerization (ATRP),[11-13] nitroxide mediated polymerization (NMP),[14-16] reversible addition-fragmentation chain transfer (RAFT) polymerization,[17-20] with RAFT seemingly being the most efficient under emulsion conditions. In conventional emulsion polymerization, low molar mass surfactants are employed to act as stabilizers,[21] preventing coagulation of the latex particles and providing the conditions for sufficient colloidal stability through an electrostatic and/or steric stabilization mechanism.[22] However, these residual surfactants can affect the quality of the final material, such as by compromising the water barrier properties of polymer latex films, thus accumulatively deteriorating the film quality.[23-25] In this context, Jiang *et al.* reported that the water solubility of polymers and their diffusion coefficient are proportional to the extent of water whitening and found that both were higher when SDS was used as the surfactant.[26] Furthermore, these films become opaque because of the different refractive indices of the dried polymer film and the water clusters formed from the absorbed water during the drying process.[27] The physically adsorbed surfactant molecules on the surface of the latex particle migrate during film formation, therefore getting unevenly distributed throughout the film.[28] Heterogeneous distributions due to the accumulation of surfactant at the top of a film can reduce its gloss and increase tackiness,[23] as well as affect its adhesive properties (*i.e.* peel strength), depending on the type and concentration of the surfactant used.[29, 30] The surfactant type and concentration also has a significant impact on the water uptake and water sensitivity of a latex film.[31]

In order to avoid the negative impact of commercial surfactants on polymer latex films, several strategies have been developed to synthesize 'surfactant-free latexes'. RAFT polymerization-induced self-assembly (PISA)[32-38] has evolved as a

versatile approach for surfactant-free emulsion or dispersion polymerization through the use of hydrophilic macroRAFT agents. Several studies on hydrophilic macroRAFT agents' potential for the stabilization of latexes have been conducted. For instance, Velasquez *et al.* synthesized surfactant-free poly(vinylidene chloride-*co*-methyl acrylate) latexes using an anionic macroRAFT agent based on poly(sodium 4-styrenesulfonate) (pSSNa). They reported that films prepared from these emulsions were transparent, and did not whiten even after immersion in water for 2 hours at 95 °C.[39] Martin-Fabiani *et al*. presented a study comparing the water sorption properties of films prepared from surfactant-free latexes stabilized by poly(methacrylic acid) (pMAA) and pSSNa macroRAFT agents, showing that films cast from pSSNa dispersion had absorbed only 4 wt.% of water after immersion in water for 3 days.[40] This value is five times lower than what was found for the films cast from pMAA dispersions, highlighting the impact of the macroRAFT agent`s type on the water barrier properties of the films. In addition, in a more recent work the same group performed *in situ* and *ex situ* small-angle neutron scattering (SANS) experiments to follow the formation of films, which differ in the nature of the stabilizer (*d*-pMAA or *d*-SDS), providing valuable insights into the way that the stabilizer mobility affects the structure of films and their properties.[41] Schreur-Piet *et al.* used pMAA oligomers and co-oligomers as precursors to stabilizers, synthesized through Co-mediated catalytic chain transfer polymerization (CCTP), and examined the influence of the chain length and their concentration on the particle size of latex particles and on the stability of the final formulation, as well as their rheological characteristics.[42, 43]

CCTP in particular is a very efficient technique for the synthesis of α-protic ω-unsaturated functional oligomers, of which the chemistry and applications have been explored by both industrial[44-46] and academic research groups.[47-51] These oligomers can be used as chain transfer agents for sequence-controlled multiblock copolymers,[52-55] for post-polymerization modifications,[56] and as stabilizers in emulsion polymerizations resulting in polymers with complex architectures.[57-59] Despite their versatility, there is limited research on the behavior of these reactive oligomers as emulsion stabilizers, and consequently, the effect of their composition and concentration on film formation has been overlooked. Therefore, there is a need for a better understanding of their potential as efficient stabilizers in the production of waterborne polymer colloids.

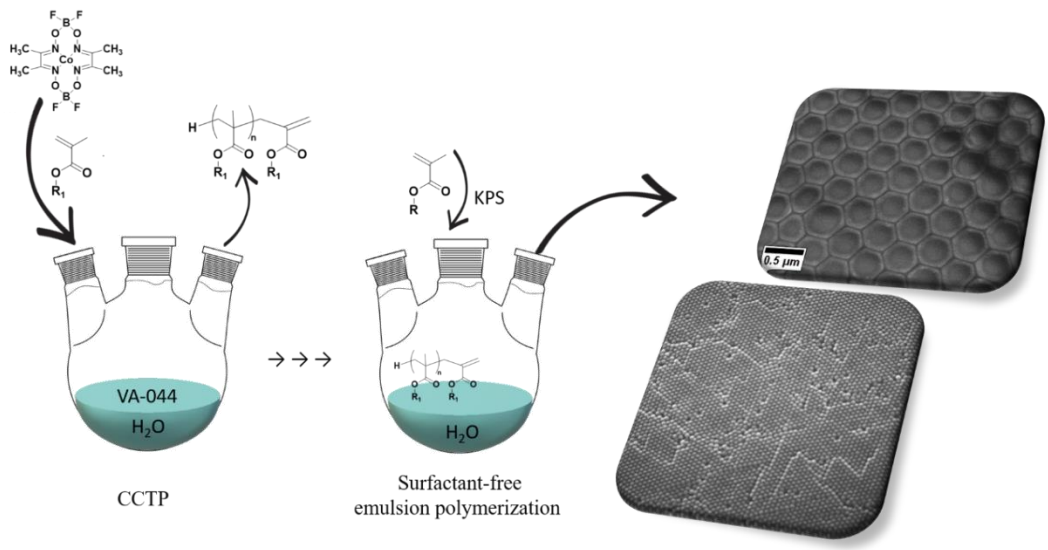

Scheme 2-1. Synthesis of ω-propenyl functional oligomers through CCTP and surfactant-free emulsion polymerization process for the preparation of monodisperse latex particles.

In this chapter, the impact of hydrophobic species and stabilizer type on the final latex are investigated, in addition to the process through which stabilization occurs. The introduction of hydrophobic monomers into aqueous solutions of a CCTP macromonomer (pMAA) resulted in latexes that were stable for over 2 years (**Scheme 2-1**). The effect of substituting pMAA for poly(glycerol monomethacrylate) (pGMMA) on the final properties of the latex was also examined. A kinetic study showed that hydrophobic monomer radicals first react with the CCTP macromonomers, leading to *in situ* amphiphilic copolymers that swell with additional monomer and polymerize through a free radical process. TGA and DSC enabled us to examine the thermal properties of the polymers. Moreover, by weighting the results by different orthogonal characterization methods (SEM, DLS, SLS), we present a statistical method to explain particle size variations due to hydrophobic monomer selection.

2.2 Results and discussion

2.2.1 Synthesis of hydrophilic oligomers through CCTP

Our initial aim was to investigate the synthesis of waterborne polymer colloids (latexes), formed through the introduction of hydrophobic monomers into homogeneous solutions of hydrophilic ω-propenyl functional oligomers. As such, pMAA "macromonomers" were synthesized in aqueous solution, following previous work from our group.[60] A solution of CoBF dissolved in monomer was fed into the reaction, and a low decomposition temperature initiator ($t_{\frac{1}{2}}$(10 hrs) = 44 °C) was used, in order to avoid exposing the catalyst to high temperatures in acidic conditions, which can lead to degradation and loss of activity. The aqueous polymerization of pGMMA led to a highly viscous solution and poor control over the molecular weight, possibly due to limited catalyst diffusion. Therefore, pGMMA was synthesized in methanol solution and it is noted that no transesterification was detected by ^{1}H NMR.

The obtained oligomers were analysed by SEC and ^{1}H NMR (**Table 2-1 & Figures 2-1 to 2-4).** ^{1}H NMR was used to determine that the pMAA oligomer had a DP_n = 21 (M_n= 1,900 g mol^{-1}) through integration of the unsaturated propenyl end group protons (region at 5.5 – 6.5 ppm) relative to the backbone protons (region 0.5-2.2 ppm). The pGMMA oligomer was obtained at a slightly higher molecular weight, based on SEC analysis, likely due to oligomers being removed during dialysis purification steps.

Table 2-1. SEC and ^{1}H NMR analysis of oligomers obtained through CCTP.

Oligomer	Mon. Conv. (%) [a]	DP_n [a]	$M_{n,\,NMR}$ (g mol^{-1}) [a]	$M_{n,\,SEC}$ [b]	$Đ$ [b]
pMAA	**100**	**21**	**1,900**	**1,900**	**2.0**
pGMMA	**70**	**10**	**1,600**	**4,200**	**1.7**

[a] Conversion was calculated *via* ^{1}H NMR in DMSO-d_6 for pMAA and in Methanol-d_4 for pGMMA.[b] Determined by DMF-SEC analysis and expressed as molecular weight relative to pMMA narrow molecular weight standards.

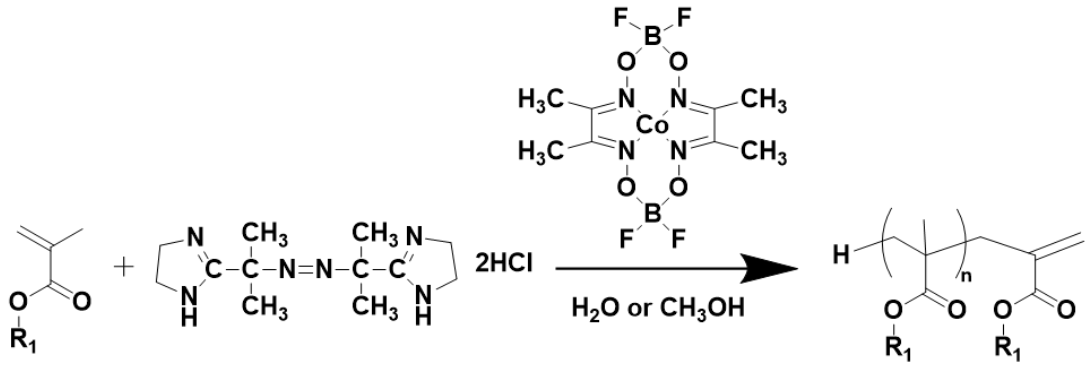

R_1 = -H, -$CH_2CH(OH)CH_2OH$

Figure 2-1. Reaction scheme for the CCTP of both MAA and GMMA.

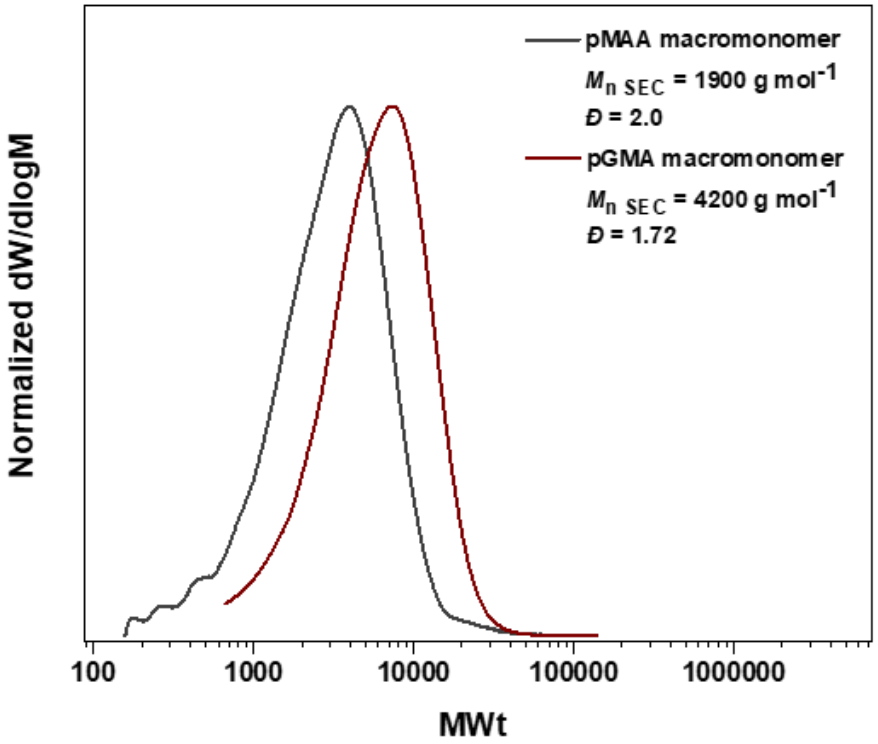

Figure 2-2. DMF-SEC derived molecular weight distributions showing the evolution of MWts of pMAA and pGMMA oligomers.

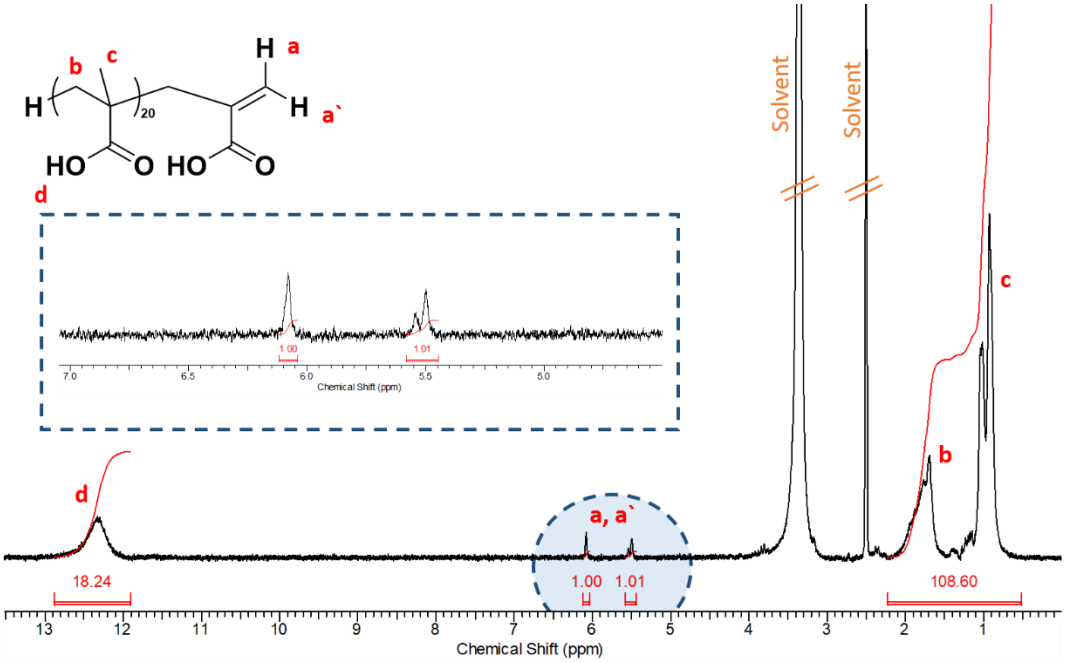

Figure 2-3. ^{1}H NMR (400 MHz) spectrum of pMAA in DMSO-d_6. DP and M_n were calculated through integration of the unsaturated propenyl end group protons (region at ~ 5.5 – 6.5 ppm relative to the backbone protons (region 0.5-2.2 ppm).

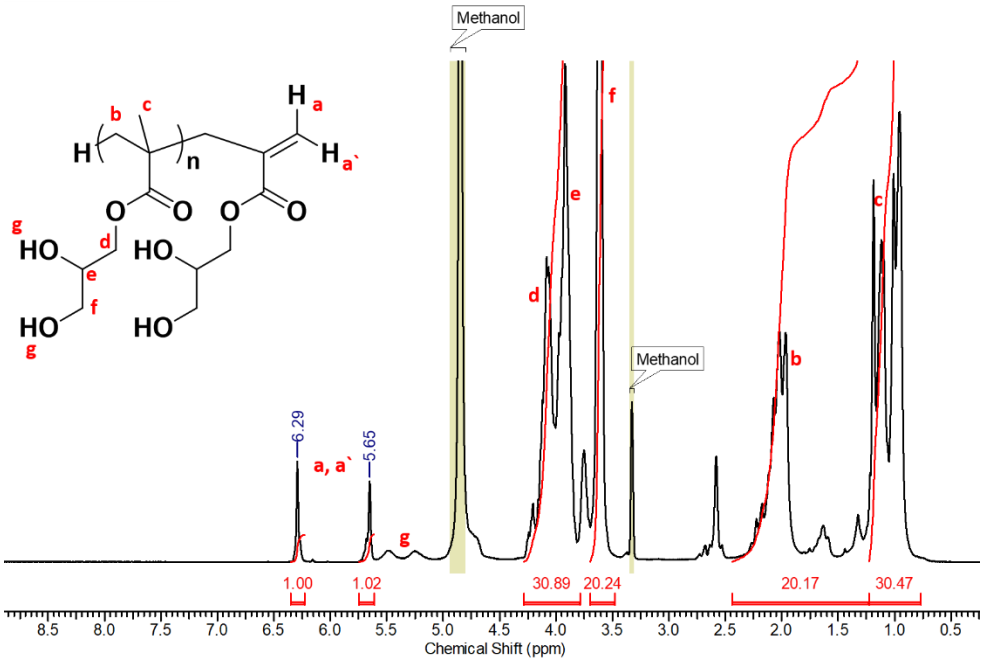

Figure 2-4. ^{1}H NMR (400 MHz) spectrum of pGMMA. DP and M_n were calculated through integration of the unsaturated propenyl end group protons (region at 5.5 – 6.5 ppm) relative to the protons of glycerol group (region 3.5 – 4.5 ppm). The spectrum was taken after removal of excess methanol and before the dialysis purification steps.

2.2.2 Kinetic study of surfactant-free emulsion polymerization of styrene

In order to explore the ability of pMAA oligomers to perform as stabilizers in the surfactant-free emulsion polymerization of hydrophobic monomers, kinetic studies under starved feed conditions were conducted (St: pMAA = 50: 1), where St and KPS were fed into a PBS solution of pMAA (pH = 7). At a pH lower than its pK_a (5.9)[39] most of the pMAA chains are uncharged, which translates into a lower hydrophilicity. By using PBS (pH=7) as the solvent, the sodium salt of the macromonomer was formed, which is highly water soluble and better able to act as a stabilizer. Aliquots were taken at regular intervals for characterization as shown in **Table 2-2**.

Table 2-2. Characterization of samples taken during kinetic studies of surfactant-free emulsion polymerization of styrene stabilized by pMAA.

Entry	Time (min)	Monomer added (g) [a]	Solid Content (%)	Particle Size (nm) [b]	St. Dev. (nm) [b]	ACC[c]
A1	0	0.00	9.180	1	0.3	1.00
A2	12.5	0.27	9.970	2	0.4	0.90
A3	25	0.54	10.84	-	-	0.77
A4	30	0.65	11.10	14	1.7	0.75
A5	35	0.76	11.41	91	16	0.66
A6	40	0.87	11.72	79	17	0.67
A7	45	0.97	12.03	92	24	0.66
A8	50	1.08	12.32	94	29	0.66
A9	60	1.30	12.94	113	35	0.57
A10	90	1.95	14.69	162	46	0.53
A11	120	2.60	16.38	207	49	0.44
A12	180	3.89	19.50	288	81	0.23
A13	240	5.19	22.42	420	107	0.22
A14	300	5.19	22.42	416	127	0.19

m_{pMAA} = 2.0 g, n_{pMAA} = 0.001 mol, m_{KPS} = 67.6 mg, n_{KPS} = 0.25 mmol, m_{St} = 5.19 g, n_{St} = 0.05 mol.
[a] Determined from the volume of monomer added. [b] Particle size and St. Dev. were determined by DLS.
[c] Determined by ^{1}H NMR analysis based on equation 1.

The SEC results show that for the first 50 minutes of feeding St, we observe a gradual shift in the mass of oligomer peak to higher molecular weight (**Figure 2-5**). This indicates that St radicals are reacting with the pMAA oligomer, by statistical copolymerization or potentially through an end-capping mechanism.[61, 62] After 50 minutes, we see evidence of a second higher molecular weight distribution forming, along with a continued increase in the oligomer peak molecular weight. Therefore, we hypothesized that the higher molecular weight peak is from conventional free-radical polymerization occurring within styrene swollen p(MAA- *co*-St) micelles. In order to verify our hypothesis and further investigate the mechanism through which latex stabilization occurs, the kinetic studies were followed by ^{1}H NMR (**Figure 2-6**). Of particular interest was how the magnitude of the olefinic protons of pMAA changes relative to the backbone methyl protons (**Figure 2-7**), which would indicate the coupling of pMAA with propagating styrenic radicals. The intensity of the olefinic proton peaks decreases relative to

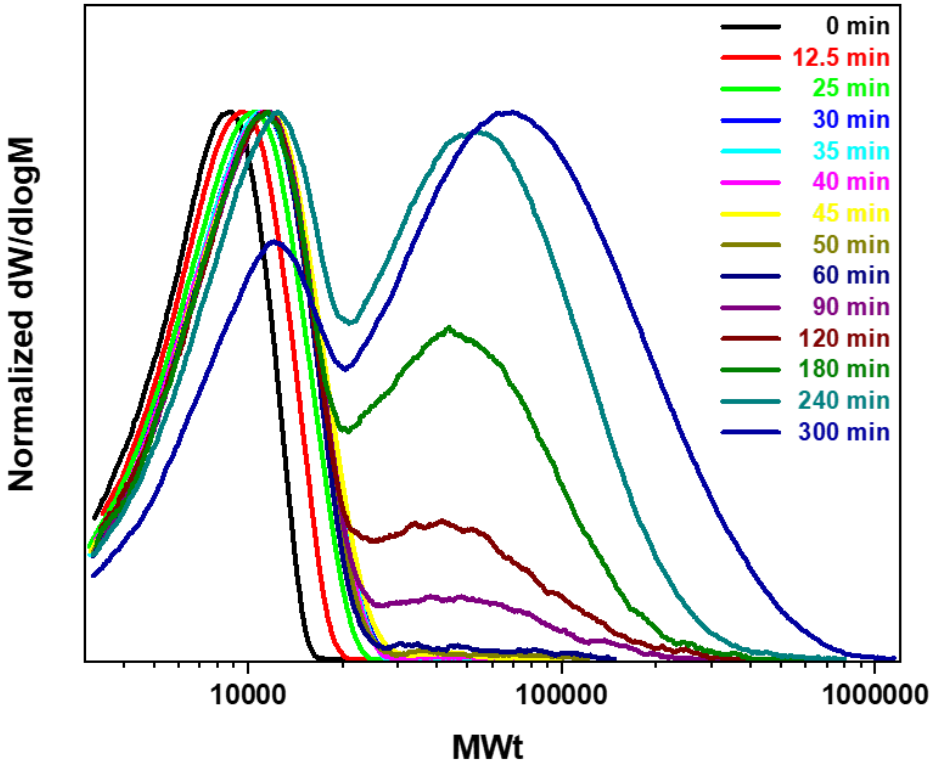

Figure 2-5. DMF-SEC derived molecular weight distributions showing the evolution of molecular weight.

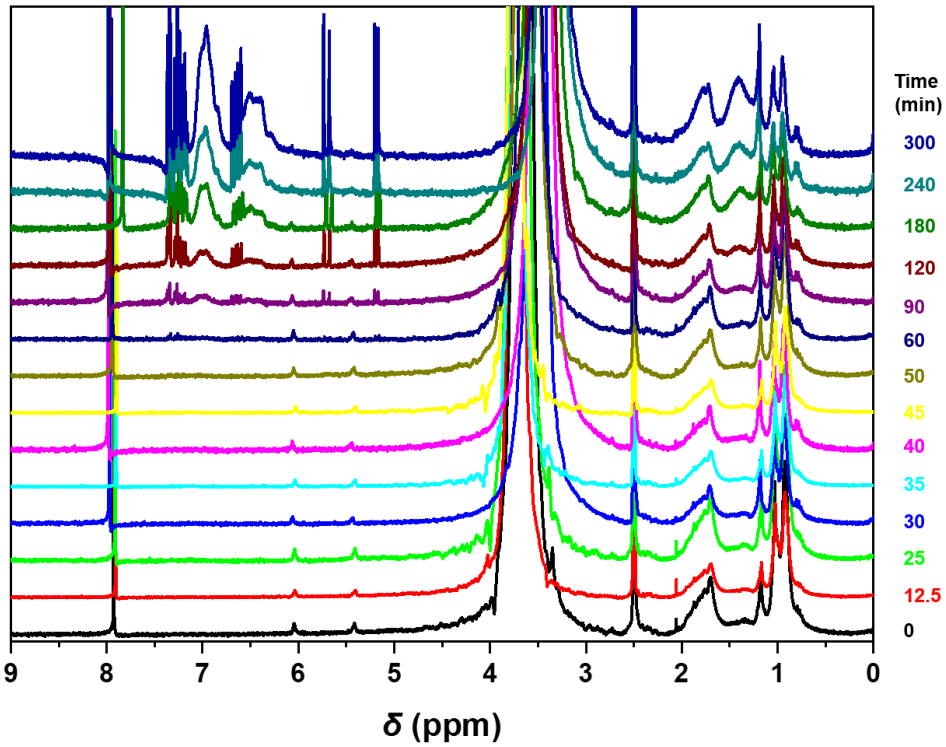

Figure 2-6. ^{1}H NMR (400 MHz) spectra of aliquots taken during the kinetic study of surfactant-free emulsion polymerization of styrene.

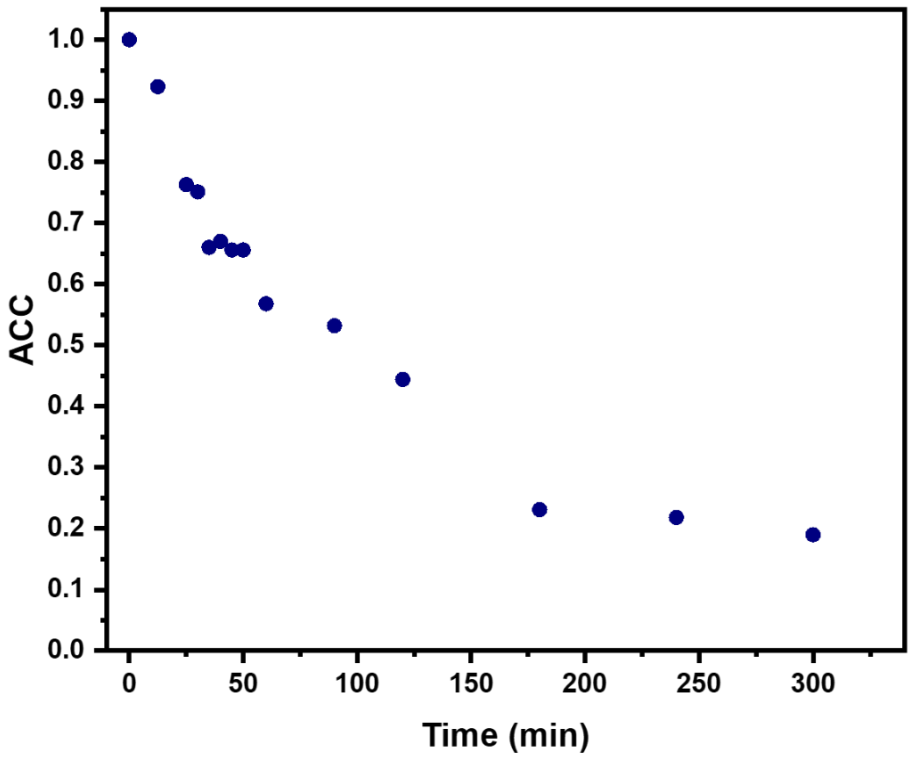

Figure 2-7. Change in ACC with time, calculated using Eq. 1 (values are given in **Table 2-2**).

the signal from the backbone CH_3 protons of the oligomer, indicating that their concentration is decreasing. The consumption of the pMAA end group through coupling with styrene (ACC)[62] was calculated as:

$$ACC = \frac{\int H_{cis,t}}{\int CH_{3,t}} \Big/ \frac{\int H_{cis,0}}{\int CH_{3,0}}, \qquad \text{Eq. 1}$$

where $H_{cis,t}$ and $H_{cis,0}$ are the cis olefinic protons of pMAA at time t and before the reaction, respectively, and $CH_{3,t}$ and $CH_{3,0}$ are the corresponding backbone methyl protons.

In order to monitor the evolution of particle size during the kinetic experiment, DLS measurements were conducted, where all the samples taken throughout the polymerization had monomodal distributions (**Figures 2-8 & 2-9**). After the initial particle formation from the homogeneous pMAA solution (50 minutes), a steady increase in particle size and a broader size dispersity is apparent. This correlates well with the SEC and NMR data, which suggest that in the initial stages (<50 minutes) the styrene is combining with the macromonomer to

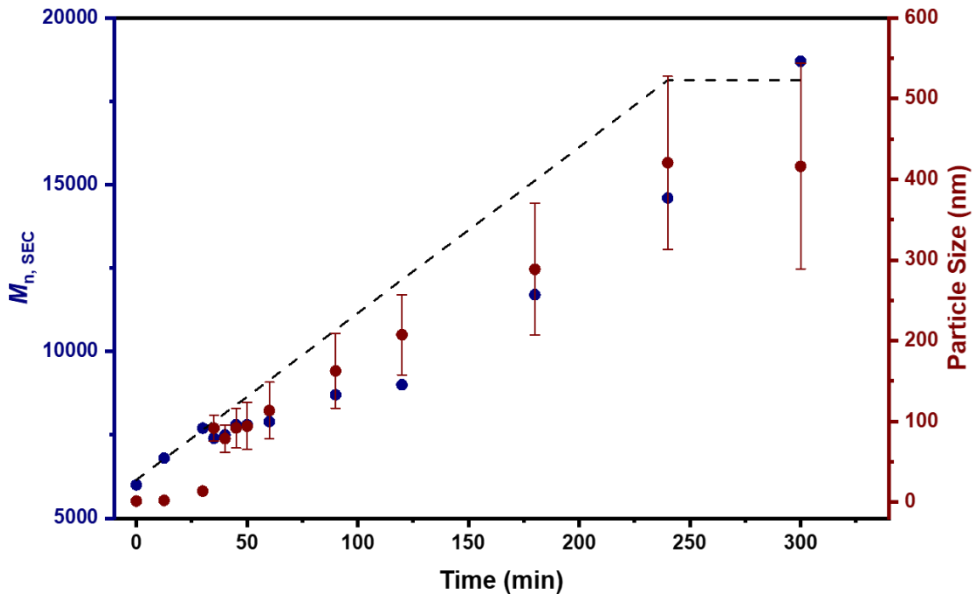

Figure 2-8. Average M_n and particle size values against time derived from SEC and DLS analysis respectively, along with feeding profile (24.4 μL min^{-1}) of styrene (dashed line).

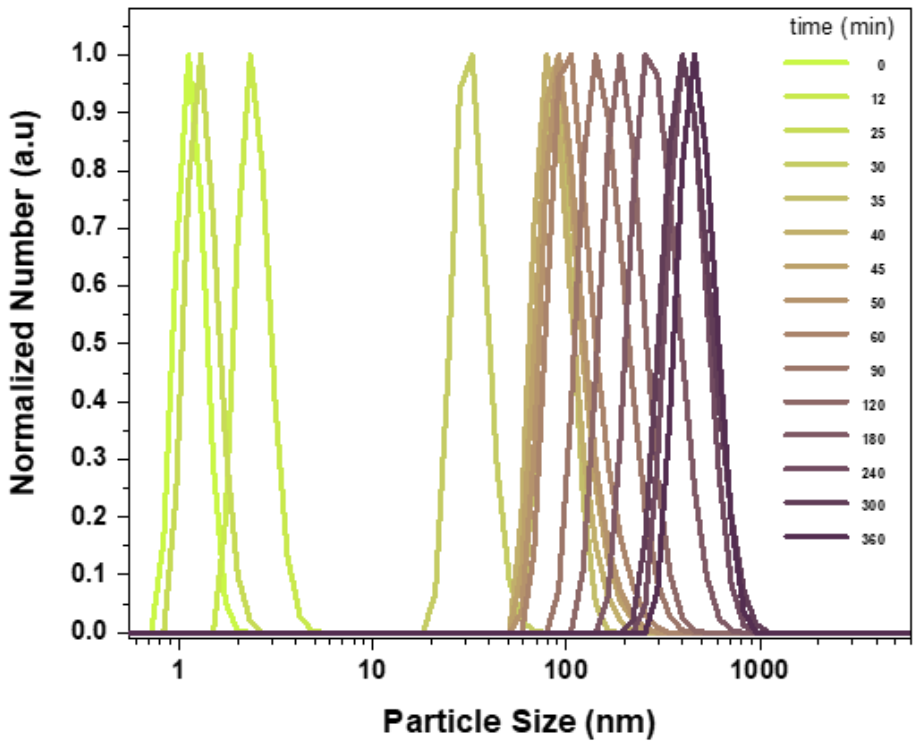

Figure 2-9. Evolution of particle size distributions from aliquots taken during the kinetic study of surfactant-free emulsion polymerization of styrene.

form a surfactant *in situ*, and subsequently these p(MAA-*co*-St) micelles swell with St and polymerize through a free-radical mechanism.

As the polymers from both pBMA and pMMA latexes were not soluble in any common solvent for SEC and ^{1}H NMR analysis without a post-polymerization methylation step, styrene was selected as the hydrophobic monomer for the kinetic experiments. However, the polymerization of methacrylic monomers in the presence of ω-propenyl functional oligomers can also result in addition-fragmentation chain transfer (AFCT) processes occurring, and so we were interested in investigating what happens after the addition of a methacrylate instead of styrene. Therefore, a latex formed from the addition of BMA under the same conditions as St was methylated using conditions that have been reported previously.[63] The SEC results, given in **Figure 2-10**, show a bimodal molecular weight distribution, indicating that broadly the same mechanism of particle formation observed when styrene was used, also occurs with methacrylates in these systems.

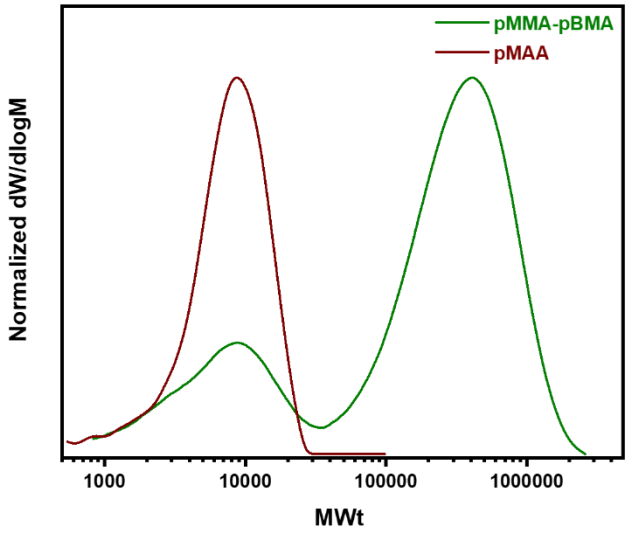

Figure 2-10. DMF-SEC with DRI detection derived molecular weight distributions showing the evolution of MWts of pMAA and the methylated pBMA latex.

2.2.3 Surfactant-free emulsion polymerization of hydrophobic monomers

Subsequent to the kinetic experiments, surfactant-free latexes of hydrophobic monomers (St, BMA and MMA) stabilized by pMAA oligomer were prepared. The molar ratio of these monomers to pMAA was varied to examine its effect on the final latex. Reactions with the highest molar ratio (200:1) were also repeated, substituting pMAA for pGMMA, in order to determine the impact of using a non-ionic stabilizer, and conventional emulsion polymerizations using SDS were also conducted as control experiments. During all polymerizations with pMAA as stabilizer in neutral pH conditions the subunits of pMAA were negatively charged, which facilitated the synthesis of stable latexes through electrostatic repulsion. To quantify the charge on the latex particle's surface, their zeta potential was measured, **Table 2-3** and in **Figure 2-11**. The zeta potential of pMAA latexes was in a range -32 mV to -36 mV, and these latexes showed good stability for more than two years when stored at room temperature. The zeta potential of the pGMMA stabilized latexes was around -6 mV, whereas the charge stabilization of the SDS stabilizer was -28.1 mV for the pSt latex, -23.7 mV for the pBMA latex and -16.5 mV for the pMMA latex.

Table 2-3. Zeta potential data for the latexes stabilized by pMAA, pGMMA and SDS 2 years after their synthesis.

Polymer	Zeta Potential (mV)	Zeta Potential St. Dev. (mV)
(L1) pSt_{20} [a]	-35	2.5
(L2) pSt_{50} [a]	-36	2.6
(L3) pSt_{100} [a]	-36	2.4
(L4) pSt_{200} [a]	-32	1.8
(L5) $pBMA_{20}$ [a]	n.d.[d]	n.d.
(L6) $pBMA_{50}$ [a]	-36	2.0
(L7) $pBMA_{100}$ [a]	-33	3.0
(L8) $pBMA_{200}$ [a]	n.d.[d]	n.d.
(L9) $pMMA_{20}$ [a]	-33	1.8
(L10) $pMMA_{50}$ [a]	-32	2.2
(L11) $pMMA_{100}$ [a]	-37	2.6
(L12) $pMMA_{200}$ [a]	-36	2.6
(L13) pSt_{200} [b]	-6	0.6
(L14) $pBMA_{200}$ [b]	-6	0.6
(L15) $pMMA_{200}$ [b]	-6	0.8
(L16) pSt [c]	-28.1	2.5
(L17) pBMA [c]	-23.7	2.8
(L18) pMMA [c]	-16.5	1.1

[a] Stabilized by pMAA. [b] Stabilized by pGMMA. [c] Stabilized by SDS, [d]n.d. = not determined.

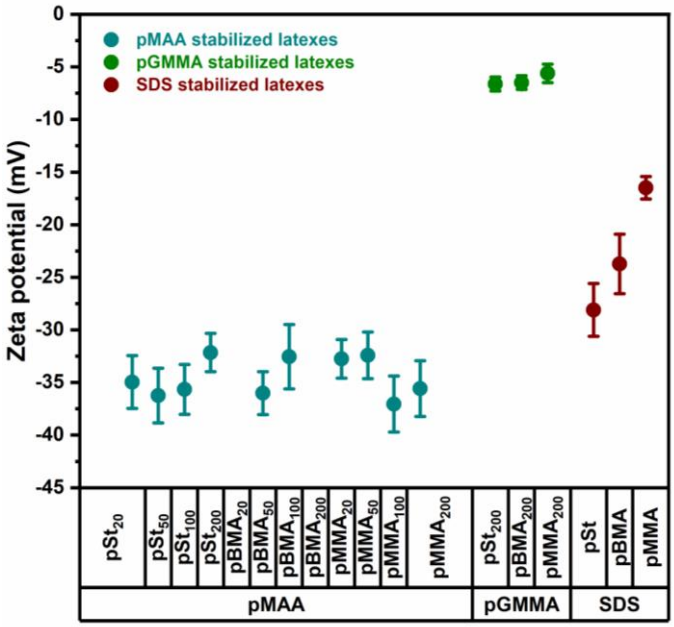

Figure 2-11. Zeta potential of the latexes stabilized by an ionic stabilizer (pMAA), a non-ionic (pGMMA) and the commercial available surfactant (SDS), 2 years after their synthesis.

SEC analysis of pSt latexes (**Figure 2-12**) show a clear shift of the pMAA oligomer peak to a higher molecular weight distribution, which confirms that the monomer is coupling with pMAA oligomer to form copolymers *in situ*. Subsequently, the p(MAA-*co*-St) micelles swell with the additional monomer, which polymerizes through a free radical mechanism. When the non-ionic pGMMA was used as stabilizer for the polymerization of St and BMA a similar mechanism to that observed when using pMAA appears to occur, as shown in the SEC traces in **Figure 2-13**.

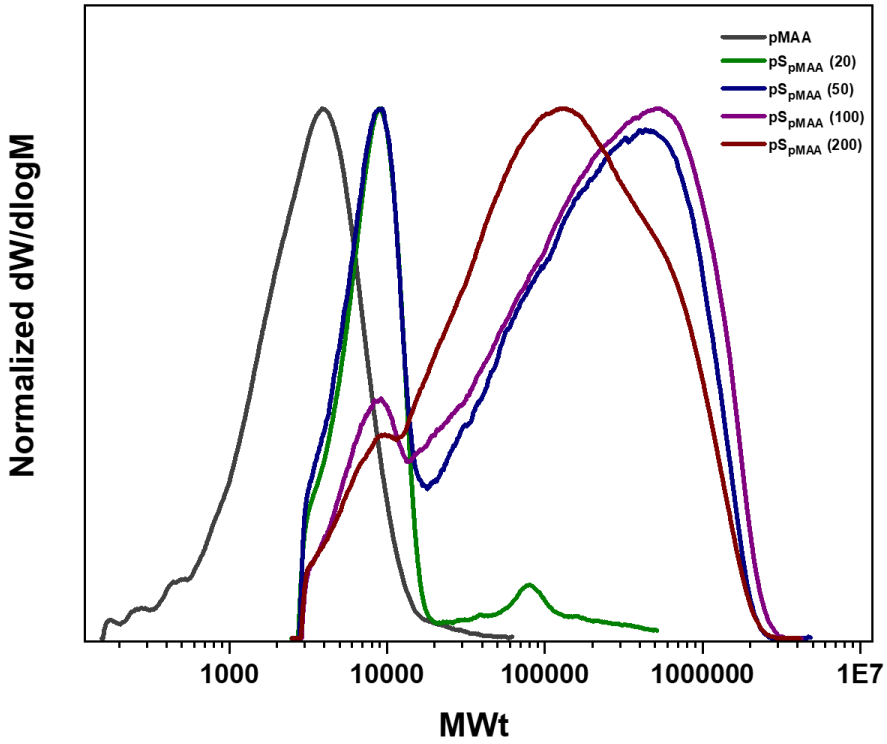

Figure 2-12. DMF-SEC with DRI detection derived molecular weight distributions showing the evolution of MWts of pSt latexes stabilized by pMAA oligomer.

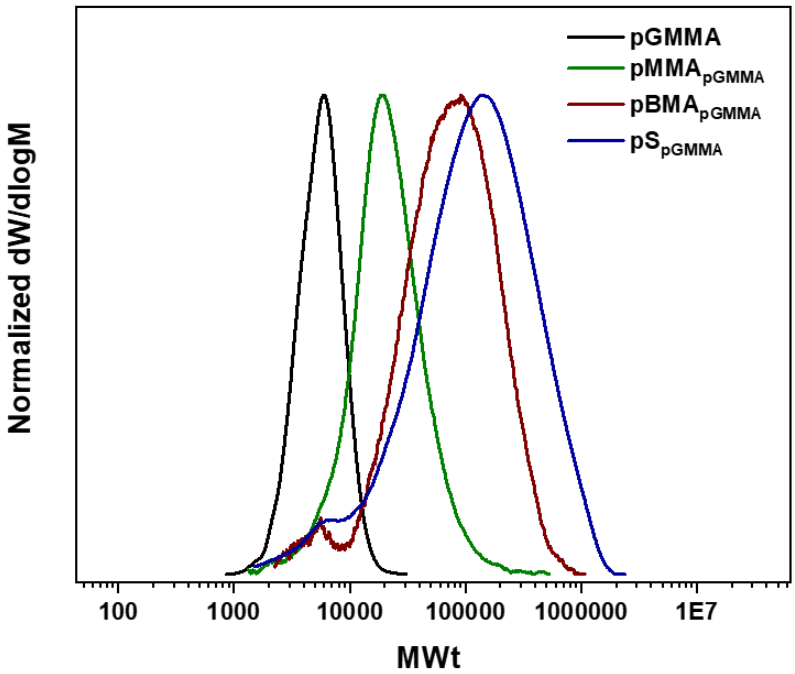

Figure 2-13. DMF-SEC with DRI detection derived molecular weights showing the evolution of MWts of pGMMA and latexes stabilized by pGMMA.

Furthermore, from the ^{1}H NMR spectra of the latexes stabilized by pGMMA, the ACC value tends to zero (**Figure 2-14**), indicating that ω-propenyl functional groups of pGMMA are consumed by the propagating St or BMA polymer chains. However, the pBMA and pMMA latexes prepared with pGMMA had poor colloidal stability, and sedimented after several weeks. This was attributed to the lower efficiency of the steric stabilization mechanism of pGMMA, in addition to their larger particle size, which is commonly observed in emulsion polymerizations stabilized by non-ionic surfactants.[64, 65]

When MMA was fed into an aqueous solution of either pMAA or pGMMA oligomers, we again observed a shift of the oligomer peak in the SEC trace to a higher molecular weight. However, in these examples the high molecular weight peak from free radical polymerization is of a significantly lower magnitude. This is most likely because of the higher water solubility of MMA, which lowers the fraction of the monomer that swells into the pMMA-oligomer micelles.

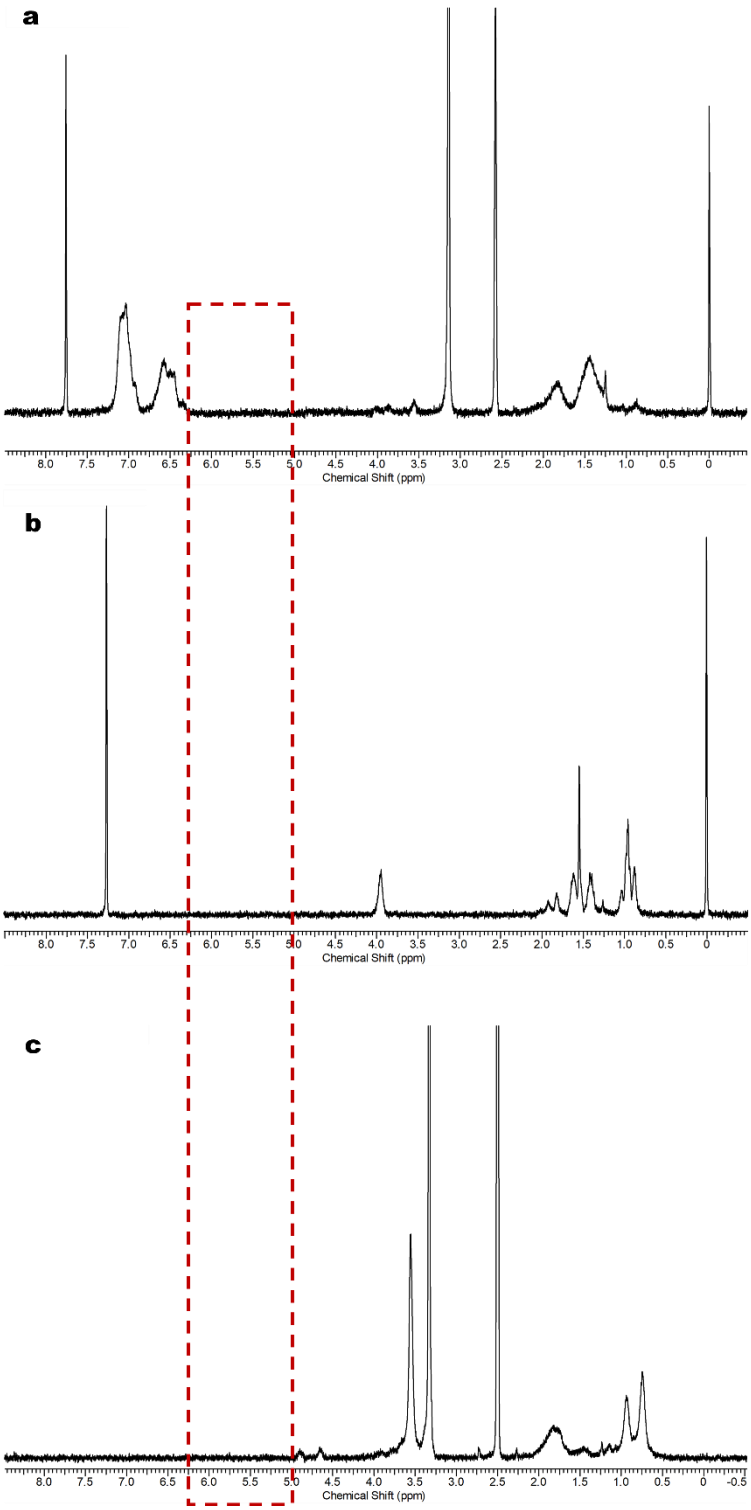

Figure 2-14. ^{1}H NMR (400 MHz) spectrum of a) pSt, b) pBMA and c) pMMA stabilized by pGMMA oligomer showing that ω-propenyl functional groups of pGMMA are consumed (there are no peaks attributed to olefinic protons in the dashed area).

In a similar study, by Heuts and colleagues, it was reported that the lower hydrophobicity of MMA inhibited the formation of a stable latex in their system.[42] The increased stability of our formed latexes might be attributed to the lower molecular weight of our pMAA stabilizer (1800 g/mol *vs* 6800 g/mol), which would lower the number of MMA units required to form micelles. However, we speculate that the predominant factor that leads to the formation of stable pMMA latexes is the higher temperature we applied for the reaction (86 °C *vs* 60 °C), as at this temperature MMA propagates faster, and therefore, will form hydrophobic chains more quickly. In order to verify this, the polymerization was repeated at 60 °C. During these reactions, large amounts of coagulum were observed prior to completion of MMA addition, which verifies our hypothesis on the importance of temperature during these reactions. It should be noted that poor colloidal stability was also observed when pGMMA was used as stabilizer for the pMMA latex, even at a reaction temperature of 86 °C, highlighting the effect of the electrostatic repulsion between pMAA units on latex stability.

The particle size of the latexes was determined by different orthogonal characterization methods (DLS, SLS and SEM) and the obtained data are shown in **Table 2-4**. DLS analysis of the latexes stabilized by pMAA show that, approximately, spherical and uniform particles and monomodal distributions are present in all cases (**Figure 2-15**), although the uncertainty associated with each estimate increases as the size of the particle increases. A general observation that can be made is that the particle size gradually increases as a higher monomer to stabilizer molar ratio is used, which is in agreement with previous studies on RAFT emulsion polymerizations in batch.[66, 67] In these studies, where exclusively diblock copolymers were prepared, the particle size was governed by the monomer to RAFT agent concentration ratio. Whereas, in our system a free radical process forms the polymer latex after the *in situ* formation of surfactants. However, the nature of the stabilizing moieties is similar in both experiments, and so when a larger [monomer]:[stabilizer] ratio is used, the same number of stabilizing groups is required to stabilize a larger volume of monomer, which leads to bigger particles.

The average particle size determined by static light scattering (SLS) is based on an analysis of variation in the scattering intensity, I, as a function of the magnitude

of the scattering vector, q. The SLS technique is more usually associated with the construction of a Zimm plot to estimate a particle size of the order $d < \lambda/10$, where λ is the wavelength of the illuminating laser.[68] However, our range of samples included particle sizes that were of the same order of magnitude as the laser wavelength (λ = 633 nm), so more appropriate models were utilized for the data analysis on a sample-by-sample basis, **Figures 2-25 to 2-27** (section 2.4.4).

Table 2-4. Particle size analysis by different orthogonal characterization methods (SEM, DLS and SLS) of latexes stabilized by an ionic stabilizer (pMAA), a non-ionic stabilizer (pGMMA) and a low molar mass surfactant (SDS).

Entry	Stabilizer	Monomer: Stabilizer	Particle Diameter (nm)		
			SEM	DLS	SLS
pSt_{20}	pMAA	20	n.d.	96 ± 32	134 ± 8
pSt_{50}	pMAA	50	276 ± 18	198 ± 42	188 ± 18
pSt_{100}	pMAA	100	226 ± 34	268 ± 26	220 ± 4.6
pSt_{200}	pMAA	200	286 ± 18	324 ± 64	286 ± 38
$pBMA_{20}$	pMAA	20	290 ± 28	490 ± 104	436 ± 28
$pBMA_{50}$	pMAA	50	n.d.	554 ± 110	506 ± 64
$pBMA_{100}$	pMAA	100	420 ± 34	520 ± 112	478 ± 24
$pBMA_{200}$	pMAA	200	550 ± 40	594 ± 104	626 ± 30
$pMMA_{20}$	pMAA	20	140 ± 30	206 ± 44	150 ± 2
$pMMA_{50}$	pMAA	50	n.d.	n.d.	216 ± 8
$pMMA_{100}$	pMAA	100	640 ± 76	730 ± 250	672 ± 114
$pMMA_{200}$	pMAA	200	330 ± 36	470 ± 92	502 ± 22
pSt_{200}	pGMMA	200	250 ± 22	n.d.	224 ± 52
$pBMA_{200}$	pGMMA	200	900 ± 126	1788 ± 402	1350 ± 382
$pMMA_{200}$	pGMMA	200	n.d.	646 ± 104	464 ± 86
pSt	SDS	-	42 ± 7	57 ± 0.52	n.d.
pBMA	SDS	-	92 ± 20	79 ± 0.34	n.d.
pMMA	SDS	-	n.d.	32 ± 0.15	n.d.

n.d. = not determined

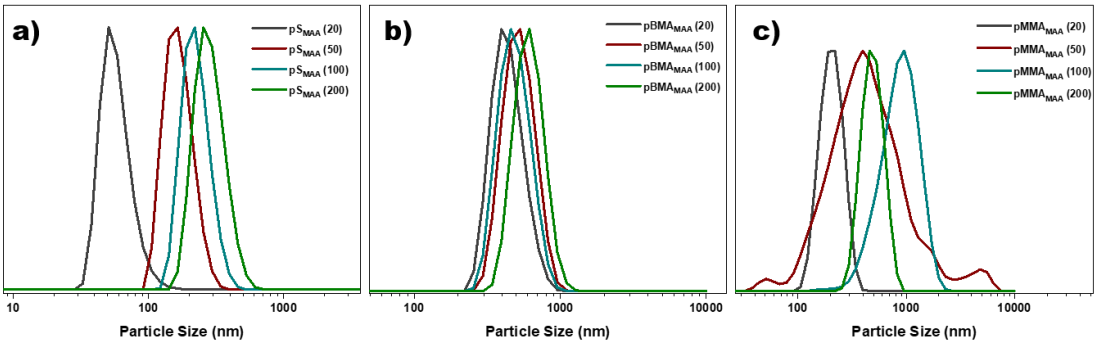

Figure 2-15. DLS particle size distributions of (a) pS and (b) pBMA and (c) pMMA latexes.

In some instances the data were consistent with a narrow particle size distribution (PSD), which is an indication of uniform latex particles; for other samples – the very largest particles – the uniformity of the sample could not be determined by SLS due to the superposition of sampling effects, **Figure 2-16**. Consequently, in these cases, average particle size by SLS was determined *via* a fit constrained such that the PSD was as indicated by DLS results.

In the pSt latexes, the uniformity of the samples is clear regardless of the hydrophilic stabilizer concentration that was used or its nature (pMAA or pGMMA) (**Figure 2-25**, section 2.4.4**)**. Moreover, an excellent match between the scattering behavior of the particles and the fitted model was observed in the case of pBMA stabilized by pMAA ([monomer]:[pMAA] ratio = 20 : 1) (**Figure 2-16g**), a pattern that is not followed when higher concentrations of BMA relative to pMAA were used (**Figure 2-26 a-c**). The effects of the stabilizers on the architecture of the final latexes can be observed in the SEM images (**Figure 2-16 a to f**), where it is apparent that the choice of the stabilizer has a significant impact on the size and uniformity of the latex particles. The SEM images indicate that the shape and size of the pSt particles remain consistent when both an ionic and a non-ionic stabilizer are used (**Figures 2-16 a & c and Figure 2-28**, section 2.4.4), resulting in well-packed, uniform and monodisperse particles after water evaporation, which naturally occurs during the sample preparation. The same pattern was observed when pMAA was used in the formation of pBMA latexes (**Figure 2-16d and Figure 2-29**, section 2.4.4), however, highly polydisperse particles with minimal packing ability were obtained with pGMMA (**Figure 2-16e**). In addition, in the pGMMA samples non-spherical particles with flattened surfaces and rounded edges are apparent. A contributing factor to the

observed morphology is likely the low T_g value (T_g = 31 °C) of these samples, which would cause deformation during sample preparation and under the electron beam during SEM measurements. Notably, very small particles (<100 nm) with poor packing and uneven distributions were

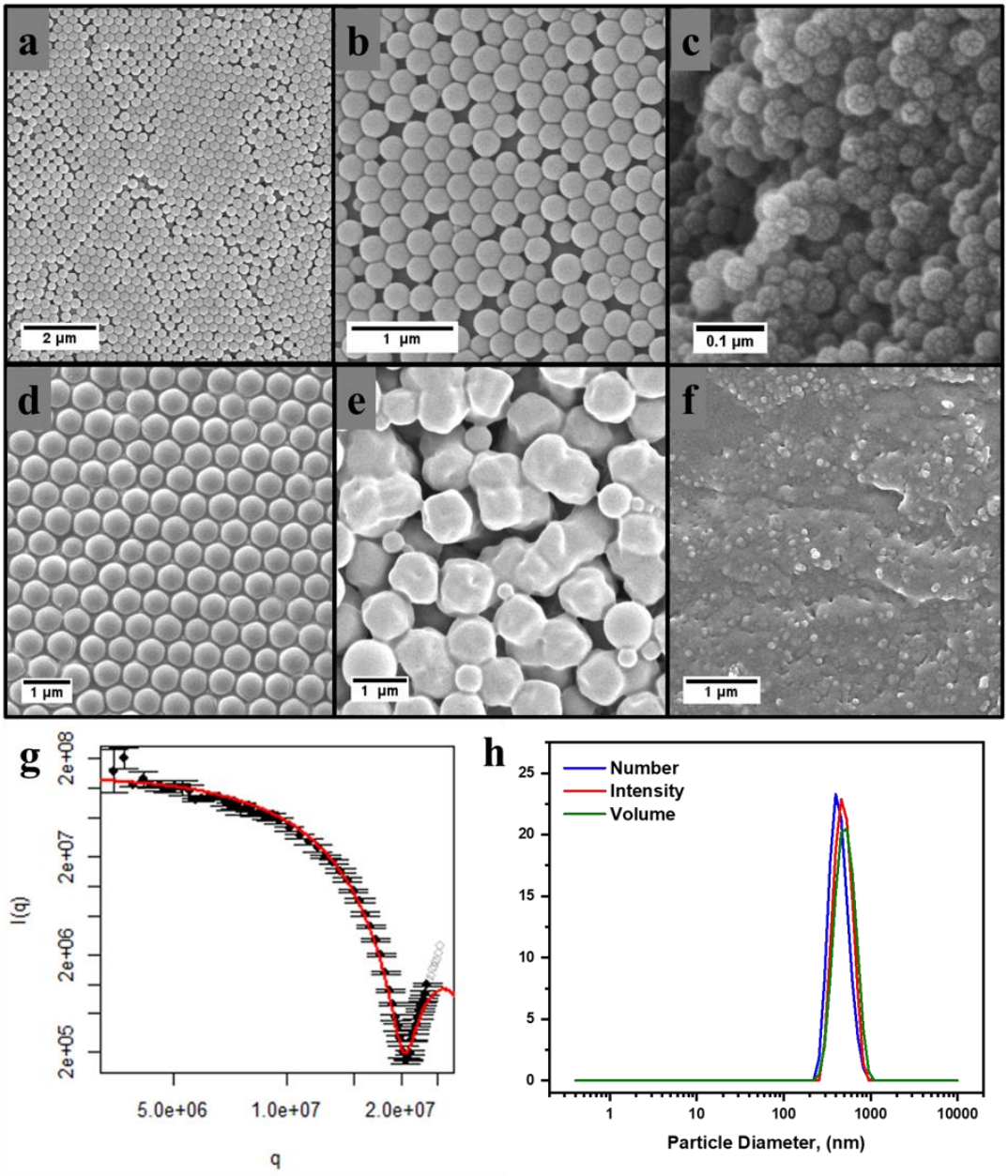

Figure 2-16. SEM images of latex particles of pSt (a-c) and pBMA (d-f), stabilized by pMAA (a and d), pGMMA (b and e) and SDS (c and f). SLS (g) and DLS (h) data for pBMA latex stabilized by pMAA with [BMA] : [pMAA] = 20, showing that the measurements are consistent with uniformly sized spheres. [Monomer] : [macromonomer] = 200 for pSt (a, d) and pBMA (b, e) latexes. For SDS stabilized latexes [SDS] = 0.5 mol% with respect to the monomer.

obtained when SDS was used with pSt (**Figure 2-16c**). The morphology of the pBMA particles stabilized by SDS was difficult to observe under SEM, as their low T_g caused the formation of a largely continuous film following sample preparation at room temperature. The pGMMA oligomer resulted in a different architecture of pMMA particles, as shown in **Figure 2-30** (section 2.4.4). the pGMMA-MMA nanoparticles coalesce to form large sponge-like particles, **Figure 2-30e**. It is also noteworthy that when a molar ratio MMA: pMAA = 50:1 was used, the behavior of the particles is different, where beaded chain like structures were observed under SEM (**Figure 2-30b**).

In order to explain the particle size behavior, all of the data collected by SEM, SLS and DLS were analyzed as one data set using R statistical software, having first omitted the measurements for one of the pMMA samples stabilized by pMAA (i.e. with [monomer]: [pMAA] ratio = 100) as a statistical outlier. **Figure 2-17** shows the estimated values for particle size by each technique for each latex stabilized by pMAA, indicating that a similar particle size was recorded for pSt and pMMA latexes, whilst a larger particle size was observed for pBMA. A linear regression model of the form $\ln(d) = \ln(RAT) + f$ was fitted to the data, weighted by the error associated with each estimated value, where d is particle diameter and RAT is monomer : pMAA ratio. In the final model, f was made a factor of two levels treating monomer type as either 'BMA' or 'St/MMA', since no statistical evidence was found to suggest that pSt and pMMA particles differ in size. According to the fitted model, for pSt or pMMA particles

$$d = \exp(4.27 \pm 0.14) \cdot RAT^{0.26\pm0.03},$$

and for pBMA particles

$$d = \exp(5.04 \pm 0.21) \cdot RAT^{0.26\pm0.03}.$$

Consequently, a pSt or pMMA particle made at monomer to oligomer ratio of 50 will be of diameter d ≈ 198 nm, while at the same monomer to oligomer ratio, pBMA particles will be diameter d ≈ 427 nm. Irrespective of monomer type, an increase in monomer to oligomer ratio by a factor of x is associated with a corresponding increase in particle size (diameter) by a factor $x^{0.26\pm0.03}$. This suggests that increasing the

monomer to oligomer ratio results in an approximately proportional increase to the volume of the particle. That the fitted value of the exponent is less than a theoretical value of $^{1}/_{3}$ might either be explained by an increase in particle dispersity as the average particle size increases or else a tendency for the sphericity of very large particles to become less precise.

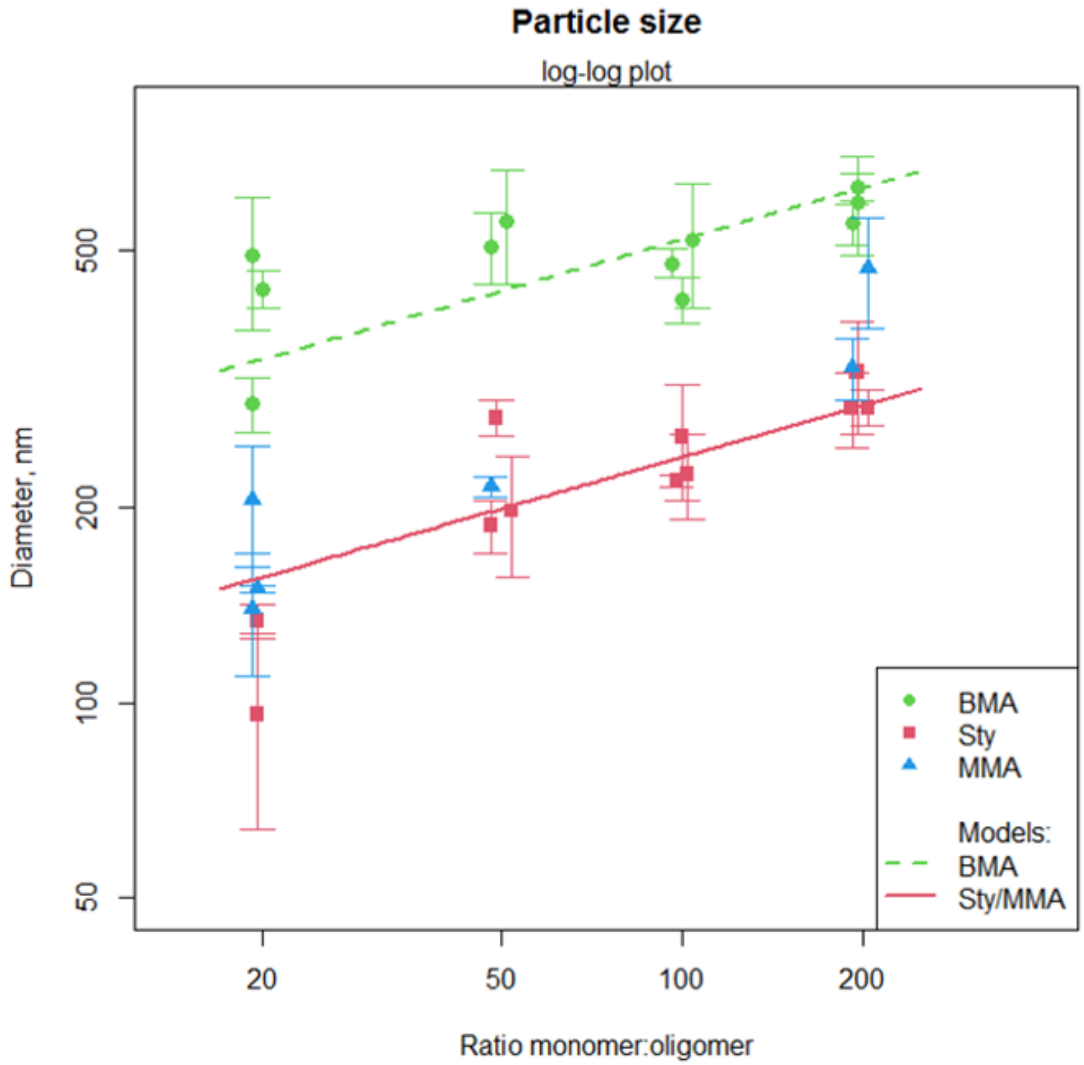

Figure 2-17. Linear Regression model to summarize results of particle size characterization by orthogonal techniques.

In order to examine the thermal properties of the latexes, TGA and DSC analyses were conducted (**Table 2-5 & Table 2-6**). From TGA, the pMAA oligomer exhibited three transition temperature ranges. Taking into account the ability of pMAA to retain water, the first transition from 35 to 105 °C is attributed to water loss (**Figure 2-31,** section 2.4.4). The second transition from 185 to 282 °C with maximum

degradation temperature at 208 °C, is the range in which polymethacrylates with ω-propenyl functional groups (in this case, pMAA) start to degrade,[69] whereas the transition from 335 to 456 °C (maximum degradation temperature at 430 °C) is the decomposition of the main chain. Thus, all polymers containing pMAA have a transition up to ~100 °C due to water loss, which is decreased with lower pMAA concentration (**Figure 2-18**).

Table 2-5. Thermal analysis of pMAA and pGMMA oligomers and pSt, pBMA and pMMA latexes.

Polymer	1st M. D. (°C)[d]	1st T. R. (°C) [e]	1st W. L. (%) [f]	2nd M. D. (°C) [d]	2nd T. R. (°C) [e]	2nd W. L. (%) [f]
pMAA	208	185-282	10	430	335-456	76
pGMMA	317	158-440	56	-	-	-
(L1) pSt_{20} [a]	208	184-230	7	420	317-460	64
(L2) pSt_{50} [a]	204	150-220	4	412	330-465	81
(L3) pSt_{100} [a]	194	140-220	3	412	343-450	86
(L4) pSt_{200} [a]	172	140-202	1	407	343-450	89
(L5) $pBMA_{20}$ [a]	-	-	-	418	202-500	59
(L6) $pBMA_{50}$ [a]	202	167-255	6	383	255-440	75
(L7) $pBMA_{100}$ [a]	220	123-247	6	386	247-413	79
(L8) $pBMA_{200}$ [a]	211	158-229	3	340	229-430	86
(L9) $pMMA_{20}$ [a]	256	176-317	7	409	317-500	51
(L10) $pMMA_{50}$ [a]	-	-	-	422	185-455	87
(L11) $pMMA_{100}$ [a]	273	238-308	5	395	308-490	46
(L12) $pMMA_{200}$ [a]	-	-	-	388	237-481	65
(L13) pSt_{200} [b]	413	343-439	97	-	-	-
(L14) $pBMA_{200}$ [b]	304	247-413	97	-	-	-
(L15) $pMMA_{200}$ [b]	291	202-413	97	-	-	-
(L16) pSt [c]	411	352-439	96	-	-	-
(L17) pBMA [c]	343	265-422	97	-	-	-
(L18) pMMA [c]	375	255-413	98	-	-	-

[a] Stabilized by pMAA. [b] Stabilized by pGMMA. [c] Stabilized by SDS. [d] M. D. = maximum degradation, [e] T. R. = temperature range and [f] W. L. = weight loss.

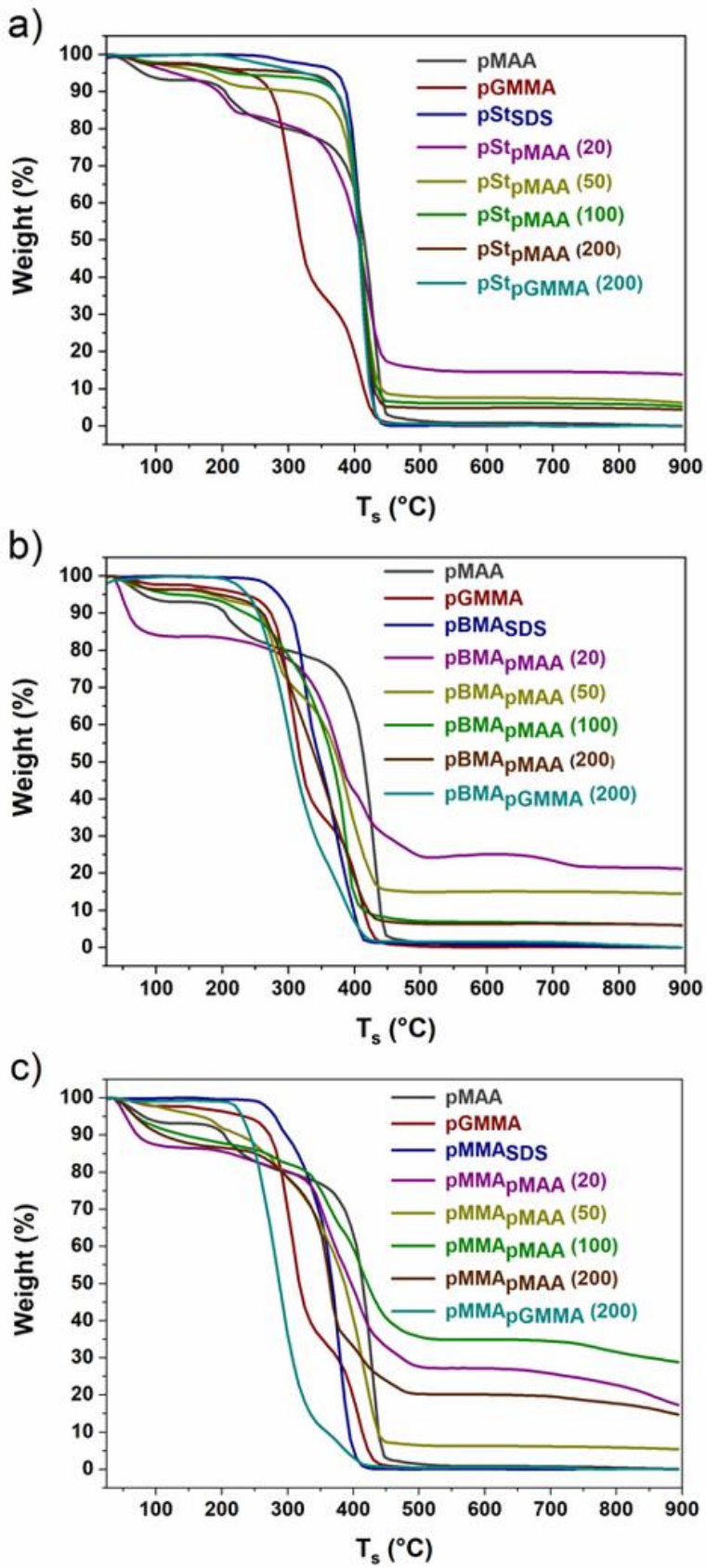

Figure 2-18. TGA thermograms of (a) pSt and (b) pBMA and (c) pMMA latexes, along with thermograms of pMAA and pGMMA macromonomers.

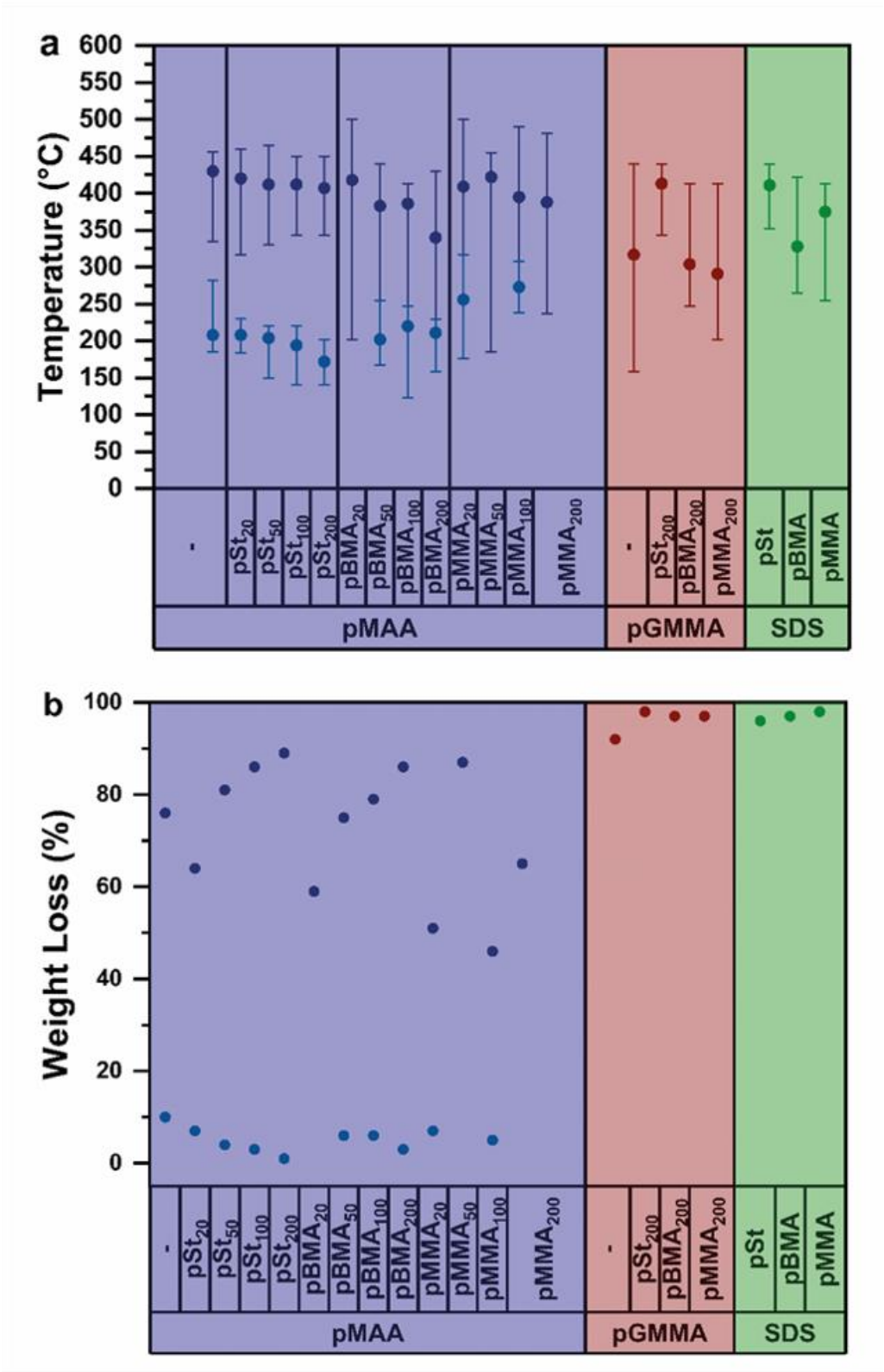

Figure 2-19. (a) Degradation temperatures of pMAA and pGMMA oligomers and pSt, pBMA and pMMA latexes. Error bars indicate the transition temperature range, at which maximum decomposition occurs. (b) Weight loss % at each decomposition temperature range of (a).

Figure 2-19a illustrates the degradation temperature of all polymers, along with the temperature range (indicated by error bars) in which the degradation occurs, and **Figure 2-19b** shows the weight loss % of the polymer due to these transitions, excluding from the analysis the transition caused by water loss. The thermal decomposition of the pSt polymers stabilized by pMAA followed the same pattern as pMAA, showing a small transition due to its degradation, which became weaker as the concentration of pMAA decreased, and then thermal stability up to 310-340 °C until their final decomposition at ~400-420 °C (**Figure 2-19a, Table 2-5,** L1-L4). The thermal decomposition of pBMA and pMMA polymers stabilized by pMAA, revealed similar transitions and behavior of the polymers. However, it is notable that in this case, by increasing the molar ratio of BMA to pMAA, the thermal stability of the polymers was slightly reduced (**Figure 2-19a**, pBMA latexes). Moreover, in contrast with pSt, polymers of pBMA and pMMA containing pMAA have wider decomposition temperature ranges, although without any significant trend. It is worth to note that the percentage weight loss from the decomposition of the main chain of pSt and pBMA polymers containing pMAA is proportional to the [monomer]:[pMAA] ratio (**Figure 2-19b**). The pGMMA oligomer shows a lower thermal stability but with similar transitions, in which a small water loss appears between 35 to 100 °C and the weight loss of side groups and backbone follows in a two-step process at 150 - 440 °C. This is also apparent in the TGA graphs of the corresponding pSt, pBMA and pMMA polymers containing pGMMA, where the decomposition occurred again in two steps. However, these polymers showed different behavior, as pSt had similar thermal stability with the pSt made with SDS, with a decomposition temperature at 411-413 °C, although based on the plot in **Figure 2-18a**, the onset temperature is slightly lower in pSt stabilized by pGMMA. In contrast, pBMA decomposes ~40 °C lower than the respective pBMA made with SDS (304 °C and 343 °C, respectively) and pMMA ~80 °C lower (291 °C and 375 °C, respectively), as expected (**Figure 2-19a**, latexes where pGMMA or SDS used).

Table 2-6. Thermal analysis of pMAA and pGMMA oligomers and pSt, pBMA and pMMA latexes.

Polymer	$T_{g,1}$ (°C) [d]	$T_{g,1}$ (°C) [e]	$T_{g,2}$ (°C) [d]	$T_{g,2}$ (°C) [e]	$T_{g,3}$ (°C) [d]	$T_{g,3}$ (°C) [e]
pMAA	-		143	141	-	
pGMMA	-3	-10	-		-	
(L1) pSt$_{20}$ [a]	-		153	148	225	223
(L2) pSt$_{50}$ [a]	105	103	-		230	221
(L3) pSt$_{100}$ [a]	105	102	-		220	213
(L4) pSt$_{200}$ [a]	104	103	-		214	213
(L5) pBMA$_{20}$ [a]	-		132	126	215	214
(L6) pBMA$_{50}$ [a]	36	26	132	124	-	
(L7) pBMA$_{100}$ [a]	34	22	129	121	-	
(L8) pBMA$_{200}$ [a]	39	23	154	153	-	
(L9) pMMA$_{20}$ [a]			180	174	221	220
(L10) pMMA$_{50}$ [a]	115	108	-		230	228
(L11) pMMA$_{100}$ [a]	139	130	-		-	
(L12) pMMA$_{200}$ [a]	115	109	-		225	219
(L13) pSt$_{200}$ [b]	4	4	-		100	98
(L14) pBMA$_{200}$ [b]	31	8	-		-	
(L15) pMMA$_{200}$ [b]	18	-4	-		109	103
(L16) pSt [c]	99	97	-		-	
(L17) pBMA [c]	32	18	-		-	
(L18) pMMA [c]	106	97	-		-	

Theor. T_g values: pMAA = 228 °C, pSt = 90 °C, pBMA = 20-50 °C and pMMA = 100-105 °C. [a] Stabilized by pMAA. [b] Stabilized by pGMMA. [c] Stabilized by SDS. [d] Midpoint. [e] Onset.

The glass transition temperature (T_g) of the polymers was determined by DSC using a heating rate of 10 °C/min (**Table 2-6**, **Figure 2-20 & Figure 2-21**). The T_g of the pMAA oligomer (143 °C) was lower than the literature value (228 °C), which is attributed to the low molecular weight of the polymer. The latexes stabilized by pMAA with a molar ratio of monomer to stabilizer of 20:1 did not have a T_g within the range of the literature values of the corresponding hydrophobic polymer (pSt, pBMA, or pMMA), but nevertheless, had two T_g values, one at 215-225 °C, which is close to the theoretical T_g of pMAA, and a second (lower transition) close to the oligomer`s T_g. This is interesting as it seems that at low monomer to oligomer ratios, the hydrophobic monomers have some compatibility with the pMAA. Moving to higher molar ratios, pSt and pBMA polymers (**Table 2-6,** L2-L4, L6-L8) had T_g values close to their theoretical values. Latexes L2-L4 of **Table 2-6** (St: pMAA = 50:1, 100:1, 200:1) also have a T_g at 214-230 °C indicating copolymer formation, where pSt and pMAA units

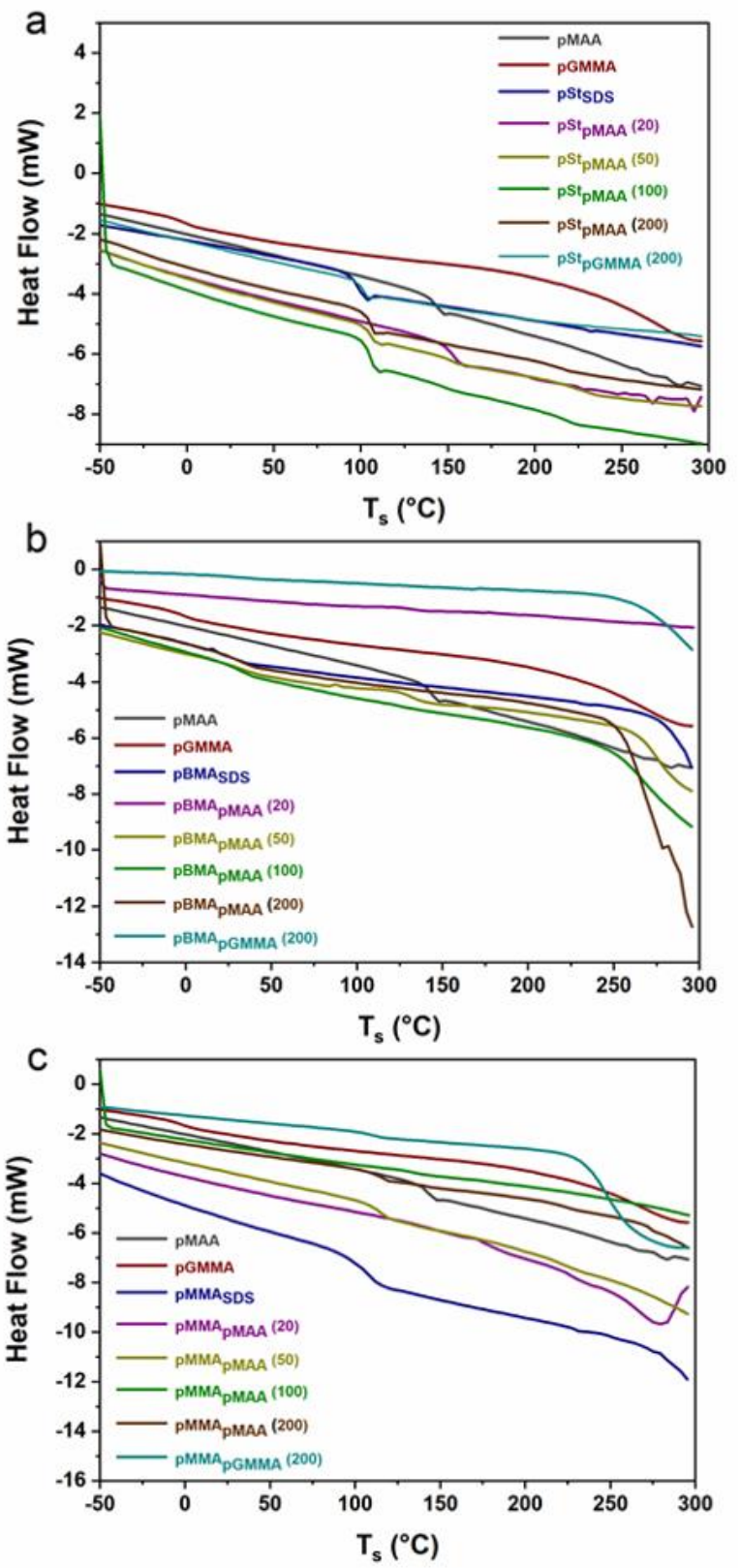

Figure 2-20. DSC thermograms of (a) pSt and (b) pBMA and (c) pMMA latexes, along with thermograms of pMAA and pGMMA oligomers.

are not compatible, while the corresponding pBMA polymers (BMA: pMAA = 50:1, 100:1, 200:1) have a second T_g at 132, 129 and 154 °C respectively. In this case, the lower T_g is attributed to pBMA particles and the higher to the copolymers of compatibilized pMAA and pBMA units. Although latexes L10 and L12 (MMA: pMAA = 50, 200) showed similar behavior as pSt, L11 (MMA: pMAA = 100) had only one T_g at 139 °C, showing a level of compatibility at this monomer to oligomer ratio. Moving to pGMMA containing latexes, pSt and pMMA show compatibility with pGMMA. They exhibit two T_g values, one close to theoretical values of pSt or pMMA respectively, due to the presence of free radical homopolymers, and a second between the T_g values of pGMMA and pSt or pMMA from the compatibilized copolymer (**Table 2-6**, L13 and L15, monomer: pGMMA = 200). Latex L14 (BMA: pGMMA =200) had a T_g value of 31 °C, suggesting that the [pGMMA] was too low to affect the T_g of the polymer. Finally, latexes L16-L18 (pSt, pBMA, pMMA made with SDS) have a good correlation between the theoretical and experimental T_g values.

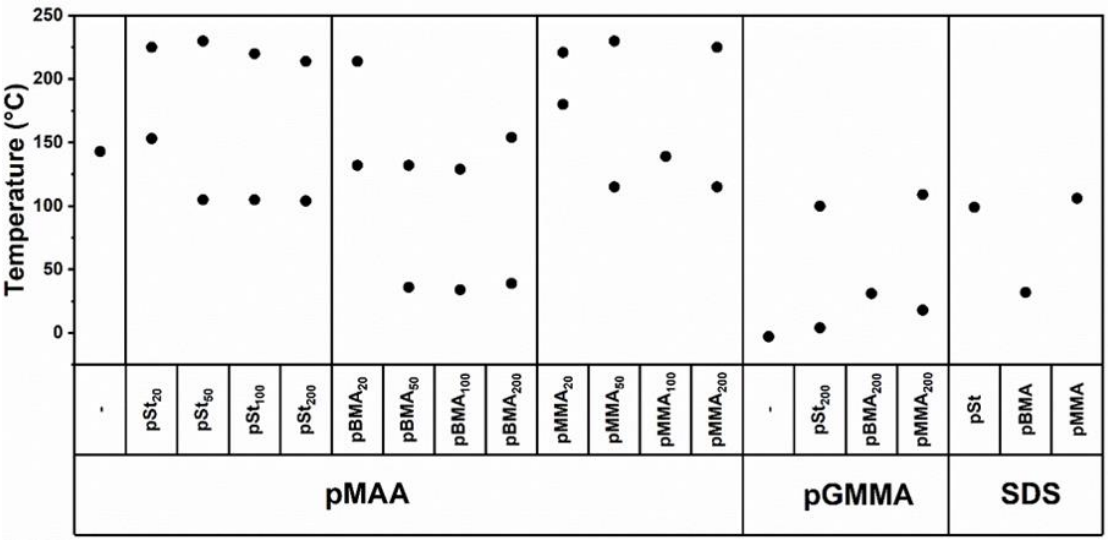

Figure 2-21. Glass transition temperatures (T_g) of pMAA and pGMMA oligomers and pSt, pBMA and pMMA latexes collected by DSC analysis.

2.3 Conclusions

In summary, a hydrophilic oligomer of pMAA, synthesized through CCTP, was used as the stabilizing agent for the surfactant-free emulsion polymerization of St, BMA and MMA with various molar ratios. Kinetic studies of the polymerization of styrene revealed the process through which the stabilization occurs; styrenic radicals react with the oligomer to form amphiphilic copolymers and the formed micelles swell with the additional monomer and polymerize through free radical polymerization. The mechanism through which the latex stabilization occurs, seems to be the same when an ionic (pMAA) or a non-ionic (pGMMA) stabilizer was used. Notably, the methylation of a carboxylated pBMA latex showed that this mechanism can be generalized to methacrylates. SEM analysis showed the formation of well-packed, uniform and monodisperse particles when pMAA was used as stabilizer. Substituting pMAA for pGMMA had a negative impact on the stability of the latex and the morphology of the latex particles, suggesting that steric stabilization is inferior to electrostatic repulsion in these systems. Finally, a linear regression model was used to summarize the particle size characterization, according to which an increase in monomer to oligomer ratio by a factor of x is associated with a corresponding increase in particle diameter by a factor $x^{0.26\pm0.03}$, or approximately $x^{1/3}$, independent of the monomer type.

2.4 Experimental section

2.4.1 Materials

Methacrylic acid (MAA, 99%), methyl methacrylate (MMA, 99%), butyl methacrylate (BMA, 99%), styrene (St, 99.9%), sodium dodecyl sulfate (SDS) and potassium persulfate (KPS) were obtained from Sigma-Aldrich and used without any further purification. Glycerol monomethacrylate (GMMA, >99.8%) was provided by GEO Specialty Chemicals, UK. Bis[(difluoroboryl) dimethylglyoximato]cobalt(II), (CoBF) was synthesized according to the literature.[70] 2,2'-Azobis[2-(2-imidazolin-2-yl)propane]dihydrochloride (VA-044) was obtained from Wako Specialty Chemical. Phosphate buffer solution (PBS), pH = 7, was prepared and used as solvent in all surfactant-free emulsion polymerizations, while deionized water (RO grade) was used for the reactions with SDS.

2.4.2 Instrumentation and Characterization techniques

Proton Nuclear Magnetic Resonance (^{1}H NMR)

^{1}H NMR spectra were recorded on Bruker DPX-300 or DPX-400 spectrometers in deuterated chloroform ($CDCl_3$), deuterated dimethyl sulfoxide (DMSO-d_6) or deuterium oxide (D_2O) as obtained from Sigma-Aldrich. Chemical shifts are given in ppm downfield from the tetramethylsilane internal standard.

Size Exclusion Chromatography (SEC)

SEC characterization was carried out on an Agilent Infinity II MDS instrument, using DMF with 5 mmol NH_4BF_4 additive as the eluent, at 50 °C, and with a flow rate of 1 mL/min. The system was equipped with differential refractive index (DRI), viscometry (VS), dual angle light scatter (LS) and variable wavelength UV detectors, 2 × PLgel Mixed D columns (300 × 7.5 mm) and a PLgel 5 μm guard column. The system was calibrated using poly(methyl methacrylate) standards (Agilent EasiVials) with molecular weights in the range of 550 - 955,000 g mol^{-1}. Prior to injecting the samples, they were filtered through a nylon membrane with a pore size of 0.22 μm.

Scanning Electron Microscopy (SEM)

SEM was performed using a Zeiss SUPRA 55-VP scanning electron microscope with a field emission electron gun (FEG). Best results were obtained when using the InLens detector with 3.5 mm working distance, 30 and 20 μm aperture and 0.5-3 kV acceleration voltage, with respect to sample tolerance. 1 μL of each sample was dissolved in 5 mL of DI water and aliquots of 7 μL were drop cast on silicon wafer chips (5 mm × 7 mm) and attached to aluminum specimen stubs. To improve contrast, gold sputter coating was applied for 15 seconds prior to imaging.

Dynamic Light Scattering (DLS)

DLS measurements were performed on a Malvern instrument Zetasizer Nano Series instrument with a detection angle of 173°, where the intensity weighted mean hydrodynamic size (Z-average) and the width of the particle size distribution (PSD) were obtained from analysis of the autocorrelation function. 10 μL of latex was diluted with 10 mL of deionized water previously filtered with 0.20 μm membrane to ensure the minimization of dust and other particulates. At least five measurements at 25 °C were made for each sample with an equilibrium time of 2 minutes before starting measurement, where the measurement time and number of repeats that contribute to each measurement was determined automatically by the proprietary software.

Zeta potential analysis

All Zetapotential measurements were performed on an Zetasizer Nano Series instrument using DTS1070 capillary cells. 10 μL of latex was diluted with 10 mL of deionized water previously filtered with 0.20 μm membrane to ensure the minimization of dust and other particulates. The cells were filled using a 1 mL disposable syringe to ensure no air bubbles were present in the cell. Samples were run at 25 ^{o}C with 2 minutes temperature stabilization time. Smoluchowski was used as the approximation with a Henry factor of 1.5. Power was set to automatic with a maximum voltage set at 200 V. Data quality was set to automatic, which performs up to a maximum of 100 measurements. Each sample was run 3 times. Refractive index, viscosity and relative permittivity of the solvent were set to 1.33, 0.89 mPa.s, 78.37 respectively, which are the values for pure water.

Static Light Scattering (SLS)

SLS measurements were performed on an ALV-CG3 instrument. For each sample, time-averaged light scattering data was collected within the angular range, $30 < \theta < 150$ ° with the sample maintained at 20 °C. Collection of data at smaller angles ($12 < \theta < 40$ °) was often precluded by the greater intensity of scattering by the larger particles. As shown in **Table 2-6**, the range of particle sizes to be measured was found to encompass approximately an order of magnitude, *i.e.*

$$48 \pm 16 < R_{DLS} < 894 \pm 201\ nm$$

Consequently, either one of two different models was used to analyze the SLS data:

<u>Model A:</u>

A 'Guinier plot' is a well-established means to estimate particle radius, by establishing the linearity of scattering data at low-q according to the relation.

<u>Model B:</u>

The data were analyzed in relation to a theoretical 'form factor' for angular dependence of scattering intensity. Scattering theory provides a variety of models that may be used to predict what is referred to as the form factor, which is specific to particle morphology. It is noteworthy that this approach to analysis of a form factor is analogous to that used for other scattering techniques for particle characterization, where the main difference is in the wavelength of the incident radiation and, consequently, the range of particle sizes they are applied to, *e.g.,* X-ray or neutron scattering. Here, we used the analytical expression provided by Pedersen to calculate the theoretical form factor for a spherical, homogeneous particle exhibiting a radius of gyration R_G, then this function being moderated to account for particle size dispersity by sampling from a lognormal distribution and calculating the average form factor weighted by scattering intensity.

Thermogravimetric Analysis (TGA)

TGA measurements were carried out on a Mettler-Toledo TGA with autosampler. N_2 gas was used with a heating rate of 10 °C min^{-1} in 70 μL alumina pans.

Differential Scanning Calorimetry (DSC)

DSC measurements were carried out on a Mettler-Toledo DSC with autosampler. The samples (in powdered form) were placed in 40 μL aluminium crucibles (with pierced lids) and were heated/cooled from -50 °C to 300 °C in a flow of N_2 with a heating rate of 10 °C min^{-1}. The results of the second heating cycle are reported in all cases.

2.4.3 Experimental procedures

Synthesis of bis[(difluoroboryl)dimethylglyoximato] cobalt(II), (CoBF)

Cobalt (II) acetate tetrahydrate was heated under vacuum at 110 °C with pressure off 2 mbar for 5-6 hours (the pink powder turns purple upon becoming anhydrous). Under nitrogen atmosphere equipped with magnetic stirrer anhydrous cobalt (II) acetate (3.14 g, 0.0126 mol) and dimethyl glyoxime (4.47 g, 0.0344 mol) were added and purged with N_2 for 1 hour. Subsequently, ethyl acetate (77.12 ml, 0.87 mol) was dried with $MgSO_4$ and decanted and isolated (filtered with gravity filtration using filter paper). The ethyl acetate was deoxygenated for 30 minutes prior to addition to the mixture. The mixture was stirred vigorously for 30 min. Boron trifluoride etherate (BF_3EtO) (13.03 mL, 0.09 mol) was deoxygenated with nitrogen and added via syringe pump over a period of 10 minutes with continues vigorous stirring. The resulting solution was heated to 55 °C and held at that temperature for 30 minutes to complete the reaction. Sodium bicarbonate (3.57 g, 0.042 mol) was added in portions to avoid excessive frothing. When the bicarbonate addition was complete the reaction mixture was cooled to 5 °C and stirred for an hour to allow product to recrystallize. Filtration was carried out in (2 x 70 mL) H_20 and (2 x 20 mL) MeOH.

FT-IR ν (cm^{-1}):3592, 3525 (OH), 2923 ($-CH_3$), 1622 (C=N), 1438 ($-CH_3$), 1383 ($-CH_3$), 1213 (N-O), 1161 ($C-CH_3$), 1085 (CH_3), 950 (B-F), 826 (B-F), 634 (B-O), 575 (C-N-O), 506 (Co-N) (**Figure 2-22**).

The synthetic method that was carried out involved the recrystallization of CoBF in a solution of 80% water and 20% methanol. Consequently, a structure with axial water ligands is assumed. This is suggested by the presence of the two peaks at 3592 and 3525 cm^{-1}. These peaks correspond to, respectively, lattice water ligands' asymmetric and symmetric stretching motion. As suggested by M. Duncan,[71] in the free gas water molecule the asymmetric: symmetric peak ratio is close to 18:1. However, and as is

visible here, in water-containing metal complexes this ratio is closer to 1:1, an observation that is corroborated by Lawson and co-workers.[72]

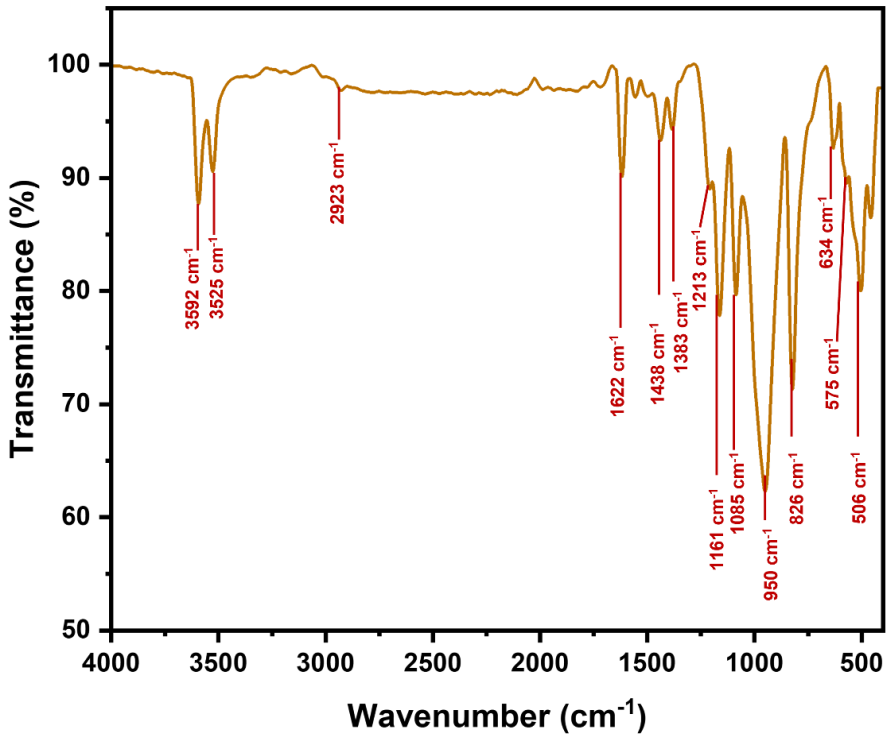

Figure 2-22. FT-IR spectrum of CoBF.

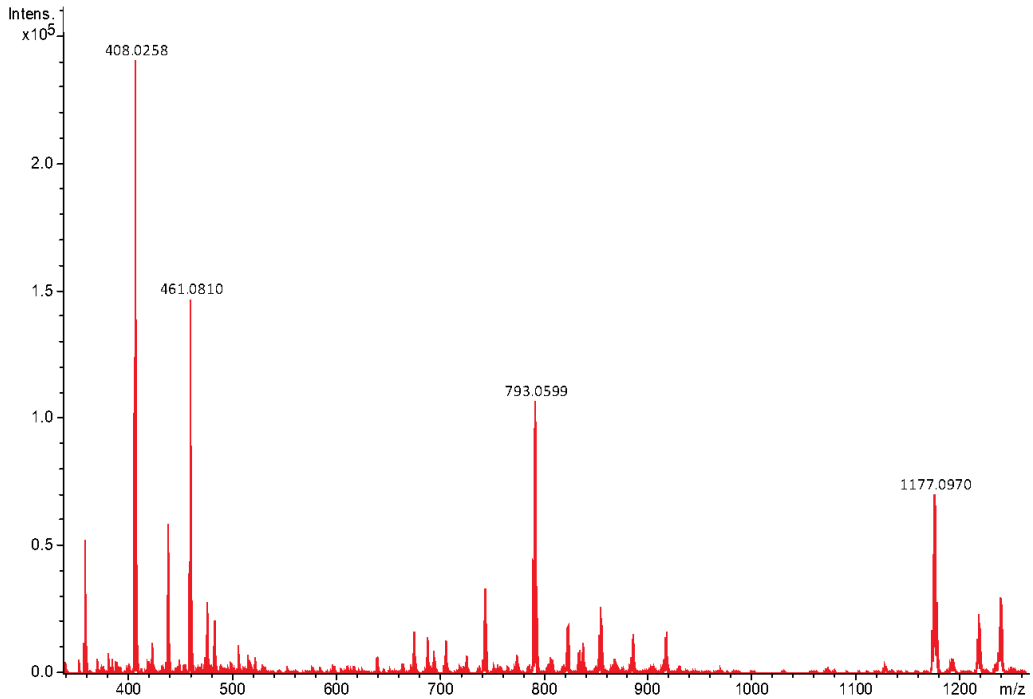

Figure 2-23. MALDI-ToF-MS spectrum of CoBF.

During MALDI-ToF-MS analysis the two axial ligands were lost, likely due to the ionization process. The theoretical value of CoBF (without axial ligands) was 384.75 Da + 22.98 Da (Na), namely 407.73 Da. The experimental value of CoBF is 408.02 Da as shown in **Figure 2-23**. The peaks at 461.08, 793.05 and 1177.09 Da correspond to CoBF adducts, ($[CoBF+2K+H]^+$, $[2CoBF+Na]^+$ and $[3CoBF+Na]^+$ respectively).

Synthesis of pMAA stabilizer by CCTP in aqueous solution

A pMAA oligomer was prepared *via* CCTP. CoBF (5.34 mg, 30 ppm relative to monomer) was added to a 100 mL round bottom flask (RBF) along with a magnetic stirrer and deoxygenated for 1 hour. Methacrylic acid (MAA, 46 mL) was added to a separate 100 mL RBF, and after deoxygenation (1 hour) 43 mL (0.5 mol) were transferred to the CoBF using a deoxygenated syringe. The mixture was stirred until full dissolution of the CoBF. In parallel, to a 500 mL 3-necked RBF VA-044 initiator (0.808 g, 2.5 mmol) and DI water (180 mL) was added, and the solution was deoxygenated for 1 h. The solution in the 3-necked flask was then heated in an oil bath to 55ºC with continuous stirring, and the monomer/CoBF solution was fed into it over 60 minutes. The reaction was continued for a further 3 h after feeding. The pMAA oligomer was purified by precipitation from methanol into chloroform and dried in a vacuum oven. ^{1}H NMR (methanol-*d*, 400 MHz) δ (ppm): ~6.2(s, *cis* **H**CH=C-), ~5.6 (d, , *trans* **H**CH=C-), ~2.5 (s, -C**H$_2$**-CR=CH$_2$), ~1.5-2.5 (m, H-C**H$_2$**-C-), ~1-1.5 (m, -C-C**H$_3$**).

Synthesis of pGMMA stabilizer by CCTP in methanol

For the synthesis of the pGMMA oligomer, GMMA (160.2 g, 1 mol) and methanol (350 mL) were added to a 1 L 3-necked RBF and deoxygenated for 1 h over ice. CoBF (26.9 mg, 70 ppm) and VA-044 (1.6164 g, 5 mmol) were added to a separate RBF which was also deoxygenated for 1 h. 50 mL of deoxygenated methanol was then added solubilizing the CoBF and VA-044, before being transferred to the GMMA solution. The reaction was then heated to 50 ºC for 18 h. Methanol and other volatiles were removed by rotary evaporation and the product dialyzed against methanol for 3 days (MWCO = 1000 Da), with the solvent exchanged twice per day. ^{1}H NMR (methanol-*d*, 400 MHz) δ (ppm): ~6.3 (s, *cis* **H**CH=C-), ~5.6 (d, , *trans* **H**CH=C-), ~4

(d, -O-C**H**$_2$-C**H**-), ~3.6 (s, -CH-C**H**$_2$-OH), ~2.5 (s, -C**H**$_2$-CR=CH$_2$), ~1.8-2,3 (m, H-C**H**$_2$-C-), ~0.8-1.3 (m, -C-C**H**$_3$).

Preparation of phosphate buffer solution

Monobasic sodium phosphate (23.996 g, 0.2 mol) was placed in a 1 L conical flask together with a magnetic stirrer. Deionized water (1 L) was added, and the mixture vigorously stirred for the preparation of solution A (0.2 M). To a second 1 L conical flask containing a magnetic stirrer bar, dibasic sodium phosphate (28.392 g, 0.2 mol) was added. Deionized water (1 L) was added, and the mixture was vigorously stirred for the preparation of solution B (0.2 M). Subsequently, 390 mL of solution A and 610 ml of solution B were mixed in a 1L bottle for the preparation of the phosphate buffer solution (pH = 7).

Synthesis of latexes via emulsion polymerization (using CCTP oligomers as stabilizers)

Emulsion polymerizations were carried out under starve-feed conditions. All experiments were conducted under nitrogen at 86 ºC and stirred at 600 rpm. First, the stabilizer (1 g) and the solvent (PBS, pH = 7) were charged in a three-necked round bottom flask and the mixture stirred and purged with nitrogen for 30 minutes. Subsequently, the reaction mixture was heated at 86 ºC and 5 minutes after reaching the desired temperature, the addition of the aqueous KPS solution and the monomer (both previously degassed for 30 minutes) started using two degassed syringes and a syringe pump (feeding time: 4 h). After completion of the addition, the reaction was stirred overnight (~16 h) under the same conditions. The reaction was terminated by introducing oxygen to the reaction media (for composition see Table 2). In all polymerizations where pGMMA was used, deionized water was used as solvent.

General procedure for the synthesis of latexes via free radical emulsion polymerization (using SDS as stabilizer)

A flask containing monomer (56.16 g, 560.93 mmol, deoxygenated for 30 min) was purged with nitrogen. 4,4'-azobis(4-cyanovaleric acid) (ACVA) (1.5 g, 5.350 mmol), SDS (1.2 g, 4.161 mmol), and 300 mL of deionized water were charged into a three-neck, 500 mL double jacketed reactor, equipped with a RTD temperature probe and

an overhead stirrer. The mixture was purged with nitrogen and stirred at 325 rpm for at least 30 min. Subsequently, the mixture was heated under inert atmosphere. When the temperature in the reactor reached 70 °C, the addition of the MMA monomer solution started using a degassed syringe and a syringe pump (feeding rate = 1.866 mL/min, feeding time = 60 min). Following completion of the addition, stirring continued for a further 60 min at 76 °C which was controlled and stabilized after the addition of the monomer.

2.4.4 Supplementary Figures and Characterization

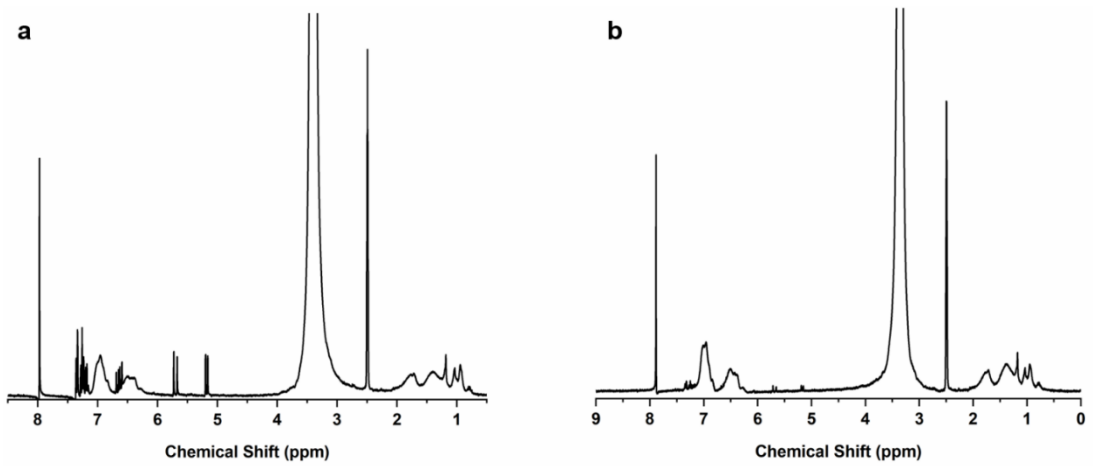

Figure 2-24. ^{1}H NMR (400 MHz) spectrum taken at a) 300 mins (entry A14) and b) 24 hours from the kinetic study of surfactant-free emulsion polymerization of styrene.

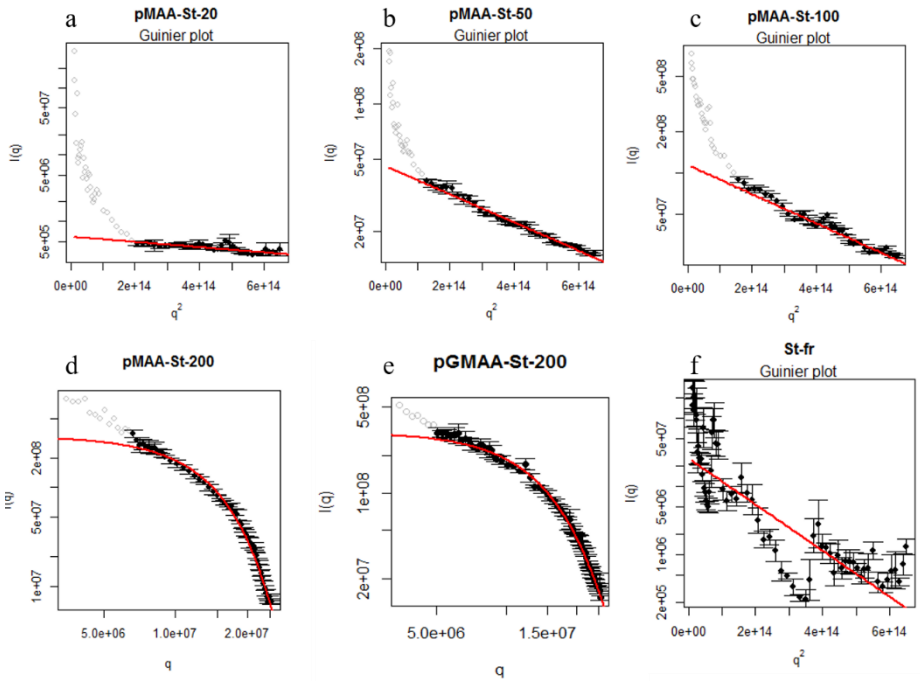

Figure 2-25. Scattering intensities, I(q) or I(q^2), as a function of the form factor (q) or (q^2), along with the corresponding fitted models for pSt latexes stabilized by pMAA, pGMMA and SDS derived by SLS. Monomer: oligomer ratio (a) 20, (b) 50, (c) 100, (d) and (e) 200. A valid fit for (f) could not be determined.

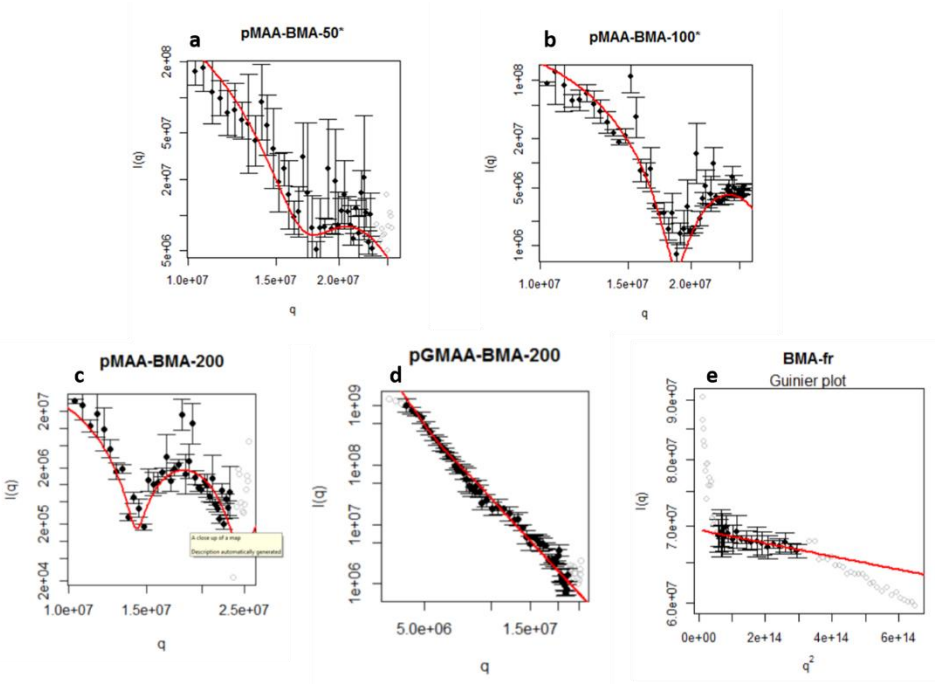

Figure 2-26. Scattering intensities, I(q) or I(q^2), as a function of the magnitude of the scattering vector, q, together with corresponding fitted models for pBMA latexes stabilized by pMAA, pGMMA and SDS derived by SLS. Monomer: oligomer ratio (a) 50, (b) 100, (c) and (d) 200. A valid fit for (e) could not be determined.

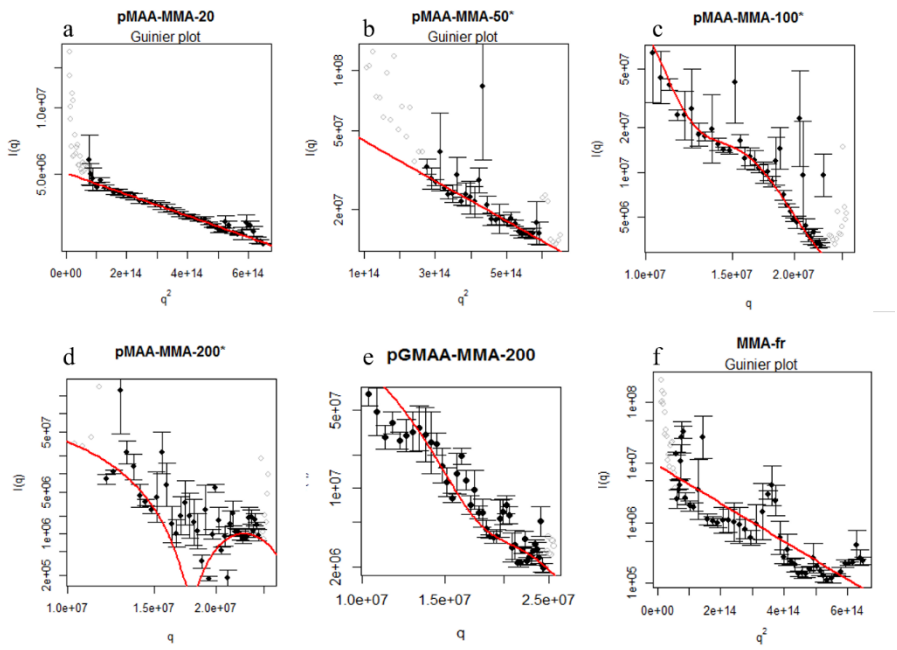

Figure 2-27. Scattering intensities, I(q) or I(q^2), as a function of the form factor (q) or (q^2), along with the corresponding fitted models for pMMA latexes stabilized by pMAA, pGMMA and SDS derived by SLS. Monomer: oligomer ratio (a) 20, (b) 50,

(c) 100, (d) and (e) 200. The validity of the fits for (d) and (e) may be considered somewhat compromised by sampling effects. A valid fit for (f) could not be determined.

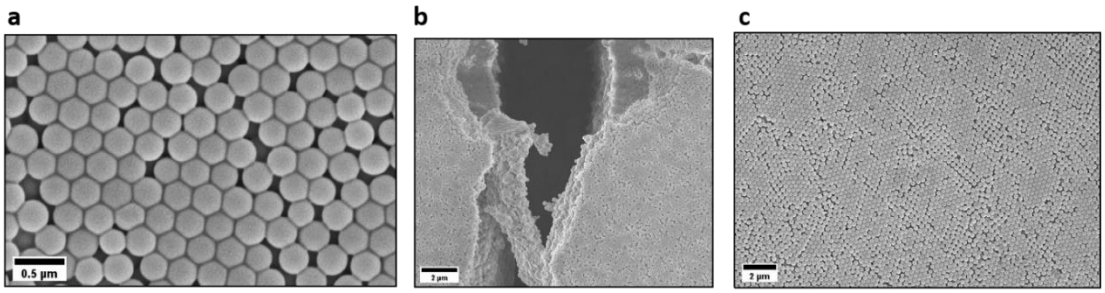

Figure 2-28. SEM images of pS latexes stabilized by pMAA with varying monomer to oligomer molar ratio. (a) monomer to oligomer ratio = 50, (b) monomer to oligomer ratio = 100 and (c) monomer to oligomer ratio = 200.

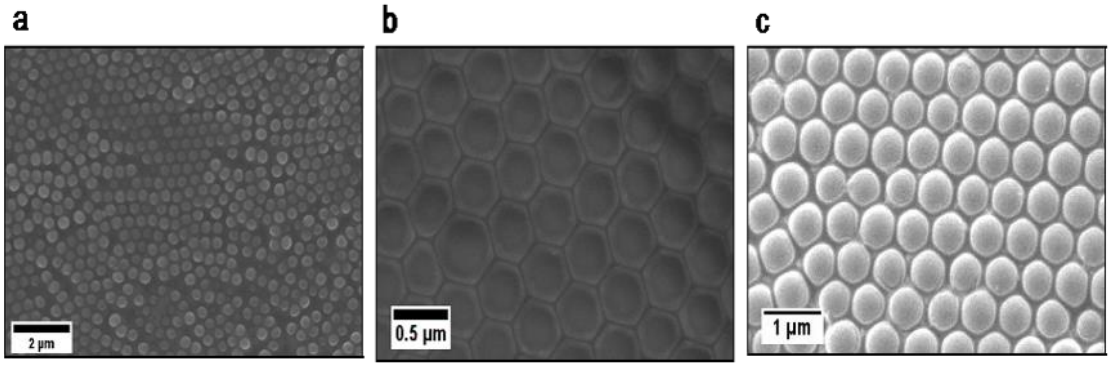

Figure 2-29. SEM images of pBMA latexes stabilized by pMAA with varying monomer to oligomer molar ratio. (a) monomer to oligomer ratio = 20, (b) monomer to oligomer ratio = 100 and (c) monomer to oligomer ratio = 200.

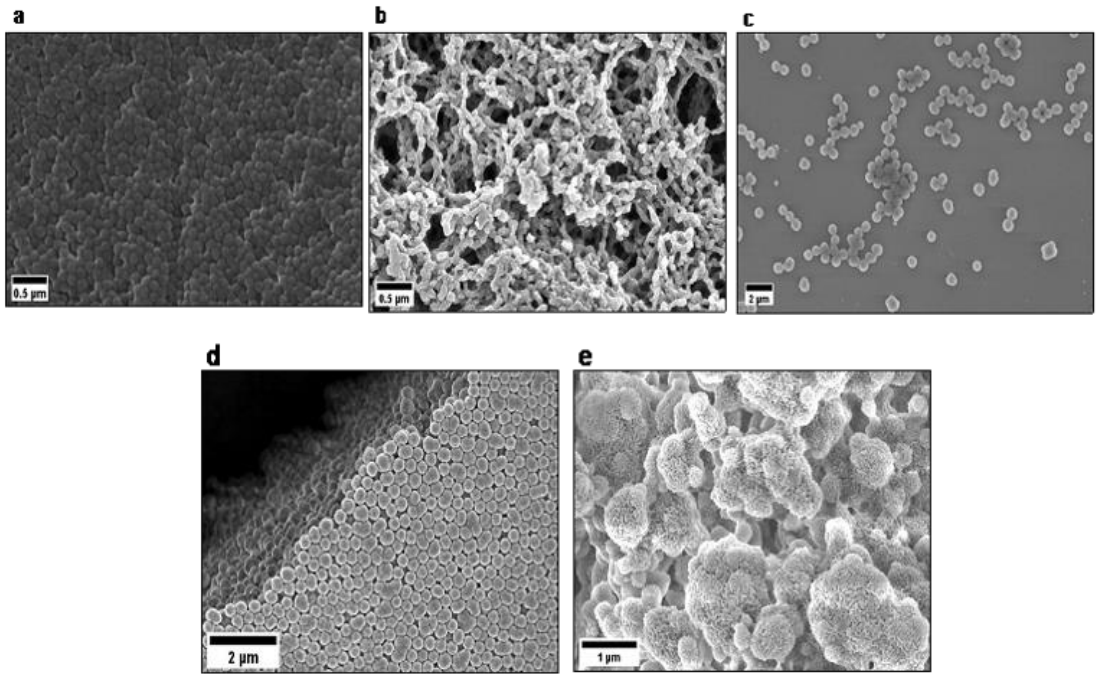

Figure 2-30. SEM images of pMMA latexes stabilized by pMAA with varying monomer to oligomer molar ratio, (a) monomer to oligomer ratio = 20, (b) monomer to oligomer ratio = 50, (c) monomer to oligomer ratio = 100, (d) monomer to oligomer ratio = 200 and (e) pMMA stabilized by pGMMA.

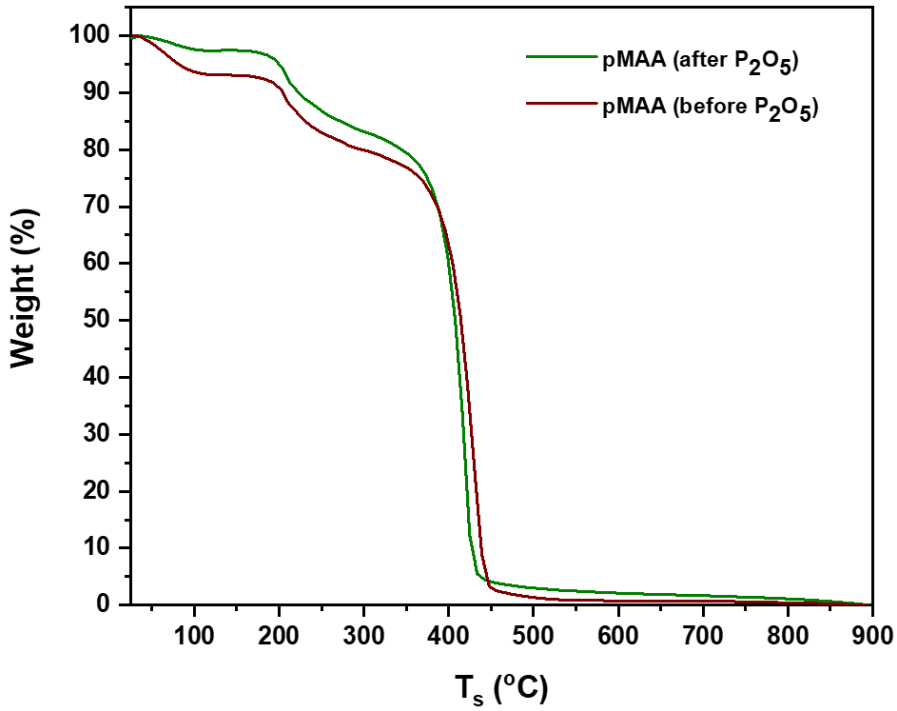

Figure 2-31. TGA thermogram of pMAA macromonomer before and after purification step with P_2O_5 for 3 hrs, showing that the transition at ~100°C is attributed to water loss.

2.5 References

1. Urban, D. T., K, *Polymer Dispersions and Their Industrial Applications* Wiley-VCH: New York: **2002**.

2. Odian, G., *Principles of Polymerization*. 4th ed.; Wiley: **2004**.

3. Dong, Y.; Argaiz, M.; He, B.; Tomovska, R.; Sun, T.; Martín-Fabiani, I., Zinc Oxide Superstructures in Colloidal Polymer Nanocomposite Films: Enhanced Antibacterial Activity through Slow Drying. *ACS Appl. Polym. Mater.* **2020,** *2* (2), 626-635.

4. Fulmer, P. A.; Wynne, J. H., Development of Broad-Spectrum Antimicrobial Latex Paint Surfaces Employing Active Amphiphilic Compounds. *ACS Appl. Mater. Interfaces* **2011,** *3* (8), 2878-2884.

5. Mulqueen, P., Recent Advances in Agrochemical Formulation. *Adv. Colloid Interface Sci.* **2003,** *106* (1), 83-107.

6. Wang, T.; Canetta, E.; Weerakkody, T. G.; Keddie, J. L.; Rivas, U., pH Dependence of the Properties of Waterborne Pressure-Sensitive Adhesives Containing Acrylic Acid. *ACS Appl. Mater. Interfaces* **2009,** *1* (3), 631-639.

7. Cunningham, M. F., Living/Controlled Radical Polymerizations in Dispersed Phase Systems. *Progress in Polymer Science* **2002,** *27* (6), 1039-1067.

8. Farcet, C.; Charleux, B.; Pirri, R., Nitroxide-Mediated Miniemulsion Polymerization of N-Butyl Acrylate: Synthesis of Controlled Homopolymers and Gradient Copolymers with Styrene. *Macromolecular Symposia* **2002,** *182* (1), 249-260.

9. Theodorou, A.; Liarou, E.; Haddleton, D. M.; Stavrakaki, I. G.; Skordalidis, P.; Whitfield, R.; Anastasaki, A.; Velonia, K., Protein-Polymer Bioconjugates Via a Versatile Oxygen Tolerant Photoinduced Controlled Radical Polymerization Approach. *Nat. Commun.* **2020,** *11* (1), 1486.

10. Liarou, E.; Han, Y.; Sanchez, A. M.; Walker, M.; Haddleton, D. M., Rapidly Self-Deoxygenating Controlled Radical Polymerization in Water Via in Situ Disproportionation of Cu(I). *Chem. Sci.* **2020,** *11* (20), 5257-5266.

11. Kim, K. H.; Kim, J.; Jo, W. H., Preparation of Hydrogel Nanoparticles by Atom Transfer Radical Polymerization of N-Isopropylacrylamide in Aqueous Media Using PEG Macro-Initiator. *Polymer* **2005,** *46* (9), 2836-2840.

12. Sugihara, S.; Sugihara, K.; Armes, S. P.; Ahmad, H.; Lewis, A. L., Synthesis of Biomimetic Poly(2-(Methacryloyloxy)Ethyl Phosphorylcholine) Nanolatexes Via Atom Transfer Radical Dispersion Polymerization in Alcohol/Water Mixtures. *Macromolecules* **2010,** *43* (15), 6321-6329.

13. Sugihara, S.; Armes, S. P.; Lewis, A. L., One-Pot Synthesis of Biomimetic Shell Cross-Linked Micelles and Nanocages by ATRP in Alcohol/Water Mixtures. *Angewandte Chemie International Edition* **2010,** *49* (20), 3500-3503.

14. Delaittre, G.; Nicolas, J.; Lefay, C.; Save, M.; Charleux, B., Surfactant-Free Synthesis of Amphiphilic Diblock Copolymer Nanoparticles Via

Nitroxide-Mediated Emulsion Polymerization. *Chemical Communications* **2005,** (5), 614-616.

15. Brusseau, S.; D'Agosto, F.; Magnet, S.; Couvreur, L.; Chamignon, C.; Charleux, B., Nitroxide-Mediated Copolymerization of Methacrylic Acid and Sodium 4-Styrenesulfonate in Water Solution and One-Pot Synthesis of Amphiphilic Block Copolymer Nanoparticles. *Macromolecules* **2011,** *44* (14), 5590-5598.

16. Groison, E.; Brusseau, S.; D'Agosto, F.; Magnet, S.; Inoubli, R.; Couvreur, L.; Charleux, B., Well-Defined Amphiphilic Block Copolymer Nanoobjects Via Nitroxide-Mediated Emulsion Polymerization. *ACS Macro Letters* **2012,** *1* (1), 47-51.

17. Chiefari, J.; Chong, Y. K.; Ercole, F.; Krstina, J.; Jeffery, J.; Le, T. P. T.; Mayadunne, R. T. A.; Meijs, G. F.; Moad, C. L.; Moad, G.; Rizzardo, E.; Thang, S. H., Living Free-Radical Polymerization by Reversible Addition−Fragmentation Chain Transfer: The RAFT Process. *Macromolecules* **1998,** *31* (16), 5559-5562.

18. Moad, G.; Rizzardo, E.; Thang, S. H., Living Radical Polymerization by the RAFT Process a First Update. *Australian Journal of Chemistry* **2006,** *59* (10), 669-692.

19. Chong, Y. K.; Le, T. P. T.; Moad, G.; Rizzardo, E.; Thang, S. H., A More Versatile Route to Block Copolymers and Other Polymers of Complex Architecture by Living Radical Polymerization: The RAFT Process. *Macromolecules* **1999,** *32* (6), 2071-2074.

20. Moad, G.; Chiefari, J.; Chong, Y. K.; Krstina, J.; Mayadunne, R. T. A.; Postma, A.; Rizzardo, E.; Thang, S. H., Living Free Radical Polymerization with Reversible Addition – Fragmentation Chain Transfer (the Life of RAFT). *Polymer International* **2000,** *49* (9), 993-1001.

21. Merritt, S. M. J.; Wemyss, A. M.; Farris, S.; Patole, S.; Patias, G.; Haddleton, D. M.; Shollock, B.; Wan, C., Gas Barrier Polymer Nanocomposite Films Prepared by Graphene Oxide Encapsulated Polystyrene Microparticles. *ACS Applied Polymer Materials* **2020,** *2* (2), 725-731.

22. Chern, C. S., Emulsion Polymerization Mechanisms and Kinetics. *Prog. Polym. Sci.* **2006,** *31* (5), 443-486.

23. Keddie, J. L., Film Formation of Latex. *Materials Science and Engineering: R: Reports* **1997,** *21* (3), 101-170.

24. Agarwal, N.; Farris, R. J., Water Absorption by Acrylic-Based Latex Blend Films and Its Effect on Their Properties. *Journal of Applied Polymer Science* **1999,** *72* (11), 1407-1419.

25. Liu, Y.; Soer, W.-J.; Scheerder, J.; Satgurunathan, G.; Keddie, J. L., Water Vapor Sorption and Diffusion in Secondary Dispersion Barrier Coatings: A Critical Comparison with Emulsion Polymers. *ACS Applied Materials & Interfaces* **2015,** *7* (22), 12147-12157.

26. Jiang, B.; Tsavalas, J. G.; Sundberg, D. C., Water Whitening of Polymer Films: Mechanistic Studies and Comparisons between Water and Solvent Borne Films. *Progress in Organic Coatings* **2017,** *105*, 56-66.

27. Lei, Y.; Child, J. R.; Tsavalas, J. G., Design and Analysis of the Homogeneous and Heterogeneous Distribution of Water Confined within Colloidal Polymer Particles. *Colloid and Polymer Science* **2013,** *291* (1), 143-156.

28. Gundabala, V. R.; Zimmerman, W. B.; Routh, A. F., A Model for Surfactant Distribution in Latex Coatings. *Langmuir* **2004,** *20* (20), 8721-8727.

29. Zhao, C.-L.; Holl, Y.; Pith, T.; Lambla, M., Surface Analysis and Adhesion Properties of Coalesced Latex Films. *British Polymer Journal* **1989,** *21* (2), 155-160.

30. Shirakbari, N.; Ebrahimi, M.; Salehi-Mobarakeh, H.; Khorasani, M., Effect of Surfactant Type and Concentration on Surfactant Migration, Surface Tension, and Adhesion of Latex Films. *Journal of Macromolecular Science, Part B* **2014,** *53* (7), 1286-1292.

31. Butler, L. N.; Fellows, C. M.; Gilbert, R. G., Effect of Surfactant Systems on the Water Sensitivity of Latex Films. *Journal of Applied Polymer Science* **2004,** *92* (3), 1813-1823.

32. Li, Y.; Armes, S. P., RAFT Synthesis of Sterically Stabilized Methacrylic Nanolatexes and Vesicles by Aqueous Dispersion Polymerization. *Angewandte Chemie International Edition* **2010,** *49* (24), 4042-4046.

33. Blanazs, A.; Ryan, A. J.; Armes, S. P., Predictive Phase Diagrams for RAFT Aqueous Dispersion Polymerization: Effect of Block Copolymer Composition, Molecular Weight, and Copolymer Concentration. *Macromolecules* **2012,** *45* (12), 5099-5107.

34. Cunningham, V. J.; Alswieleh, A. M.; Thompson, K. L.; Williams, M.; Leggett, G. J.; Armes, S. P.; Musa, O. M., Poly(Glycerol Monomethacrylate)–Poly(Benzyl Methacrylate) Diblock Copolymer Nanoparticles Via RAFT Emulsion Polymerization: Synthesis, Characterization, and Interfacial Activity. *Macromolecules* **2014,** *47* (16), 5613-5623.

35. Charleux, B.; Delaittre, G.; Rieger, J.; D'Agosto, F., Polymerization-Induced Self-Assembly: From Soluble Macromolecules to Block Copolymer Nano-Objects in One Step. *Macromolecules* **2012,** *45* (17), 6753-6765.

36. Hill, M. R.; Carmean, R. N.; Sumerlin, B. S., Expanding the Scope of RAFT Polymerization: Recent Advances and New Horizons. *Macromolecules* **2015,** *48* (16), 5459-5469.

37. Boissé, S.; Rieger, J.; Belal, K.; Di-Cicco, A.; Beaunier, P.; Li, M.-H.; Charleux, B., Amphiphilic Block Copolymer Nano-Fibers Via RAFT-Mediated Polymerization in Aqueous Dispersed System. *Chemical Communications* **2010,** *46* (11), 1950-1952.

38. Lesage de la Haye, J.; Martin-Fabiani, I.; Schulz, M.; Keddie, J. L.; D'Agosto, F.; Lansalot, M., Hydrophilic Macroraft-Mediated Emulsion Polymerization: Synthesis of Latexes for Cross-Linked and Surfactant-Free Films. *Macromolecules* **2017,** *50* (23), 9315-9328.

39. Velasquez, E.; Rieger, J.; Stoffelbach, F.; D'Agosto, F.; Lansalot, M.; Dufils, P.-E.; Vinas, J., Surfactant-Free Poly(Vinylidene Chloride) Latexes Via

One-Pot RAFT-Mediated Aqueous Polymerization. *Polymer* **2016,** *106*, 275-284.

40. Martín-Fabiani, I.; Lesage de la Haye, J.; Schulz, M.; Liu, Y.; Lee, M.; Duffy, B.; D'Agosto, F.; Lansalot, M.; Keddie, J. L., Enhanced Water Barrier Properties of Surfactant-Free Polymer Films Obtained by Macroraft-Mediated Emulsion Polymerization. *ACS Applied Materials & Interfaces* **2018,** *10* (13), 11221-11232.

41. Martín-Fabiani, I.; Makepeace, D. K.; Richardson, P. G.; Lesage de la Haye, J.; Venero, D. A.; Rogers, S. E.; D'Agosto, F.; Lansalot, M.; Keddie, J. L., In Situ Monitoring of Latex Film Formation by Small-Angle Neutron Scattering: Evolving Distributions of Hydrophilic Stabilizers in Drying Colloidal Films. *Langmuir* **2019,** *35* (10), 3822-3831.

42. Schreur-Piet, I.; Heuts, J. P. A., In Situ Stabilizer Formation from Methacrylic Acid Macromonomers in Emulsion Polymerization. *Polymer Chemistry* **2017,** *8* (43), 6654-6664.

43. Schreur-Piet, I.; van Herk, A. M.; Laven, J.; Heuts, J. P. A., Synthesis and Rheological Characterization of Latexes Stabilized by Methacrylic Acid Containing Macromonomers. *Industrial & Engineering Chemistry Research* **2019,** *58* (46), 21105-21117.

44. Abbey, K. J.; Trumbo, D. L.; Carlson, G. M.; Masola, M. J.; Zander, R. A., Synthesis and Copolymerization Behavior of Methacrylate Dimers. *J. Macromol. Sci. Part A: Polym. Chem.* **1993,** *31* (13), 3417-3424.

45. Janowicz, A. H. US Pat., 4694054. **1987**.

46. Haddleton, D. M., Muir, A. V. G., Leeming, S. W. WO Pat., 95/17435. **1995**.

47. Gridnev, A., The 25th Anniversary of Catalytic Chain Transfer. *J. Macromol. Sci. Part A: Polym. Chem.* **2000,** *38* (10), 1753-1766.

48. Suddaby, K. G.; Haddleton, D. M.; Hastings, J. J.; Richards, S. N.; O'Donnell, J. P., Catalytic Chain Transfer for Molecular Weight Control in the Emulsion Polymerization of Methyl Methacrylate and Methyl Methacrylate−Styrene. *Macromolecules* **1996,** *29* (25), 8083-8091.

49. Roberts, G. E.; Davis, T. P.; Heuts, J. P. A.; Ball, G. E., Monomer Substituent Effects in Catalytic Chain Transfer Polymerization: Tert-Butyl Methacrylate and Dimethyl Itaconate. *Macromolecules* **2002,** *35* (27), 9954-9963.

50. Heuts, J. P. A.; Smeets, N. M. B., Catalytic Chain Transfer and Its Derived Macromonomers. *Polym. Chem.* **2011,** *2* (11), 2407-2423.

51. Haddleton, D. M.; Maloney, D. R.; Suddaby, K. G.; Muir, A. V. G.; Richards, S. N., Catalytic Chain Transfer Polymerisation (CCTP) of Methyl Methacrylate: Effect of Catalyst Structure and Reaction Conditions on Chain Transfer Coefficient. *Macromol. Symp.* **1996,** *111* (1), 37-46.

52. Engelis, N. G.; Anastasaki, A.; Nurumbetov, G.; Truong, N. P.; Nikolaou, V.; Shegiwal, A.; Whittaker, M. R.; Davis, T. P.; Haddleton, D. M., Sequence-Controlled Methacrylic Multiblock Copolymers Via Sulfur-Free RAFT Emulsion Polymerization. *Nature Chemistry* **2017,** *9* (2), 171-178.

53. Engelis, N. G.; Anastasaki, A.; Whitfield, R.; Jones, G. R.; Liarou, E.; Nikolaou, V.; Nurumbetov, G.; Haddleton, D. M., Sequence-Controlled Methacrylic Multiblock Copolymers: Expanding the Scope of Sulfur-Free RAFT. *Macromolecules* **2018,** *51* (2), 336-342.

54. Shegiwal, A.; Wemyss, A. M.; Schellekens, M. A. J.; de Bont, J.; Town, J.; Liarou, E.; Patias, G.; Atkins, C. J.; Haddleton, D. M., Exploiting Catalytic Chain Transfer Polymerization for the Synthesis of Carboxylated Latexes Via Sulfur-Free RAFT. *Journal of Polymer Science Part A: Polymer Chemistry* **2019,** *57* (3), E1-E9.

55. Shegiwal, A.; Wemyss, A. M.; Liarou, E.; Town, J.; Patias, G.; Atkins, C. J.; Marathianos, A.; Lester, D. W.; Efstathiou, S.; Haddleton, D. M., Polymerisable Surfactants for Polymethacrylates Using Catalytic Chain Transfer Polymerisation (CCTP) Combined with Sulfur Free-RAFT in Emulsion Polymerisation. *Eur. Polym. J.* **2020,** *125*, 109491.

56. Atkins, C. J.; Patias, G.; Town, J. S.; Wemyss, A. M.; Eissa, A. M.; Shegiwal, A.; Haddleton, D. M., A Simple and Versatile Route to Amphiphilic Polymethacrylates: Catalytic Chain Transfer Polymerisation (CCTP) Coupled with Post-Polymerisation Modifications. *Polymer Chemistry* **2019,** *10* (5), 646-655.

57. Lotierzo, A.; Schofield, R. M.; Bon, S. A. F., Toward Sulfur-Free RAFT Polymerization Induced Self-Assembly. *ACS Macro Letters* **2017,** *6* (12), 1438-1443.

58. Lotierzo, A.; Longbottom, B. W.; Lee, W. H.; Bon, S. A. F., Synthesis of Janus and Patchy Particles Using Nanogels as Stabilizers in Emulsion Polymerization. *ACS Nano* **2019,** *13* (1), 399-407.

59. Atkins, C.; Seow, D. K.; Burns, G.; Town, J. S.; Hand, R. A.; Lester, D. W.; Cameron, N. R.; Haddleton, D.; Eissa, A. M., Branched Macromonomers from Catalytic Chain Transfer Polymerisation (CCTP) as Precursors for Emulsion-Templated Porous Polymers. *Polymer Chemistry* **2020,** *11* (23), 3841-3848.

60. Haddleton, D. M.; Depaquis, E.; Kelly, E. J.; Kukulj, D.; Morsley, S. R.; Bon, S. A. F.; Eason, M. D.; Steward, A. G., Cobalt-Mediated Catalytic Chain-Transfer Polymerization (CCTP) in Water and Water/Alcohol Solution. *J. Macromol. Sci. Part A: Polym. Chem.* **2001,** *39* (14), 2378-2384.

61. Patias, G.; Wemyss, A. M.; Efstathiou, S.; Town, J. S.; Atkins, C. J.; Shegiwal, A.; Whitfield, R.; Haddleton, D. M., Controlled Synthesis of Methacrylate and Acrylate Diblock Copolymers Via End-Capping Using CCTP and FRP. *Polymer Chemistry* **2019,** *10* (47), 6447-6455.

62. Yamada, B.; Oku, F.; Harada, T., Substituted Propenyl End Groups as Reactive Intermediates in Radical Polymerization. *Journal of Polymer Science Part A: Polymer Chemistry* **2003,** *41* (5), 645-654.

63. Kühnel, E.; Laffan, D. D. P.; Lloyd-Jones, G. C.; Martínez del Campo, T.; Shepperson, I. R.; Slaughter, J. L., Mechanism of Methyl Esterification of Carboxylic Acids by Trimethylsilyldiazomethane. *Angewandte Chemie International Edition* **2007,** *46* (37), 7075-7078.

64. Unzueta, E.; Forcada, J., Semicontinuous Emulsion Copolymerization of Methyl Methacrylate and N-Butyl Acrylate: 2. Effect of Mixed Emulsifiers in Unseeded Polymerization. *Polymer* **1995,** *36* (22), 4301-4308.

65. Feiz, S.; Navarchian, A. H., Emulsion Polymerization of Styrene: Simulation the Effects of Mixed Ionic and Non-Ionic Surfactant System in the Presence of Coagulation. *Chemical Engineering Science* **2012,** *69* (1), 431-439.

66. Rieger, J.; Stoffelbach, F.; Bui, C.; Alaimo, D.; Jérôme, C.; Charleux, B., Amphiphilic Poly(Ethylene Oxide) Macromolecular RAFT Agent as a Stabilizer and Control Agent in Ab Initio Batch Emulsion Polymerization. *Macromolecules* **2008,** *41* (12), 4065-4068.

67. Chaduc, I.; Girod, M.; Antoine, R.; Charleux, B.; D'Agosto, F.; Lansalot, M., Batch Emulsion Polymerization Mediated by Poly(Methacrylic Acid) Macroraft Agents: One-Pot Synthesis of Self-Stabilized Particles. *Macromolecules* **2012,** *45* (15), 5881-5893.

68. Andersson, M.; Wittgren, B.; Wahlund, K.-G., Accuracy in Multiangle Light Scattering Measurements for Molar Mass and Radius Estimations. Model Calculations and Experiments. *Analytical Chemistry* **2003,** *75* (16), 4279-4291.

69. Heuts, J. P. A.; Muratore, L. M.; Davis, T. P., Preparation and Characterization of Oligomeric Terpolymers of Styrene, Methyl Methacrylate and 2-Hydroxyethyl Methacrylate: A Comparison of Conventional and Catalytic Chain Transfer. *Macromolecular Chemistry and Physics* **2000,** *201* (18), 2780-2788.

70. Zhang, Q.; Slavin, S.; Jones, M. W.; Haddleton, A. J.; Haddleton, D. M., Terminal Functional Glycopolymers Via a Combination of Catalytic Chain Transfer Polymerisation (CCTP) Followed by Three Consecutive Click Reactions. *Polym. Chem.* **2012,** *3* (4), 1016-1023.

71. Duncan, M. A., Metal Cation Coordination and Solvation Studied with Infrared Spectroscopy in the Gas Phase. In *Physical Chemistry of Cold Gas-Phase Functional Molecules and Clusters*, Ebata, T.; Fujii, M., Eds. Springer Singapore: Singapore, 2019; pp 157-194.

72. Lawson, E. E.; Edwards, H. G. M.; Johnson, A. F., Vibrational Spectroscopic Characterization of Cobalt Dimethylglyoxime Boron Difluoride Ag. *Spectrochimica Acta Part A: Molecular Spectroscopy* **1994,** *50* (11), 1899-1907.

Chapter 3: *Amphiphilic macromonomers for the development of stable cyantraniliprole dispersions. Application of thin polymeric coating around cyantraniliprole particles*

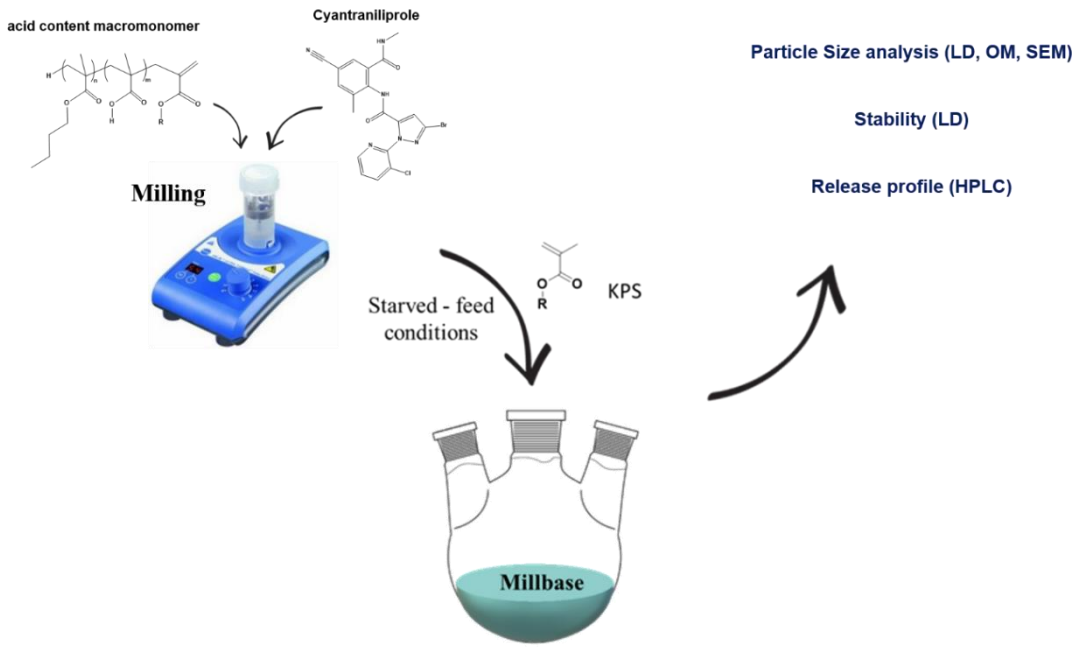

In this chapter, ω-unsaturated amphiphilic CCTP macromonomers were synthesized and used for the development of stable dispersions of an anthranilic diamide insecticide, cyantraniliprole (CYNT). In order to verify the particle size (desired particle size ~2-10 μm) and the stability of the active ingredient (AI) dispersions, light scattering (laser diffraction, LD) and microscopy (optical microscopy, OM) techniques were used. Following the optimization of the milling process, the encapsulation of cyantraniliprole particles through the surfactant-free emulsion polymerisation of methyl methacrylate/*n*-butyl acrylate mixture (MMA/*n*-BA, 10:1) under starved-feed conditions was investigated. The extraction of cyantraniliprole particles was followed by High Performance Liquid Chromatography (HPLC) giving

insights on the release profile of the cyantraniliprole particles. Scanning Electron Microscopy (SEM) was used for the determination of latex coating around cyantraniliprole particles.

3.1 Introduction

Global population growth over the past decades has triggered the need for food demand and therefore for higher agricultural yields.[1] In consequence, state-of the-art technologies have been developed and introduced in the agricultural field for plant protection and enhancement of crop products.[2-4] More than a million tones of agrochemical products; fertilizers, pesticides, herbicides, etc. are used in farm fields every year. Directing and keeping agrochemicals at the desired target can be challenging, as a range of loss mechanisms could occur to reduce the effectiveness of a crop protection product.[5, 6] The main reasons include degradation by photolysis, hydrolysis, leaching, washing away by rain and microbial activity. Hence, the majority of research groups, both in academia and industry, have focused on the development of sustainable and efficacious agrochemicals. Sustainability entails high yields and agricultural practices that have acceptable environmental consequences in land conversions, water use and contamination of ecosystems by agrochemicals.[7] Efficacy for plant protection can be achieved by several ways, such as by control release, targeted delivery, enhanced bioavailability, increased leaf adhesion and improved stability of the AI in the environment.[8]

Insecticides are a type of pesticide that is used to specifically target and kill insects. In the market they can be found in the form of seed or soil treatments or sprayed mixtures and are almost always a formulation of more than one component.[9] Formulations can be divided into three main categories; liquid formulations (emulsifiable concentrates, solutions, aerosols, etc.), dry or solid formulations (baits, granules, pellets, wettable powders, etc.) and formulations that cannot be clearly classified as liquid or dry/solid formulations (microencapsulated materials, water soluble packets, fumigants, etc.).[10] Microencapsulated formulations contain particles of the liquid or dry AI covered by a polymeric coating, are mixed with water and sprayed in the same manner as other sprayable formulations. Industries are interested in polymer microencapsulation technology due to the choices it offers.[11-13] In general, the microencapsulated particles are designed to release their contents when exposed to a particular trigger. The release of the particles can be controlled from a variety of stimuli such as temperature,[14, 15] humidity,[16] the soil composition[17] or a combination

of factors. Delayed or slow release of the AI prolongs its effectiveness, allowing for fewer and less precisely timed applications.

Anthranilic diamides are an exceptionally active class of insecticides, with a mode of action targeting the ryanodine receptors (RyRs) in insect muscle cells.[18] These receptors have a significant role in muscle function, regulating the release of calcium from internal stores.[19] Anthranilic diamide insecticides, like cyantraniliprole (3-bromo-1-(3-chloro-2-pyridinyl)-*N*-[4-cyano-2-methyl-6-[(methyl amino)carbonyl] phenyl]-1H-pyrazole-5-carboxamide, **Scheme 3-1**) bind to these receptors, resulting in uncontrolled release and depletion of internal calcium, preventing further muscle spasm. Therefore, insects treated with cyantraniliprole show rapid cessation of feeding, lethargy, regurgitation, muscle paralysis and ultimately death.[20]

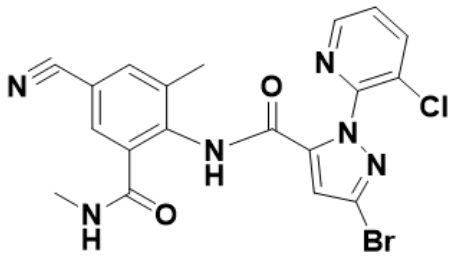

Scheme 3-1. Structure of cyantraniliprole, a diamide insecticide.

Currently, cyantraniliprole is applied to a field in a simple aqueous dispersion, however, this method is inefficient as the insecticide is quickly released into the ground and can be washed off into surrounding ground water. Controlling the release of cyantraniliprole would reduce loss due to wash off and possibly eliminate the need for multiple and precisely timed applications. Hence, microencapsulated formulations of cyantraniliprole have the potential to offer a sustainable release as well as reduce an environmental concern. Amphiphilic macromonomers could enable the application of thin polymeric coating around individual particles and offer the advantage of being able to be performed directly to dispersed AI particles in an aqueous system.[21-24]

As described in Chapter 2, CCTP (**Scheme 3-2)** is an efficient and versatile technique for the synthesis of low molecular weight functional polymers in free radical polymerization (FRP).[25-27] The technique is based on the use of certain low spin [Co(II)] complexes which catalyze the chain transfer to monomer reaction[28-30] and also provides a high level of vinyl ω- end group functionality.[31, 32] Due to their high chain

transfer constants, [Co(II)] complexes are efficient in low concentrations (ppm to monomer). The effectiveness of the catalysts, and the fact that radical addition to the vinyl end group of CCTP macromonomers forms adducts that readily undergo *β*-scission, allow them to function as addition-fragmentation chain transfer agents (CTAs) and render CCTP extensively applicable in industry.[33]

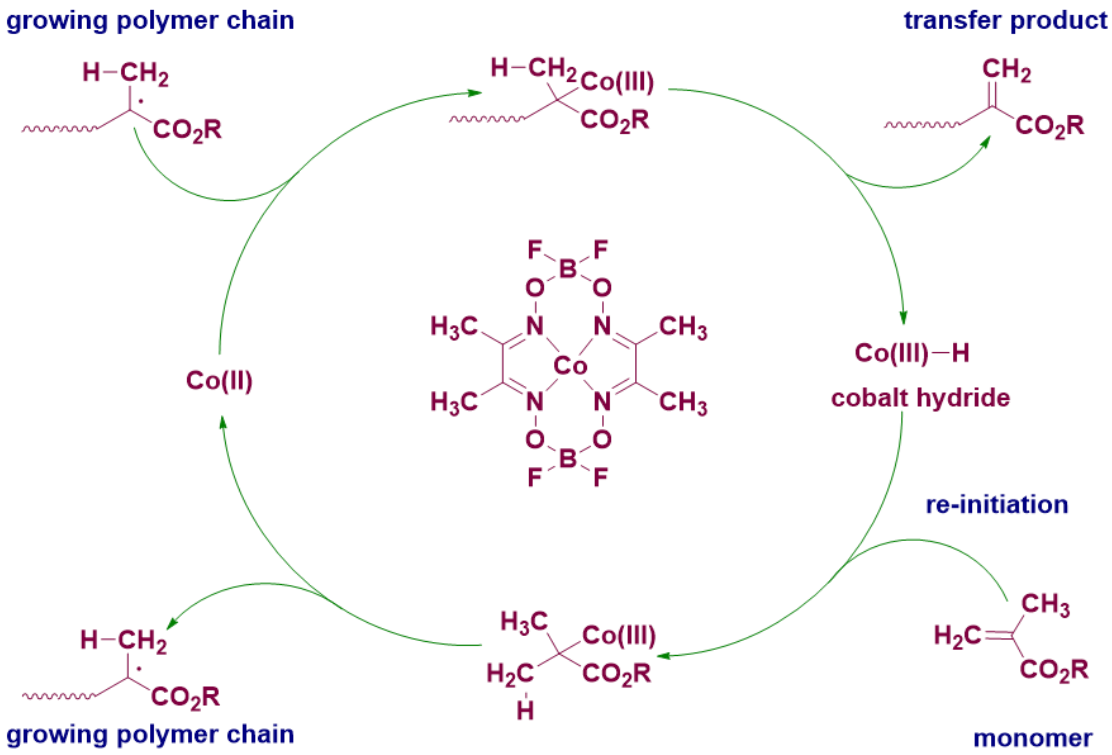

Scheme 3-2. Proposed catalytic cycle for CoBF-mediated CCTP.[25, 27]

In this chapter, *ω*-unsaturated amphiphilic macromonomers were synthesized *via* Catalytic Chain Transfer Polymerization with the use of CoBF, as chain transfer agent (CTA). Subsequently, these macromonomers were used for the development of stable dispersions of the anthranilic diamide insecticide, cyantraniliprole. The encapsulation of cyantraniliprole would prolong the release of the AI following the application to a target area. Thus, formulations of coated cyantraniliprole particles were prepared under starved-feed emulsion polymerization of a mixture of methyl methacrylate (MMA) and *n*-butyl methacrylate (*n*-BA). The particle size (desired particle size ~2-10 μm) and the stability of the dispersions and formulations were followed by light scattering (laser diffraction, LD), optical microscopy (OM) and scanning electron microscopy (SEM). Furthermore, the release profile of the

cyantraniliprole particles was investigated using High Performance Liquid Chromatography (HPLC).

3.2 Results and discussion

3.2.1 Synthesis of amphiphilic macromonomers though CCTP

The main idea behind this work is to apply a thin polymeric coating around the particles of an insecticide, cyantraniliprole, to prolong the release of the AI following the application to a target area. Previously, Ali *et al.* and Loiko *et al.* synthesized short amphiphilic co-oligomers that dispersed particles of a hydrophobic clay (gibbsite) in aqueous solutions.[21, 34] These were subsequently chain extended using starved-feed emulsion polymerization to successfully encapsulate the particles, without the need for the co-oligomers to be chemically immobilized on to the particle`s surface.

In order to generate amphiphilic co-oligomers, Ali *et al.* used a Reversible Addition-Fragmentation chain transfer (RAFT) based technique, whereas Loiko *et al.* used Atom Transfer Radical Polymerization (ATRP). We, however, are using CCTP to synthesize ω-unsaturated macromonomers of butyl methacrylate (BMA) and *tert*-butyl methacrylate (*t*-BMA). Acidic hydrolysis of the *tert*-butyl groups resulted in amphiphilic methacrylic macromonomers, which will subsequently be used to disperse the cyantraniliprole particles.

Initially, a series of polymerizations of BMA were conducted altering the concentration of CoBF in order to identify the amount required as to achieve the desired molecular weight (~2,000 g mol^{-1}), **Scheme 3-3**. Briefly, polymerizations with four [BMA]/[CoBF] ratios (4, 8, 12, 16 ppm of CoBF) were conducted using an azo-initiator (V-65) in toluene and stopped at low conversions, to minimize termination and keep [monomer]/[CTA] ratios relatively consistent. An identical experiment in the absence of CoBF resulted in the typical free radical polymerization with significantly higher M_n value. The ^{1}H NMR spectrum of the pBMA macromonomer synthesized

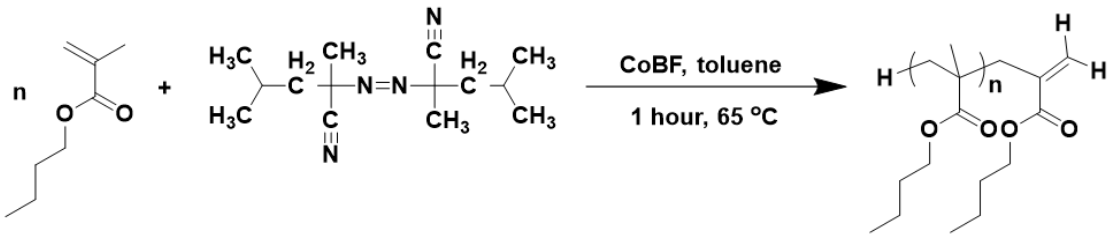

Scheme 3-3. Synthesis of pBMA macromonomer through CCTP.

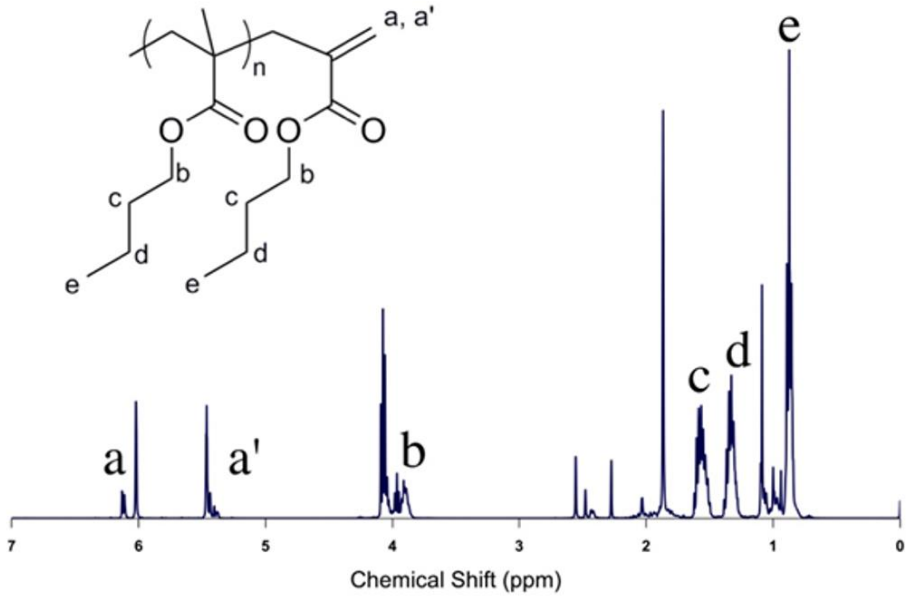

Figure 3-1. ^{1}H NMR spectrum of pBMA macromonomer synthesized using 16 ppm of CoBF

using 16 ppm of CoBF (**Figure 3-1**) shows that the vinyl peaks (a and a`) are present in the macromonomer and the integrated intensity of these peaks was compared with the CH_2 protons (b) to calculate the monomer conversion (28%), which is predictable low given the short reaction time (1 hour).

Varying CoBF concentration resulted in the tuning of the molecular weights, as expected, since higher CoBF concentration leads to more chain transfer events, thus the molecular weight is reduced, **Figure 3-2**. The molecular weight (M_n) measured by SEC and used to calculate the reciprocal of the degree of polymerization (1/DP). Using the pseudo-Mayo equation (equation 1),[35] plotting 1/DP against [CoBF]/[BMA] gives a good straight line with slope C_T = 17,700 (**Figure 3-3**) considering the chain transfer activity of other reaction components to be negligible. The value of C_T of the batch of CoBF used in these experiments, is in good agreement with literature values in the range of 16,000 – 28,000.[36]

$$\frac{1}{DP} = \frac{1}{DP_0} + C_T \frac{[Co]}{[M]} \qquad [1]$$

where DP is the degree of polymerisation, DP_0 is the degree of polymerisation in the absence of a chain transfer agent, and $[Co]$ and $[M]$ are the CoBF and monomer concentrations, respectively.

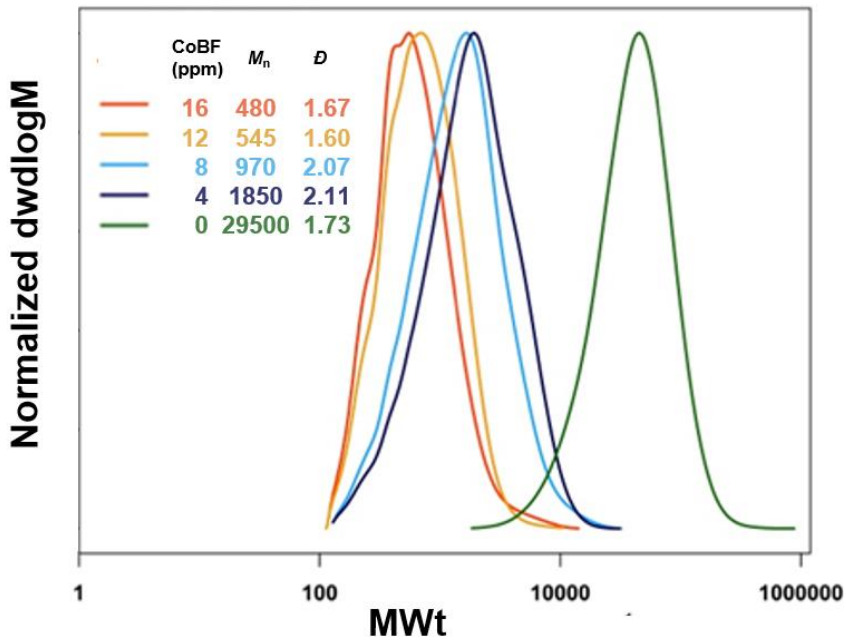

Figure 3-2. $CHCl_3$-SEC derived molecular weight distributions showing the evolution of MWts of pBMA using different amounts of CoBF.

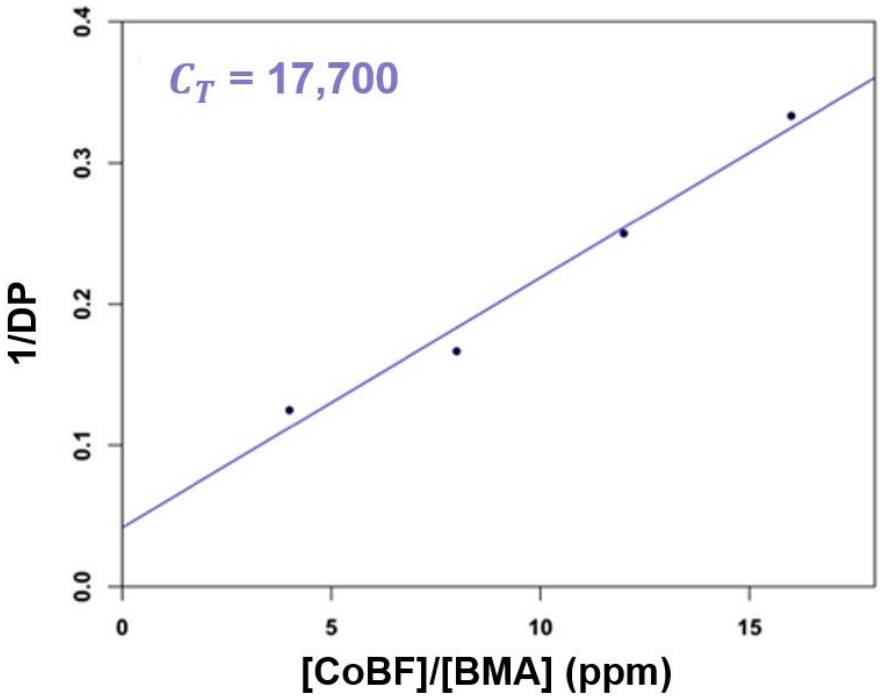

Figure 3-3. Pseudo - Mayo plot showing the calculation of the chain transfer constant (C_T) using Equation 1.

To obtain macromonomers with M_n of approximately 2,000 g mol^{-1} (DP = 14), it was calculated from the pseudo-Mayo plot in **Figure 3-3** that 1.68 ppm of CoBF relative to the monomer was needed. Considering that the catalytic activity of CoBF will be similar for BMA and *tert*-BMA, three statistical copolymers were synthesized with a targeted content of *tert*-butyl groups of 60, 70 and 80% (**Scheme 3-4**, **Table 3-1**). Consequently, acidic hydrolysis of the *tert*-butyl groups resulted in the amphiphilic statistical copolymers p(MAA-*stat*-BMA) with different acid content, maintaining the functionality of the end-group (**Scheme 3-5**, **Table 3-2)**.

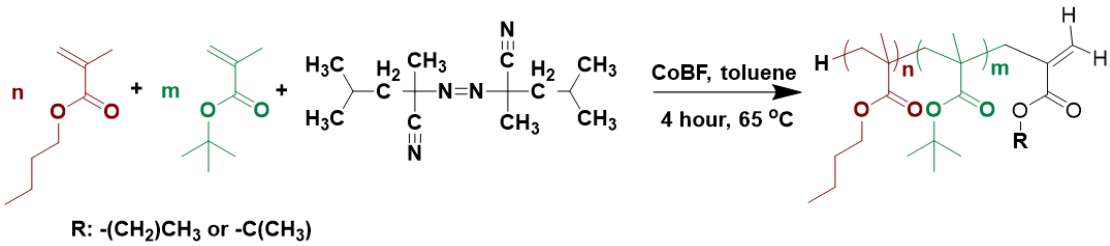

Scheme 3-4. Synthesis of p(*t*BMA–*stat*–BMA) statistical macromonomers through CCTP.

Table 3-1. ^{1}H NMR and SEC analysis of p(*t*BMA–*stat*–BMA) statistical macromonomers.

Entry	*t*BMA (%)	BMA (%)	Mon. Conversion (%)^a	$M_{n\ SEC}{}^b$	$Đ^b$
1	60	40	85	1,700	1.79
2	70	30	83	1,300	1.80
3	80	20	82	1,300	1.83

^{a} Conversion was calculated *via* ^{1}H NMR in $CDCl_3$.
^{b} Determined by THF-SEC analysis and expressed as molecular weight equivalents to pMMA narrow molecular weight standards.

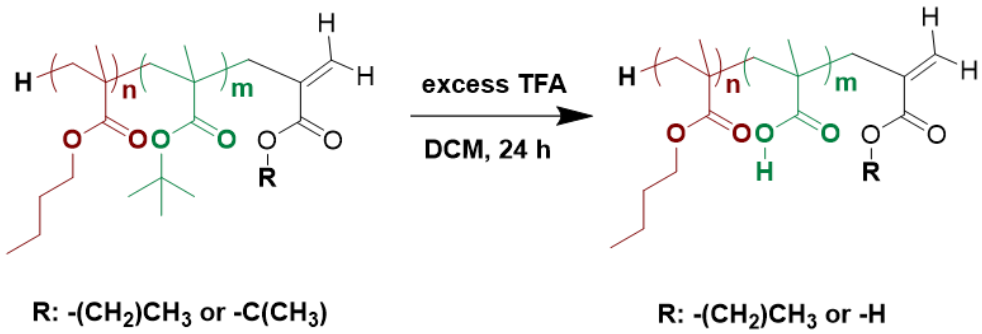

Scheme 3-5. Acidic hydrolysis of p(*t*BMA–*stat*–BMA) for the preparation of p(MAA–*stat*–BMA) statistical macromonomers.

Table 3-2. ^{1}H NMR and SEC analysis after the acidic hydrolysis of p(*t*BMA–*stat*–BMA) statistical macromonomers.

Entry	MAA (%)	BMA (%)	MAA (DP)[a]	BMA (DP)[a]	M_n (g mol^{-1})[a]	$M_{n\ SEC}$[b]	$Đ$[b]
1	60	40	10	5	1,600	1,700	1.24
2	70	30	9	3	1,200	3,100	1.34
3	80	20	10	2	1,200	1,800	1.25

[a] Molecular weight and DP was calculated *via* ^{1}H NMR in DMSO-d_6.
[b] Determined by DMF-SEC analysis and expressed as molecular weight equivalents to pMMA narrow molecular weight standards.

In **Figures 3-4** to **3-9**, ^{1}H NMR and SEC analysis of the macromonomers before and after hydrolysis of the *tert*-butyl groups, are shown. The absence of the peak at 1.42 ppm shows that the *tert*-butyl groups have been successfully deprotected. This is further confirmed by the presence of the peak from acid protons, the region of which is expanded in each figure. Comparing the vinyl end group integrals (~5.5-6.5 ppm) with those of CH_2 peak of pBMA (~3.7-4.0 ppm) and the acidic proton (~12 ppm) gave an indication of the molecular weight of the amphiphilic macromonomers, as well as their DP.

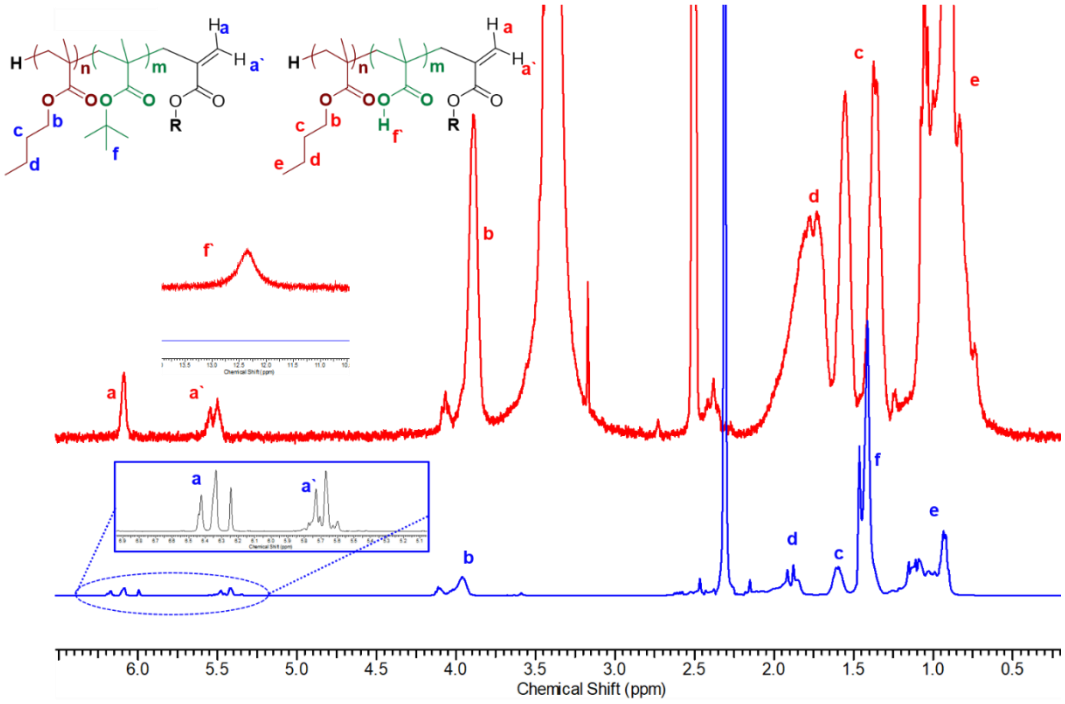

Figure 3-4. ^{1}H NMR spectra of p(*t*BMA-*stat*-BMA) macromonomer (blue trace) and p(MAA-*stat*-BMA) macromonomer (red trace). Acid content: 60%.

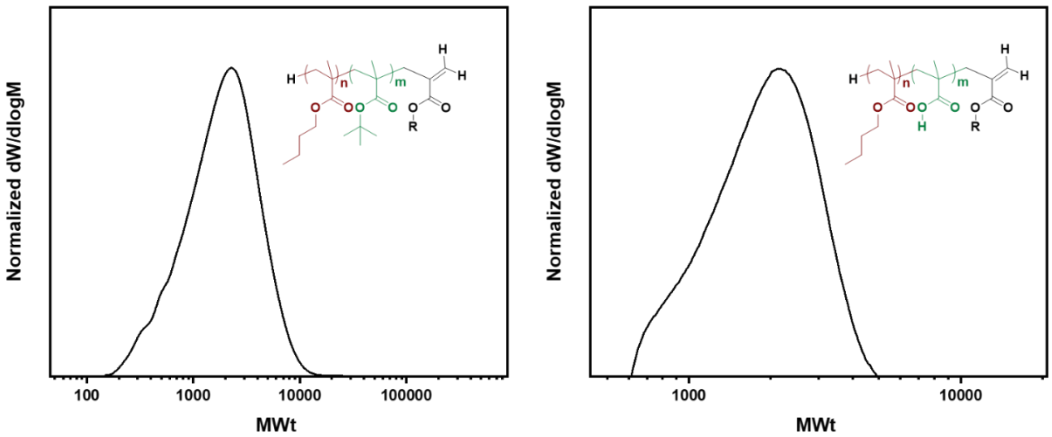

Figure 3-5. THF-SEC derived molecular weight distribution of p(*t*BMA-*stat*-BMA) macromonomer (left) and p(MAA-*stat*-BMA) macromonomer (right). Acid content: 60%.

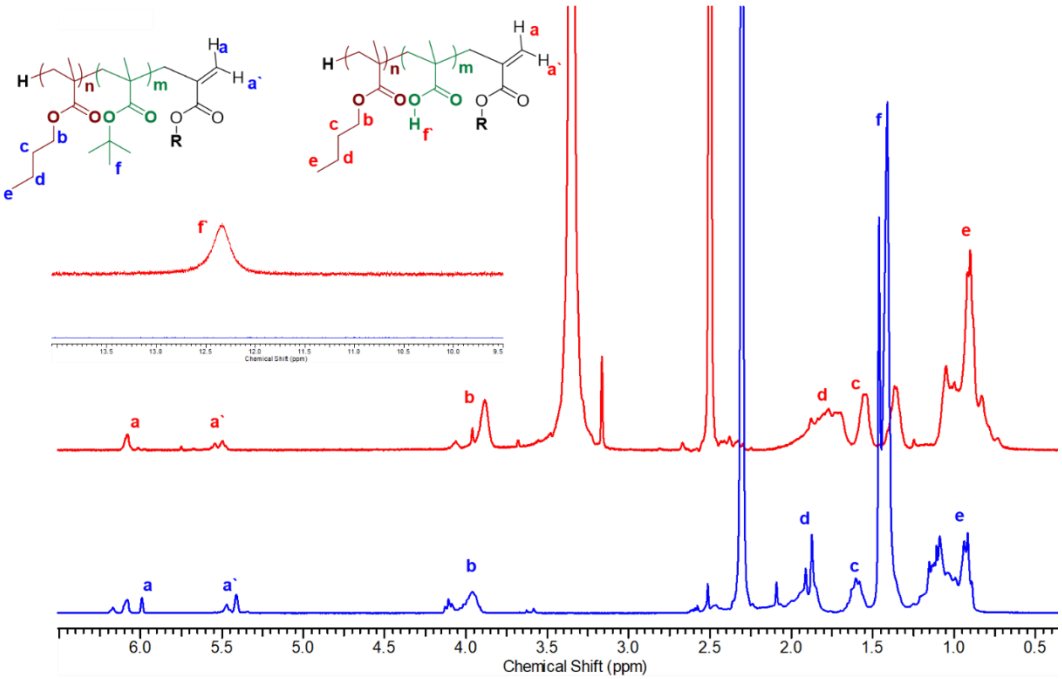

Figure 3-6. ^{1}H NMR spectra of p(*t*BMA-*stat*-BMA) macromonomer (blue trace) and p(MAA-*stat*-BMA) macromonomer (red trace). Acid content: 70%.

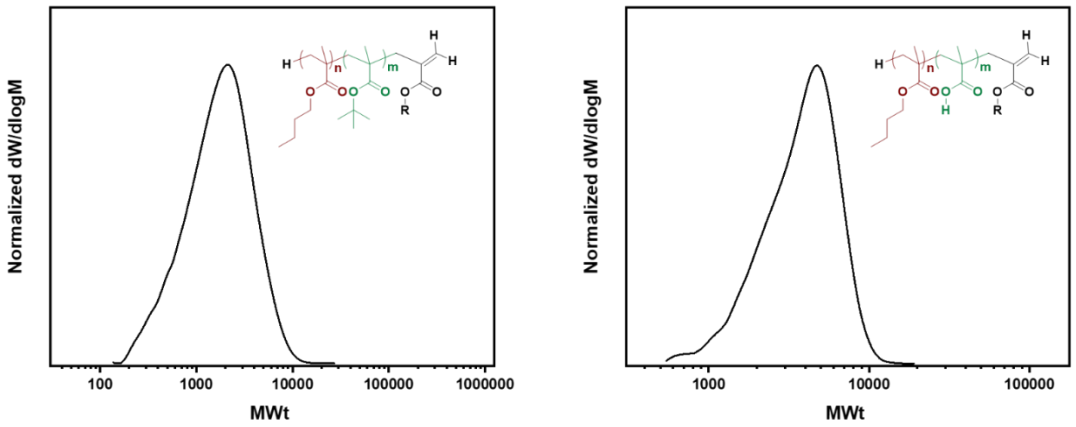

Figure 3-7. THF-SEC derived molecular weight distribution of p(*t*BMA-*stat*-BMA) macromonomer (left) and p(MAA-*stat*-BMA) macromonomer (right). Acid content: 70%.

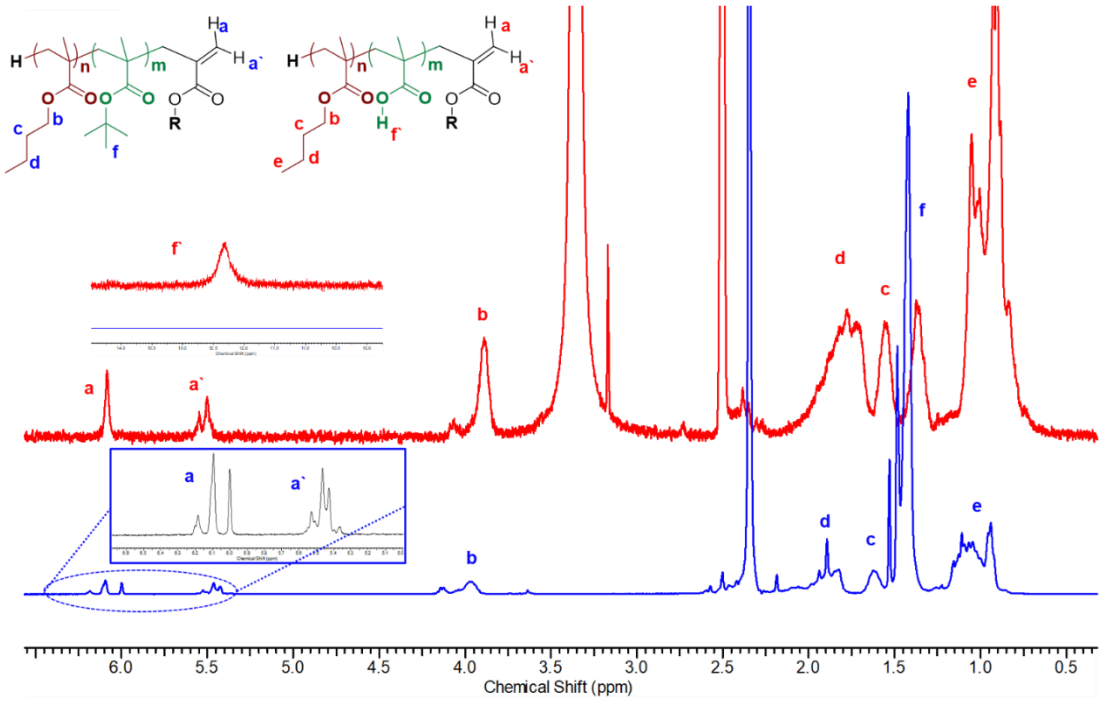

Figure 3-8. ^{1}H NMR spectra of p(*t*BMA-*stat*-BMA) macromonomer (blue trace) and p(MAA-*stat*-BMA) macromonomer (red trace). Acid content: 80%.

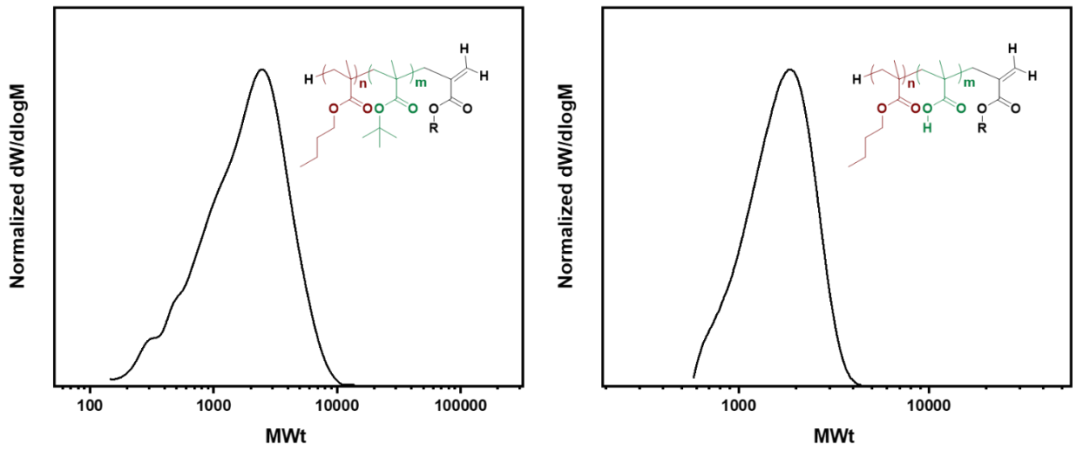

Figure 3-9. THF-SEC derived molecular weight distribution of p(*t*BMA-*stat*-BMA) macromonomer (left) and p(MAA-*stat*-BMA) macromonomer (right). Acid content: 80%.

SEC analysis of the macromonomers proved to be challenging, as the deprotection of the *tert*-butyl groups resulted in macromonomers composed of more than 60% of methacrylic acid, which made them insoluble in the organic solvents used for GPC analysis, for example, $CHCl_3$ or THF and partially soluble in DMF. The samples were run using DMF as the eluent after their filtration. It has been previously observed that the DMF-GPC analysis of methacrylic acid gives higher M_n values than expected. Furthermore, higher molar mass fractions of the polymer might have been removed during filtration, thus leading to dispersity values as low as those observed for the amphiphilic macromonomers.

In order to confirm the percentage of acid functionality in each macromonomer, matrix assisted laser desorption-ionization time of flight mass spectroscopy (MALDI-ToF-MS) was used, revealing that the chemical composition is in agreement with the expected values. More specifically, peaks with the same DP but different chemical composition had different intensity, for example expanded spectra in a specific region *m/z* 1,040 to 1,200 in **Figures 3-10** to **3-12.** Chemical analysis and comparison of the percentage of each peak across the spectrum showed that the acid functionality in the macromonomers was 62, 68 and 77%, thus confirming that the targeted acid content, 60, 70 and 80%, has been achieved.

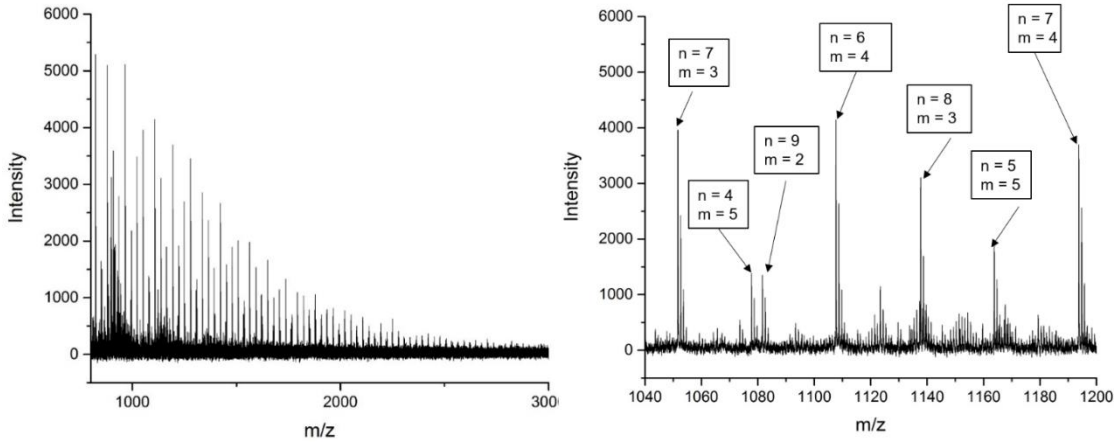

Figure 3-10. MALDI-ToF-MS spectrum of the p(MAA$_{10}$-*stat*-BMA$_5$) macromonomer (left) and expanded region showing peaks of several copolymeric chains (right). Acid content: 60%.

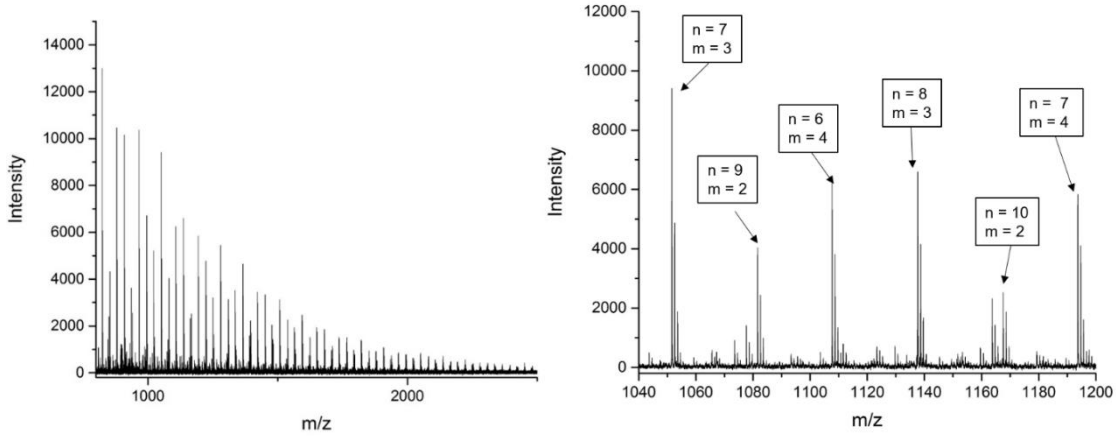

Figure 3-11. MALDI-ToF-MS spectrum of the p(MAA$_9$-*stat*-BMA$_3$) macromonomer (left) and expanded region showing peaks of several copolymeric chains (right). Acid content: 70%.

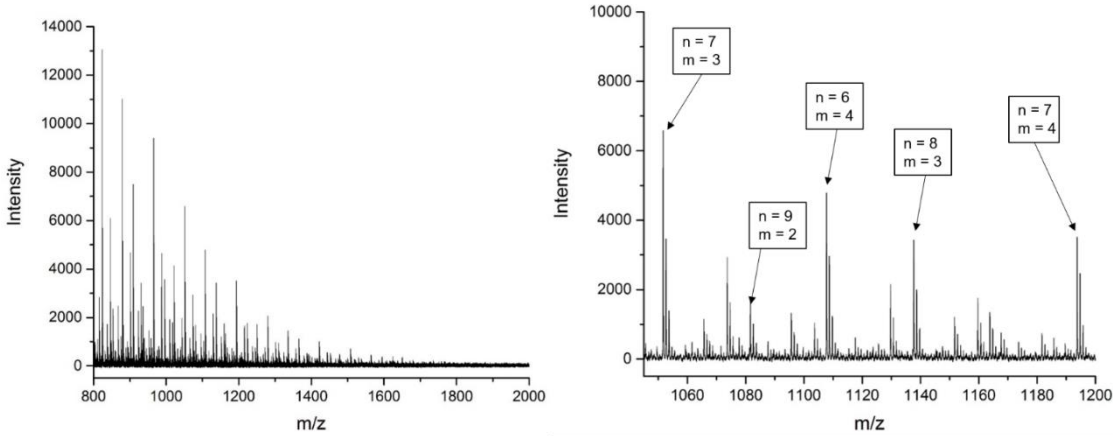

Figure 3-12. MALDI-ToF-MS spectrum of the p(MAA$_{10}$-*stat*-BMA$_2$) macromonomer (left) and expanded region showing peaks of several copolymeric chains (right). Acid content: 80%.

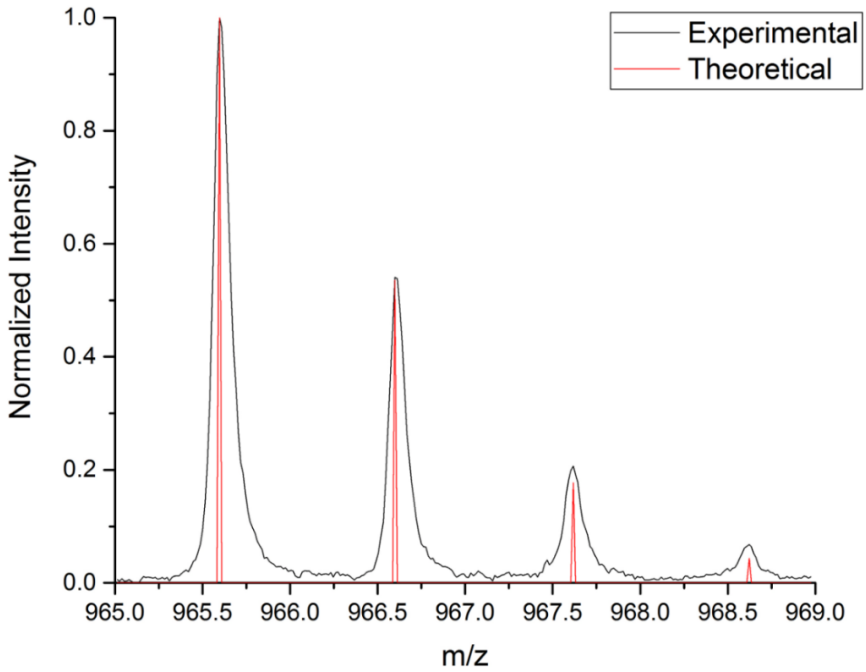

Figure 3-13. Comparison of experimental and theoretical isotopic pattern of p(MAA$_{10}$-*stat*-BMA$_5$), showing no saturation of the macromonomer.

Moreover, full copolymer formation was observed along with no evidence of homopolymers or saturated macromonomers. The normalized intensity of the theoretical and experimental isotopic distributions were overlayed and show excellent match, **Figure 3-13**. In the case of saturation, namely loss of the double bond of the end-group, the intensity of the peak that corresponds to *m/z* = 967.6 Da would have been higher than the theoretical value.

3.2.2 Dispersion of cyantraniliprole particles in aqueous solution

Cyantraniliprole has a very low solubility value in water (14.2 mg/L at 20 ^{o}C) and has a particle size in the range of few nm to 4 μm and the particles are highly irregular in shape(**Figure 3-14**). In water cyantraniliprole forms big aggregates (>50 μm, **Figure 3-15a**). In this study, amphiphilic macromonomers were used in order to evaluate their ability to perform as efficient dispersants of cyantraniliprole particles with a desired particle size range of 2-10 μm.

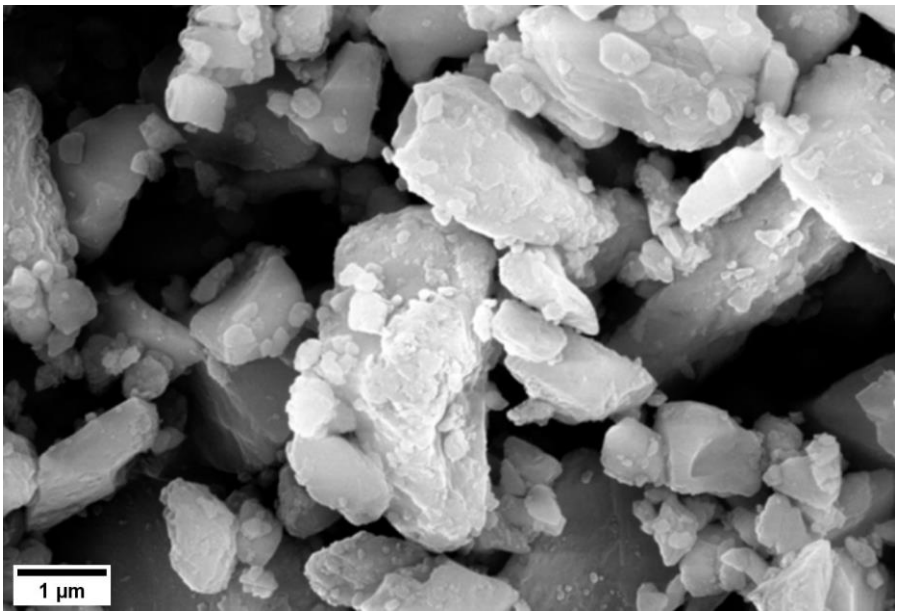

Figure 3-14. SEM image of cyantraniliprole, showing that the particles are of a wide range of sizes and are highly irregular in their shape.

Initial dispersion tests took place by using different amounts of the 70% acid content macromonomer. 0.05 g, 0.1 g and 0.2 g were weighed into vials and 10 mL of water was added to each, with an additional 10 mL of buffer being added to a separate vial to be used as a control sample. To dissolve the macromonomer, 5 drops of 2 M KOH was added to each sample, including the control, and all were left stirring overnight. As has been reported previously by Sharma *et al.*[37], controlling the pH and maintain a value of around 7 is important to avoid fast hydrolysis of the insecticide. After measuring and finding the pH to be around 7, to each vial was added 2 g of cyantraniliprole particles and all were vortexed for approximately 5 minutes. Subsequently, the samples were sonicated using a Branson Digital Sonifier (probe

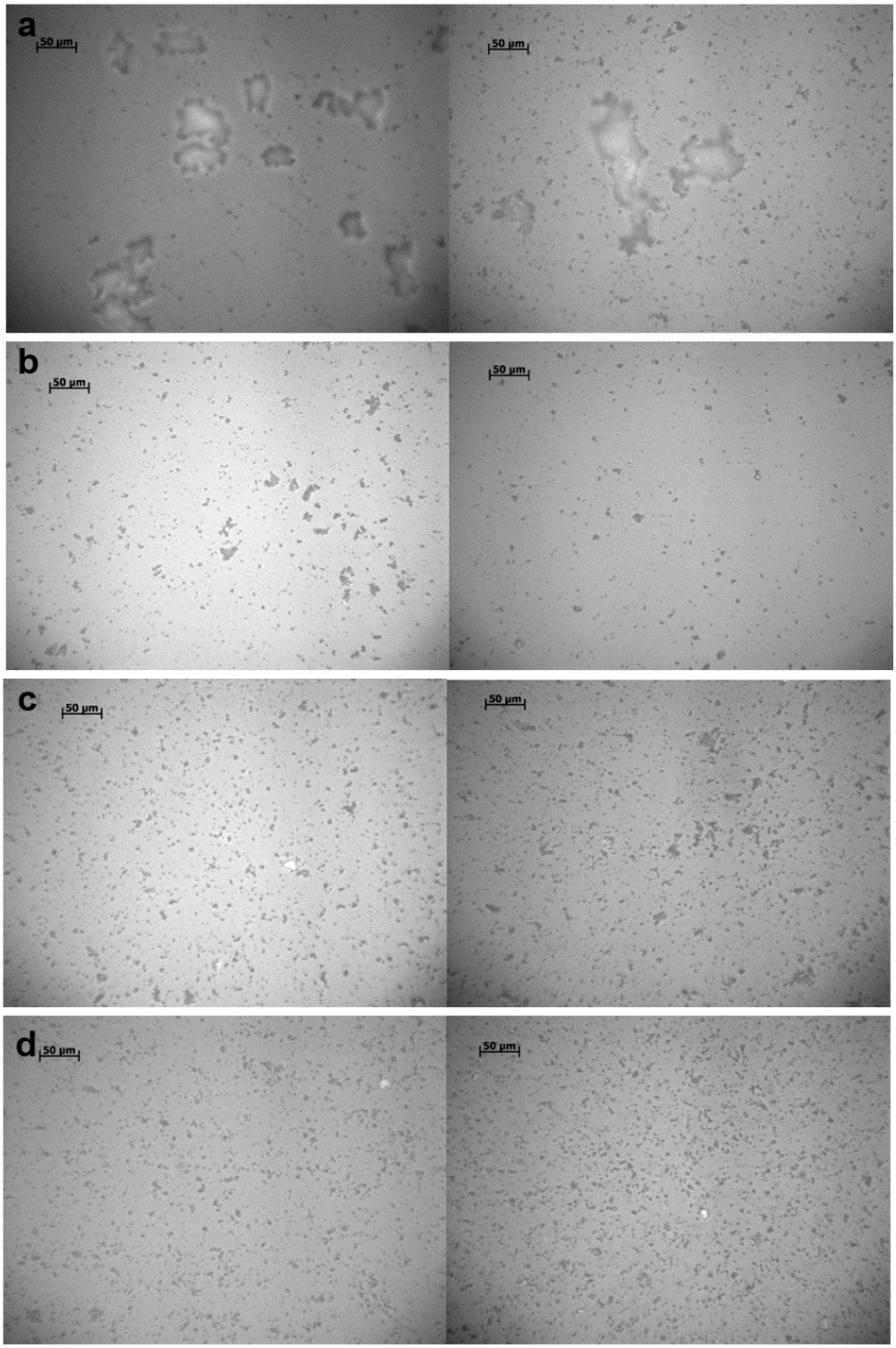

Figure 3-15. Optical microscopy images taken of **a)** cyantraniliprole only, control sample, where no macromonomer was added, cyantraniliprole particles where **b)** 0.05 g ([MM] : [CYNT] = 2.5 w/w%), **c)** 0.1 g ([MM] : [CYNT] = 5 w/w%) and **d)** 0.2 g ([MM] : [CYNT] = 10 w/w%) of the amphiphilic macromonomer were added.

model: 102-C) at 30% for 1 minute. Optical microscopy (OM) images of these samples show that the p(MAA-*stat*-BMA) macromonomer can be used to disperse the particles of cyantraniliprole and that 2.5, 5 and 10 w/w % of macromonomer to insecticide particles appears to produce well dispersed samples, **Figure 3-15**.

Based on these results, further studies were required to investigate the *optimum* ratio between the macromonomer and cyantraniliprole, as well as the stability of the AI dispersions. Thus, several [macromonomer] : [cyantraniliprole] ([MM] : [CYNT]) ratios were applied for the preparation of AI dispersions (**Table 3-3**), using an IKA Ultra TURRAX Tube Drive Disperser for the milling process (**Figure 3-16**). The cyantraniliprole mass was kept at 10 w/w % for these experiments. Three different time intervals were used for the milling of cyantraniliprole (1, 5 and 10 minutes), whereas the particle size was followed by laser diffraction (LD) and optical microscopy (OM).

Milling of the cyantraniliprole particles resulted in AI dispersions with a mean particle size in the desired range of ~2–10 μm according to LD analysis (**Figure 3-17**). However, populations of larger particles were apparent, especially when lower milling times were applied along with low [MM] : [CYNT] ratios, which proved to be insufficient for the successful dispersion of the whole amount of cyantraniliprole particles. This was observed on the AI dispersions where the 60% and the 70% macromonomer were used to stabilize the AI particles (**Figure 3-17 a, b, d, & e**). On the other hand, when the 80% acid content macromonomer was used, bigger particles were present at high [MM] : [CYNT] ratio (**Figure 3-17 g & h**). In this case, this might be attributed to the excess of the macromonomer which probably led to aggregates with poor dispersion properties.

Table 3-3. Dispersion tests using IKA Ultra TURRAX Tube Drive Disperser for the milling process of cyantraniliprole

Entry	Acid Content MM (%)	[MM] : [CYNT]	Time (min)
1	60	0.1 %	1, 5, 10
2	60	0.5 %	1, 5, 10
3	60	1 %	1, 5, 10
4	60	5 %	1, 5, 10
5	70	0.1 %	1, 5, 10
6	70	0.5 %	1, 5, 10
7	70	1 %	1, 5, 10
8	70	5 %	1, 5, 10
9	80	0.1 %	1, 5, 10
10	80	0.5	1, 5, 10
11	80	1 %	1, 5, 10
12	80	5 %	1, 5, 10

Figure 3-16. IKA Ultra TURRAX Tube Drive Disperser used for the milling process of cyantraniliprole in this study.

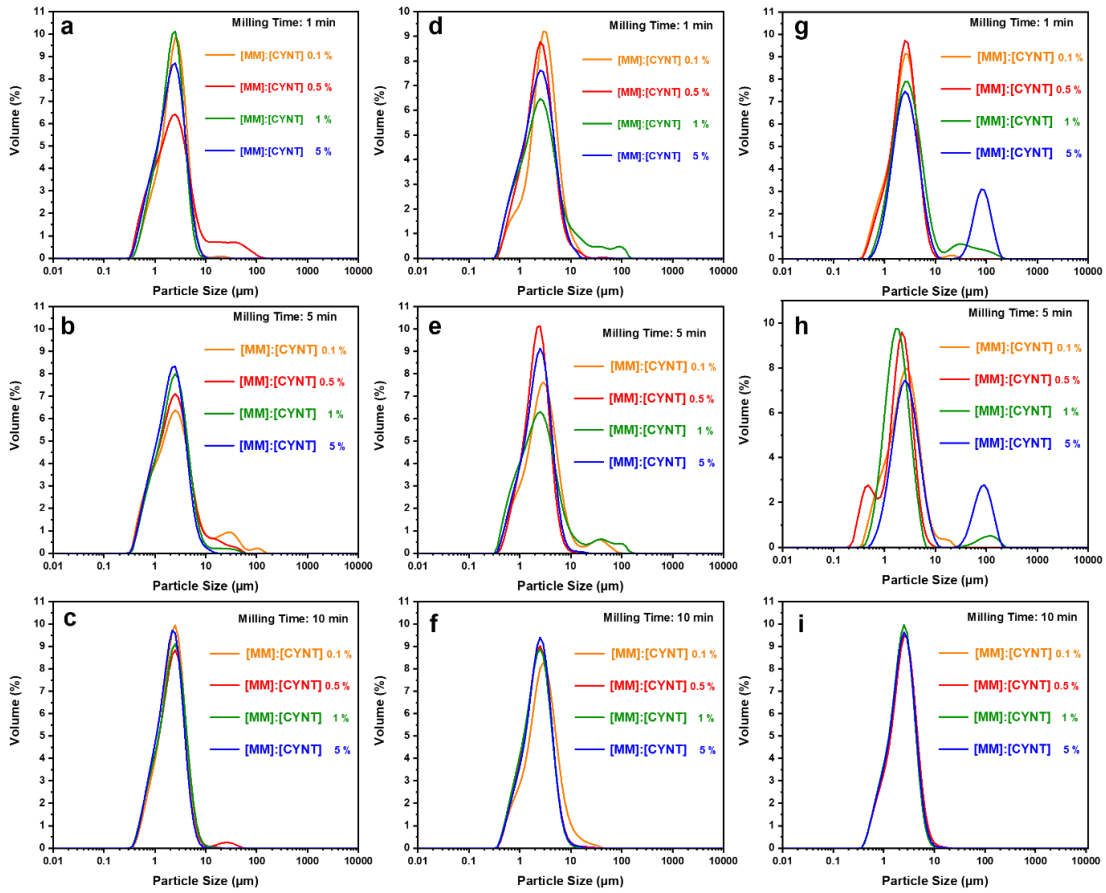

Figure 3-17. Laser Diffraction analysis showing the particle size of cyantraniliprole after the milling process using various concentrations of **a)**, **b)** and **c)** 60% acid content macromonomer, **d)**, **e)** and **f)** 70% acid content macromonomer and **g)**, **h)** and **i)** 80% acid content macromonomer.

Optical microscopy images correlate well with results from LD measurements, as shown in **Figure 3-18**. The particles with bigger size are apparent in images where the samples were milled for 1 and 5 minutes, although the mean particle size is in the desired range (**Figure 3-18 a, b, d, e, g & h**). However, a milling time of 10 minutes resulted in dispersions with a single particle size distribution (**Figure 3-18 c, f & i**). Additional optical microscopy images of the AI dispersions can be found in section *3.4.4 Supplementary Figures and Tables* (**Figures 3-44** to **3-46**).

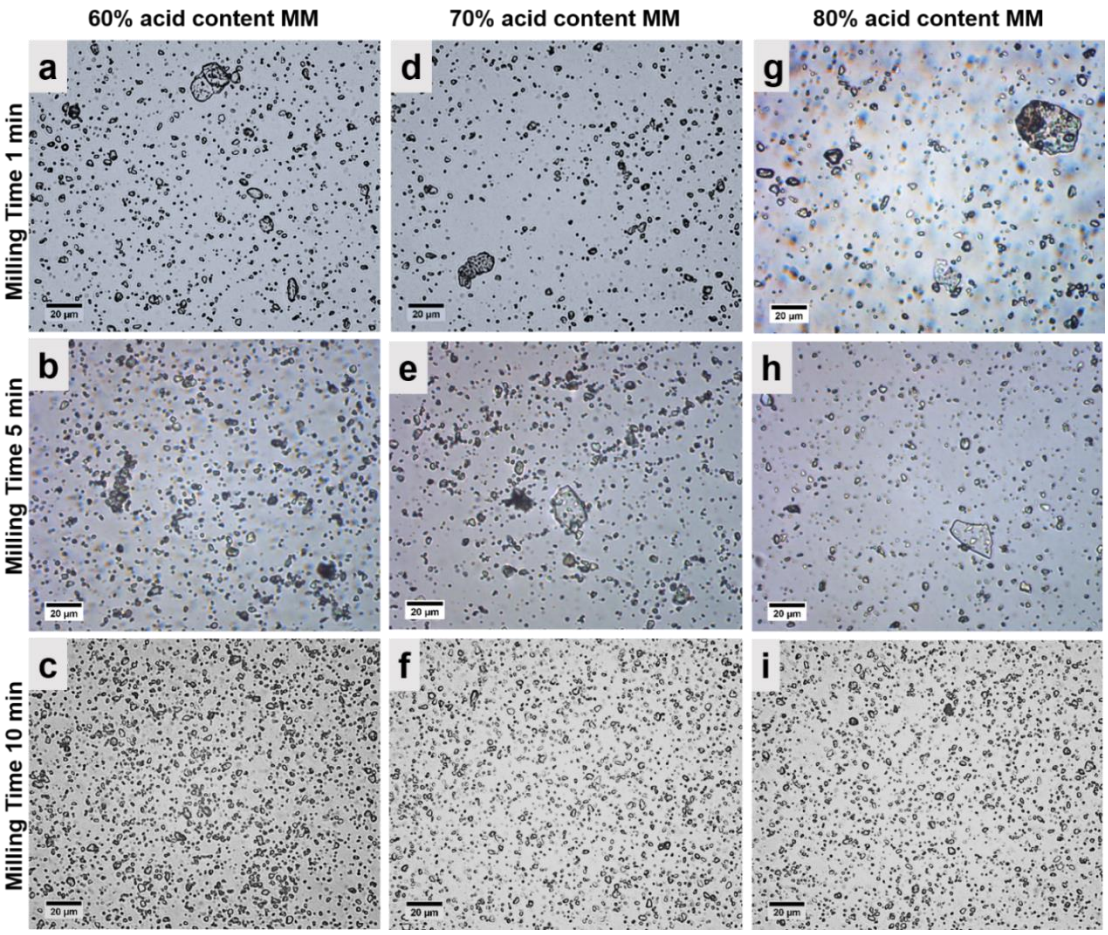

Figure 3-18. Optical microscopy images of cyantraniliprole dispersions using **a)**, **b)** and **c)** 60% acid content macromonomer. **d)**, **e)** and **f)** 70% acid content macromonomer. **g)**, **h)** and **i)** 80% acid content macromonomer. [MM] : [CYNT] = 1%. Scale bar 20 µm.

Based on these results the *optimum* milling time for the preparation of AI dispersions was 10 minutes independently of the [MM] : [CYNT] ratio. Therefore, the next step was to verify the stability of these AI dispersions. LD measurements and OM images of the samples milled for 10 minutes showed that excellent stability could be maintained even one week after the milling process, **Figure 3-19 & 3-20**.

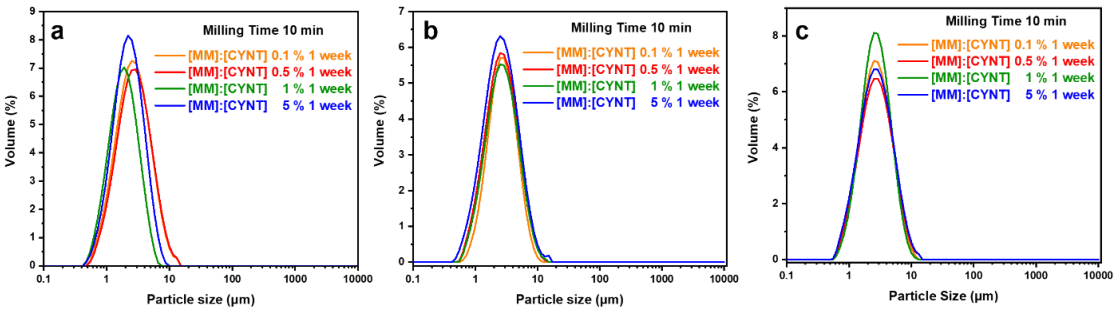

Figure 3-19. Laser Diffraction measurements of cyantraniliprole dispersions using **a)** 60% acid content macromonomer, **b)** 70% acid content macromonomer and **c)** 80% acid content macromonomer. The measurements were taken 1 week after the milling process.

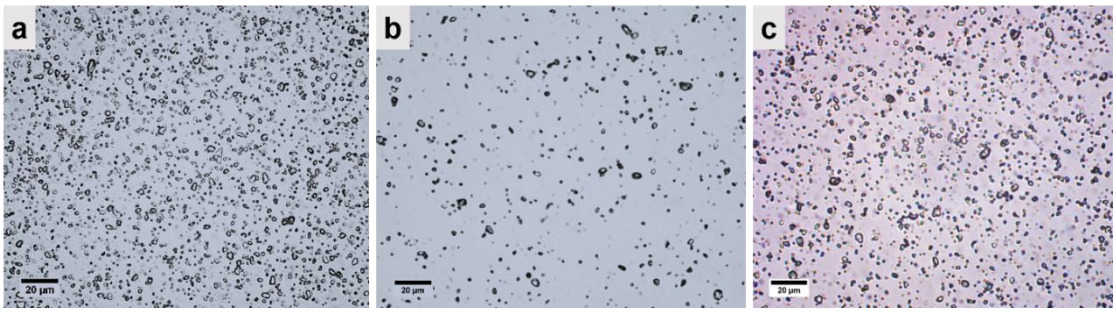

Figure 3-20. Optical microscopy images of cyantraniliprole dispersions using **a)** 60% acid content macromonomer, **b)** 70% acid content macromonomer and **c)** 80% acid content macromonomer. The images were taken one week after the milling process. Scale bar 20 μm.

3.2.3 Formulations of coated cyantraniliprole particles under starved-feed emulsion polymerization

Surfactant-free emulsion polymerization of hydrophobic monomers in the presence of cyantraniliprole dispersions, would have been resulted in the application of polymeric coating around AI particles directly performed in an aqueous system. A simple process, similar to this described in the previous chapter, was followed, **Scheme 3-6**. The latexes should meet several technical criteria in order to be suitable

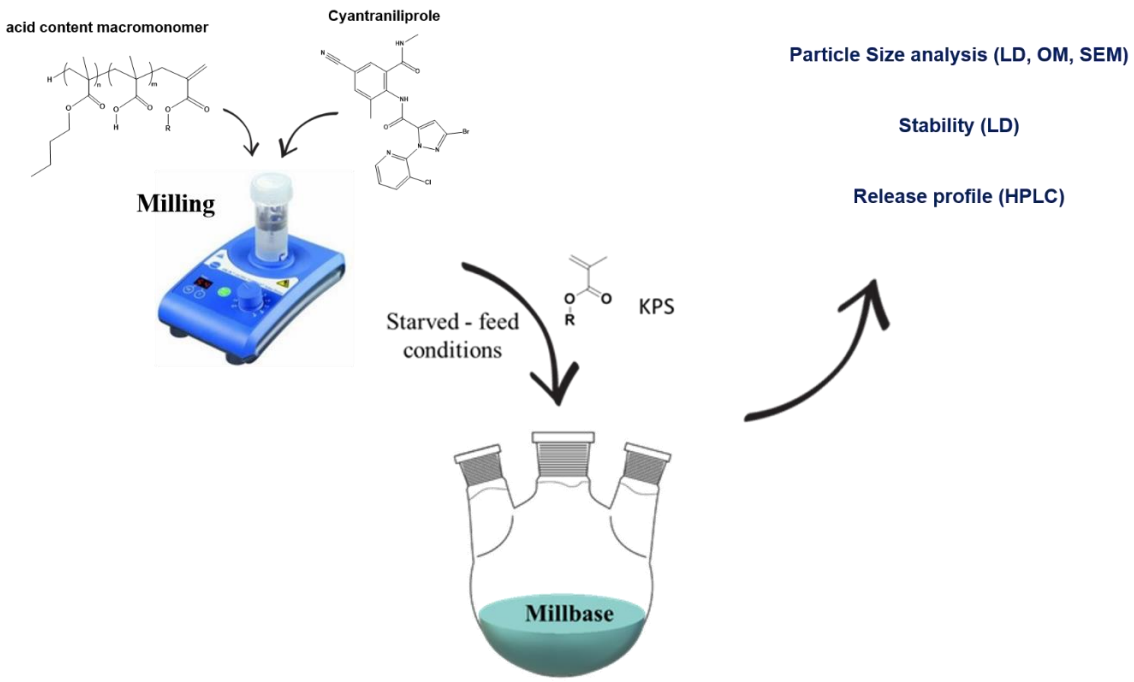

Scheme 3-6. Surfactant-free emulsion polymerization of hydrophobic monomer for the application of polymeric coating around cyantraniliprole particles.

for coating applications,[38] such as the glass transition temperature (T_g) of the obtained polymers, which should be similar to the ambient temperature during film formation. Therefore, different w/w% of a mixture of MMA : BA (10 : 1) with respect to the mass of cyantraniliprole dispersion (millbase) were used for the application of coatings with different length around cyantraniliprole particles. The formed polymer particles, in the presence of cyantraniliprole dispersion, will accumulate around cyantraniliprole particles, thus entrapping the AI. The role of the amphiphilic macromonomer in this process is to stabilize the cyantraniliprole dispersion, as well as the emulsion polymerization of the MMA/BA mixture.

Moreover, they should be produced in high solids content and feature relatively small particle size (0.2 – 1μm). The amount of cyantraniliprole used in this study was 10 w/w% with respect to the total mass of the mixture. Further experiments with increased amounts of cyantraniliprole were conducted (20 and 30 w/w%) to explore the possibility of higher solids content formulations. The particle size can be controlled by using starved-feed conditions to avoid formation of monomer droplets in the aqueous phase, which can reduce the colloidal stability resulting in AI-free polymer particles, as well as to lead in lower encapsulation efficiency.[34]

The encapsulation of cyantraniliprole and the release profile were followed by High Performance Liquid Chromatography (HPLC), thus a calibration curve for cyantraniliprole was required (for calibration method see *section 3.4.2*). The determination of the critical micelle concentration (CMC) of the amphiphilic macromonomer (80% acid content) was investigated using a Drop Shape Analysis system (DSA100). The CMC was determined by measuring the surface tension (SFT) of a concentration series. In general, above the CMC, the SFT is extensively independent of the concentration. The CMC results from the intersection between the regression straight line of the linearly dependent region and the straight line passing through the plateau. However, in this study the SFT never reached a plateau, even at high macromonomer concentrations (as high as 12 g L^{-1}), indicating that macromonomer`s concentrations used for the dispersion of the AI were below the CMC (**Figure 3-21**).

Based on this, dispersions where [MM] : [CYNT] = 0.1% was used for the coating application experiments. The concentration of the monomer mixture was selected to be 5, 10 and 15 w/w % with respect to the millbase. The 80% acid content macromonomer was used, the initiator was potassium persulfate, KPS (0.5 mol% with respect to monomer), the reaction temperature 86 ^{o}C, the feeding time 22 hours, the initial pH = 7 and the reaction time after the feeding was 1 hour. The final pH (~ 5.5) of these latexes dropped from the initial pH, probably due to the formation of sulfuric acid from KPS. This could lower the solubility of the macromonomer and therefore its ability to stabilize the emulsion polymerization process, resulting in coagulation. This was further confirmed by LD measurements, where bigger particles were present (**Figure 3-22**). Nevertheless, HPLC analysis of the formulations showed that an increase of the percentage of monomer mixture with respect to cyantraniliprole resulted in a decrease of the absorption`s intensity, as expected (**Figure 3-23**). An experiment using millbase with [MM] : [CYNT] = 1% led to a stable formulation, where the mean particle size of the coated cyantraniliprole particles was close to the desired range of 2-10 µm. Moreover, less coagulation was observed by increasing the macromonomer concentration from 0.1 to 1% with respect to cyantraniliprole. LD measurements of the formulation prepared with $W_{(MMA:BA)}$: $W_{Millbase}$ = 15% showed that excellent stability can be retained even after 2 weeks, **Figure 3-24**. The results indicate a particle size of the latex particles approximately 1 µm and a mean particle

size of the cyantraniliprole particles of 10 µm. HPLC chromatograms of the millbase and cyantraniliprole formulation are shown in **Figure 3-25**.

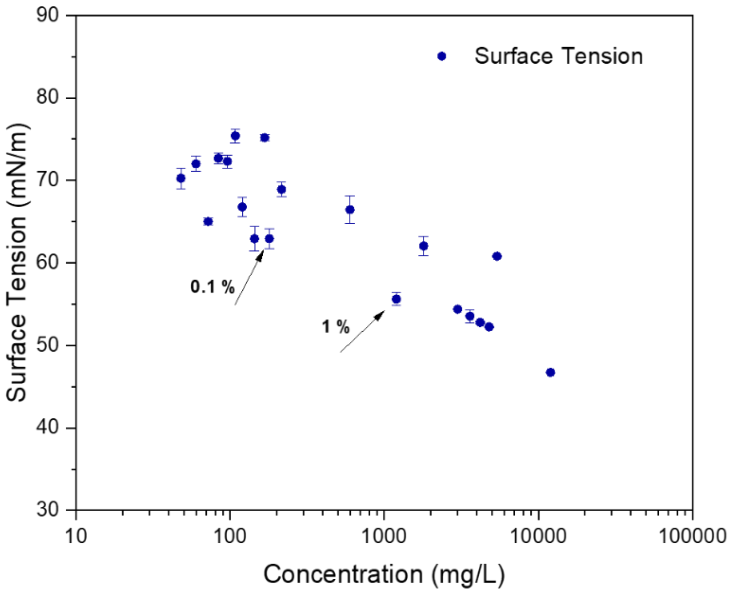

Figure 3-21. Determination of CMC by measuring the SFT of a concentration series for the 80% acid content macromonomer. [MM] : [CYNT] = 0.1% and 1% were used for the coating application studies.

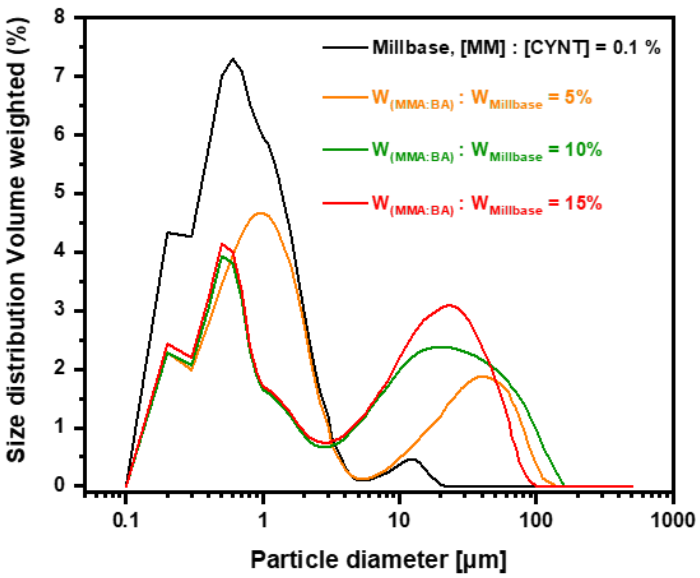

Figure 3-22. LD measurement of millbase, [MM] : [CYNT] = 0.1% (black trace) and coating application experiments, where $W_{(MMA:BA)}$: $W_{Millbase}$ = 5% (orange trace), $W_{(MMA:BA)}$: $W_{Millbase}$ = 10% (green trace) and $W_{(MMA:BA)}$: $W_{Millbase}$ = 15% (red trace).

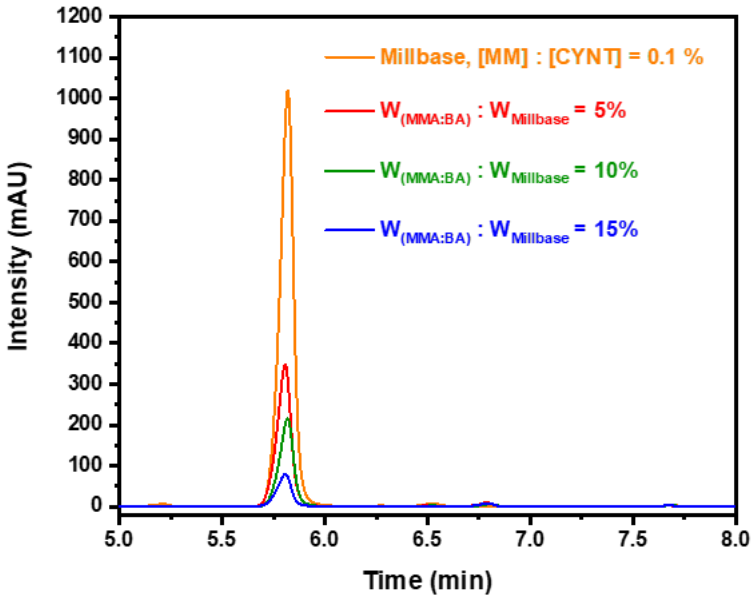

Figure 3-23. HPLC chromatograms of millbase, [MM] : [CYNT] = 0.1% (orange trace) and coating application experiments, where $W_{(MMA:BA)}$: $W_{Millbase}$ = 5% (red trace), $W_{(MMA:BA)}$: $W_{Millbase}$ = 10% (green trace) and $W_{(MMA:BA)}$: $W_{Millbase}$ = 15% (blue trace).

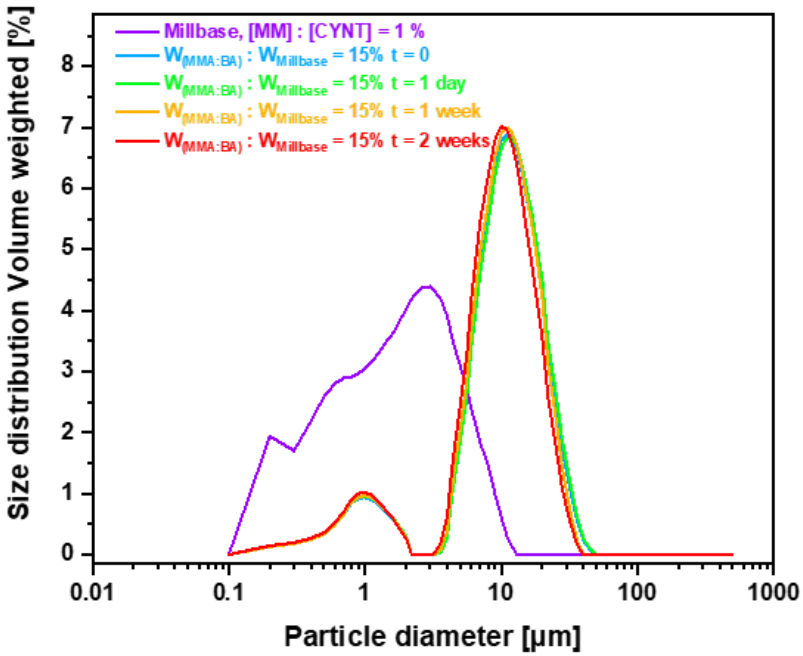

Figure 3-24. LD measurements of cyantraniliprole formulation prepared with $W_{(MMA:BA)}$: $W_{Millbase}$ = 15% in different times. Macromonomer with 80% acid content was used.

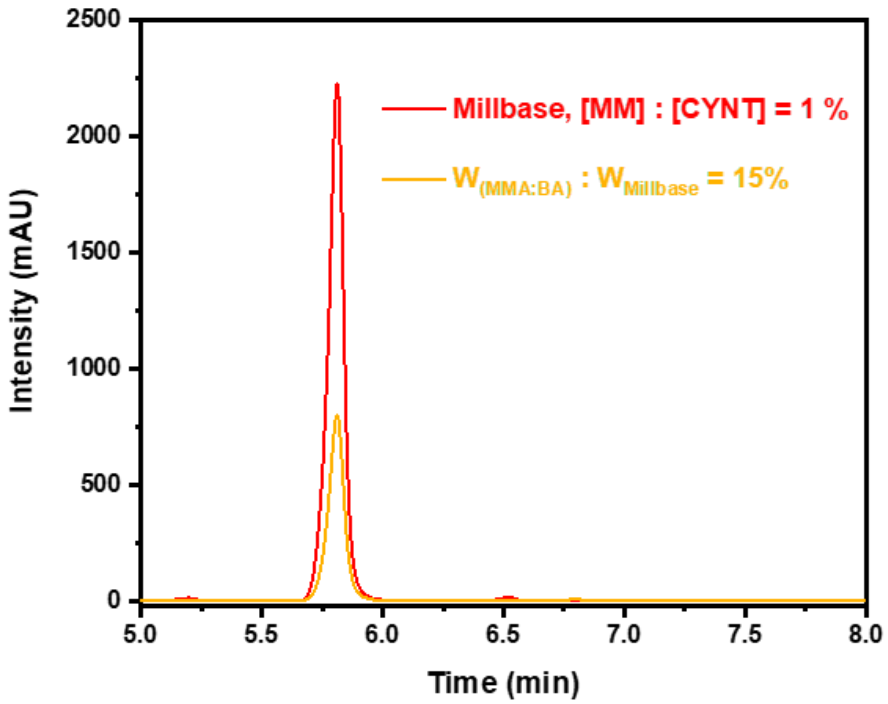

Figure 3-25. HPLC chromatograms of millbase, [MM] : [CYNT] = 1% and cyantraniliprole formulation, where $W_{(MMA:BA)}$: $W_{Millbase}$ = 15%.

The release profile of cyantraniliprole was followed by HPLC. A known amount of the formulation was introduced in various volumes (0, 1, 2 and 3 mL) of 0.1 w/w % aqueous formic acid solution and subsequently 10 mL of a mixture of ethyl acetate and ethanol were added. Formic acid and ethanol were used in order to supply a greater contact area between the aqueous and organic phase. Various volumes of the aqueous solutions were used to examine if slow release of cyantraniliprole particles can be controlled. Aliquots were taken from the organic phase at different times to investigate the extraction of cyantraniliprole from the aqueous phase to the organic phase (**Figure 3-26**). As expected, when no aqueous formic acid solution is added, fast release of cyantraniliprole was observed without further release of the AI, indicating that the whole amount had been extracted (**Figure 3-26 a**). Addition of 1 mL of aqueous formic acid solution (0.1 w/w%) led to fast release of the AI after 2 hours and very slow release after that (**Figure 3-26 b**). By further increasing the volume of the aqueous phase slower release was observed, in terms of amount of the AI being extracted at the same time intervals (**Figure 3-26 c & d**). This suggests that control over the slow release of cyantraniliprole can be monitored by increasing the aqueous to organic phase ratio.

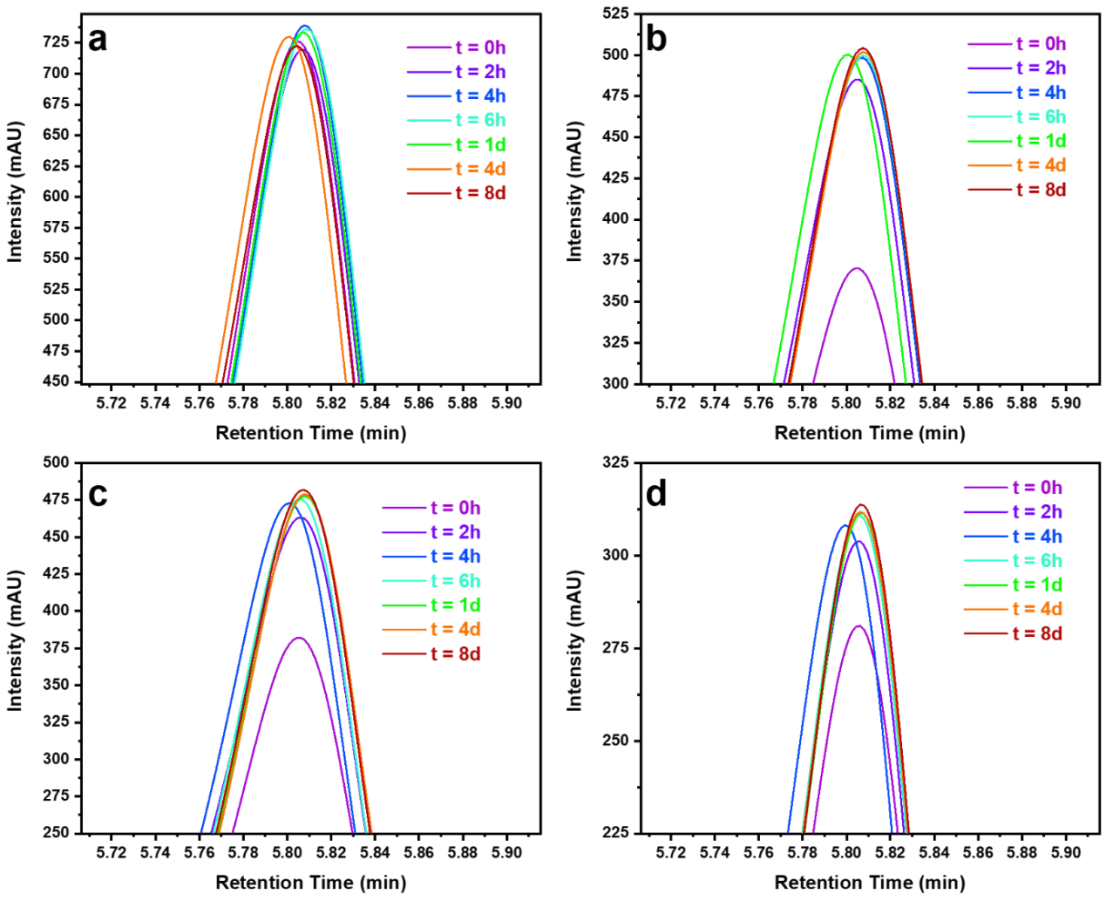

Figure 3-26. Investigation on the release profile of cyantraniliprole from aqueous to organic media using HPLC analysis. Chromatograms are shown in expanded regions: **a)** 0 mL aq. Formic acid solution, **b)** 1 mL aq. Formic acid solution, **c)** 2 mL aq. Formic acid solution and **d)** 3 mL aq. Formic acid solution. Organic solvents: Ethyl acetate : Ethanol 10 : 1.

The release profile of coated cyantraniliprole for the formulation described above is shown, **Figure 3-27**. HPLC analysis revealed slow release of AI the first 4 hours and relatively fast extraction of particles the first day, after which a plateau was reached (**Figure 3-27 b**).

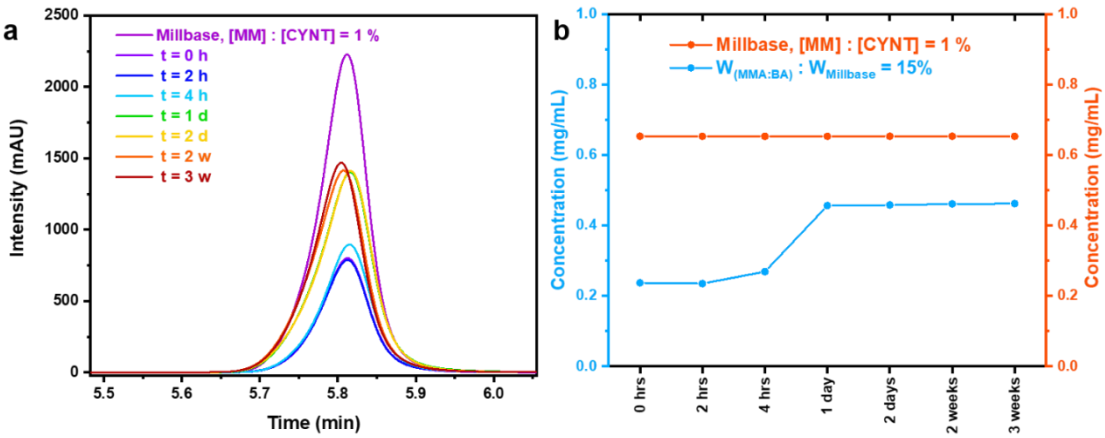

Figure 3-27. Release profile of coated cyantraniliprole particles from formulation: Millbase [MM] : [CYNT] = 1%, $W_{(MMA:BA)}$: $W_{Millbase}$ = 15%. **a)** HPLC chromatograms of millbase and extracted cyantraniliprole at different time intervals and **b)** initial cyantraniliprole concentration (orange) and concentration of extracted cyantraniliprole at different time intervals (cyan). The concentration was calculated based on the calibration curve obtained by HPLC analysis.

Additional experiments were carried out in order to investigate the impact of initial AI concentration, the percentage of coating and the choice of solvent on the stability, the release profile and the final performance of the obtained formulations.

Increasing the initial AI concentration from 10 to 20 w/w % led to a less stable formulation, **Figure 3-28 a**. The particle size of the latex particles is in a range from 100 nm to 2 µm, whereas the mean AI size = 10 µm. Although this is in the desired particle size range, a shoulder on the higher particle sizes is apparent. The release profile was the same as previously described, where AI concentration was 10 w/w % with respect to the total mass of millbase (**Figure 3-28 b**). It is noted that the macromonomer concentration was the same; 1 w/w % with respect to cyantraniliprole. An attempt to increase the AI`s solids content to 50 w/w % led to a millbase with high viscosity and solidification of the polymerization mixture, indicating limitations on the preparation of stable cyantraniliprole dispersions in high solids content.

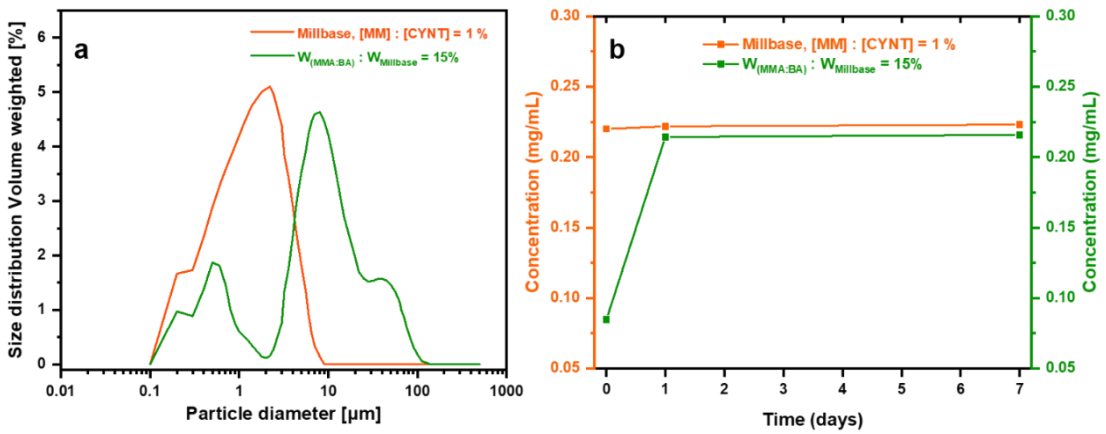

Figure 3-28. a) LD measurement of cyantraniliprole formulation with $W_{(MMA:BA)}$: $W_{Millbase}$ = 15% with 20 w/w % initial cyantraniliprole concentration and **b)** release profile of coated cyantraniliprole. Concentration was calculated based on the calibration curve obtained by HPLC analysis.

Subsequently, the 60% acid content macromonomer was used to disperse cyantraniliprole particles in water and the formed dispersions were used for the coating application reactions, where various $W_{(MMA:BA)}$: $W_{Millbase}$ ratios were explored. Initially, 5 w/w % of monomer mixture with respect to millbase resulted in stable formulation with mean particle size of 11 µm. LD measurements after the completion of the reaction and one week later showed similar stability, (**Figure 3-29 a**). The extraction of cyantraniliprole followed the same pattern as previously, resulting in full release of the particles after one day (**Figure 3-29 b**). By increasing the $W_{(MMA:BA)}$: $W_{Millbase}$ ratio to 10% again stable formulation was obtained, however, the mean particle size was 23-24 µm (**Figure 3-30 a**). Also, slower release of the coated particles was observed, as well as no full extraction after two weeks (**Figure 3-30 b**). Further increase to 30 w/w % had similar results regarding the particle size (~25 µm) and the stability of the cyantraniliprole formulation (**Figure 3-31 a**). In this case, no significant extraction of cyantraniliprole particles was observed (**Figure 3-31 b**).

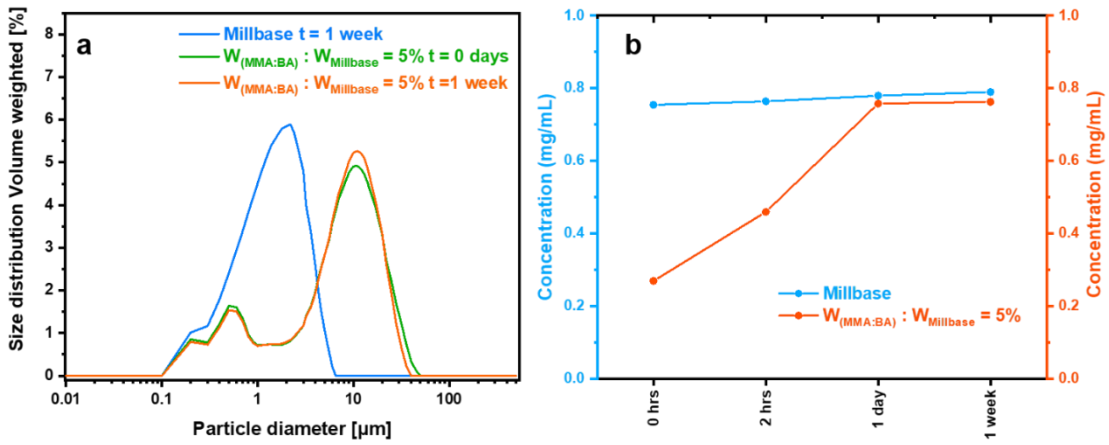

Figure 3-29. a) LD measurement of cyantraniliprole formulation with $W_{(MMA:BA)}$: $W_{Millbase}$ = 5% with 10 w/w % initial cyantraniliprole concentration and **b)** release profile of coated cyantraniliprole. Concentration was calculated based on the calibration curve obtained by HPLC analysis.

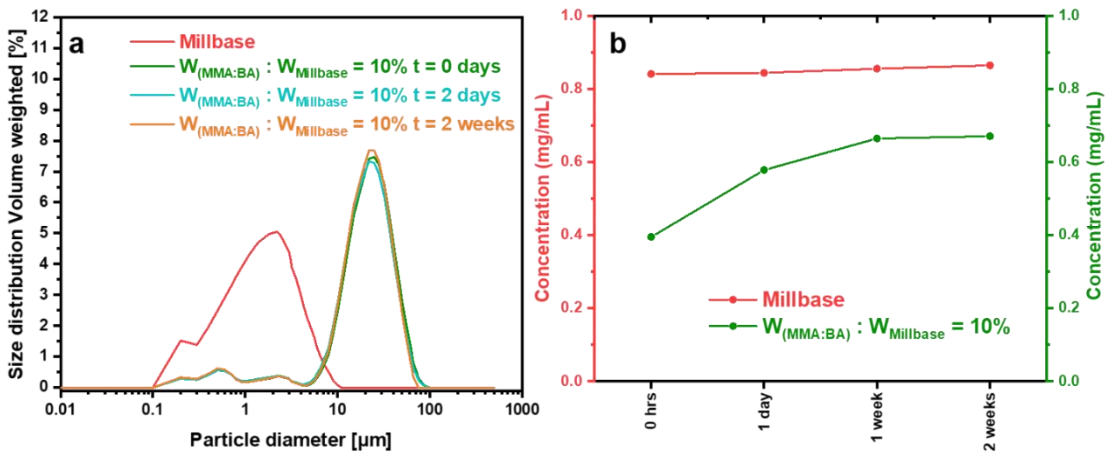

Figure 3-30. a) LD measurement of cyantraniliprole formulation with $W_{(MMA:BA)}$: $W_{Millbase}$ = 10% with 10 w/w % initial cyantraniliprole concentration and **b)** release profile of coated cyantraniliprole. Concentration was calculated based on the calibration curve obtained by HPLC analysis.

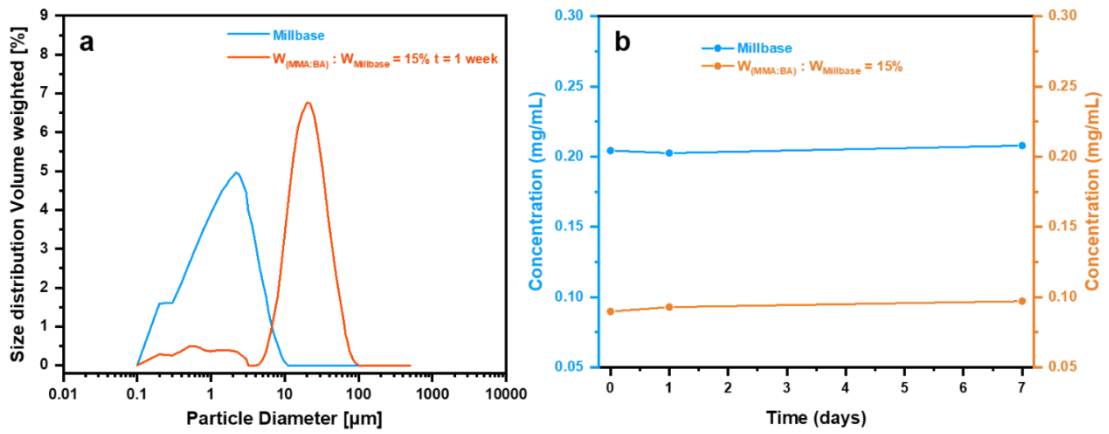

Figure 3-31. a) LD measurement of cyantraniliprole formulation with $W_{(MMA:BA)}$: $W_{Millbase}$ = 15% with 10 w/w % initial cyantraniliprole concentration and **b)** release profile of coated cyantraniliprole. The concentration was calculated based on the calibration curve obtained by HPLC analysis.

The next series of experiments included the investigation of various solids content of cyantraniliprole formulations in phosphate buffer solution (PBS) with pH = 7. For this purpose, the 60% acid content macromonomer (1 w/w % with respect to cyantraniliprole) was dissolved in PBS and used to disperse cyantraniliprole with different solids content, 10, 20 and 30 w/w %. Cyantraniliprole dispersions were stable with a mean particle size of 2 µm (**Figure 3-32 a**), indicating that the amphiphilic macromonomer is more efficient when PBS is used. This might be attributed to the pH value, which was same before and after the reaction (pH = 7), thus maintaining the solubility of the macromonomer. Coating application experiments were taken place with $W_{(MMA:BA)}$: $W_{Millbase}$ = 10% resulting in stable formulations without any sign of coagulation. When the cyantraniliprole solids content was equal to 10 or 20 w/w % the mean particle size was lower than 10 µm even after 2 weeks. However, increase of solids content to 30 w/w % led to a formulation with two different populations of cyantraniliprole particles; one with mean particle size of 8-9 µm and a second of 70 µm (**Figure 3-32 b**). HPLC analysis of the formulations showed immediate release of cyantraniliprole particles after 10 minutes (**Figure 3-33**).

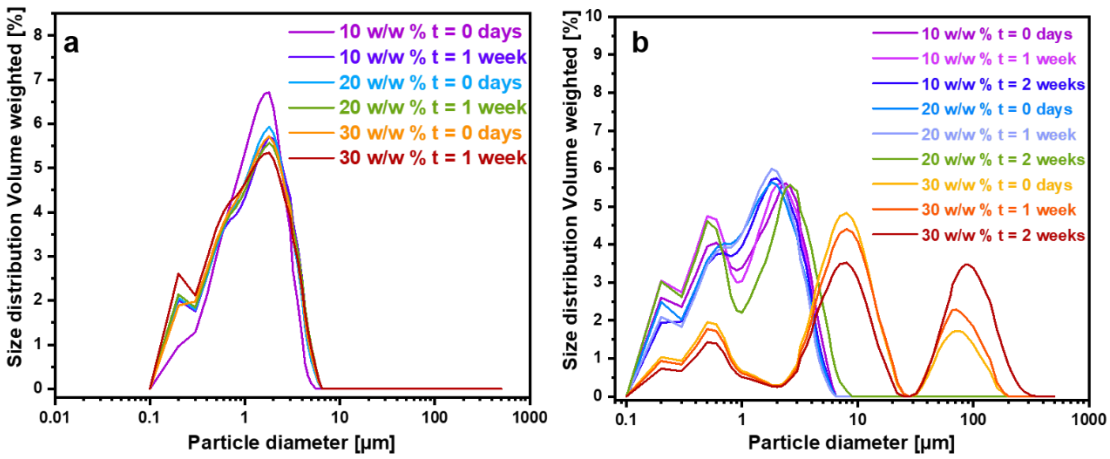

Figure 3-32. LD measurements of **a)** cyantraniliprole dispersions and **b)** cyantraniliprole formulations stabilized by 60% acid content macromonomer. Cyantraniliprole solids content: 10, 20 and 30 w/w%. $W_{(MMA:BA)}$: $W_{Millbase}$ = 10%

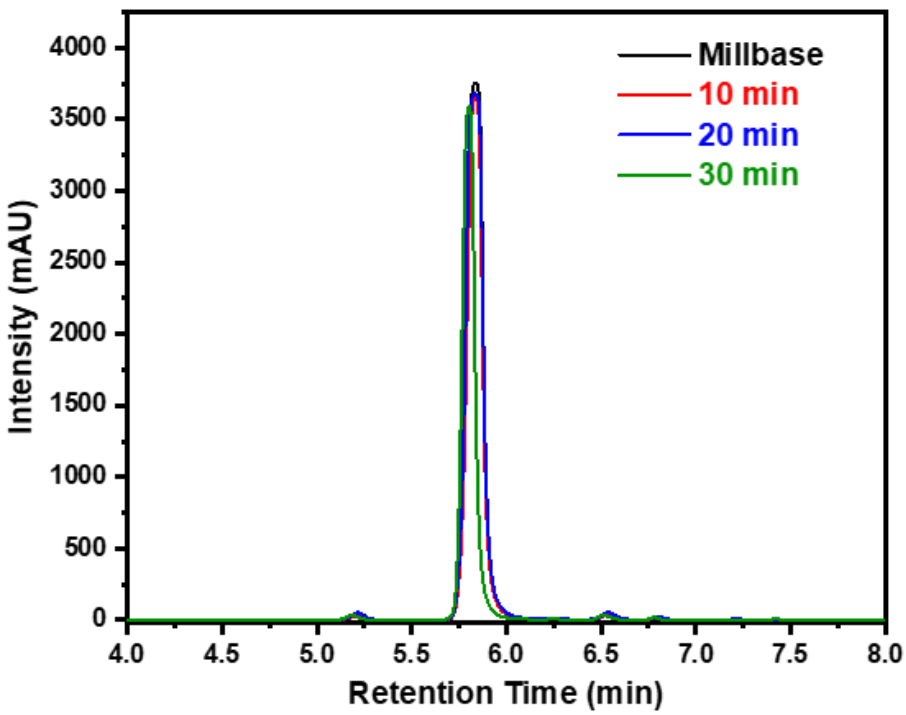

Figure 3-33. HPLC chromatograms of cyantraniliprole formulation in PBS with solids content 20 w/w %, showing immediate release of the particles.

The encapsulation efficiency and the weight % of cyantraniliprole formulations in PBS (**Figure 3-34**, **Table 3-5** in section *3.4.4 Supplementary Figures and Tables*) was calculated by the following equations:

$$\text{Weight \% CYNT} = \frac{\text{Amount CYNT extracted}}{\text{Total amount of solids}} \text{ x } 100 \qquad [2]$$

$$\text{Encapsulation Efficiency \%} = \frac{\text{Amount CYNT extracted}}{\text{Initial amount CYNT in formulation}} \text{ x } 100 \qquad [3]$$

The particle sample was prepared using dried particles at 2 mg mL^{-1} in 80% acetonitrile in water and then sonicated for 30 minutes to release cyantraniliprole from latex particles. Subsequently, the sample was filtered to remove any insoluble polymeric material. HPLC measurements using the method described previously, confirmed the amount of extracted cyantraniliprole. Initial concentration of cyantraniliprole was determined by its concentration in the millbase.

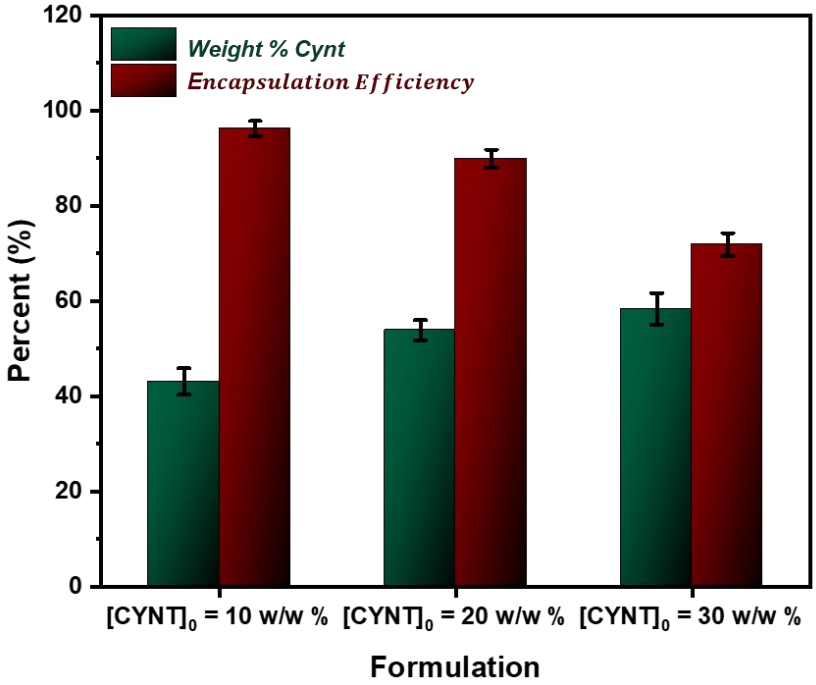

Figure 3-34. Weight % of cyantraniliprole and encapsulation efficiency of cyantraniliprole formulations in PBS.

To observe the morphology of the particles scanning electron microscopy (SEM) images were taken. An image of aggregated cyantraniliprole particles is given in **Figure 3-35**. The accumulation of latex particles around cyantraniliprole is confirmed in **Figures 3-36 & 3-37**. Although latex particles enclose cyantraniliprole particles and during polymer evaporation lead to a polymeric coating on the particulate matter, the excess latex particles form large agglomerates, **Figure 3-38**. In order to remove the excess of latex particles, samples from the formulations were centrifuged in a three cycle process. A known amount of formulation was added in a falcon tube and deionized water was added. The sample was centrifuged for 15 minutes. After

centrifugation the sediment was redispersed in water and the same process was followed two more times. Finally, the morphology of coated cyantraniliprole particles was observed by SEM, **Figures 3-39 & 3-40**.

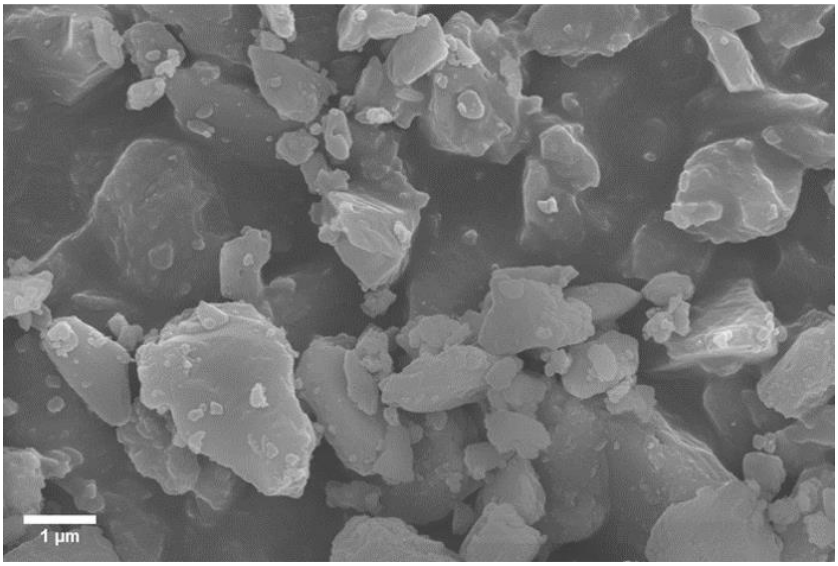

Figure 3-35. SEM image of aggregated cyantraniliprole particles.

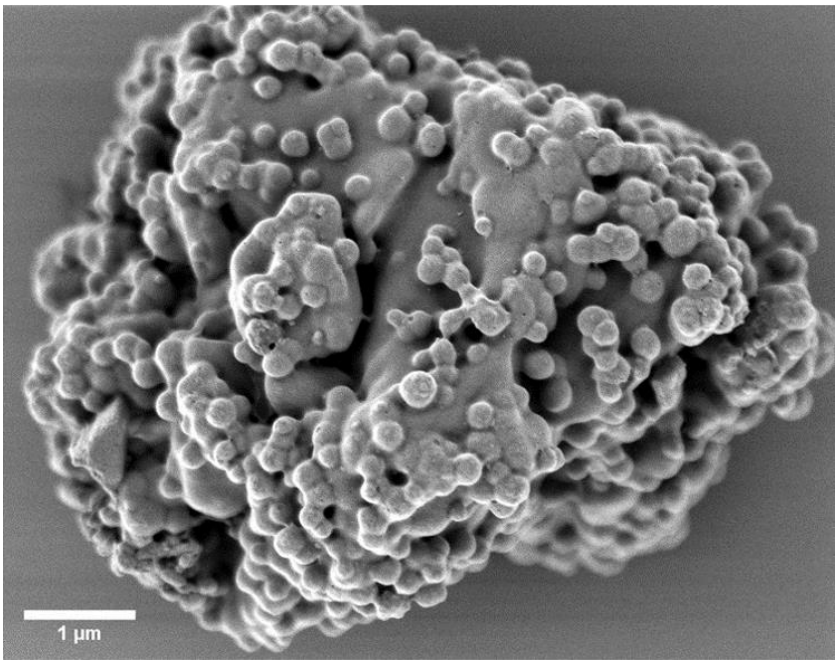

Figure 3-36. SEM image of coated cyantraniliprole particle. Latex particle accumulation around cyantraniliprole particle.

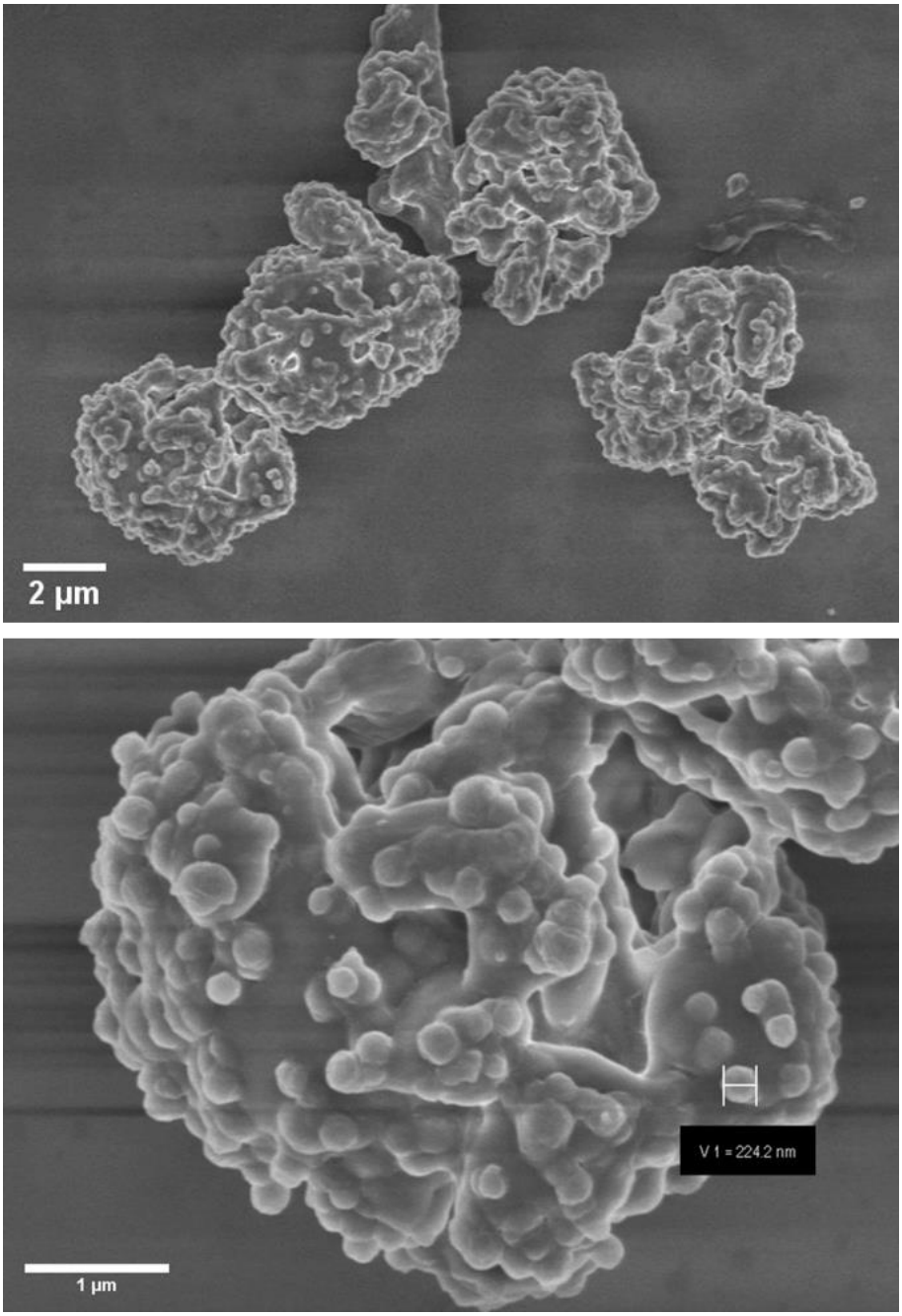

Figure 3-37. SEM image of coated cyantraniliprole particles.

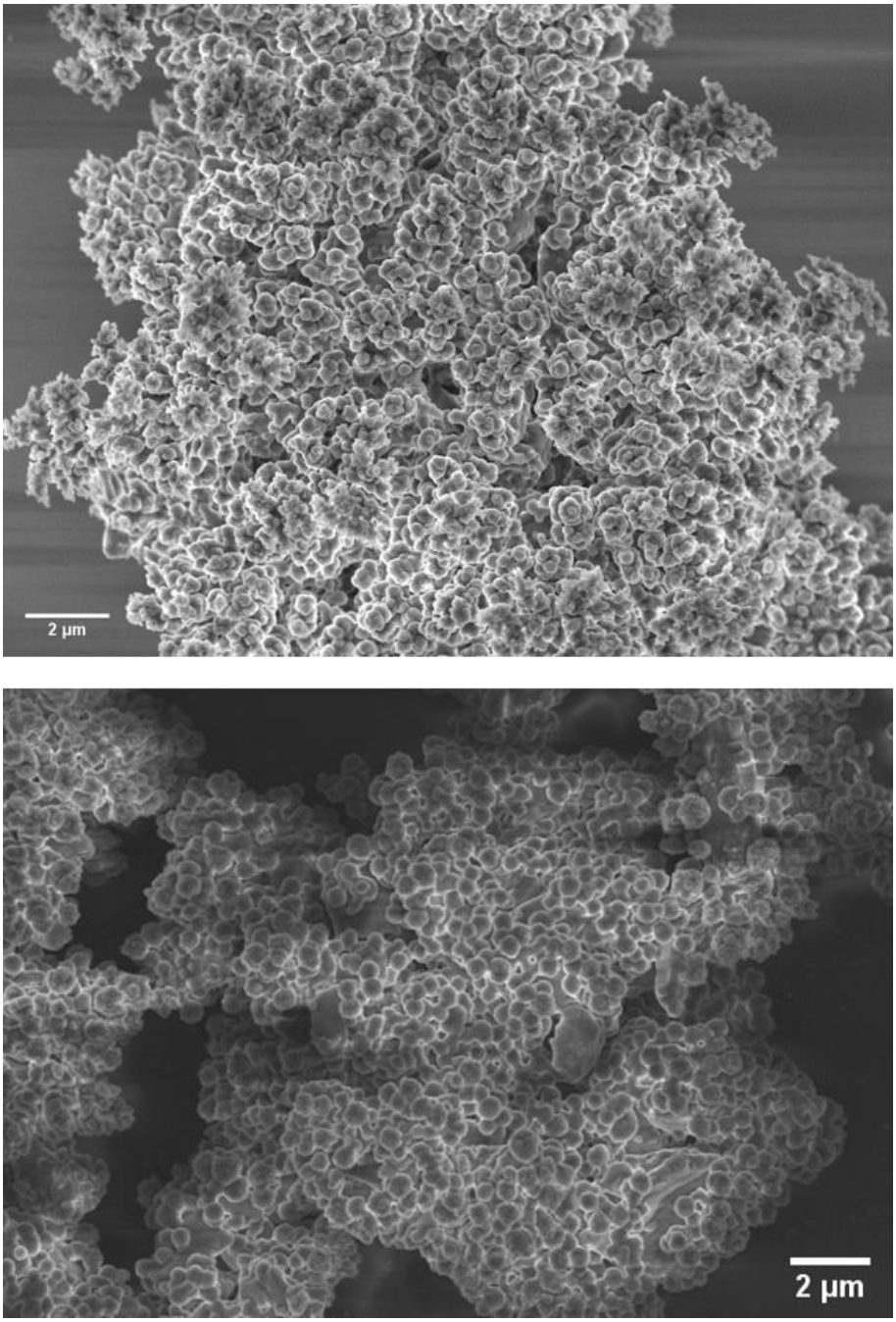

Figure 3-38. SEM images of latex particles agglomerates.

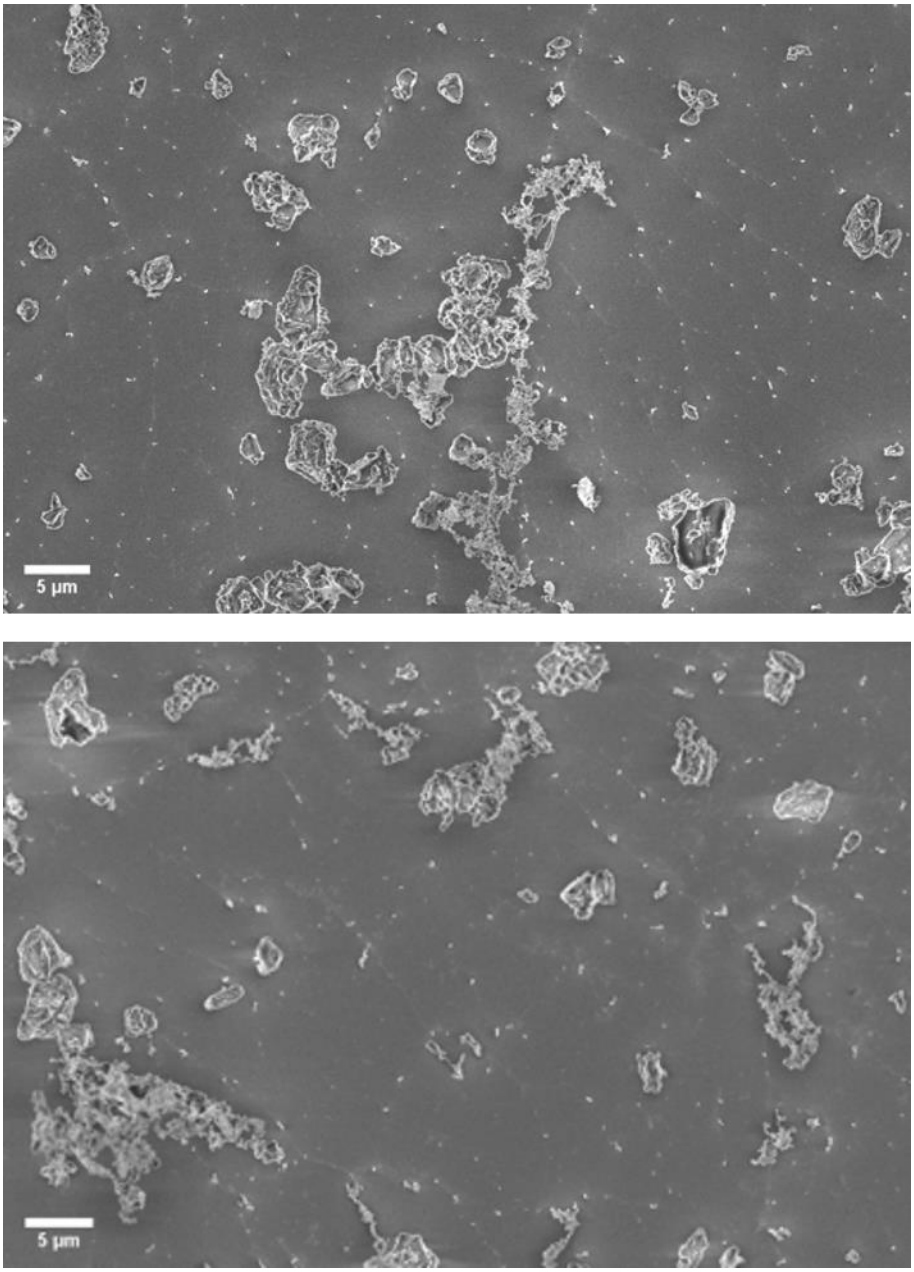

Figure 3-39. SEM images of coated cyantraniliprole particles after the removal of excess latex particles.

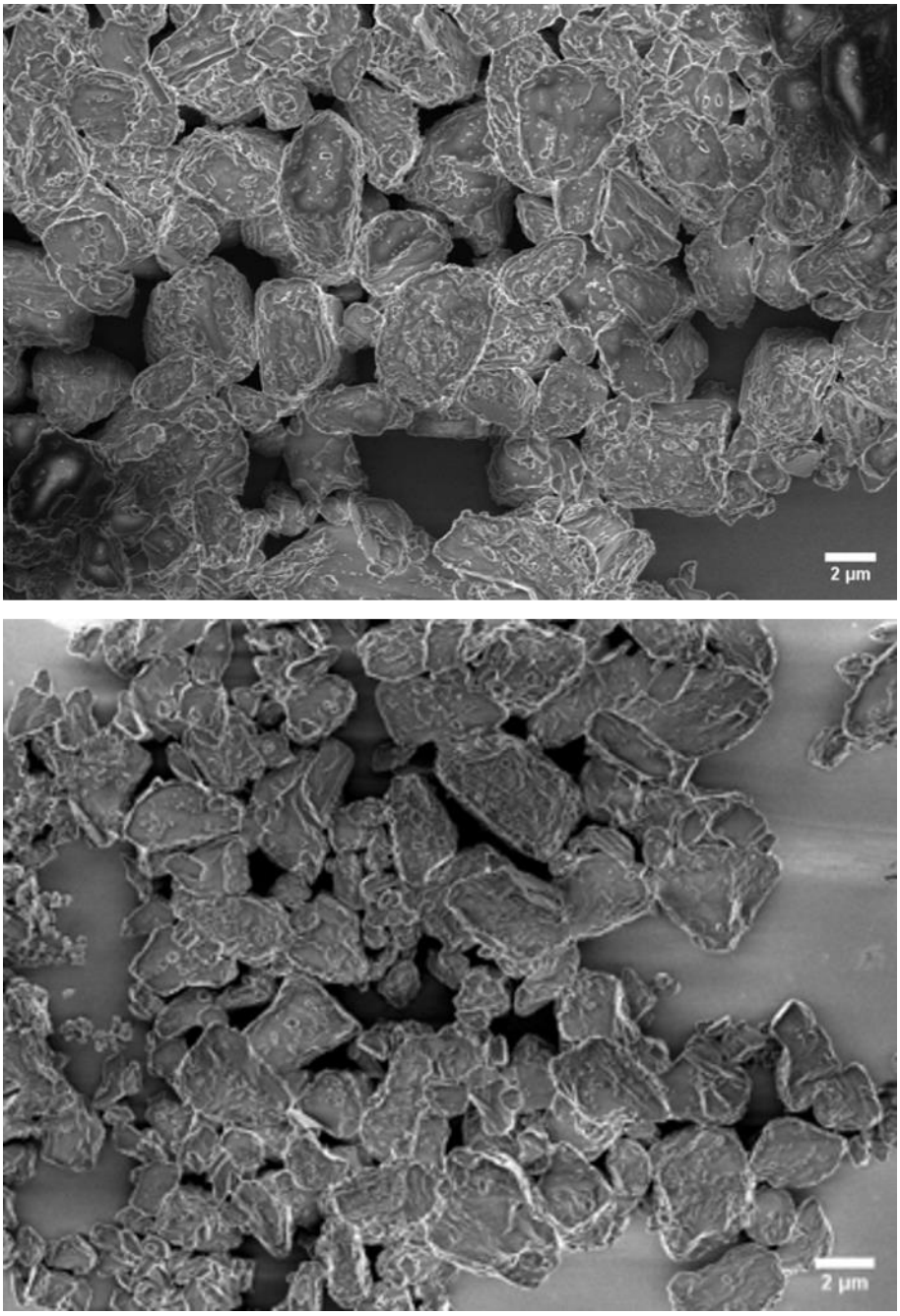

Figure 3-40. SEM images of coated cyantraniliprole particles after the removal of excess latex particles.

3.3 Conclusions

In summary, ω-unsaturated macromonomers were synthesized *via* CCTP and were used in the development of stable AI dispersions in an aqueous system. The macromonomers were statistical copolymers of various methacrylic acid and butyl methacrylate compositions, p(MAA-*stat*-BMA) and were obtained through the hydrolysis of p(*t*BMA-*stat*-BMA). Matrix assisted laser desorption-ionization time of flight mass spectrometry (MALDI-ToF-MS) was used to confirm that the targeted chemical composition of the macromonomers was achieved.

The amphiphilic macromonomers were used, in various concentrations, for the milling of the anthranilic insecticide, cyantraniliprole. Laser diffraction and optical microscopy analysis confirmed the ability of the macromonomers to stabilize and disperse cyantraniliprole in aqueous systems (water, PBS). A milling time of 10 minutes was found to be the *optimum* in order to develop stable AI dispersions, independently of the macromonomer concentration used (with respect to cyantraniliprole).

Furthermore, investigation on the application of polymeric coating around the insecticide particles was conducted through the surfactant-free emulsion polymerization of a monomer mixture (MMA : BA =10 : 1) under starved-feed conditions. Initial experiments taken place in water (pH adjustment with 2 M aq. KOH solution) showed that an increase of [MM] : [CYNT] ratio was required, such the macromonomer be able to participate both in the stabilization of cyantraniliprole dispersions and the stabilization of the emulsion polymerization process. Moreover, the release profile of cyantraniliprole was investigated through an extraction process using aq. formic acid solution and a mixture of ethyl acetate and ethanol. Interestingly, by increasing the volume of the aqueous phase, slower release of the insecticide to the organic phase was observed.

In addition, the same process was followed for the application of polymeric coating around the insecticide particles in phosphate buffer solution (PBS, pH = 7). The reaction proved to proceed more efficiently in PBS rather than water, as no coagulation was observed and the obtained formulations retain their stability for more than three weeks, based on LD measurements. The weight % of cyantraniliprole in

these formulations was over 40% and the encapsulation efficiency higher than 70%, as found by HPLC analysis. Finally, scanning electron microscopy (SEM) was used to observe the morphology of the coated particles, confirming the accumulation of latex particles around cyantraniliprole.

3.4 Experimental section

3.4.1 Materials

Butyl methacrylate (BMA, 99%), *tert*-butyl methacrylate (*t*BMA, 98%), methyl methacrylate (MMA, 99%), butyl acrylate (BA, >99%), and potassium persulfate (KPS) were purchased from Sigma-Aldrich and used without any further purification unless otherwise stated. 2,2'-Azobis(2,4-dimethylvaleronitrile) (V-65 initiator) was purchased from Wako. Cyantraniliprole was provided by Syngenta UK. Bis(boron difluorodimethylglyoximate)cobalt (CoBF) was synthesized according to the literature.[39] Laboratory supplies of toluene (Fisher Scientific, Analytical Regent Grade), methanol (VWR Chemicals, 100%) were used.

3.4.2 Instrumentation and Characterization techniques

Initial experiments for the milling of cyantraniliprole were taken place using a Branson Digital Sonifier (probe model: 102-C). In order to have comparable results, feedback regarding the milling equipment was provided by Syngenta, thus IKA Ultra TURRAX Disperser was used for the milling process.

Proton Nuclear Magnetic Resonance (^{1}H NMR)

^{1}H NMR spectra were recorded on Bruker DPX-300 or DPX-400 spectrometers in deuterated chloroform ($CDCl_3$), deuterated dimethyl sulfoxide (DMSO-d_6) or deuterium oxide (D_2O) as obtained from Sigma-Aldrich. Chemical shifts are given in ppm downfield from the tetramethylsilane internal standard.

Size Exclusion Chromatography (SEC)

SEC measurements of p(*t*BMA-*stat*-BMA) macromonomers were carried out using THF as the eluent with an Agilent 390-LC MDS instrument equipped with differential refractive index (DRI), viscometry (VS), dual angle light scatter (LS) and dual wavelength UV detectors. The system was equipped with 2 x PLgel Mixed C columns (300 x 7.5 mm) and a PLgel 5 µm guard column. The eluent was THF with 2% TEA (triethylamine) and 0.01% BHT (butylated hydroxytoluene) additives. Samples were run at 1 mL / min at 30ºC. Poly(methyl methacrylate) standards (Agilent EasyVials)

were used to create a third order calibration between 550 g mol^{-1} and 1,568,000 g mol^{-1}. Analytical samples were filtered through a GVHP membrane with 0.22 μm pore size before injection.

SEC measurements of pBMA macromonomers were carried out using an Agilent Infinity II 1260 MDS instrument equipped with differential refractive index (DRI), viscometry (VS), dual angle light scatter (LS) and multiple wavelength UV detectors. The system was equipped with 2 x PLgel Mixed C columns (300 x 7.5 mm) and a PLgel 5 µm guard column. The eluent was $CHCl_3$ run at 1 ml/min at 30 ºC. Poly(methyl methacrylate) standards (Agilent EasiVials) were used to create a 3rd order calibration between 1,020,000 – 1,840 g mol^{-1}. Analyte samples were filtered through 0.22 µm pore size GVHP filters before injection. Respectively, experimental molar mass ($M_{n,SEC}$) and dispersity ($Đ$) values of synthesized polymers were determined by conventional calibration using Agilent GPC/SEC software.

SEC characterization of p(MAA-*stat*-BMA) macromonomers was carried out on an Agilent Infinity II MDS instrument, using DMF with 5 mmol NH_4BF_4 additive as the eluent, at 50 °C, and with a flow rate of 1 mL/min. The system was equipped with differential refractive index (DRI), viscometry (VS), dual angle light scatter (LS) and variable wavelength UV detectors, 2 × PLgel Mixed D columns (300 × 7.5 mm) and a PLgel 5 μm guard column. The system was calibrated using poly(methyl methacrylate) standards (Agilent EasyVials) with molecular weights in the range of 550 - 955,000 g mol^{-1}. Prior to injecting the samples, they were filtered through a nylon membrane with a pore size of 0.22 μm.

Respectively, experimental molar mass ($M_{n,SEC}$) and dispersity ($Đ$) values of synthesized polymers were determined by conventional calibration using Agilent GPC/SEC software (version A.02.01).

Matrix-assisted laser desorption/ionization time-of-flight

MALDI-ToF-MS measurements were conducted using a Bruker Daltonics Ultraflex II MALDI-ToF mass spectrometer, equipped with a nitrogen laser delivering 2 ns laser pulses at 337 nm with positive ion ToF detection performed using an accelerating voltage of 25 kV. Solutions in dimethylformamide (DMF) (50 µL) of *trans*-2-[3-(4-*tert*-butylphenyl)-2-methyl-2-propyldene] malononitrile (DCTB) as a matrix

(saturated solution), sodium iodide as the cationization agent (1.0 mg mL^{-1}) and sample (1.0 mg mL^{-1}) were mixed, and 0.7 µL of the mixture was applied to the target plate. Spectra were recorded in reflectron mode calibrated with poly(ethylene glycol) monomethyl ether (PEG-Me) 1900 kDa.

Laser Diffraction

Laser diffraction measurements were carried out on a Malvern Mastersizer 2000 in wet mode and on an Anton-Paar Particle Size Analyser. Water was used as dispersant. The sample was stirred and sonicated for 5 minutes prior to the actual measurement.

Optical Microscopy

Optical microscopy images were taken using a Zeiss STEMI 2000 microscope. To prepare the samples for imaging, 5 drops of each sample was added to a vial containing 4 mL of water. The vial was then vigorously shaken, and 1 drop was pipetted on to a microscope slide. A coverslip was put in place and the slide was imaged (20 or 50 × magnification).

Scanning Electron Microscopy (SEM)

SEM was performed using a Zeiss SUPRA 55-VP scanning electron microscope with a field emission electron gun (FEG). Best results were obtained when using the InLens detector with 3.5 mm working distance, 30 and 20 μm aperture and 0.5-3 kV acceleration voltage, with respect to sample tolerance. 1 μL of each sample was dissolved in 5 mL of DI water and aliquots of 7 μL were drop cast on silicon wafer chips (5 mm × 7 mm) and attached to aluminum specimen stubs. To improve contrast, gold sputter coating was applied for 15 seconds prior to imaging.

High Performance Liquid Chromatography (HPLC)

HPLC measurements were carried out on an Agilent 1260 Infinity series stack equipped with an Agilent 1260 binary pump and degasser. Samples were injected using Agilent 1260 autosampler. The HPLC was fitted with a Kinetex 5U EVO C18 100 Å column. Detection was achieved using an Agilent 1260 variable wavelength detector monitoring at 269 nm. The mobile phase consisted of acetonitrile and water. The HPLC method used in this study is already described in section 3.2.

Calibrants were made between 0.01 mg mL^{-1} and 1.00 mg mL^{-1} in 80% acetonitrile in water. The HPLC method used a Kinetex 5U EVO C18 100A short column, using a solvent gradient system, **Table 3-4**. The calibrants were run, along with a blank of 80% acetonitrile in water, **Figure 3-41**. The peak of cyantraniliprole is shown to be at around 6 minutes. In **Figure 3-42** the 5-7 minute range of the same spectra of calibrants is shown. By using the integration results from these calibrants a calibration curve was generated for cyantraniliprole (**Figure 3-43**).

Table 3-4. Development of HPLC method for cyantraniliprole formulations.

Time (min)	A (%)	B (%)
0	90	10
2	90	10
8	10	90
10	10	90
10.1	90	10
15	90	10

A: water, B: acetonitrile. HPLC was operated at 30 ºC with a flow rate 1.5 mL min^{-1}. The pressure limits were 0-400 bar. Injection volume: 10 µL. λ = 269 nm.

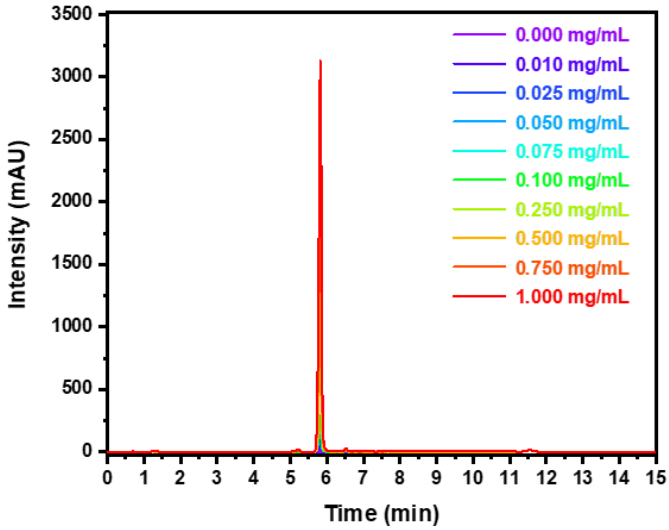

Figure 3-41. HPLC chromatograms of cyantraniliprole calibrants in 80% acetonitrile in water, run using a Kinetex 5U EVO C18 100A column.

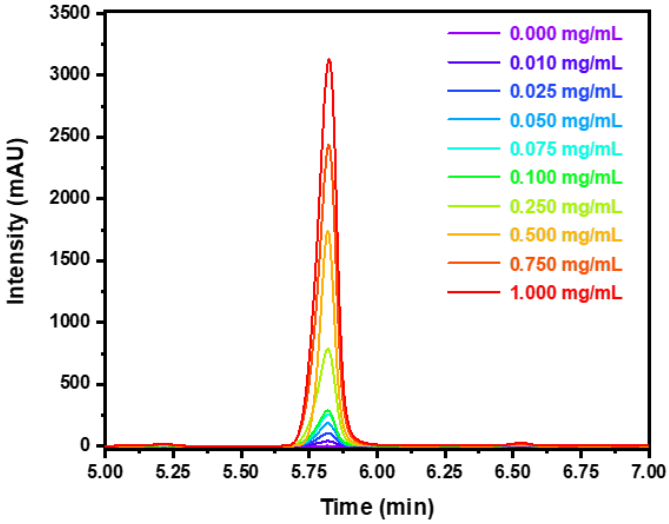

Figure 3-42. Expanded HPLC spectra of cyantraniliprole calibrants.

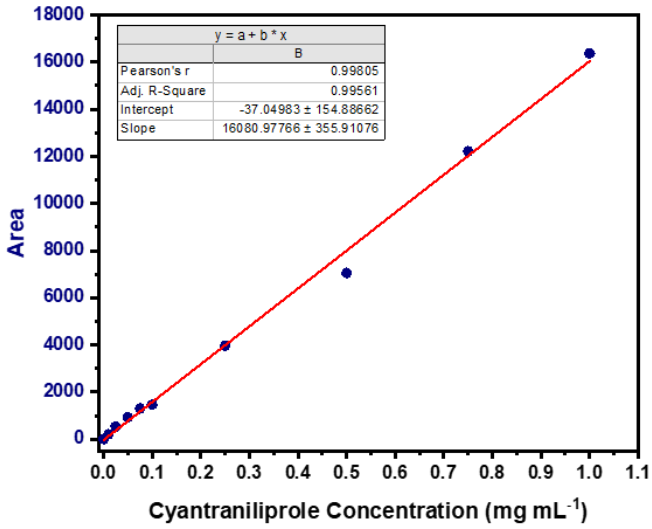

Figure 3-43. Calibration curve for cyantraniliprole.

Drop Shape Analyzer

Drop Shape Analyzer measurements (pendant drop) were carried out on a Kruss DSA 100. The SFT of a series of samples with various concentrations of the 80% acid content macromonomer was determined. Samples concentration was varied from 40 µg/L to 12 g/L.

3.4.3 Experimental procedures

Synthesis of pBMA macromonomers through CCTP in toluene

In separate round bottom flasks, 4.007 mg of CoBF and 60 mL of methanol were degassed for 2 hours. Using a degassed syringe, 50 mL of the methanol was transferred to dissolve the CoBF to form a stock solution. To five small Schlenk flasks containing a magnetic stirrer, which had been evacuated using a vacuum line and refilled with nitrogen, was added 0 µL, 192 µL, 384 µL, 576 µL and 786 µL of the CoBF stock solution, and the solvent was removed under reduced pressure, leaving behind a known weight of CoBF. To another small Schlenk flask was added 248 mg of V-65 initiator and 40 mL of toluene, which were degassed by freeze-pump-thawing three times. A stock of butyl methacrylate was also degassed using a nitrogen line for 1 hour. The reaction mixtures were assembled by adding 1.59 mL (1.42 g, 0.01 mol) of butyl methacrylate to each of the Schlenk flasks containing CoBF, before 2 mL of the initiator solution. These reactions were identical except for the catalyst concentration, which ranged: 0, 4, 8, 12 and 16 ppm of CoBF relative to the monomer concentration. The Schlenk flasks were freeze-pump-thawed a final three times to ensure any oxygen introduced during the solvent transfer was removed before being placed in an oil bath at 65ºC for 1 hour with continuous stirring. At the end of this time, the flasks were plunged into liquid nitrogen to stop the reactions. Toluene was removed by rotary evaporation, and samples were prepared for ^{1}H NMR and SEC analysis.

Synthesis of p(tBMA-stat-BMA) macromonomers through CCTP in toluene

In separate round bottom flasks, 3 mg of CoBF and 60 mL of methanol were degassed for 2 hours. Using a degassed syringe 40 mL of the methanol was transferred to dissolve the CoBF to form a stock solution. To three small Schlenk flasks containing a magnetic stirrer, which had been evacuated using a vacuum line and refilled with nitrogen, was added 200 µL of the CoBF stock solution, and the solvent was removed under reduced pressure, leaving behind 0.015 mg of CoBF. To another small Schlenk flask was added 100 mg of V-65 initiator and 8 mL of toluene, which were degassed by freeze-pump-thawing three times. The reaction mixtures were assembled by adding 2.6 mL (2.275 g, 0.016 mol), 2.28 mL (1.995 g, 0.014 mol), 1.95 mL (1.706 g, 0.012 mol) of degassed *t*BMA and 0.64 (0.572 g, 0.004 mol), 0.95 mL (0.849 g, 0.006 mol),

1.27 mL (1.135 g, 0.008 mol) of degassed BMA to each of the Schlenk flasks containing CoBF, before 2 mL of the initiator solution. The Schlenk flasks were freeze-pump-thawed a final three times to ensure any oxygen introduced during the solvent transfer was removed before being placed in an oil bath at 65ºC for 1 hour with continuous stirring. At the end of this time, the flasks were plunged into liquid nitrogen to stop the reactions. Toluene was removed by rotary evaporation, and samples were prepared for ^{1}H NMR and SEC analysis.

Hydrolysis of tert-butyl groups

Known quantities of p(*t*BMA$_n$-*stat*-BMA$_m$) macromonomers were weighed in to separate round bottom flasks and dissolved in DCM. A 5-fold molar excess of TFA with respect to the *tert*-butyl groups was then added to each round bottom flask and the reaction was stirred at room temperature for 24 hours with a reflux condenser in place. The DCM was then removed by rotary evaporation, and the macromonomers were washed with additional DCM and then methanol to remove residual TFA.

Preparation of macromonomer stock solution (10w/w %)

1 g of macromonomer was weighed and placed into a 20 mL vial and 10 mL of water was added. To dissolve the macromonomer, 5 drops of 2 M KOH from a Pasteur pipette was added and the mixture was left stirring overnight. After total dissolution of the macromonomer the pH was measured and found to be 7. In the preparation of macromonomer stock solution in PBS (pH = 7) the macromonomer was soluble, thus the addition of KOH was not necessary.

Dispersion of cyantraniliprole using CCTP macromonomers

In IKA ultra Turrax BMT-G tubes (total volume capacity 15 mL) cyantraniliprole (1.2 g, 10 w/w % with respect to total volume of the mixture) was weighed, along with glass balls (3 g) for its milling at IKA disperser. The desired amount of macromonomer was added from the stock solution and the tube was filled up with deionized water to total mass of 12 g (excluding the mass of glass balls). Subsequently, the tube was placed at the IKA disperser and the milling process started for the desired amount of time using maximum speed mode. The same process was followed when PBS was used as the solvent.

Surfactant-free emulsion polymerization of MMA:BA in the presence of cyantraniliprole dispersions

In a typical reaction: In a 50 ml round bottom flask a mixture of methyl methacrylate (MMA) and butyl acrylate (BA) in a ratio 10:1 was degassed for 30 minutes. To another 50 ml round bottom flask, potassium persulfate (KPS) solution in water was degassed for 30 minutes. Meanwhile, the cyantraniliprole dispersion was added to a three-necked round bottom flask and was degassed for 1 hour. Then, the three-necked round bottom flask was placed in an oil bath at 86 ºC and left under stirring for approximately 15 minutes. When the temperature of the millbase reached 86 ºC, the addition of the monomer mixture and the initiator solution started by the use of two degassed syringes and a syringe pump (feeding time 22 hours). When the addition was over, stirring continued for another 2 h under the same conditions. The reaction was terminated by introducing oxygen to the reaction media.

3.4.4 Supplementary Figures and Tables

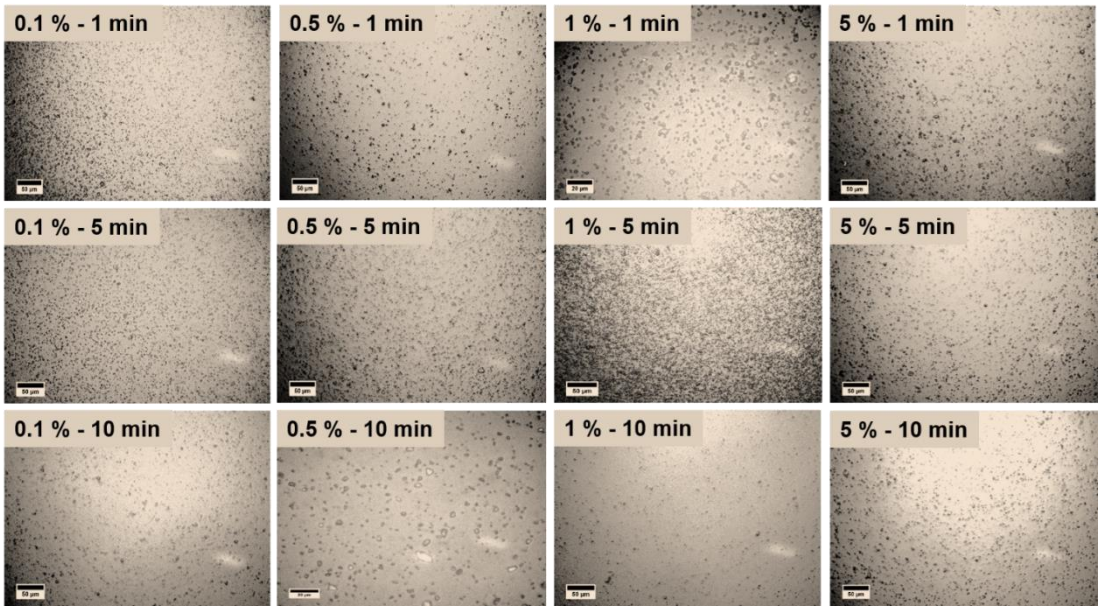

Figure 3-44. Optical microscopy images of cyantraniliprole dispersions using 60% acid content macromonomer.

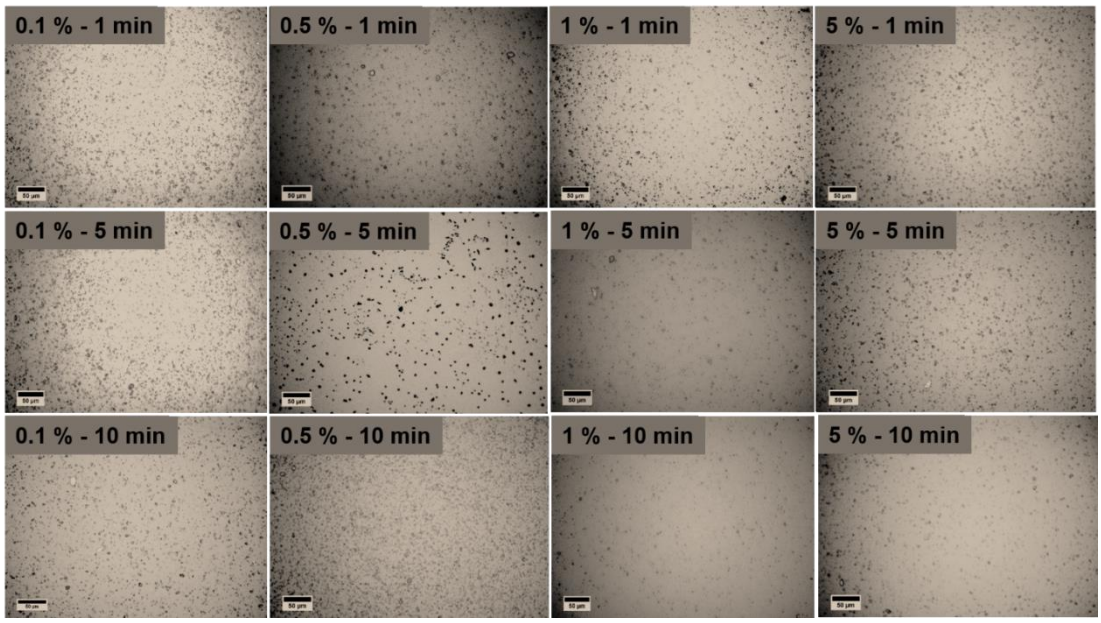

Figure 3-45. Optical microscopy images of cyantraniliprole dispersions using 70% acid content macromonomer.

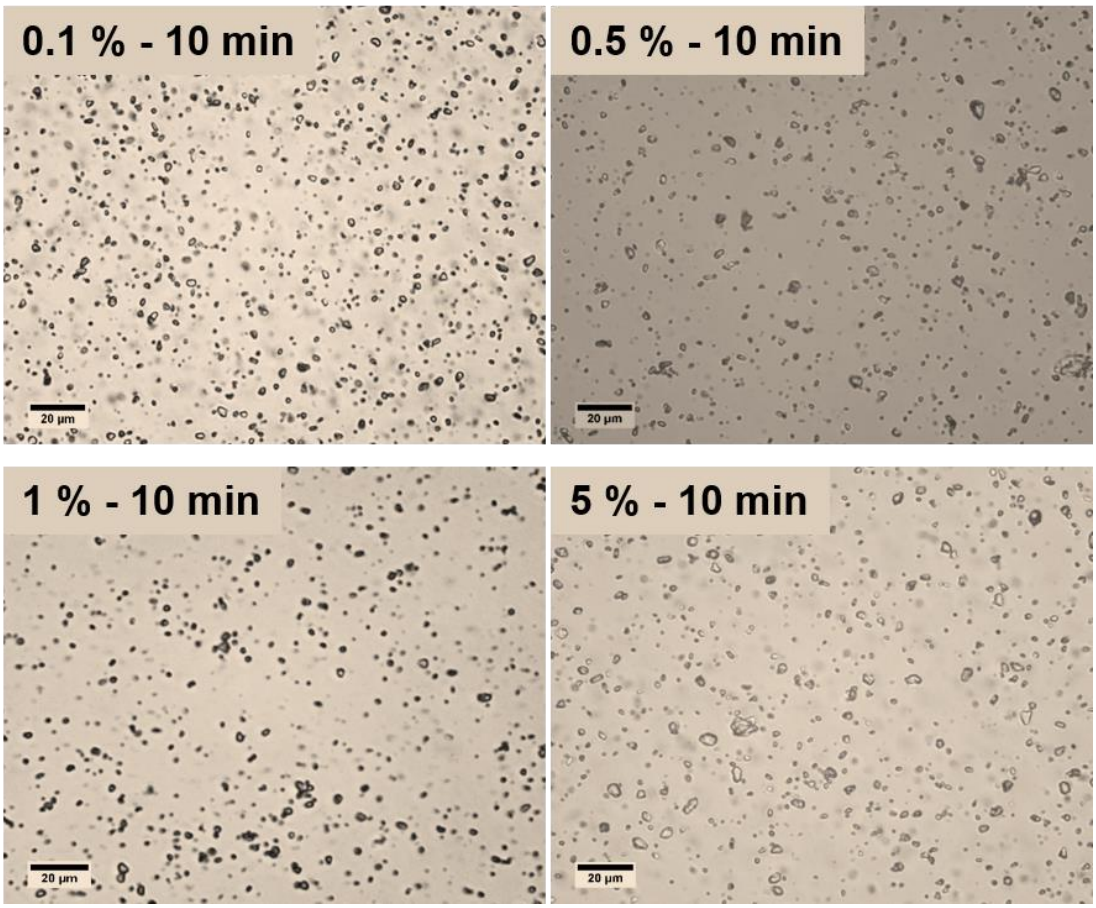

Figure 3-46. Optical microscopy images of cyantraniliprole dispersions using 80% acid content macromonomer.

Table 3-5. Encapsulation efficiency and cyantraniliprole weight % of formulations prepared in PBS, using 60% acid content macromonomer.

$[CYNT]_0$ (w/w %)	E. E. (%)	CYNT weight %
10	96 ± 1.6	43 ± 2.8
20	90 ± 1.9	54 ± 2.1
30	72 ± 2.4	59 ± 3.3

[MM] was 1 w/w % with respect to cyantraniliprole and $W_{MMA : BA}$ was 10 w/w % with respect to millbase mass.

3.5 References

1. Gogos, A.; Knauer, K.; Bucheli, T. D., Nanomaterials in Plant Protection and Fertilization: Current State, Foreseen Applications, and Research Priorities. *Journal of Agricultural and Food Chemistry* **2012,** *60* (39), 9781-9792.

2. Kah, M.; Hofmann, T., Nanopesticide Research: Current Trends and Future Priorities. *Environment International* **2014,** *63*, 224-235.

3. Orts, W. J.; Sojka, R. E.; Glenn, G. M., Biopolymer Additives to Reduce Erosion-Induced Soil Losses During Irrigation. *Industrial Crops and Products* **2000,** *11* (1), 19-29.

4. Yang, Y.; Tong, Z.; Geng, Y.; Li, Y.; Zhang, M., Biobased Polymer Composites Derived from Corn Stover and Feather Meals as Double-Coating Materials for Controlled-Release and Water-Retention Urea Fertilizers. *Journal of Agricultural and Food Chemistry* **2013,** *61* (34), 8166-8174.

5. Aktar, M. W.; Sengupta, D.; Chowdhury, A., Impact of Pesticides Use in Agriculture: Their Benefits and Hazards. *Interdiscip Toxicol* **2009,** *2* (1), 1-12.

6. Kah, M.; Kookana, R. S.; Gogos, A.; Bucheli, T. D., A Critical Evaluation of Nanopesticides and Nanofertilizers against Their Conventional Analogues. *Nature Nanotechnology* **2018,** *13* (8), 677-684.

7. Tilman, D.; Cassman, K. G.; Matson, P. A.; Naylor, R.; Polasky, S., Agricultural Sustainability and Intensive Production Practices. *Nature* **2002,** *418* (6898), 671-677.

8. Kah, M.; Beulke, S.; Tiede, K.; Hofmann, T., Nanopesticides: State of Knowledge, Environmental Fate, and Exposure Modeling. *Critical Reviews in Environmental Science and Technology* **2013,** *43* (16), 1823-1867.

9. Symonds, B. L.; Thomson, N. R.; Lindsay, C. I.; Khutoryanskiy, V. V., Rainfastness of Poly(Vinyl Alcohol) Deposits on Vicia Faba Leaf Surfaces: From Laboratory-Scale Washing to Simulated Rain. *ACS Applied Materials & Interfaces* **2016,** *8* (22), 14220-14230.

10. Fishel, F., Pesticide Formulations. *EDIS* **2010,** *4*.

11. Rai, M. K.; Asthana, P.; Singh, S. K.; Jaiswal, V. S.; Jaiswal, U., The Encapsulation Technology in Fruit Plants—a Review. *Biotechnology Advances* **2009,** *27* (6), 671-679.

12. Green, J. M.; Beestman, G. B., Recently Patented and Commercialized Formulation and Adjuvant Technology. *Crop Protection* **2007,** *26* (3), 320-327.

13. Hack, B.; Egger, H.; Uhlemann, J.; Henriet, M.; Wirth, W.; Vermeer, A. W. P.; Duff, D. G., Advanced Agrochemical Formulations through Encapsulation Strategies? *Chemie Ingenieur Technik* **2012,** *84* (3), 223-234.

14. Bibi, S.; Lattmann, E.; Mohammed, A. R.; Perrie, Y., Trigger Release Liposome Systems: Local and Remote Controlled Delivery? *Journal of Microencapsulation* **2012,** *29* (3), 262-276.

15. Chilkoti, A.; Dreher, M. R.; Meyer, D. E.; Raucher, D., Targeted Drug Delivery by Thermally Responsive Polymers. *Advanced Drug Delivery Reviews* **2002,** *54* (5), 613-630.

16. Wright, T. P.; Hader, J. D.; McMeeking, G. R.; Petters, M. D., High Relative Humidity as a Trigger for Widespread Release of Ice Nuclei. *Aerosol Science and Technology* **2014,** *48* (11), i-v.

17. De Nobili, M.; Contin, M.; Mondini, C.; Brookes, P. C., Soil Microbial Biomass Is Triggered into Activity by Trace Amounts of Substrate. *Soil Biology and Biochemistry* **2001,** *33* (9), 1163-1170.

18. Cordova, D.; Benner, E. A.; Sacher, M. D.; Rauh, J. J.; Sopa, J. S.; Lahm, G. P.; Selby, T. P.; Stevenson, T. M.; Flexner, L.; Gutteridge, S.; Rhoades, D. F.; Wu, L.; Smith, R. M.; Tao, Y., Anthranilic Diamides: A New Class of Insecticides with a Novel Mode of Action, Ryanodine Receptor Activation. *Pesticide Biochemistry and Physiology* **2006,** *84* (3), 196-214.

19. Meissner, G., Ryanodine Receptor/Ca2+ Release Channels and Their Regulation by Endogenous Effectors. *Annual Review of Physiology* **1994,** *56* (1), 485-508.

20. Insecticide Resistance Management Global Guidelines for IRAC Group 28 (Diamide) Insecticides. https://irac-online.org/.

21. Ali, S. I.; Heuts, J. P. A.; Hawkett, B. S.; van Herk, A. M., Polymer Encapsulated Gibbsite Nanoparticles: Efficient Preparation of Anisotropic Composite Latex Particles by RAFT-Based Starved Feed Emulsion Polymerization. *Langmuir* **2009,** *25* (18), 10523-10533.

22. Perreira, A. C.; Pearson, S.; Kostadinova, D.; Leroux, F.; D'Agosto, F.; Lansalot, M.; Bourgeat-Lami, E.; Prévot, V., Nanocomposite Latexes Containing Layered Double Hydroxides Via RAFT-Assisted Encapsulating Emulsion Polymerization. *Polymer Chemistry* **2017,** *8* (7), 1233-1243.

23. Delafresnaye, L.; Dugas, P.-Y.; Lansalot, M.; Bourgeat-Lami, E., Innovative Method for Laponite Encapsulation into Polymer Latex Particles by Clay Cluster-Seeded Emulsion Polymerization. *Macromolecules* **2020,** *53* (1), 39-50.

24. Chaparro, T. C.; Silva, R. D.; Dugas, P.-Y.; D'Agosto, F.; Lansalot, M.; Martins dos Santos, A.; Bourgeat-Lami, E., Laponite®-Based Colloidal Nanocomposites Prepared by RAFT-Mediated Surfactant-Free Emulsion Polymerization: The Role of Non-Ionic and Anionic Macroraft Polymers in Stability and Morphology Control. *Polymer Chemistry* **2021,** *12* (1), 69-81.

25. Davis, T. P.; Kukulj, D.; Haddleton, D. M.; Maloney, D. R., Cobalt-Mediated Free-Radical Polymerization of Acrylic Monomers. *Trends Polym. Sci.* **1995,** *3* (11), 365-373.

26. Gridnev, A., The 25th Anniversary of Catalytic Chain Transfer. *J. Macromol. Sci. Part A: Polym. Chem.* **2000,** *38* (10), 1753-1766.

27. Heuts, J. P. A.; Roberts, G. E.; Biasutti, J. D., Catalytic Chain Transfer Polymerization: An Overview. *Aust. J. Chem.* **2002,** *55* (7), 381-398.

28. Davis, T. P.; Haddleton, D. M.; Richards, S. N., Controlled Polymerization of Acrylates and Methacrylates1. *J. Macromol. Sci. Part C* **1994,** *34* (2), 243-324.

29. Smirnov, B. R.; Marchenko, A. P.; Korolev, G. V.; Bel'govskii, I. M.; Yenikolopyan, N. S., Kinetic Study of Catalysis of the Chain Transfer Reaction to Monomer in the Radical Polymerization of Methyl Methacrylate. *Polym. Sci. U.S.S.R.* **1981,** *23* (5), 1158-1168.

30. Smirnov, B. R.; Plotnikov, V. D.; Ozerkovskii, B. V.; Roshchupkin, V. P.; Yenikolopyan, N. S., Catalysis of Chain Transfer and Oligometer Structure in Radical Polymerization of Styrene in the Presence of Cobalt Complexes of Porphyrins. *Polym. Sci. U.S.S.R.* **1981,** *23* (11), 2807-2816.

31. Anastasaki, A.; Waldron, C.; Nikolaou, V.; Wilson, P.; McHale, R.; Smith, T.; Haddleton, D. M., Polymerization of Long Chain [Meth]Acrylates by Cu(0)-Mediated and Catalytic Chain Transfer Polymerisation (CCTP): High Fidelity End Group Incorporation and Modification. *Polym. Chem.* **2013,** *4* (15), 4113-4119.

32. Maloney, D. R.; Hunt, K. H.; Lloyd, P. M.; Muir, A. V. G.; Richards, S. N.; Derrick, P. J.; Haddleton, D. M., Polymethylmethacrylate End-Group Analysis by Matrix-Assisted Laser Desorption Ionisation Time-of-Flight Mass Spectrometry (MALDI-ToF-MS). *J. Chem. Soc., Chem. Commun.* **1995,** (5), 561-562.

33. Antonelli Joseph A., B. C. T., Darmon Michael J. Method of Preparing Macrmonomer Compositions. US5362826A, **1994**.

34. Loiko, O. P.; Spoelstra, A. B.; van Herk, A. M.; Meuldijk, J.; Heuts, J. P. A., An Atrp-Based Approach Towards Water-Borne Anisotropic Polymer–Gibbsite Nanocomposites. *Polymer Chemistry* **2016,** *7* (20), 3383-3391.

35. Mayo, F. R., Chain Transfer in the Polymerization of Styrene: The Reaction of Solvents with Free Radicals1. *J. Am. Chem. Soc.* **1943,** *65* (12), 2324-2329.

36. Heuts, J. P. A.; Smeets, N. M. B., Catalytic Chain Transfer and Its Derived Macromonomers. *Polym. Chem.* **2011,** *2* (11), 2407-2423.

37. Sharma, A. K.; Zimmerman, W. T.; Lowrie, C.; Chapleo, S., Hydrolysis of Chlorantraniliprole and Cyantraniliprole in Various pH Buffer Solutions. *Journal of Agricultural and Food Chemistry* **2014,** *62* (16), 3531-3536.

38. Lesage de la Haye, J.; Martin-Fabiani, I.; Schulz, M.; Keddie, J. L.; D'Agosto, F.; Lansalot, M., Hydrophilic Macroraft-Mediated Emulsion Polymerization: Synthesis of Latexes for Cross-Linked and Surfactant-Free Films. *Macromolecules* **2017,** *50* (23), 9315-9328.

39. Zhang, Q.; Slavin, S.; Jones, M. W.; Haddleton, A. J.; Haddleton, D. M., Terminal Functional Glycopolymers Via a Combination of Catalytic Chain Transfer Polymerisation (CCTP) Followed by Three Consecutive Click Reactions. *Polym. Chem.* **2012,** *3* (4), 1016-1023.

Chapter 4: *Photo-induced copper-RDRP in continuous flow without external deoxygenation*

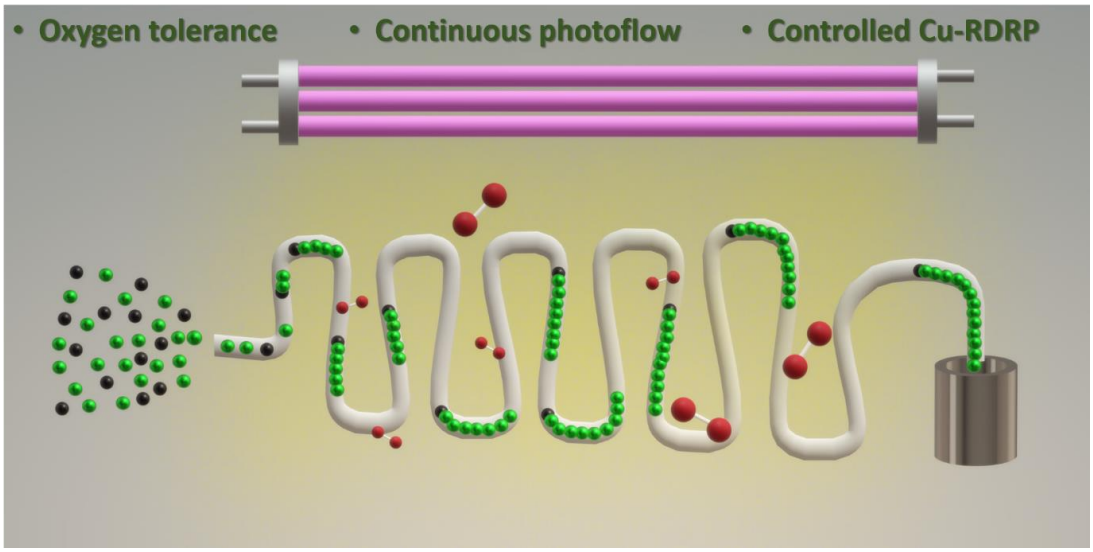

Photo-induced Cu-RDRP of acrylates in a continuous flow reactor without the need for deoxygenation or addition of external deoxygenation agents. Optimization of the catalyst concentration and the flow rate/residence time leads to well-defined polyacrylates with controlled molecular weights, excellent initiator efficiency, high end-group fidelity polymers and product uniformity, a multifunctional initiator was also used to demonstrate the versatility of the system.

4.1 Introduction

Controlled radical polymerization (CRP) techniques such as atom-transfer radical polymerization (ATRP),[1-3] single electron transfer-living radical polymerization (SET-LRP),[4, 5] reversible addition–fragmentation chain-transfer polymerization (RAFT),[6-9] and nitroxide-mediated polymerization (NMP),[10] have expanded the capability of polymer synthesis, allowing access to a plethora of new materials.[11, 12] Among the benefits, the ability to externally regulate these techniques with various stimuli has further expanded the scope of their applications. The use of light as a stimulus allows for excellent spatial and temporal control thus expanding their applications.[13-17]

Nevertheless, CRP techniques are often not available to undergraduate laboratories or those lacking specialist equipment for efficient deoxygenation. Oxygen is a radical inhibitor, scavenging both primary and propagating radicals leading to the formation of peroxy radicals and hydroperoxides altering irreversibly the reaction components (initiator, catalyst, etc.) and having an overall detrimental effect.[18-20] Although the various traditional deoxygenation techniques applied prior to polymerization (freeze-pump-thaw, N_2/Ar sparging, glove box equipment, etc.) provide efficient oxygen removal, they can be disadvantageous due to their high cost and implementation time. In order to circumvent this, different approaches have been made so as to replace conventional deoxygenation in Cu-mediated reversible deactivation radical polymerization [21-27] and photo-induced electron transfer (PET) RAFT.[28-30] PET-RAFT, has employed various reducing agents (*i.e.* ascorbic acid,[31, 32] photo-redox catalysts[33, 34]) which have been successfully used for the efficient removal of oxygen in both batch reactions and in continuous flow processes.[35]

Polymerizations in continuous flow (CF) reactors are of interest since they have been proved to be efficient alternatives to batch reactions[36-39] and by providing the ability to produce large volumes in short times,[40] have introduced an industrialized way of materials production.[41, 42] Continuous flow RAFT has been developed and exploited, for example by CSIRO where the ingress of oxygen through the tubing was problematic and avoided by using steel tubing to prevent quenching of the radical process by oxygen,[43] and more recently making use of the light penetration of

millimetre-size fluoropolymer tubing giving multigrams/kgs of RAFT polymer per day.[44] In 2013, Haddleton *et al* reported that a simple, easy to construct, bench-top plug flow reactor consisting of PTFE tubing with a Cu(0)-wire was used for the SET-LRP of methyl acrylate leading to polymers with narrow dispersities and high end-group fidelity.[45] CF processes have been fully exploited when combined with light as an external stimulus.[37, 46-48] Hawker and coworkers investigated the light-mediated polymerization of MMA using four widely available tubing materials giving insights into the impact of oxygen diffusivity on polymerization kinetics.[49] Junkers and colleagues has recently reported on the CF synthesis of core crosslinked star polymers *via* a photo induced copper mediated system. This system required prior nitrogen sparging and showed an elegant route to an interesting tool to continuously produce star polymers without intermediate purification[50] Efficiency of light penetration is increased due to the high surface area-to-volume ratio leading to more uniform irradiation and resulting in better control over the polymerization.[38] As a result, significant amounts of polymers are obtained through a user-friendly approach, with the ability to easily regulate the reaction parameters (flow rate, residence time, light intensity, etc.). On account of this, the scope of CF polymerizations has been expanded with the replacement of traditional deoxygenation in PET-RAFT polymerization.[30, 51] However, to the best of our knowledge, there is no example of a photoinduced copper mediated process that does not require deoxygenation in CF reactors. The recent publications by Liarou, Haddleton and colleagues, which inspired this research, demonstrated the importance of all the components for the oxygen consumption in the reaction mixture.[21, 22]

In this chapter, the photo-induced Cu-RDRP of acrylates in a continuous flow reactor, without the requirement of applying any type of deoxygenation or using externally added reagents, is introduced and discussed (**Scheme 4-1**). Optimization of the flow rate/residence time as well as the [EBiB] : [Cu(II)Br_2] : [Me_6Tren] ratio leads to the synthesis of well-defined poly(acrylates). The versatility of this approach is further confirmed with the synthesis of different molar mass polymers ($M_{n,SEC}$ ~ 2,300 – 26,000 g mol^{-1}), as well as the synthesis of an 8-arm star pMA homopolymer and the high end-group fidelity maintained is demonstrated through nucleophilic thio-bromine substitution with thioglycerol.

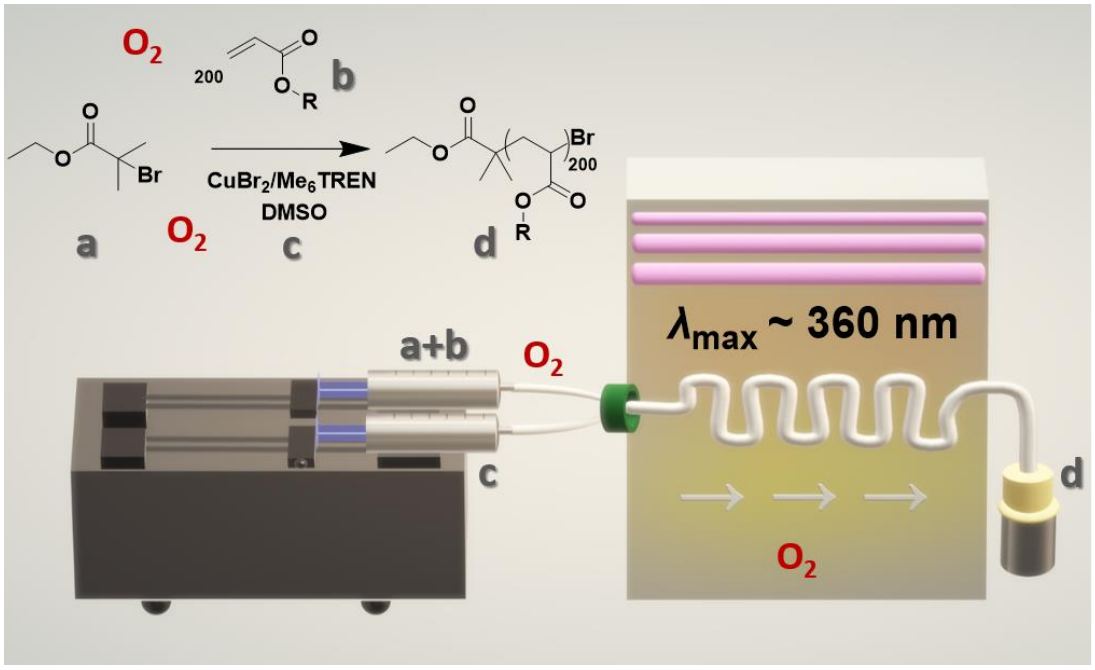

Scheme 4-1. Reaction scheme and setup for the photo-induced Cu-RDRP in continuous flow with a: EBiB, b: Monomer, c: $CuBr_2/Me_6Tren$/DMSO and d: final polymer.

4.2 Results and Discussion

In order to explore the ability of this system to perform without deoxygenation in a continuous flow reactor, methyl acrylate (MA) was used as monomer, ethyl α-bromoisobutyrate (EBiB) as initiator, tris(2-(dimethylamino)ethyl)-amine (Me_6Tren) as ligand, $Cu(II)Br_2$ as the copper source, and DMSO as solvent. In this chemistry the copper(II) is reduced following photoexcitation of the ligand and subsequent energy transfer.[52] The copper(I) complex is prone to both oxidation and disproportionation.[53] Disproportionation leads to copper(0) which is susceptible to rapid oxidation.[54] One of the primary aims was to design a user-friendly process, able to provide uniform irradiation for the continuous flow.

In this system, the photoexcitation of free ligand (Me_6Tren) leads to the C-Br bond homolysis of the initiator resulting in an initiating radical, a radical cation of the ligand and its analogous counterion, Br^-.[15] In the presence of monomer, the initiating radical mediates the propagation, whereas the deactivating species ($Cu^{II}Br_2/Me_6Tren$) maintain the control over the polymerization. Thus, the stoichiometry of the reagents in the polymerization mixture is essential for the production of well-defined polymers. A [$Cu(II)Br_2$] : [Me_6Tren] = 1:1 ratio means that the whole amount of the ligand is complexed with $Cu(II)Br_2$ and therefore the photoactivation will not occur. It was found that when this ratio is 1:2, 1:3 and 1:6 the polymerization of MA was proceeded in high conversions (90 -95 %), narrow dispersities (1.05 – 1.07), and very good agreement between theoretical and experimental M_n value (slightly better when the ratio was 1:6), proving that excess of ligand is required for successful photoactivation.[15] In this work the ratio of [$Cu(II)Br_2$] : [Me_6Tren] = 1:6 was kept for all the experiments in order to maintain large excess of the ligand.

Based on this, initial experiments took place by the preparation of the reaction mixture using the ratio [MA] : [I] : [$Cu(II)Br_2$] : [Me_6Tren] = [50] : [1] : [0.02] : [0.12] and its transfer to a syringe. Consequently, the syringe (wrapped with foil) was put in a syringe pump and was connected to a 3 meter PFA tubing located in the chamber of a UVP crosslinker with λ_{max}= 365 nm, ending outside of the UVP chamber and connected with the foil-wrapped collection vessel. The

reaction was conducted by using two different flow rates, 6 and 10 μL/min, leading to residence times of 3.25 and 2 hours (which is the time the solution is irradiated in the tubing), respectively. The monomer conversion was 89% and 81%, respectively, however, aliquots taken from the syringe showed monomer conversion of 21% and 10%, indicating that polymerization can occur even before the intended irradiation of the solution (**Figures 4-1 & 4-2**). In order to eliminate the polymerization reaction in the syringe, two more reactions were conducted by lowering the residence time to 30 and 60 minutes. Although the monomer conversion in the syringe was 2% and 3% respectively, the conversion after irradiation was limited to 29% for a residence time of 60 minutes and 8% when the solution was irradiated for 30 minutes (**Figure 4-1 & 4-2**).

Therefore, a different set-up was required for the preparation of the polymerization mixture just before its introduction into the chamber of the UVP crosslinker. Consequently, the set-up included a dual syringe pump, a mixing tee, 3-meter PFA tubing located in the chamber of the UVP crosslinker with λ_{max}= 365 nm, ending outside of the UVP chamber and connected with the foil-wrapped collection vessel (**Scheme 4-2**). In this set-up, one syringe contains the solution of the complex (Cu(II)Br_2, Me_6Tren and DMSO) and a second contains the monomer/initiator solution (MA/EBiB).

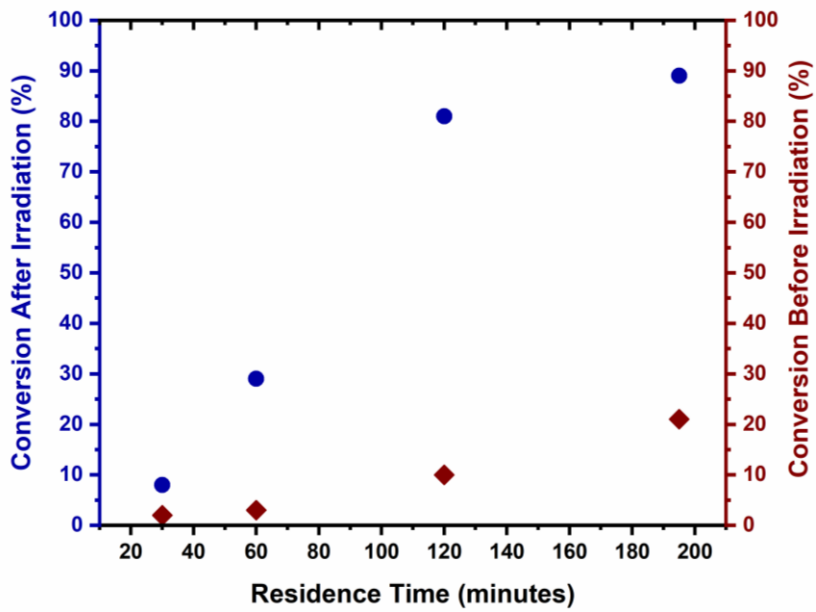

Figure 4-1. Conversion versus residence time plot of the targeted pMA_{50} showing the monomer conversion before and after irradiation under different flow rates.

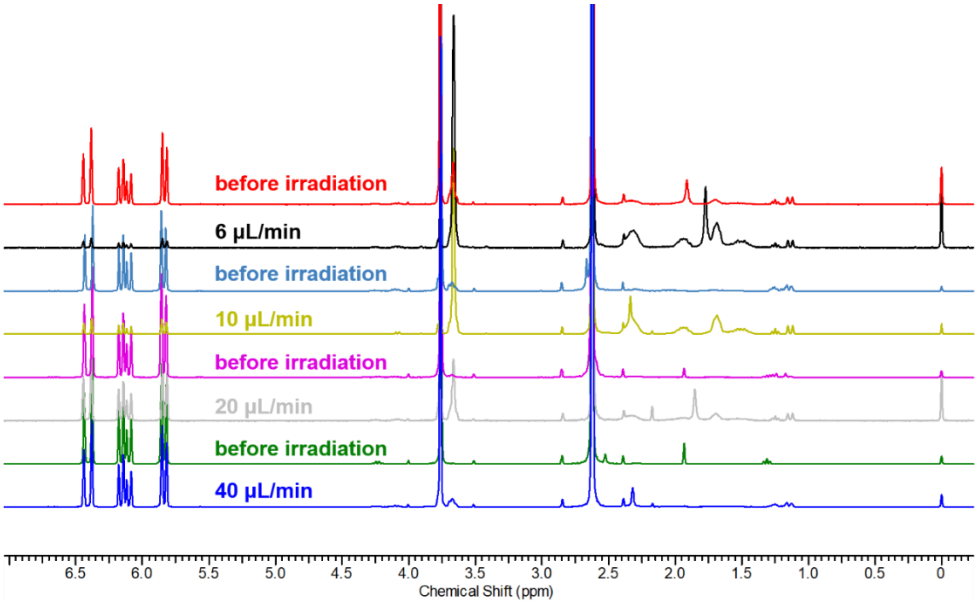

Figure 4-2. ^{1}H NMR spectra of the targeted pMA_{50} synthesized *via* photoinduced Cu-RDRP in continuous flow without deoxygenation. Conversion was determined by comparing the integrals of monomeric vinyl protons (~5.7-6.5 ppm) to polymer signal (~3.56-3.87 ppm).

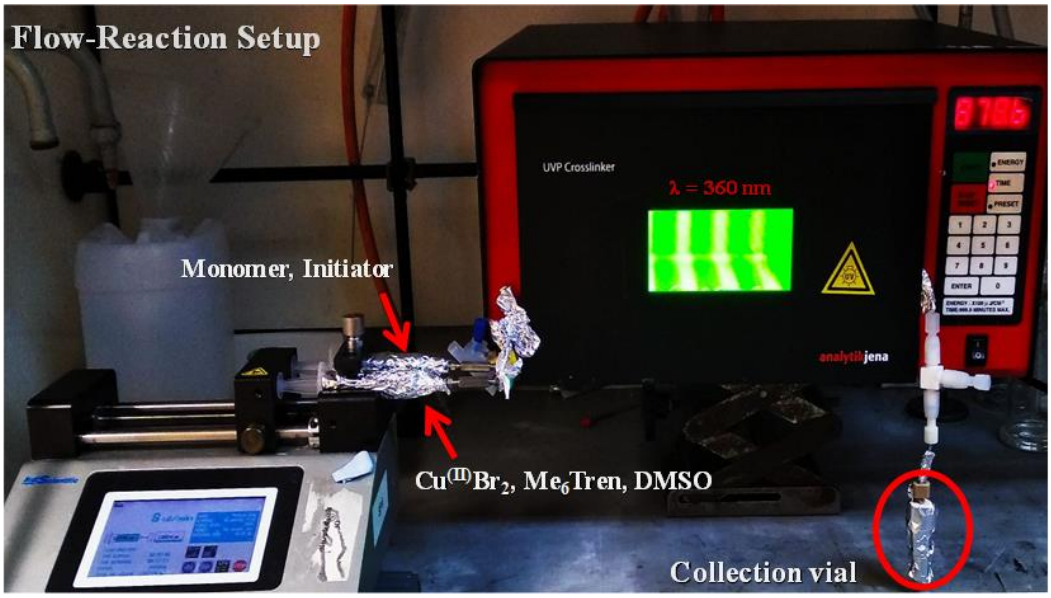

Scheme 4-2. Continuous flow reactor setup.

Taking into consideration that by using this set-up no polymerization could take place before irradiation, the polymerization of MA with targeted DP_n = 50 was conducted using the ratio [MA] : [I] : [Cu(II)Br_2] : [Me_6Tren] = [50] : [1] : [0.02] : [0.12] with a flow rate of 6 μL/min (residence time = 3.25 hours). The monomer conversion, theoretical molecular weight, experimental

molecular weight and dispersity values were 87%, 4,000, 4,800 and 1.10 respectively, whereas no monomer conversion was observed in the syringe containing the monomer and the initiator. Building on this, various DPs of pMA (DP_n = 25, 100 and 200) were targeted under the same conditions (**Table 4-1, Figure 4-3**). Albeit the polymerization was proceeded to acceptable conversions for DP_n = 25 (88%) and 100 (67%), no polymerization took place when DP_n = 200 was targeted. Thus, further studies were required for the optimization of reaction conditions in order to obtain polymers with higher molecular weights.

Table 4-1. ^{1}H NMR, SEC analysis and flow rates for the pMA with different DPs obtained through photoinduced Cu-RDRP in continuous flow without deoxygenation.[a]

DP	Flow rate (µL/min)	Residence time (min)	Mon. Conv.[b] (%)	$M_{n,th.}$ (g mol^{-1})	$M_{n,GPC}$[c]	Đ
25	6	3 h 15	88	2,100	2,900	1.11
50	6	3 h 15	87	4,000	4,500	1.08
100	6	3 h 15	67	6,000	6300	1.16
200	6	3 h 15	0	-	-	-

[a] In all polymerizations, the volume ratio of monomer to solvent was maintained 1 : 1 and [I] : [Cu(II)Br$_2$] : [Me$_6$Tren] = [1] : [0.02] : [0.12]. [b] Conversion was calculated *via* ^{1}H NMR in *d*-CHCl$_3$. [c] Determined by THF-SEC analysis and expressed as molecular weight equivalents to pMMA narrow molecular weight standards.

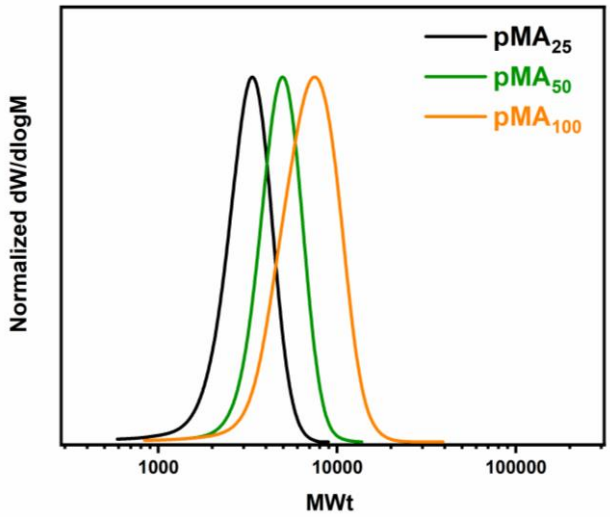

Figure 4-3. THF-SEC derived molecular weight distributions of pMA with targeted DP_n=25-100 synthesized *via* non-deoxygenated photoinduced Cu-RDRP in continuous flow.

Based on the findings in the batch system (near-quantitative conversion after ~ 2.5 hours) (**Figure 4-4**), the polymerization of MA with targeted DP_n = 200 was conducted using the ratio [MA] : [I] : [Cu(II)Br_2] : [Me_6Tren] = [200] : [1] : [0.02] : [0.12] with a flow rate = 8 μL/min (residence time = 2.5 hours).

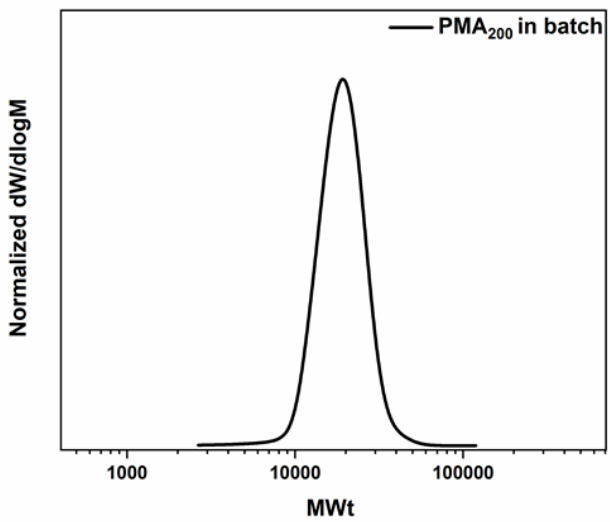

Figure 4-4. THF-SEC derived molecular weight distributions for targeted pMA_{200} synthesized in batch process without deoxygenation for 3 h in the UVP crosslinker with [MA] : [I] : [Cu(II)Br_2] : [Me_6Tren] = [200] : [1] : [0.02] : [0.12]. The results obtained were: conversion 97%, $Đ$ = 1.18 and $M_{n,SEC}$=22,300 ($M_{n,th}$.= 16,900 g mol^{-1}).

In contrast to the equivalent batch process, no polymerization took place. In a batch reaction the headspace is eliminated by conducting the reaction in a fully filled reaction vessel. However in the continuous flow set up the presence of oxygen is significant since it can be found dissolved in the reaction solution or localized in the tubing acting as "*headspace*", therefore it could decelerate the oxygen consumption process and ultimately the polymerization reaction. Liarou and Haddleton *et al.* have reported previously that in a batch reaction with 20 or 12 mL of headspace, oxygen did not fully consumed even after 1 hour, thus affecting the reaction time.[21] In another work from the same group it was reported that an increase of the copper complex concentration contributed to fast oxygen consumption.[22] It is noted that copper(II) salts are classified as "Generally Regarded As Safe" (GRAS) compounds by the FDA. Based on these findings, we hypothesized that increasing both the concentration of Cu(II)Br_2 and Me_6Tren with respect to initiator, faster oxygen consumption could

contribute to an acceptable conversion of monomer to polymer. However, no polymerization was seen under these conditions. The lack of polymerization (**Table 4-2, entries 1&2**) was attributed to the low amounts of copper complex which proved insufficient to both participate in oxygen consumption and generate active species for the polymerization. Although the ratio [Cu(II)Br_2] : [Me_6Tren] = [0.04] : [0.24] resulted in zero monomer conversion (**Table 4-2, entry 2**), it resulted in 46% monomer conversion when 6 μL/min was applied, which further corroborates that longer reaction times are required when the headspace cannot be eliminated. In order to overcome this, higher amounts of the copper complex were used with [Cu(II)Br_2] : [Me_6Tren] = [0.08] : [0.48], yielding pMA_{200} with 46% monomer conversion (**Table 4-2, entry 3, Figure 4-5**).

Table 4-2. ^{1}H NMR and SEC analysis for all the non-deoxygenated photoinduced Cu-RDRP with different [Cu(II)Br_2] : [Me_6Tren] ratios for pMA_{200}. [a,b]

Entry	[I] : [$CuBr_2$] : [Me_6Tren]	Mon. Conv. [c] (%)	$M_{n,th.}$ (g mol^{-1})	$M_{n,GPC}$ [d]	Đ
1	1 : 0.02 : 0.12	0	-	-	-
2	1 : 0.04 : 0.24	0	-	-	-
3	1 : 0.08 : 0.48	46	8,100	11,200	1.16
4	1 : 0.16 : 0.96	77	13,500	13,600	1.17
5	1 : 0.32 : 1.92	75	13,100	14,000	1.23

[a] In all polymerizations, the volume ratio of monomer to solvent was maintained 1 : 1. [b] Flow rate 8 μL/min. [c] Conversion was calculated *via* ^{1}H NMR in *d*-$CDCl_3$. [d] Determined by THF SEC analysis and expressed as molecular weight equivalents to pMMA narrow molecular weight standards.

The deviations between theoretical and experimental M_n values for the latter might be attributed to the oxygen consumption, taking place at this stage of the polymerization, leading to a reduction of initiator efficiency. As low monomer conversion and initiator efficiency were obtained, we envisaged that further increase of the copper complex concentration was needed in order to achieve sufficient oxygen consumption and higher monomer conversions. Consequently, [Cu(II)Br_2] : [Me_6Tren] = [0.16] : [0.96] was used, resulting in 77% monomer conversion, good agreement between theoretical and experimental molecular weights ($M_{n,SEC}$ = 13,600, $M_{n,\ th.}$ = 13,500) and low dispersity (*Đ* = 1.17) (**Table 4-2, entry 4, Figures 4-5 & 4-6**). Interestingly, the

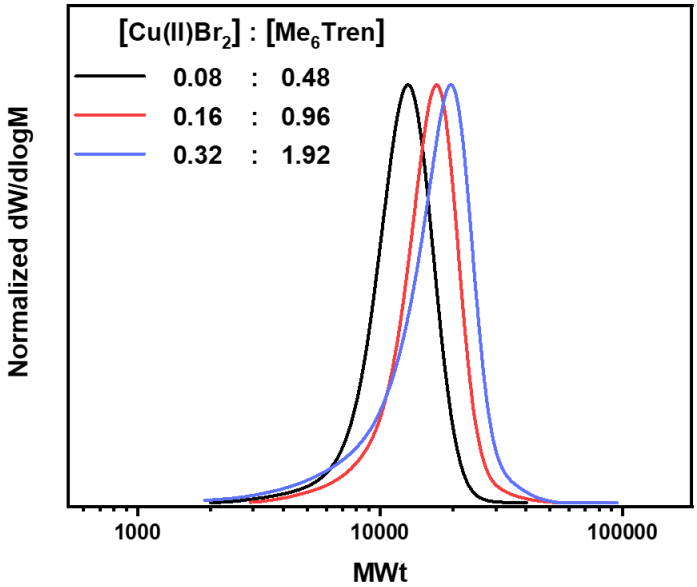

Figure 4-5. SEC derived molecular weight distributions for targeted pMA_{200} synthesized *via* non-deoxygenated photoinduced Cu-RDRP in continuous flow with different [Cu(II)Br2] : [Me6Tren] ratios.

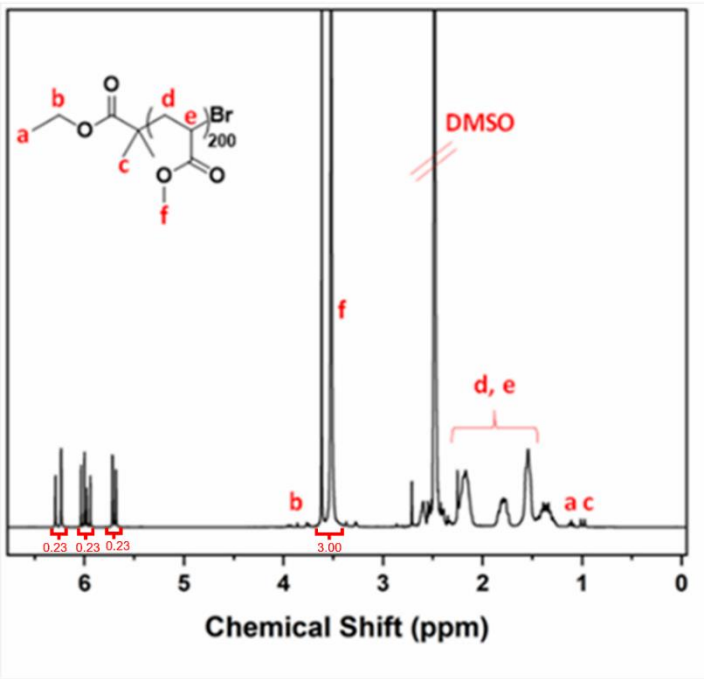

Figure 4-6. ^{1}H NMR of targeted pMA_{200} synthesized *via* photoinduced Cu-RDRP in continuous flow without deoxygenation. Conversion (77%) was determined by comparing the integrals of monomeric vinyl protons (~5.7-6.5 ppm) to polymer signal (~3.56-3.87 ppm).

continuous flow process provided high initiator efficiency when compared with a batch process, where deviations between experimental and theoretical M_n values were present (**Figure 4-4**).[22] It is noteworthy that when higher amounts of $Cu(II)Br_2$ and Me_6Tren were used (0.32 eq. and 1.92 eq., respectively), a slightly higher dispersity was observed ($Đ$ = 1.23) and no further increase in the monomer conversion was obtained (**Figure 4-5, Table 4-2, entry 5**). Hence, the ratio [EBiB] : [$Cu(II)Br_2$] : [Me_6Tren] = [1] : [0.16] : [0.96] was selected for further investigation of this non-deoxygenated system in continuous flow process (**Table 4-2, entry 4**).

Consequently, identical samples were prepared and polymerized with different flow rates leading to different residence times (**Table 4-3**). MA with targeted DP_n = 200 was polymerized with [EBiB] : [$Cu(II)Br_2$] : [Me_6Tren] =[1] : [0.16] : [0.96] (**Figure 4-7**). Initially, a flow rate of 80 µL/min resulted in a residence time of 15 minutes. The monomer conversion was as low as 4%, indicating that longer residence times are required for the polymerization to proceed to acceptable conversions. Therefore, a flow rate of 40 µL/min led to an increase of the monomer conversion to 16% (**Table 4-3, entry 2**) and continued to increase steadily for all the samples with residence times up to 200 minutes (**Table 4-3, entries 2-9, Figure 4-8 & 4-9**), where good control over the polymerization was achieved, with low dispersities and good agreement between $M_{n,th}$ and $M_{n,SEC}$ suggesting good initiator efficiency (**Figure 4-7 & Figure 4-10)**. The monomer conversion reached its highest value (85%), when a flow rate of 6 µL/min was used. In order to achieve even higher conversions, lower flow rates (longer residence times) were used. When a flow rate of 5 µL/min was used, the results were similar to 6 µL/min (**Table 4-3, entry 9**). With flow rates of 4 µL/min and 2 µL/min, the monomer conversion remained constant at 84-85%, but higher MWts were obtained (**Table 4-3**, **entry 11&12**). This might be attributed to the prolonged residence times in the reactor and the extended exposure to oxygen, which can induce termination events.

Table 4-3. ^{1}H NMR and SEC analysis for the non-deoxygenated photo-induced Cu-RDRP conducted under different flow rates for pMA_{200}.[a]

Entry	Flow rate (μL/min)	Res. Time (min)	Mon. Conv.[b] (%)	$M_{n,th.}$ (g mol^{-1})	$M_{n,GPC}$[c]	$Đ$[c]
1	80	15	4	-	-	-
2	40	30	16	-	-	-
3	30	40	30	5,400	5,500	1.08
4	20	60	39	6,900	8,200	1.18
5	15	80	56	9,800	9,200	1.20
6	12	100	59	10,400	11,900	1.20
7	10	120	69	12,100	12,800	1.19
8	8	150	77	13,500	13,600	1.17
9	6	200	85	14,800	14,300	1.15
10	5	240	84	14,700	14,300	1.15
11	4	300	85	14,800	15,400	1.21
12	2	600	84	14,700	16,400	1.23

[a] In all polymerizations, the volume ratio of monomer to solvent was maintained 1 : 1 and [EBiB] : [Cu(II)Br_2] : [Me_6Tren] =[1] : [0.16] : [0.96]. [b] Conversion was calculated via ^{1}H NMR in *d*-$CDCl_3$. [c] Determined by THF SEC analysis and expressed as molecular weight equivalents to pMMA narrow molecular weight standards.

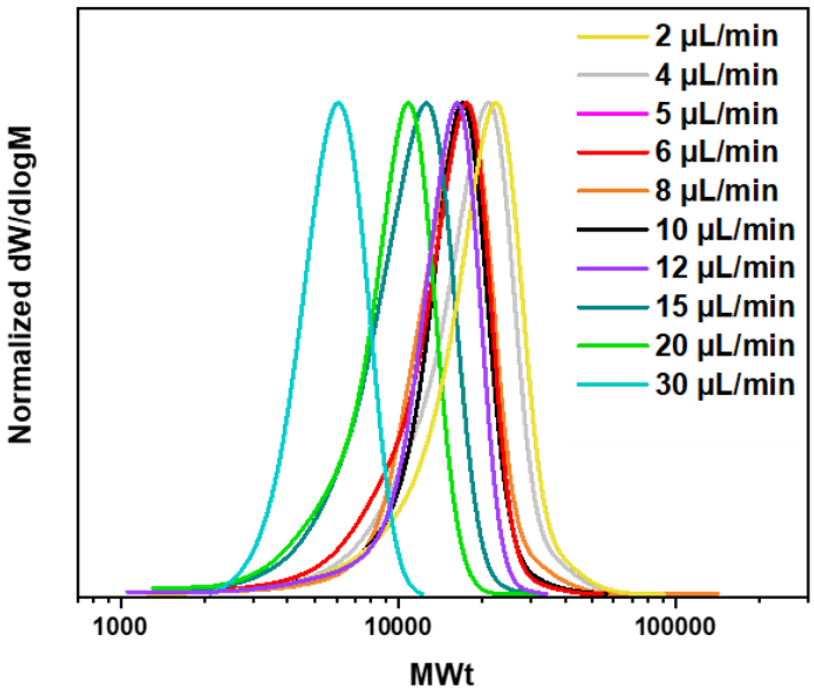

Figure 4-7. THF-SEC derived molecular weight distributions showing the evolution of MWts.

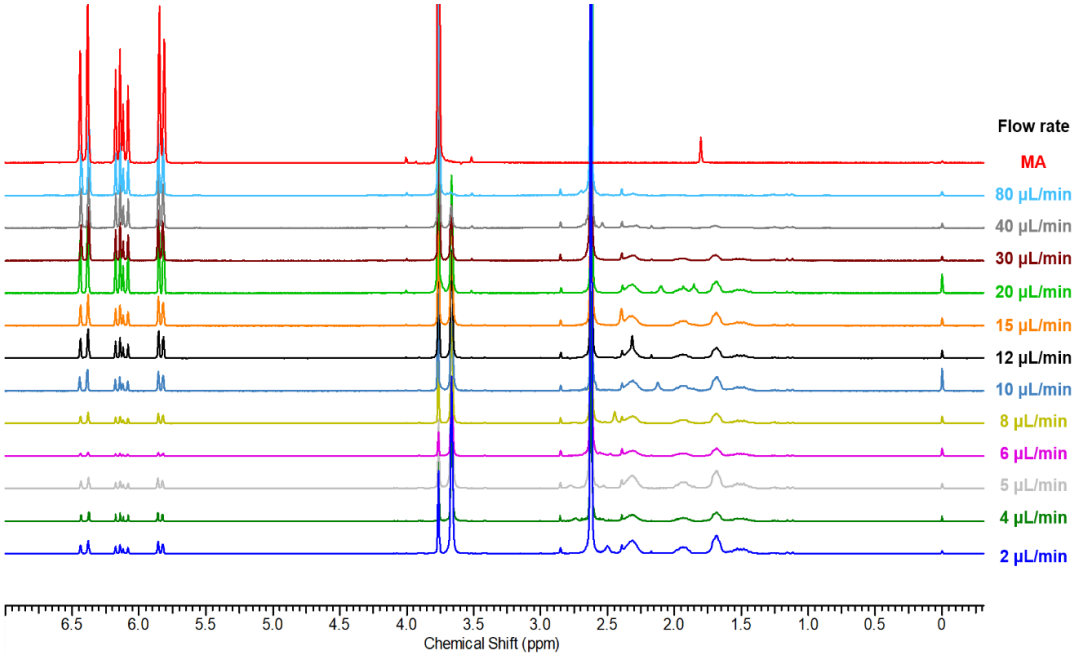

Figure 4-8. ^{1}H NMR spectra of the –Br terminated pMA_{200} showing the conversion of MA with increased residence times. Conditions : [MA] : [I] : [Cu(II)Br_2] : [Me_6Tren] = [200] : [1] : [0.16] : [0.96].

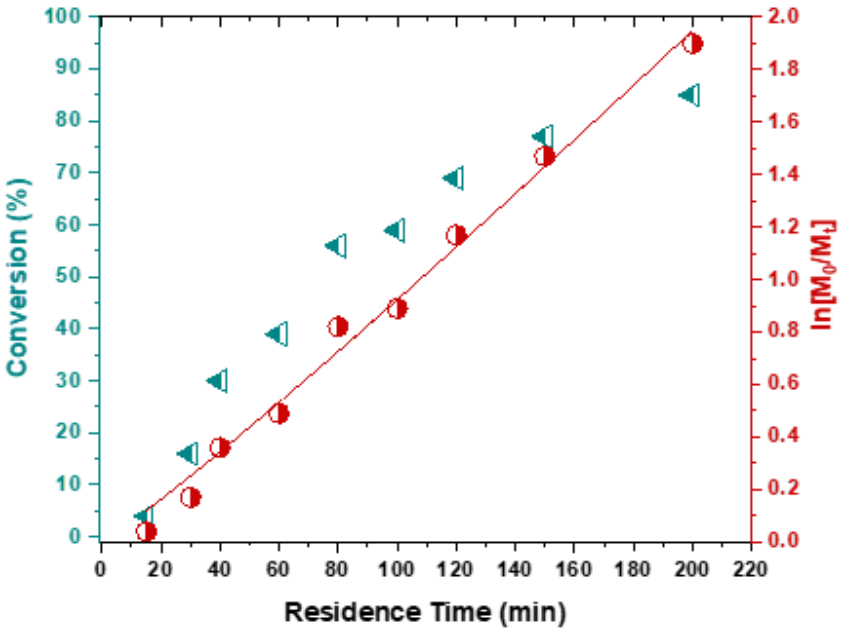

Figure 4-9. Kinetic plots of ln[M_0/M_t] (right, red) and conversion (left, dark cyan) versus residence time. Conditions: [EBiB] : [Cu(II)Br_2] : [Me_6Tren] = [1] : [0.16] : [0.96].

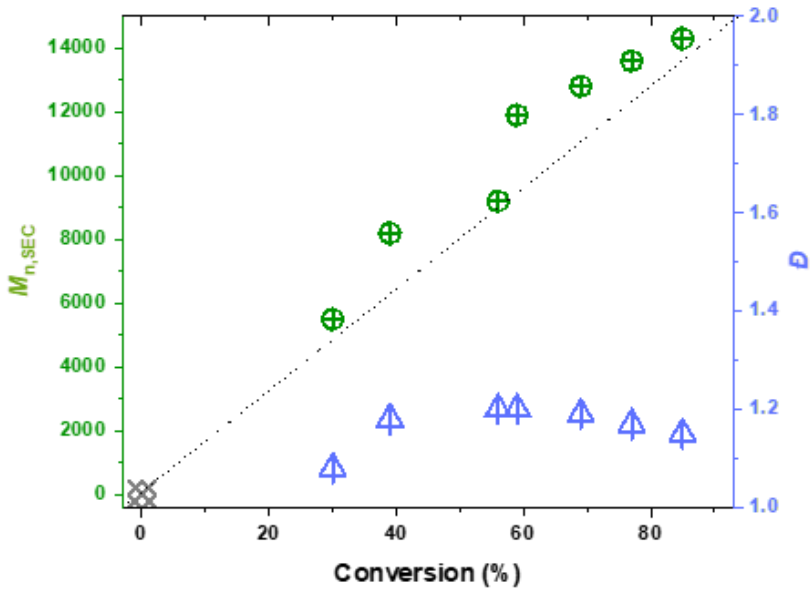

Figure 4-10. Plots of M_n versus conversion (left, green) and dispersity ($Đ$) versus conversion (right, blue). Conditions: [EBiB] : [Cu(II)Br$_2$] : [Me$_6$Tren] = [1] : [0.16] : [0.96].

Furthermore, the molecular characteristics of the sample run at different times in the reactor were the same for the whole volume of the polymer, corroborating the uniformity of the system. In all cases, polymers have shown almost identical monomer conversions (84 - 85%), as well as molecular weights and dispersities (M_n = 15,400 – 15,700 and $Đ$ = 1.15 – 1.19) independently of collection time (**Table 4-4, Figure 4-11**). These results confirm that after the total oxygen consumption at the early stages of the polymerization, oxygen diffusion through the tubing during the reaction cannot have significant effects on the polymerization.

A further requirement for a controlled radical polymerization is the retention of the chain end, which enables the functionalization of the obtained polymers.[55] In order to explore the ω-Br functionality in this system, matrix assisted laser desorption-ionization time-of-flight mass spectrometry (MALDI-ToF-MS) was employed for pMA$_{25}$,[56] revealing a predominant single peak distribution corresponding to the bromine-capped polymer chains (**Figure 4-12b, c**), with a calculated mass for bromine terminated polymer with DP$_n$ = 25 of 2369.9 Da and an observed mass of 2370.1 Da. A small second distribution observed was attributed to a small degree of fragmentation during the MALDI-ToF-MS process. Since this suggested that the active end-groups were preserved, thioglycerol was used for the thio-bromine substitution of the well-

Table 4-4. ^{1}H NMR and SEC analysis for pMA_{200} passed through the tubing reactor at different timeframes and obtained through photoinduced Cu-RDRP in continuous flow without deoxygenation.[a]

Time after first elution	Mon. Conv.[b] (%)	$M_{n,th.}$ (g mol^{-1})	$M_{n,SEC}$[c]	Đ
5 min	84	14,700	15,700	1.18
10 min	84	14,700	15,500	1.19
30 min	85	14,800	15,600	1.18
45 min	85	14,800	15,500	1.17
1 h	85	14,800	15,500	1.19
2 h	85	14,800	15,400	1.15
3 h	85	14,800	15,500	1.18

[a] In all polymerizations, the volume ratio of monomer to solvent was maintained 1 : 1 and [EBiB] : [Cu(II)Br_2] : [Me_6Tren] = [1] : [0.16] : [0.96].
[b] Conversion was calculated *via* ^{1}H NMR in $CDCl_3$.
[c] Determined by THF SEC analysis and expressed as molecular weight equivalents to pMMA narrow molecular weight standards.

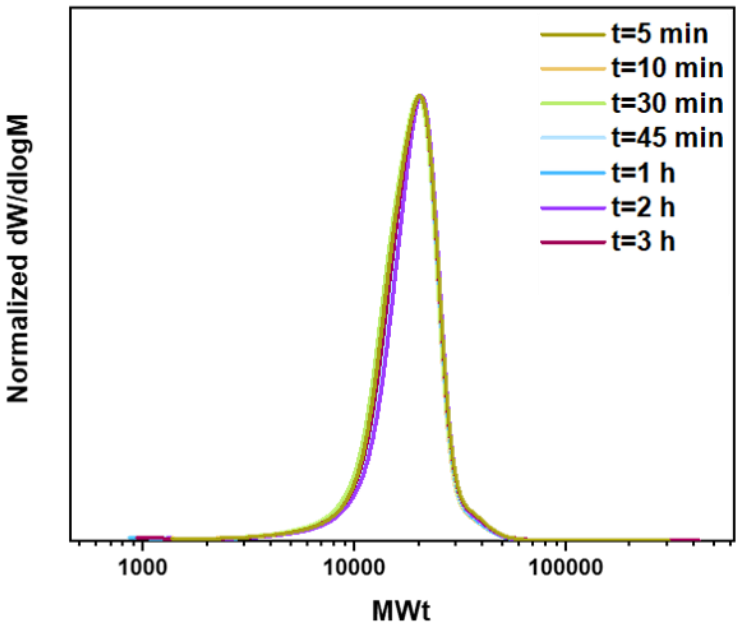

Figure 4-11. THF- SEC derived molecular weight distributions for pMA_{200} passed through the tubing reactor at different times. Conditions : [MA] : [I] : [Cu(II)Br_2] : [Me_6Tren] = [200] : [1] : [0.16] : [0.96].

defined pMA_{25} so as to introduce a different functionality for the non-deoxygenated polymer (**Figure 4-12a**). Thus, 1 mol equivalent of pure pMA_{25} was dissolved in methyl ethyl ketone and 1.5 equivalents of 1-thioglycerol in the presence of triethylamine (1.5 eq.) were added and left under stirring for 2 hours. After the thio-bromine substitution, MALDI-ToF-MS showed full shift of the -Br terminated chains and revealed the thioglycerol-functionalized pMA_{25} (**Figure 4-12 c & d and Figure 4-13**), with a calculated mass of 2397.0 Da and an observed mass of 2397.3 Da. The

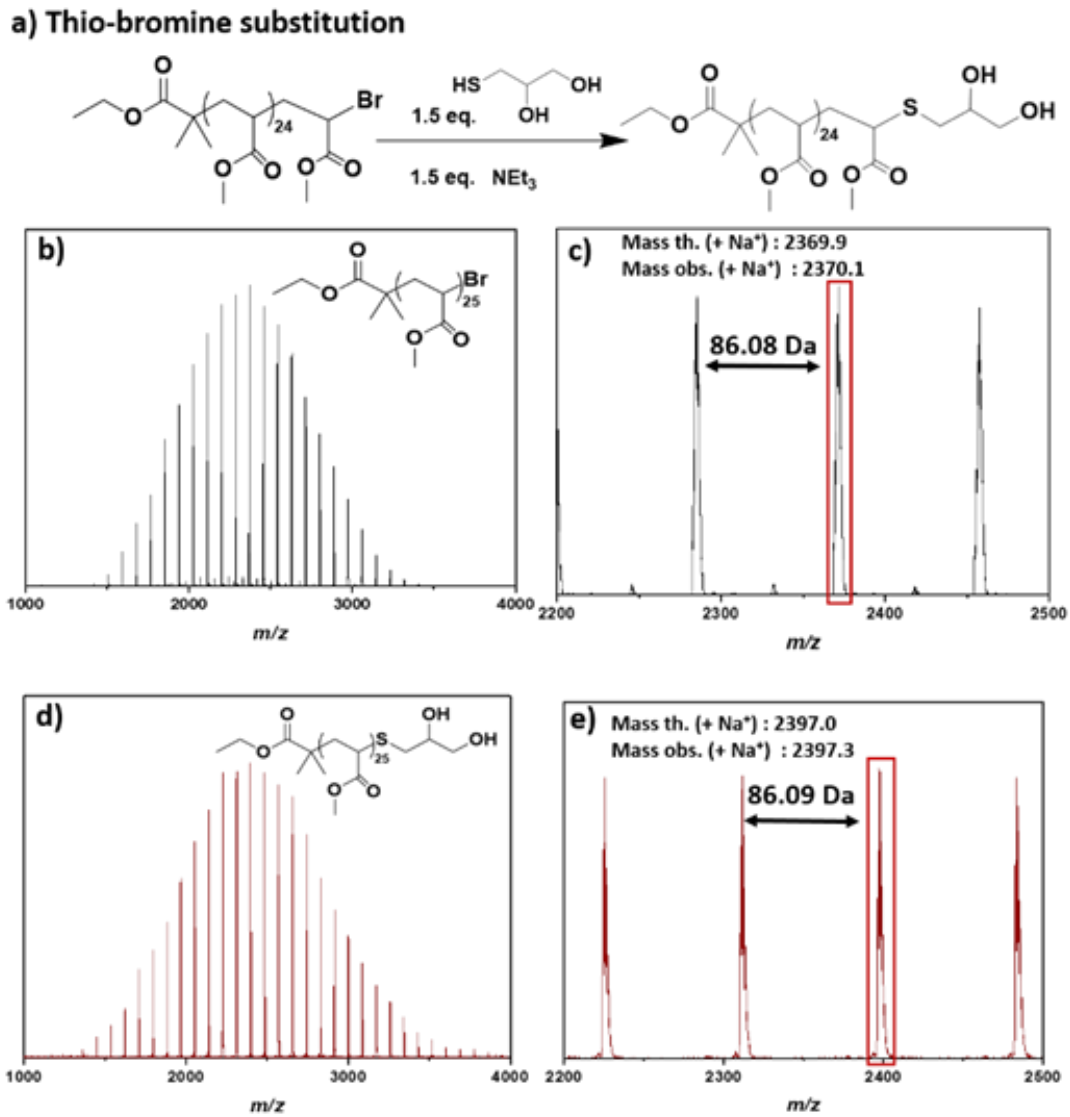

Figure 4-12. **a)** Reaction scheme for the thio-bromine substitution of pMA_{25} with thioglycerol and MALDI-ToF spectra for **b), c)** -Br substituted pMA_{25} and **d), e)** -thioglycerol substituted pMA_{25}

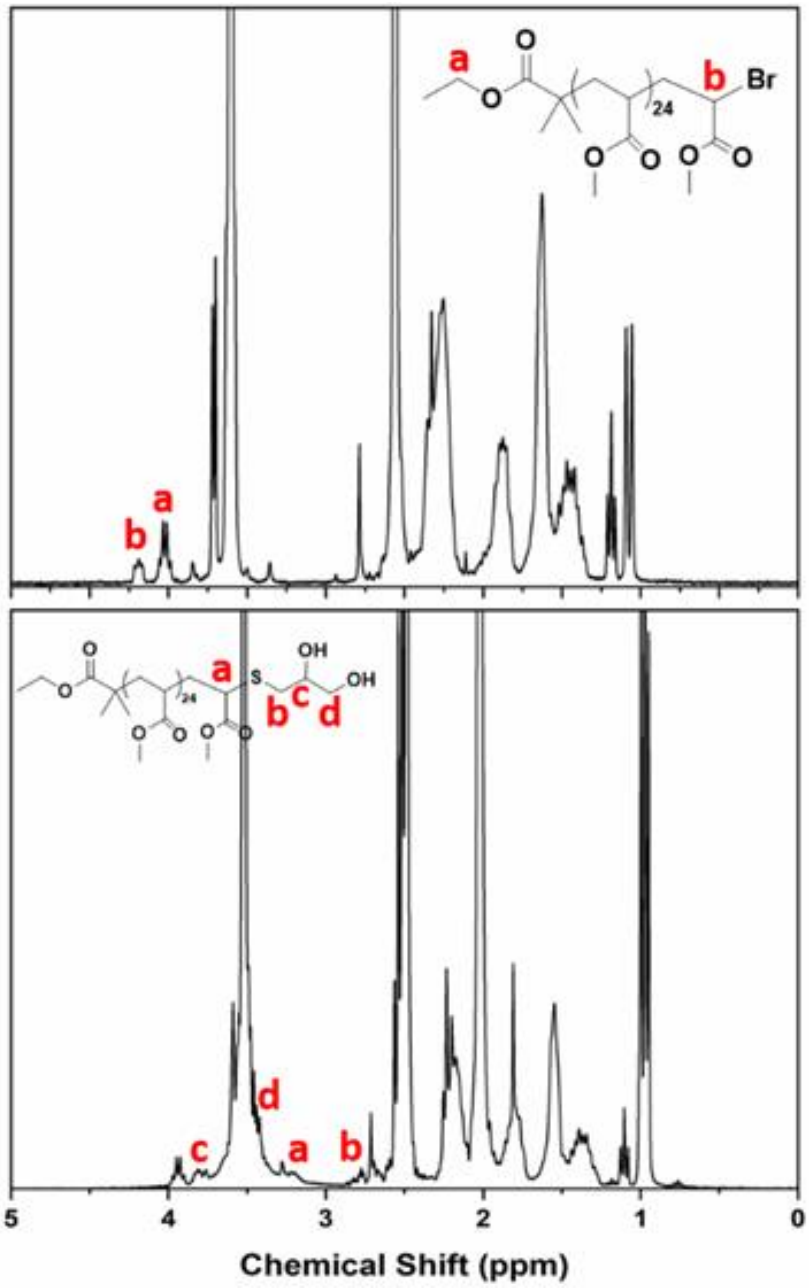

Figure 4-13. ^{1}H NMR spectra of the –Br terminated pMA_{25} (top) and thioglycerol terminated pMA_{25} (bottom).

single peak distribution observed for the substituted pMA, corroborated our hypothesis that the small distribution observed in the –Br capped sample corresponded to the MALDI-ToF-MS process.

In order to examine the ability to produce different molar masses, various DPs of pMA (25-400) were targeted with [Cu(II)Br_2] : [Me_6Tren] = [0.16] : [0.96]. Since the production of different molar masses requires different polymerization times,

different flow rates (residence times) were applied for this purpose (**Table 4-5**). As a result, molecular weights from 2,300 to 26,400 g mol^{-1} were achieved **(Figure 4-14)**.

Table 4-5. ^{1}H NMR, SEC analysis and flow rates for the pMA with different DPs obtained through photoinduced Cu-RDRP in continuous flow without deoxygenation.[a]

DP	Flow rate (µL/min)	Residence time	Mon. Conv.[b] (%)	$M_{n,th.}$ (g mol^{-1})	$M_{n,GPC}$[c]	Đ
25	6	3 h 15 min	99	2,300	2,300	1.12
50	6	3 h 15 min	97	4,400	4,300	1.12
200	6	3 h 15 min	85	14,800	14,300	1.15
400	3	6 h 30 min	72	25,000	26,400	1.28

[a] In all polymerizations, the volume ratio of monomer to solvent was maintained 1 : 1.
[b] Conversion was calculated *via* ^{1}H NMR in *d*-$CHCl_3$.
[c] Determined by THF-SEC analysis and expressed as molecular weight equivalents to pMMA narrow molecular weight standards.

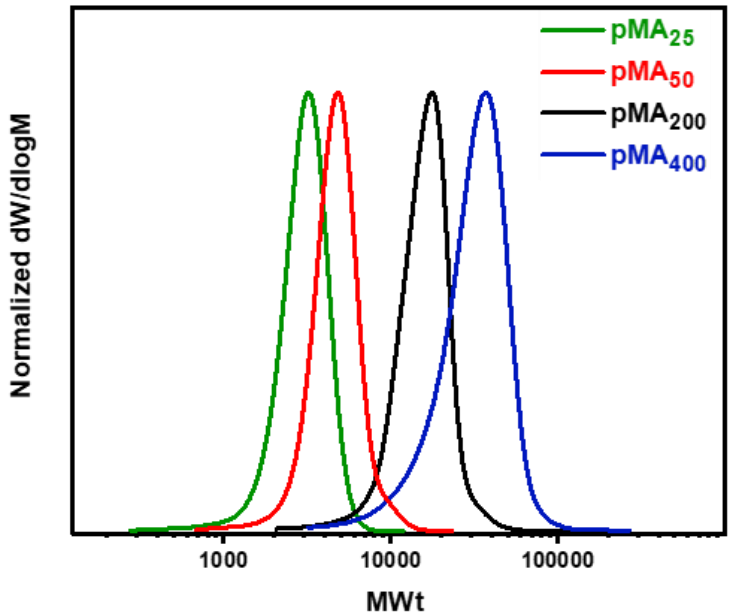

Figure 4-14. THF-SEC derived molecular weight distributions of pMA with targeted DP_n=25-400 synthesized *via* non-deoxygenated photoinduced Cu-RDRP in continuous flow.

As discussed previously and recently reported, all the components of this system contribute to the oxygen consumption. Thus, when higher DPs are targeted the initiator and catalyst concentrations are lower and in combination with the extended exposure to oxygen can affect the initiator efficiency and compromise the monomer conversion. The latter was observed in the case of pMA with targeting DP_n = 400, where the residence time was 6 hours and 40 minutes, leading to monomer conversion of 72% and small deviations between theoretical and experimental M_n values.

Apart from various molar masses, the non-deoxygenated CF polymerization of hydrophobic and hydrophilic monomers was examined with *n*-butyl acrylate (*n*-BA) and poly(ethylene glycol) methyl ether acrylate ($PEGA_{480}$). The polymerizations of *n*-BA and $PEGA_{480}$ with targeted DP_n = 50 and 20 respectively, were attempted using [Cu(II)Br_2] : [Me_6Tren] = [0.02] : [0.12]. With a flow rate of 6 μL/min, the conversion of *n*-BA to p(*n*-BA) was 53% with good agreement between theoretical and experimental M_n values (**Table 4-6, Figure 4-15).** For the polymerization of $PEGA_{480}$ with a flow rate of 4 μL/min the monomer conversion was 87% and the experimental M_n value was twice the theoretical indicating dimerization of the polymer (**Table 4-6, Figure 4-16**). The outcome of these polymerizations is that both hydrophobic and hydrophilic monomers are compatible with this CF system. Thus, the polymerizations were repeated with the *optimum* conditions of [Cu(II)Br_2] : [Me_6Tren] = [0.16] : [0.96]

Table 4-6. ^{1}H NMR, SEC analysis and flow rates for pBA with targeted DP_n = 50 and $pPEGA_{480}$ with targeted DP_n = 20 through photoinduced Cu-RDRP in continuous flow without deoxygenation.[a]

Polymer	Flow rate (μL/min)	Residence time (hours)	Mon. Conv.[b] (%)	$M_{n,th.}$ (g mol^{-1})	$M_{n,GPC}$[c]	Đ
pBA[d]	6	3.25	53	3,600	3,700	1.29
pBA[e]	6	3.25	95	6,300	6,300	1.16
$pPEGA_{480}$[d]	4	6	87	8,500	16,900	1.18
$pPEGA_{480}$[e]	6	3.25	80	7,900	10,100	1.14

[a] In all polymerizations, the volume ratio of monomer to solvent was maintained 1 : 1.
[b] Conversion was calculated *via* ^{1}H NMR in d-$CHCl_3$.
[c] Determined by THF-SEC analysis and expressed as molecular weight equivalents to pMMA narrow molecular weight standards.
[d] [Cu(II)Br_2] : [Me_6Tren] = [0.02] : [0.12]
[e] [Cu(II)Br_2] : [Me_6Tren] = [0.16] : [0.96]

with a flow rate of 6 μL/min for both *n*-BA and $PEGA_{480}$, leading to polymers with good agreement between theoretical and experimental M_n values, low dispersities (*Đ* = 1.14-1.16) and high conversions (**Table 4-6, Figures 4-17 to 4-20)**.

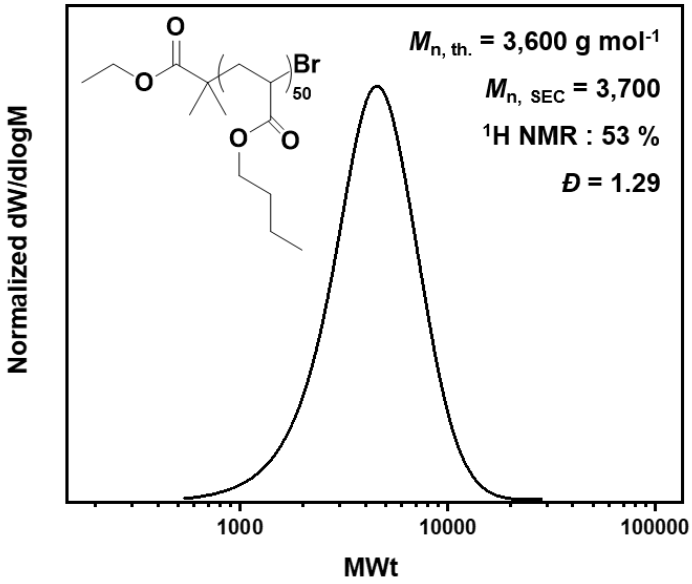

Figure 4-15. THF-SEC derived molecular weight distributions and molecular characteristics of $p(n\text{-BA})_{50}$ synthesized *via* non-deoxygenated photoinduced Cu-RDRP in continuous flow, using $[Cu(II)Br_2]$: $[Me_6Tren]$ = [0.02] : [0.12] with a flow rate of 6 μL/min.

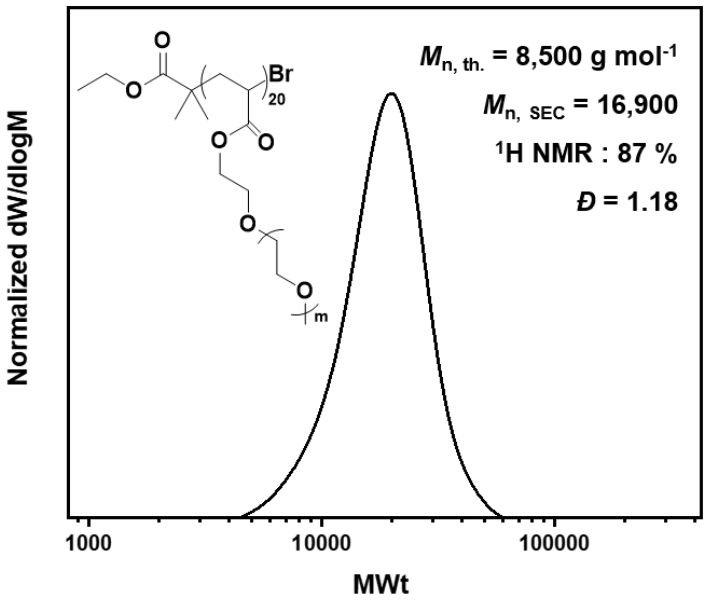

Figure 4-16. THF-SEC derived molecular weight distributions and molecular characteristics of targeted $p(PEGA_{480})_{20}$ synthesized *via* non-deoxygenated

photoinduced Cu-RDRP in continuous flow, using [Cu(II)Br_2] : [Me_6Tren] = [0.02] : [0.12] with a flow rate of 4 μL/min.

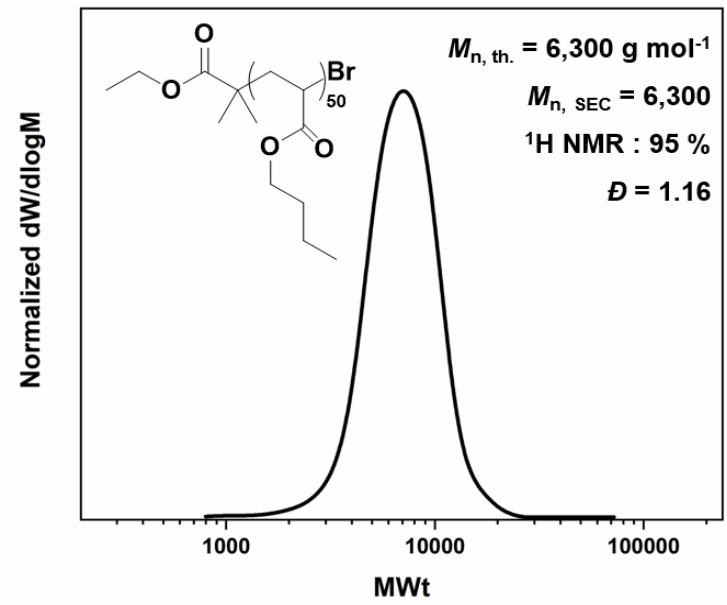

Figure 4-17. THF-SEC derived molecular weight distributions and molecular characteristics of p(*n*-BA)$_{50}$ synthesized *via* non-deoxygenated photoinduced Cu-RDRP in continuous flow, using the *optimum* conditions of [Cu(II)Br_2] : [Me_6Tren] = [0.16] : [0.96] with a flow rate of 6 μL/min.

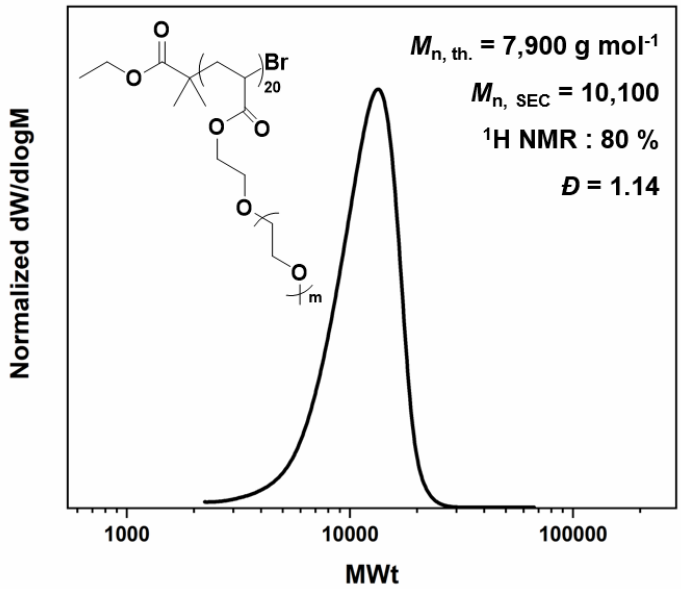

Figure 4-18. THF-SEC derived molecular weight distributions and molecular characteristics of targeted p(PEGA$_{480}$)$_{20}$ synthesized *via* non-deoxygenated photoinduced Cu-RDRP in continuous flow, using the *optimum* conditions of [Cu(II)Br_2] : [Me_6Tren] = [0.16] : [0.96] with a flow rate of 6 μL/min.

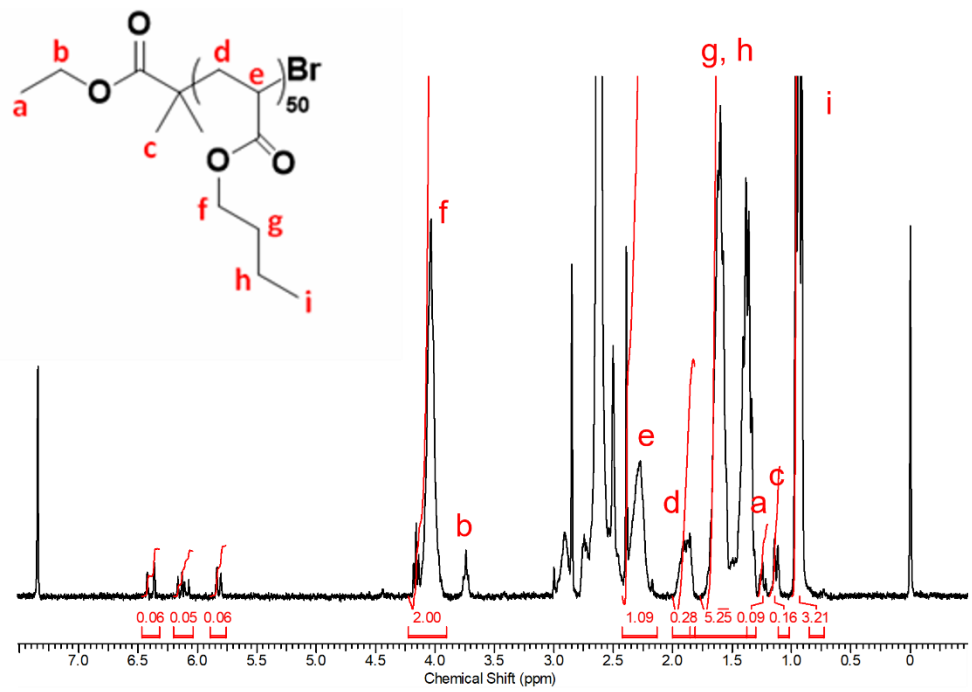

Figure 4-19. ^{1}H NMR of p(*n*-BA)$_{50}$ synthesized *via* photoinduced Cu-RDRP in continuous flow without deoxygenation, using the *optimum* conditions of [Cu(II)Br$_2$] : [Me$_6$Tren] = [0.16] : [0.96] with a flow rate of 6 µL/min. Conversion (95%) was determined by comparing the integrals of monomeric vinyl protons (~5.7-6.5 ppm) to polymer signal (~4-4.3 ppm).

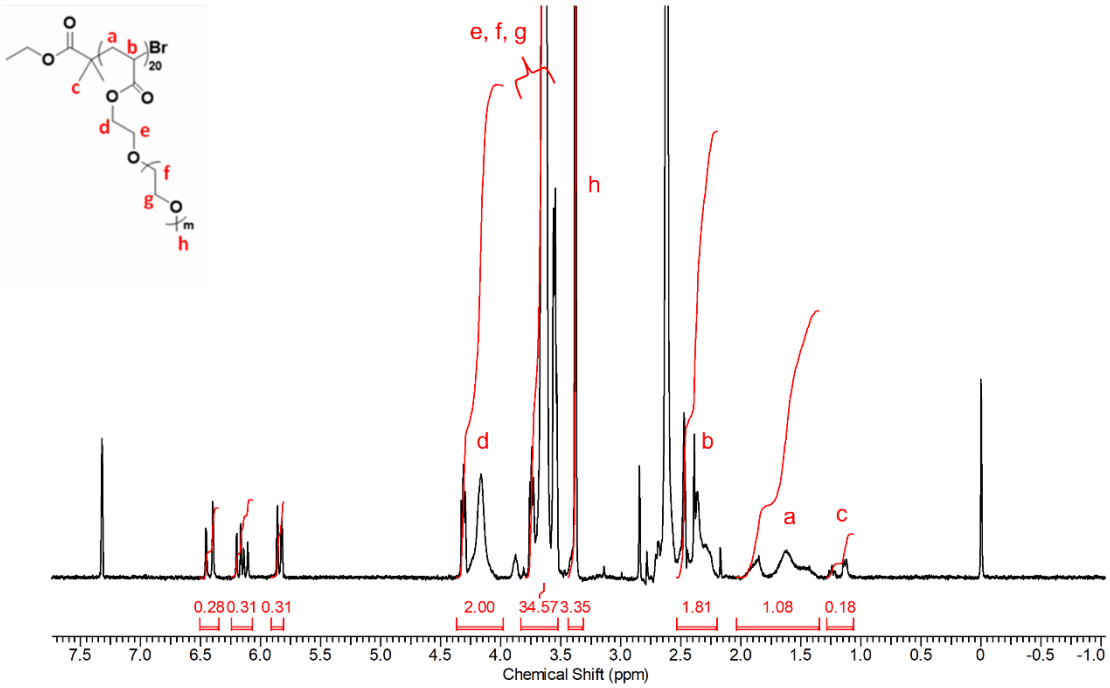

Figure 4-20. ^{1}H NMR of targeted p(PEGA$_{480}$)$_{20}$ synthesized *via* photoinduced Cu-RDRP in continuous flow without deoxygenation, using the *optimum* conditions of [Cu(II)Br$_2$] : [Me$_6$Tren] = [0.16] : [0.96] with a flow rate of 6 µL/min. Conversion

(80%) was determined by comparing the integrals of monomeric vinyl protons (~5.7-6.5 ppm) to polymer signal (~4-4.3 ppm).

In addition to the synthesis of linear polymers, we were interested in different architectures, since their properties have gained a lot of academic and industrial interest.[57, 58] For this purpose, an 8-arm initiator (octa-O-isobutyryl bromide lactose initiator) was used for the synthesis of a pMA star homopolymer with targeted DP_n=200. Following [Cu(II)Br_2] : [Me_6Tren] = [0.16] : [0.96] and 6 μL/min flow rate, a well-defined pMA star was obtained (**Scheme 4- 3, Figures 4-21 & 4-22**). It is noted that for the synthesis of star polymers the ratio of [Cu(II)Br_2] : [Me_6Tren] is attributed to the amount required for each active centre of the initiator. In this case, where an 8-arm initiator was used, each active centre requires 1/8 of the total amount of the complex. Thus, each arm of the pMA star homopolymer with targeted DP_n = 200, consists of 25 monomeric units of MA.

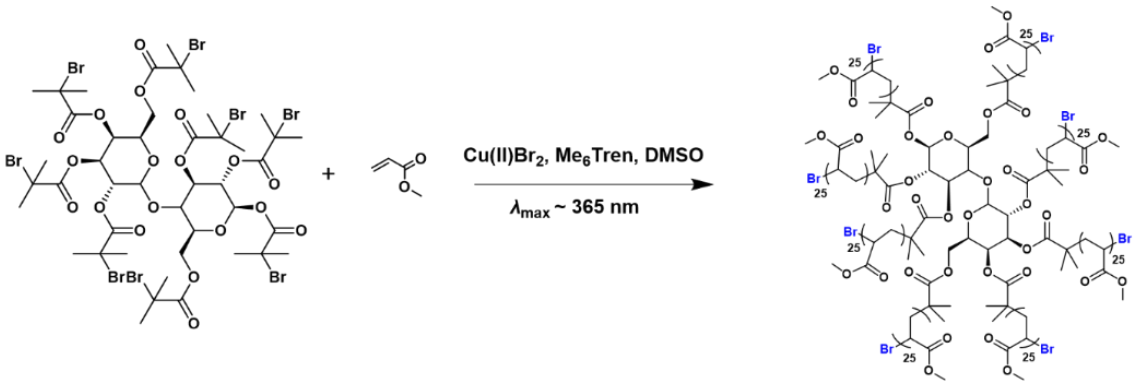

Scheme 4-3. Reaction scheme for the synthesis of 8-arm pMA_{200} star homopolymer through non-deoxygenated photoinduced Cu-RDRP in continuous flow with [Cu(II)Br_2] : [Me_6Tren] = [0.16] : [0.96] and 6 μL/min flow rate.

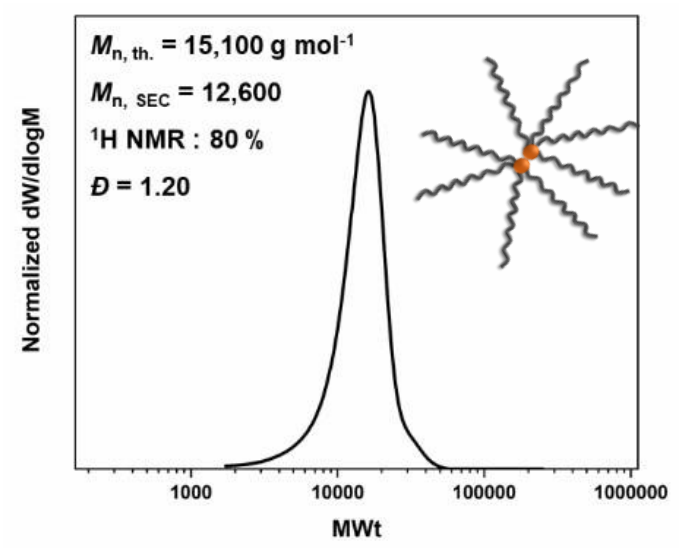

Figure 4-21. THF-SEC derived molecular weight distributions and molecular characteristics of the 8-arm pMA_{200} star polymer synthesized *via* non-deoxygenated photoinduced Cu-RDRP in continuous flow with [Cu(II)Br_2] : [Me_6Tren] = [0.16] : [0.96] and 6 µL/min flow rate.

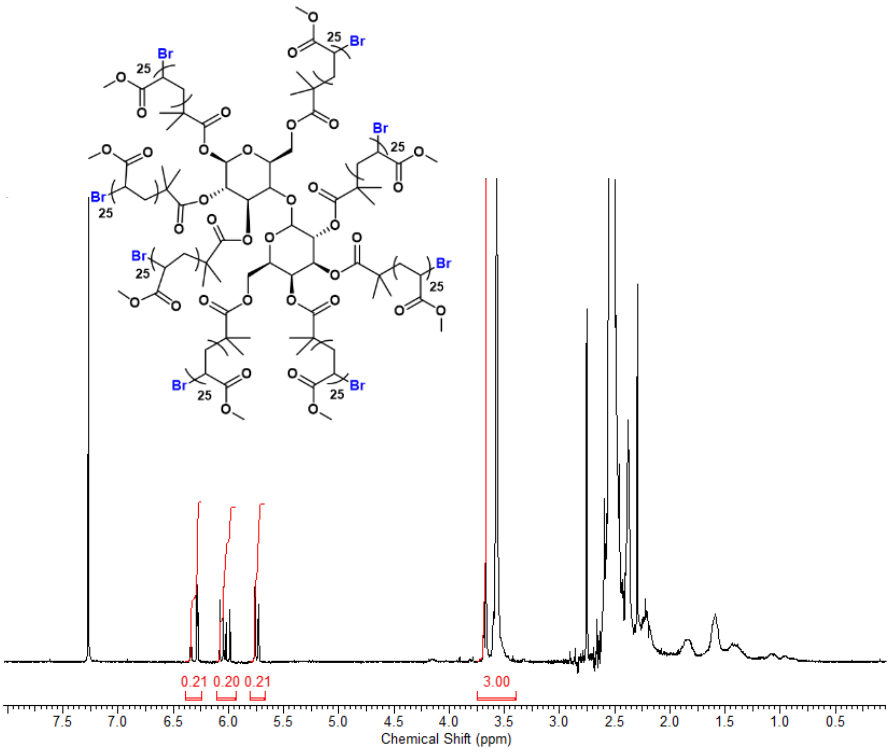

Figure 4-22. ^{1}H NMR and scheme of the 8-arm pMA_{200} star polymer synthesized *via* non-deoxygenated photoinduced Cu-RDRP in continuous flow with [Cu(II)Br_2] : [Me_6Tren] = [0.16] : [0.96] and 6 µL/min flow rate.

4.3 Conclusions

In this chapter, a photo-induced Cu-RDRP of acrylates in continuous flow without the addition of extrinsic oxygen scavengers or reducing agents, is presented and discussed. The photo reduction of copper(II) and subsequent disproportion of copper(I) to copper(0) provide a regenerating process which results in the rapid consumption of oxygen. Low polymer dispersities, control over the molecular weights and high monomer conversions were obtained, after optimization of the copper catalyst loadings and residence times. Without external deoxygenation, good initiator efficiency was evident and high end-group fidelity was maintained, allowing for post polymerization modification. The robustness of the system is further corroborated with the synthesis of sophisticated architectures, as well as hydrophobic and hydrophilic polymers through a user-friendly setup.

4.4 Experimental section

4.4.1 Materials

Methyl acrylate (MA, 99%), n-butyl acrylate (n-BA), poly(ethylene glycol) methyl ether acrylate ($PEGA_{480}$), ethyl α-bromoisobutyrate (EBiB, 98%), copper(II) bromide ($Cu(II)Br_2$, 99%) and dimethyl sulfoxide (DMSO) were purchased from Sigma-Aldrich and used as received unless otherwise stated. Tris-(2-(dimethylamino)ethyl)amine (Me_6Tren) was synthesized according to the literature and stored in the fridge.[59]

4.4.2 Instrumentation and Characterization techniques

Proton Nuclear Magnetic Resonance (^1H NMR)

^1H NMR spectra were recorded on Bruker DPX-300 or DPX-400 spectrometers in deuterated chloroform ($CDCl_3$) or deuterium oxide (D_2O) obtained from Sigma-Aldrich. Chemical shifts are given in ppm downfield from the internal standard tetramethylsilane. Monomer conversions were determined *via* ^1H NMR spectroscopy by comparing the integrals of monomeric vinyl protons to polymer signals.

Size Exclusion Chromatography (SEC)

SEC measurements were carried out using THF as the eluent with an Agilent 390-LC MDS instrument equipped with differential refractive index (DRI), viscometry (VS), dual angle light scatter (LS) and dual wavelength UV detectors. The system was equipped with 2 x PLgel Mixed C columns (300 x 7.5 mm) and a PLgel 5 µm guard column. The eluent was THF with 2% TEA (triethylamine) and 0.01% BHT (butylated hydroxytoluene) additives. Samples were run at 1 mL / min at 30°C. Poly(methyl methacrylate) standards (Agilent EasiVials) were used to create a third order calibration between 550 g mol^{-1} and 1,568,000 g mol^{-1}. Analytical samples were filtered through a GVHP membrane with 0.22 μm pore size before injection. Respectively, experimental molar mass ($M_{n,SEC}$) and dispersity ($Đ$) values of synthesized polymers were determined by conventional calibration using Agilent GPC/SEC software (version A.02.01).

Matrix-assisted laser desorption/ionization time-of-flight

MALDI-ToF-MS measurements were conducted using a Bruker Daltonics Ultraflex II MALDI-ToF mass spectrometer, equipped with a nitrogen laser delivering 2 ns laser pulses at 337 nm with positive ion ToF detection performed using an accelerating voltage of 25 kV. Solutions in tetrahydrofuran (THF) (50 µL) of *trans*-2-[3-(4-*tert*-butylphenyl)-2-methyl-2-propyldene] malononitrile (DCTB) as a matrix (saturated solution), sodium iodide as the cationization agent (1.0 mg mL^{-1}) and sample (1.0 mg mL^{-1}) were mixed, and 0.7 µL of the mixture was applied to the target plate. Spectra were recorded in reflectron mode calibrated with poly(ethylene glycol) monomethyl ether (PEG-Me) 1900 kDa.

Continuous flow reactor setup

All of the tubing, connections, fittings and ferrules were purchased from Thames Restek. The dual syringe infusion pump was purchased from kD Scientific (model LEGATO® 101). The tubing reactors and the connecting tubing were made of PFA (1/16" × 1.0 mm ID). The length of tubing that was used for the reaction was 3 m. For best mixing results a Cheminert mixing tee 1/4"- 28 for 1/16" tubing, 0.75 mm bore, CTFE was used. As light source, a UVP ultraviolet crosslinker from Analytic Jena (model CL-1000) with λ_{max} = 365 nm was used. A septum-sealed glass vial was wrapped with foil, connected with the tubing reactor and used as collection vessel.

4.4.3 Experimental procedures

Typical procedure for the synthesis of pMA_{50} in continuous flow without deoxygenation, using one syringe.

In a vial containing a previously sonicated solution of $Cu(II)Br_2$ (5 mg, 0.02 eq.), Me_6Tren (35.3 µL, 0.12 eq.) and 5 mL DMSO, MA (5 mL, 50 eq.) and EBiB (162 µL, 1 eq.) were added and transferred to a 10 mL syringe. The syringe was wrapped with foil and was connected to the female Luer adaptors of the tubing and adjusted to the pump. The continuous flow polymerization was left to commence in the UVP crosslinker chamber under λ_{max} = 365 nm. The sample was collected in a sealed and foil-wrapped vial, connected with the tubing reactor (similar as **Scheme 4-2** but using one syringe). Conversions were measured using ^1H NMR in $CDCl_3$ and SEC analysis

was conducted in THF after the samples having been passed through neutral alumina for the removal of copper salts.

The same procedure was followed for the synthesis of pMA with targeted DP_n = 25, 100 and 200. The flow rate was adjusted according to the desired residence time.

Calculation of the amounts of the reagents

For 5 mL (monomer) scale reaction with [EBiB] : [Me_6Tren] : [Cu(II)Br_2] = [1] : [0,18] : [0.02].

$DP_n = [M]_0 / [I]_0$ (conversion).

Assuming full conversion: Targeted $DP_n = [M]_0 / [I]_0$, where $[M]_0$ is the concentration of the monomer and $[I]_0$ the concentration of the initiator.

m_{MA} (g) = d_{MA} (g mL^{-1}) V_{MA} (mL), n_{MA} (mol) = m_{MA} (g) / Mr_{MA} (g mol^{-1})

n_{EBiB} (mol) = n_{MA} (mol) / DP_n, m_{EBiB} (g) = n_{EBiB} (mol) Mr_{EBiB} (g mol^{-1}),

V_{EBiB} (mL) = m_{EBiB} (g) / d_{EBiB} (g mL^{-1})

$n_{Cu(II)Br2}$ (mol) = n_{EBiB} (mol) 0.02, $m_{Cu(II)Br2}$ (g) = $n_{Cu(II)Br2}$ (mol) $Mr_{Cu(II)Br2}$ (g mol^{-1})

$n_{Me6Tren}$ = n_{EBiB} (mol) 0.18, $m_{Me6Tren}$ (g)= $n_{Me6Tren}$ (mol) $Mr_{Me6Tren}$ (g mol^{-1}),

$V_{Me6Tren}$ (mL) = $m_{Me6Tren}$ (g) / $d_{Me6Tren}$ (g mL^{-1})

Typical procedure for the synthesis of pMA_{200} in continuous flow without deoxygenation, using two syringes.

A 5 mL plastic syringe was charged with a previously sonicated solution of Cu(II)Br_2 (10 mg, 0.16 eq.), Me_6Tren (70 µL, 0.96 eq.) and 5 mL DMSO and a second 5 mL plastic syringe was charged with MA (5 mL, 200 eq.) and EBiB (40 µL, 1 eq.). The two syringes were wrapped with foil and were connected to the female Luer adaptors of the tubing and adjusted to the pump. The continuous flow polymerization was left to commence in the UVP crosslinker chamber under λ_{max} = 365 nm. The sample was collected in a sealed and foil-wrapped vial, connected with the tubing reactor (**Scheme 4-2**). Conversions were measured using ^{1}H NMR in $CDCl_3$ and SEC analysis was

conducted in THF after the samples having been passed through neutral alumina for the removal of copper salts.

The same procedure was followed for the synthesis of pMA with targeted DP_n = 25, 50 and 400. The flow rate was adjusted according to the desired residence time.

Thio-bromine substitution for the functionalization of pMA_{25}.

In a vial containing stirring bar, purified pMA_{25} (1 g, 0.43mmol, 1 mol eq.) was dissolved in methyl ethyl ketone and 1-thio glycerol (55 µL, 0.63 mmol, 1.5 eq.) and triethylamine (89 µL, 0.63 mmol, 1.5 eq.) were added. The mixture left under stirring for 2 hours. Aliquots were taken for ^{1}H NMR and mass spectroscopy analysis.

Typical procedure for the synthesis of $p(n\text{-}BA)_{50}$ in continuous flow without deoxygenation.

A 5 mL plastic syringe was charged with a previously sonicated solution of $Cu(II)Br_2$ (25 mg, 0.16 eq.), Me_6Tren (179 µL, 0.96 eq.) and 5 mL DMSO and a second 5 mL plastic syringe was charged with *n*-BA (5 mL, 50 eq.) and EBiB (102 µL, 1 eq.). The two syringes were wrapped with foil and were connected to the female Luer adaptors of the tubing and adjusted to the pump. The continuous flow polymerization was left to commence in the UVP crosslinker chamber under λ_{max} = 365 nm. The sample was collected in a sealed and foil-wrapped vial, connected with the tubing reactor. Conversions were measured using ^{1}H NMR in $CDCl_3$ and SEC analysis was conducted in THF after the samples having been passed through neutral alumina for the removal of copper salts.

Typical procedure for the synthesis of $p(PEGA_{480})_{20}$ in continuous flow without deoxygenation.

A 5 mL plastic syringe was charged with a previously sonicated solution of $Cu(II)Br_2$ (20 mg, 0.16 eq.), Me_6Tren (146 µL, 0.96 eq.) and 5 mL DMSO and a second 5 mL plastic syringe was charged with $PEGA_{480}$ (5 mL, 50 eq.) and EBiB (83 µL, 1 eq.). The two syringes were wrapped with foil and were connected to the female Luer adaptors of the tubing and adjusted to the pump. The continuous flow polymerization was left to commence in the UVP crosslinker chamber under λ_{max} = 365 nm. The

sample was collected in a sealed and foil-wrapped vial, connected with the tubing reactor. Conversions were measured using ^{1}H NMR in $CDCl_3$ and SEC analysis was conducted in THF after the samples having been passed through neutral alumina for the removal of copper salts.

Typical procedure for the synthesis of 8-arm star pMA homopolymer in continuous flow without deoxygenation.

A 5 mL plastic syringe was charged with a previously sonicated solution of Cu(II)Br_2 (2 mg, 0.16 eq.), Me_6Tren (14 μL, 0.96 eq.) and 5 mL DMSO and a second 5 mL plastic syringe was charged with 4 mL DMSO, MA (1 mL, 200 eq.) and 8-arm initiator (83.6 mg, 1 eq.). The two syringes were wrapped with foil and were connected to the female Luer adaptors of the tubing and adjusted to the pump. The continuous flow polymerization was left to commence in the UVP crosslinker chamber under λ_{max} = 365 nm. The sample was collected in a sealed and foil-wrapped vial, connected with the tubing reactor. Conversions were measured using ^{1}H NMR in $CDCl_3$ and SEC analysis was conducted in THF after the samples having been passed through neutral alumina for the removal of copper salts.

Purification of pMA homopolymers.

Following the completion of the reaction pMA homopolymer was precipitated in cold H_2O/methanol mixture with volume ratio of 1:4 under stirring. Removal of the solvent mixture was followed by the dissolution of the polymer in THF and addition of $MgSO_4$. Subsequently, THF was removed under reduced pressure using a rotary evaporator and the polymer was dried in a vacuum oven at 40 ^oC for 2 days.

Purification of p(n-BA)$_{50}$ homopolymer.

The polymerization of n-BA in DMSO resulted in a biphasic system with a polymer rich bottom phase and solvent rich (and residual monomer) top phase. The solvent phase was removed and the polymer was dissolved in minimal amount of THF. After dissolution the polymer was precipitated in water methanol mixture and the process was continued as described for the pMA homopolymers.

Purification of p(PEGA$_{480}$)$_{20}$ homopolymer.

The purification of p(PEGA$_{480}$)$_{20}$ was achieved through dialysis against water for 5 days and the polymer was obtained after freeze drying for 2 days.

4.5 References

1. Kato, M.; Kamigaito, M.; Sawamoto, M.; Higashimura, T., Polymerization of Methyl Methacrylate with the Carbon Tetrachloride/Dichlorotris-(Triphenylphosphine)Ruthenium(II)/Methylaluminum Bis(2,6-Di-Tert-Butylphenoxide) Initiating System: Possibility of Living Radical Polymerization. *Macromolecules* **1995,** *28* (5), 1721-1723.

2. Wang, J.-S.; Matyjaszewski, K., Controlled/"Living" Radical Polymerization. Atom Transfer Radical Polymerization in the Presence of Transition-Metal Complexes. *J. Am. Chem. Soc.* **1995,** *117* (20), 5614-5615.

3. Ribelli, T. G.; Lorandi, F.; Fantin, M.; Matyjaszewski, K., Atom Transfer Radical Polymerization: Billion Times More Active Catalysts and New Initiation Systems. *Macromol. Rapid Commun.* **2019,** *40* (1), 1800616.

4. Rosen, B. M.; Percec, V., Single-Electron Transfer and Single-Electron Transfer Degenerative Chain Transfer Living Radical Polymerization. *Chem. Rev.* **2009,** *109* (11), 5069-5119.

5. Percec, V.; Guliashvili, T.; Ladislaw, J. S.; Wistrand, A.; Stjerndahl, A.; Sienkowska, M. J.; Monteiro, M. J.; Sahoo, S., Ultrafast Synthesis of Ultrahigh Molar Mass Polymers by Metal-Catalyzed Living Radical Polymerization of Acrylates, Methacrylates, and Vinyl Chloride Mediated by Set at 25 °C. *J. Am. Chem. Soc.* **2006,** *128* (43), 14156-14165.

6. Chiefari, J.; Chong, Y. K.; Ercole, F.; Krstina, J.; Jeffery, J.; Le, T. P. T.; Mayadunne, R. T. A.; Meijs, G. F.; Moad, C. L.; Moad, G.; Rizzardo, E.; Thang, S. H., Living Free-Radical Polymerization by Reversible Addition−Fragmentation Chain Transfer: The RAFT Process. *Macromolecules* **1998,** *31* (16), 5559-5562.

7. Barner, L.; Davis, T. P.; Stenzel, M. H.; Barner-Kowollik, C., Complex Macromolecular Architectures by Reversible Addition Fragmentation Chain Transfer Chemistry: Theory and Practice. *Macromolecular Rapid Communications* **2007,** *28* (5), 539-559.

8. Perrier, S., 50th Anniversary Perspective: RAFT Polymerization—a User Guide. *Macromolecules* **2017,** *50* (19), 7433-7447.

9. Ng, G.; Yeow, J.; Chapman, R.; Isahak, N.; Wolvetang, E.; Cooper-White, J. J.; Boyer, C., Pushing the Limits of High Throughput PET-RAFT Polymerization. *Macromolecules* **2018,** *51* (19), 7600-7607.

10. Hawker, C. J.; Bosman, A. W.; Harth, E., New Polymer Synthesis by Nitroxide Mediated Living Radical Polymerizations. *Chem. Rev.* **2001,** *101* (12), 3661-3688.

11. Jones, G. R.; Whitfield, R.; Anastasaki, A.; Risangud, N.; Simula, A.; Keddie, D. J.; Haddleton, D. M., Cu(0)-RDRP of Methacrylates in DMSO: Importance of the Initiator. *Polymer Chemistry* **2018,** *9* (18), 2382-2388.

12. Whitfield, R.; Anastasaki, A.; Jones, G. R.; Haddleton, D. M., Cu(0)-RDRP of Styrene: Balancing Initiator Efficiency and Dispersity. *Polymer Chemistry* **2018,** *9* (34), 4395-4403.

13. Pan, X.; Tasdelen, M. A.; Laun, J.; Junkers, T.; Yagci, Y.; Matyjaszewski, K., Photomediated Controlled Radical Polymerization. *Progress in Polymer Science* **2016,** *62*, 73-125.

14. Chen, M.; Zhong, M.; Johnson, J. A., Light-Controlled Radical Polymerization: Mechanisms, Methods, and Applications. *Chem. Rev.* **2016,** *116* (17), 10167-10211.

15. Anastasaki, A.; Nikolaou, V.; Zhang, Q.; Burns, J.; Samanta, S. R.; Waldron, C.; Haddleton, A. J.; McHale, R.; Fox, D.; Percec, V.; Wilson, P.; Haddleton, D. M., Copper(II)/Tertiary Amine Synergy in Photoinduced Living Radical Polymerization: Accelerated Synthesis of *ω*-Functional and *α,ω*-Heterofunctional Poly(Acrylates). *J. Am. Chem. Soc.* **2014,** *136* (3), 1141-1149.

16. Yagci, Y.; Jockusch, S.; Turro, N. J., Photoinitiated Polymerization: Advances, Challenges, and Opportunities. *Macromolecules* **2010,** *43* (15), 6245-6260.

17. Fors, B. P.; Hawker, C. J., Control of a Living Radical Polymerization of Methacrylates by Light. *Angew. Chem. Int. Ed.* **2012,** *51* (35), 8850-8853.

18. Yeow, J.; Chapman, R.; Gormley, A. J.; Boyer, C., Up in the Air: Oxygen Tolerance in Controlled/Living Radical Polymerisation. *Chem. Soc. Rev.* **2018,** *47* (12), 4357-4387.

19. Bhanu, V. A.; Kishore, K., Role of Oxygen in Polymerization Reactions. *Chem. Rev.* **1991,** *91* (2), 99-117.

20. Ligon, S. C.; Husár, B.; Wutzel, H.; Holman, R.; Liska, R., Strategies to Reduce Oxygen Inhibition in Photoinduced Polymerization. *Chemical Reviews* **2014,** *114* (1), 557-589.

21. Liarou, E.; Whitfield, R.; Anastasaki, A.; Engelis, N. G.; Jones, G. R.; Velonia, K.; Haddleton, D. M., Copper-Mediated Polymerization without External Deoxygenation or Oxygen Scavengers. *Angew. Chem. Int. Ed.* **2018,** *57* (29), 8998-9002.

22. Liarou, E.; Anastasaki, A.; Whitfield, R.; Iacono, C. E.; Patias, G.; Engelis, N. G.; Marathianos, A.; Jones, G. R.; Haddleton, D. M., Ultra-Low Volume Oxygen Tolerant Photoinduced Cu-RDRP. *Polym. Chem.* **2019,** *10* (8), 963-971.

23. Wang, Y.; Fu, L.; Matyjaszewski, K., Enzyme-Deoxygenated Low Parts Per Million Atom Transfer Radical Polymerization in Miniemulsion and Ab Initio Emulsion. *ACS Macro Lett.* **2018,** *7* (11), 1317-1321.

24. Enciso, A. E.; Fu, L.; Lathwal, S.; Olszewski, M.; Wang, Z.; Das, S. R.; Russell, A. J.; Matyjaszewski, K., Biocatalytic "Oxygen-Fueled" Atom Transfer Radical Polymerization. *Angew. Chem. Int. Ed.* **2018,** *57* (49), 16157-16161.

25. Yang, Q.; Lalevée, J.; Poly, J., Development of a Robust Photocatalyzed ATRP Mechanism Exhibiting Good Tolerance to Oxygen and Inhibitors. *Macromolecules* **2016,** *49* (20), 7653-7666.

26. Fleischmann, S.; Rosen, B. M.; Percec, V., SET-LRP of Acrylates in Air. *Journal of Polymer Science Part A: Polymer Chemistry* **2010,** *48* (5), 1190-1196.

27. Liarou, E.; Han, Y.; Sanchez, A. M.; Walker, M.; Haddleton, D. M., Rapidly Self-Deoxygenating Controlled Radical Polymerization in Water Via in Situ Disproportionation of Cu(I). *Chem. Sci.* **2020,** *11* (20), 5257-5266.

28. Chapman, R.; Gormley, A. J.; Stenzel, M. H.; Stevens, M. M., Combinatorial Low-Volume Synthesis of Well-Defined Polymers by Enzyme Degassing. *Angewandte Chemie International Edition* **2016,** *55* (14), 4500-4503.

29. Chapman, R.; Gormley, A. J.; Herpoldt, K.-L.; Stevens, M. M., Highly Controlled Open Vessel RAFT Polymerizations by Enzyme Degassing. *Macromolecules* **2014,** *47* (24), 8541-8547.

30. Tanaka, J.; Gurnani, P.; Cook, A. B.; Häkkinen, S.; Zhang, J.; Yang, J.; Kerr, A.; Haddleton, D. M.; Perrier, S.; Wilson, P., Microscale Synthesis of Multiblock Copolymers Using Ultrafast RAFT Polymerisation. *Polymer Chemistry* **2019,** *10* (10), 1186-1191.

31. Ng, G.; Yeow, J.; Xu, J.; Boyer, C., Application of Oxygen Tolerant PET-RAFT to Polymerization-Induced Self-Assembly. *Polymer Chemistry* **2017,** *8* (18), 2841-2851.

32. Yeow, J.; Chapman, R.; Xu, J.; Boyer, C., Oxygen Tolerant Photopolymerization for Ultralow Volumes. *Polymer Chemistry* **2017,** *8* (34), 5012-5022.

33. Xu, J.; Jung, K.; Atme, A.; Shanmugam, S.; Boyer, C., A Robust and Versatile Photoinduced Living Polymerization of Conjugated and Unconjugated Monomers and Its Oxygen Tolerance. *Journal of the American Chemical Society* **2014,** *136* (14), 5508-5519.

34. Yeow, J.; Joshi, S.; Chapman, R.; Boyer, C., A Self-Reporting Photocatalyst for Online Fluorescence Monitoring of High Throughput RAFT Polymerization. *Angewandte Chemie International Edition* **2018,** *57* (32), 10102-10106.

35. Corrigan, N.; Rosli, D.; Jones, J. W. J.; Xu, J.; Boyer, C., Oxygen Tolerance in Living Radical Polymerization: Investigation of Mechanism and Implementation in Continuous Flow Polymerization. *Macromolecules* **2016,** *49* (18), 6779-6789.

36. Rubens, M.; Latsrisaeng, P.; Junkers, T., Visible Light-Induced Iniferter Polymerization of Methacrylates Enhanced by Continuous Flow. *Polymer Chemistry* **2017,** *8* (42), 6496-6505.

37. Junkers, T.; Wenn, B., Continuous Photoflow Synthesis of Precision Polymers. *Reaction Chemistry & Engineering* **2016,** *1* (1), 60-64.

38. Buss, B. L.; Miyake, G. M., Photoinduced Controlled Radical Polymerizations Performed in Flow: Methods, Products, and Opportunities. *Chemistry of Materials* **2018,** *30* (12), 3931-3942.

39. Reis, M. H.; Davidson, C. L. G.; Leibfarth, F. A., Continuous-Flow Chemistry for the Determination of Comonomer Reactivity Ratios. *Polymer Chemistry* **2018,** *9* (13), 1728-1734.

40. Diehl, C.; Laurino, P.; Azzouz, N.; Seeberger, P. H., Accelerated Continuous Flow RAFT Polymerization. *Macromolecules* **2010,** *43* (24), 10311-10314.

41. Wiles, C.; Watts, P., Continuous Flow Reactors: A Perspective. *Green Chemistry* **2012,** *14* (1), 38-54.

42. Steinbacher, J. L.; McQuade, D. T., Polymer Chemistry in Flow: New Polymers, Beads, Capsules, and Fibers. *Journal of Polymer Science Part A: Polymer Chemistry* **2006,** *44* (22), 6505-6533.

43. Hornung, C. H.; Guerrero-Sanchez, C.; Brasholz, M.; Saubern, S.; Chiefari, J.; Moad, G.; Rizzardo, E.; Thang, S. H., Controlled RAFT Polymerization in a Continuous Flow Microreactor. *Organic Process Research & Development* **2011,** *15* (3), 593-601.

44. Gardiner, J.; Hornung, C. H.; Tsanaktsidis, J.; Guthrie, D., Continuous Flow Photo-Initiated RAFT Polymerisation Using a Tubular Photochemical Reactor. *European Polymer Journal* **2016,** *80*, 200-207.

45. Burns, J. A.; Houben, C.; Anastasaki, A.; Waldron, C.; Lapkin, A. A.; Haddleton, D. M., Poly(Acrylates) Via SET-LRP in a Continuous Tubular Reactor. *Polymer Chemistry* **2013,** *4* (17), 4809-4813.

46. Ramsey, B. L.; Pearson, R. M.; Beck, L. R.; Miyake, G. M., Photoinduced Organocatalyzed Atom Transfer Radical Polymerization Using Continuous Flow. *Macromolecules* **2017,** *50* (7), 2668-2674.

47. Wenn, B.; Conradi, M.; Carreiras, A. D.; Haddleton, D. M.; Junkers, T., Photo-Induced Copper-Mediated Polymerization of Methyl Acrylate in Continuous Flow Reactors. *Polymer Chemistry* **2014,** *5* (8), 3053-3060.

48. Chen, M.; Johnson, J. A., Improving Photo-Controlled Living Radical Polymerization from Trithiocarbonates through the Use of Continuous-Flow Techniques. *Chemical Communications* **2015,** *51* (31), 6742-6745.

49. Melker, A.; Fors, B. P.; Hawker, C. J.; Poelma, J. E., Continuous Flow Synthesis of Poly(Methyl Methacrylate) Via a Light-Mediated Controlled Radical Polymerization. *Journal of Polymer Science Part A: Polymer Chemistry* **2015,** *53* (23), 2693-2698.

50. Vrijsen, J. H.; Osiro Medeiros, C.; Gruber, J.; Junkers, T., Continuous Flow Synthesis of Core Cross-Linked Star Polymers Via Photo-Induced Copper Mediated Polymerization. *Polymer Chemistry* **2019,** *10* (13), 1591-1598.

51. Peng, J.; Xu, Q.; Ni, Y.; Zhang, L.; Cheng, Z.; Zhu, X., Visible Light Controlled Aqueous RAFT Continuous Flow Polymerization with Oxygen Tolerance. *Polymer Chemistry* **2019**.

52. Frick, E.; Anastasaki, A.; Haddleton, D. M.; Barner-Kowollik, C., Enlightening the Mechanism of Copper Mediated PhotoRDRP Via High-Resolution Mass Spectrometry. *J. Am. Chem. Soc.* **2015,** *137* (21), 6889-6896.

53. Zhang, Q.; Wilson, P.; Li, Z.; McHale, R.; Godfrey, J.; Anastasaki, A.; Waldron, C.; Haddleton, D. M., Aqueous Copper-Mediated Living Polymerization: Exploiting Rapid Disproportionation of CuBr with Me_6Tren. *J. Am. Chem. Soc.* **2013,** *135* (19), 7355-7363.

54. Lligadas, G.; Percec, V., A Comparative Analysis of Set-Lrp of Ma in Solvents Mediating Different Degrees of Disproportionation of Cu(I)Br. *Journal of Polymer Science Part A: Polymer Chemistry* **2008,** *46* (20), 6880-6895.

55. Anastasaki, A.; Willenbacher, J.; Fleischmann, C.; Gutekunst, W. R.; Hawker, C. J., End Group Modification of Poly(Acrylates) Obtained Via ATRP: A User Guide. *Polymer Chemistry* **2017,** *8* (4), 689-697.

56. Town, J. S.; Jones, G. R.; Haddleton, D. M., MALDI-LID-ToF/ToF Analysis of Statistical and Diblock Polyacrylate Copolymers. *Polymer Chemistry* **2018,** *9* (37), 4631-4641.

57. Whitfield, R.; Anastasaki, A.; Truong, N. P.; Wilson, P.; Kempe, K.; Burns, J. A.; Davis, T. P.; Haddleton, D. M., Well-Defined PDMAEA Stars Via Cu(0)-Mediated Reversible Deactivation Radical Polymerization. *Macromolecules* **2016,** *49* (23), 8914-8924.

58. Buss, B. L.; Beck, L. R.; Miyake, G. M., Synthesis of Star Polymers Using Organocatalyzed Atom Transfer Radical Polymerization through a Core-First Approach. *Polymer Chemistry* **2018,** *9* (13), 1658-1665.

59. Ciampolini, M.; Nardi, N., Five-Coordinated High-Spin Complexes of Bivalent Cobalt, Nickel, Andcopper with Tris(2-Dimethylaminoethyl)Amine. *Inorganic Chemistry* **1966,** *5* (1), 41-44.

Chapter 5: *Dihydrolevoglucosenone (Cyrene^{TM}) as a bio-renewable solvent for Cu(0)-mediated reversible deactivation radical polymerization (RDRP) without external deoxygenation*

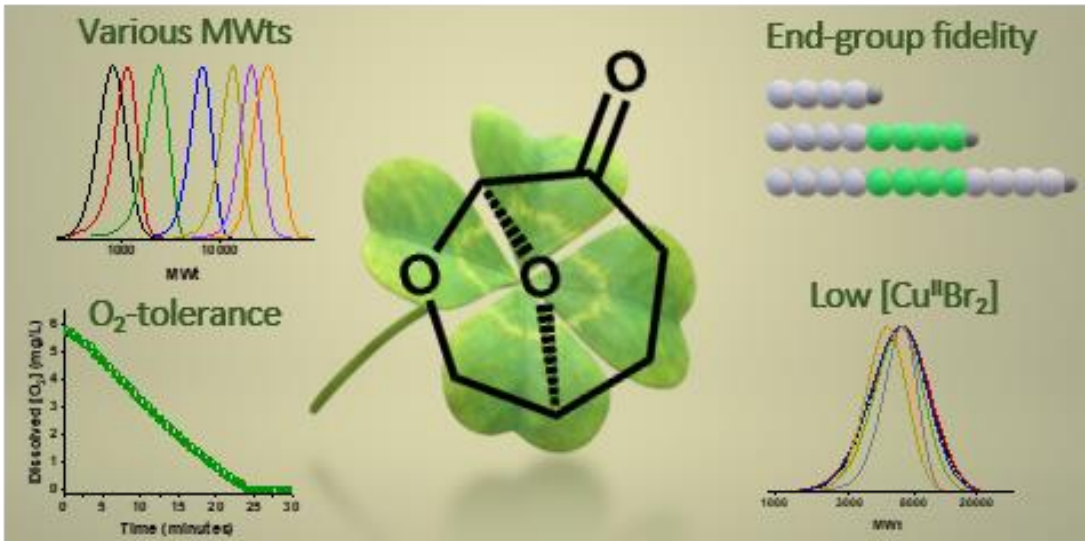

In this chapter, a biorenewable compound, dihydrolevoglucosenone (Cyrene^{TM}) is used as an effective dipolar aprotic solvent for Cu(0) wire-mediated reversible deactivation radical polymerization (Cu(0) wire mediated RDRP) of various monomers without any external deoxygenation being applied. The solvent is used to give products with a broad range of molar masses (M_n ~ 700 – 28,000), *in-situ* chain extension and as low as 7.8 x 10^{-4} eq. of [Cu(II)Br_2] relative to initiator.

5.1 Introduction

Controlled radical polymerization (CRP) has enabled the synthesis of a large number of well-defined materials,[1-6] with well-defined shape, different functionalities and molecular architectures.[7, 8] Amongst them, Cu-mediated reversible deactivation radical polymerization (Cu-RDRP) has evolved into an efficient technique in academia for the polymerization of many functional vinyl monomers, including hydrophilic and hydrophobic (meth)acrylates, styrenics and (meth)acrylamides using a many different dipolar solvents (*e.g.* water, DMSO, DMF, NMP), adding to the versatility of this technique.[9-11] However, many of these solvents have been added to the "*Registration, Evaluation, Authorisation and Restriction of Chemicals*" (REACH) restricted substances list due to their negative environmental effects and are becoming undesirable reagents in many applications. In this context, several solvent selection guides have been published in order to replace many commonly used volatile organic solvents or compounds that could form toxic gases upon incineration (CO_x, NO_x, SO_x), with solvents derived from natural or/and renewable resources.[12-14]

Dihydrolevoglucosenone (Cyrene™) is a bio-based and fully biodegradable (99% in 14 days) aprotic dipolar solvent that can be synthesized in a two-step process from biomass, mainly from cellulose.[15, 16] Cyrene™ is not mutagenic, has a median lethal dose (LD_{50}) > 2000 mg kg^{-1} (above the value of high toxicity solvents, 50 mg kg^{-1}) and it is hardly ecotoxic.[17] Therefore, it has potential as a greener and safer alternative to widely used dipolar aprotic solvents, such as DMF, NMP, DMAc and DMSO which are widely used today.[17-19] Furthermore, Cyrene™ has similar solvating behavior with the abovementioned solvents, demonstrating similar Hansen solubility parameters.[20] A further characteristic of Cyrene™ is that it is completely miscible with water, since it is in equilibrium with its hydrate (a geminal diol), in contrast to most conventional ketones in water.[21] Cyrene™ is currently manufactured on a relatively small scale by Circa Group in Tasmania leading to relatively high prices when compared to DMSO. However, as of 2020 new 1000 and 5000 tonne plants were planned for construction in Europe which should reduce the costs to become within 1.5-2 of DMSO at current pricing.[22]

Recently, Cyrene has attracted significant interest as a bio-degradable solvent in the synthesis of metal–organic frameworks,[17] synthetic transformations,[20] metal catalyzed processes,[23] in the synthesis of ureas[24] and amides.[25, 26] Moreover, upon further hydrogenation, Cyrene could lead to more renewable chemicals that can be used as precursors for drugs, flavors and polymers.[27] In the field of polymer synthesis, the use of Cyrene as solvent has been underexplored to date, with few examples of its use being as a co-solvent in low toxicity solvent systems for polyamideimide and polyamide amic acid resin manufacture,[28] in sustainable membrane preparation[29] and in membrane performance tests of interpenetrating polymer networks.[30] Conversely, in some cases Cyrene has been used as a monomer precursor. In a recent work , Ray *et al.* reported the development of bio-acrylic polymers from a methacrylic monomer synthesized from Cyrene.[31] This monomer was polymerized under different free radical polymerization conditions (bulk, solution and emulsion) and it was found that polymers obtained from emulsion polymerization had higher yields and molecular weights, in contrast with solution polymerization.

In this chapter, the use of Cyrene as a bio-alternative solvent for the polymerization of various monomers using Cu(0) wire-mediated RDRP without applying any external deoxygenation or addition of external additives is described (**Scheme 5-1**). Well-defined polymers with high conversions, narrow molecular weight distributions and high end-group fidelity were obtained, enabling the synthesis of diblock and triblock copolymers. Moreover, a wide range of molar masses from 700 to 28,000 g mol^{-1} (targeted DP_n = 5 - 800) of poly(methyl acrylate) (pMA) were obtained in the absence of deoxygenation and with Cyrene as solvent. The use of a low catalyst concentration was investigated for the Cu(0) wire-RDRP of MA (targeted DP_n = 50), to test the limits of this system. Finally, the oxygen tolerance profile of the polymerization was elucidated by employing an oxygen probe.

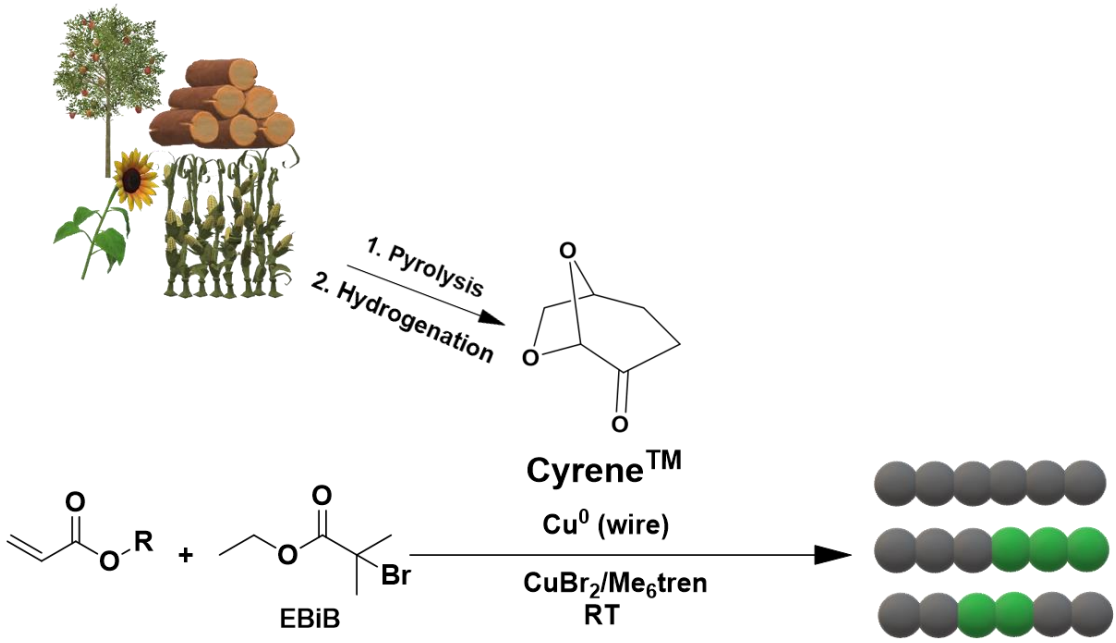

Scheme 5-1. Oxygen tolerant Cu(0) wire-mediated RDRP in Cyrene, a bio-alternative solvent derived from biomass (cellulose) in a two-step process.[15]

5.2 Results and Discussion

The choice of solvent is important for a successful Cu-RDRP process due to the effect on the rate of the polymerization,[32, 33] the solubility of the Cu complexes, monomers and polymers,[34-36] as well as potential of solvent coordination to the copper.[37] Initially, in order to investigate Cyrene as a solvent for Cu(0) wire-mediated RDRP, polymerizations were conducted under an inert nitrogen atmosphere. For this purpose, MA was used as monomer (targeted DP_n = 50), ethyl α-bromoisobutyrate (EBiB) as initiator, 5 cm of Cu(0) wire and $Cu(II)Br_2$ as copper source and the aliphatic multidentate ligand tris(2-(dimethylamino)ethyl)-amine (Me_6Tren) as ligand with Cyrene as solvent (**Table 5-1, Entry 1, Figure 5-1 a & 5-3 a**). Polymerization was carried out at ambient temperature with [EBiB] : [Me_6Tren] : [$Cu(II)Br_2$] = 1 : 0.18 : 0.05 (as previously reported when DMSO was used as solvent[38]), leading to pMA_{50} with high monomer conversion (>95% after 18 hrs), $M_{n,\,NMR}$ = 4,400 g mol^{-1} and $Đ_{SEC}$ = 1.09. These results are comparable with previously reported polymerization of MA in DMSO, where monomer conversion was higher than 99.9% after 18 hrs, M_n = 5,700 and $Đ_{SEC}$ = 1.06.[38] It is noted that, although it has previously been reported that under basic conditions and in the presence of amines, Cyrene can exhibit sensitivity, no evidence of side reactions was observed in this study (**Figure 5-1 b**).[23] This might be attributed to the low concentrations of Me_6Tren (18.7 mM for pMA_{50}), as well as the ambient temperature that the reactions took place. Apart from EBiB, the possibility to use the more hydrophobic dodecyl 2-bromoisobutyrate as an initiator for the polymerization of MA (targeted DP_n = 50) was explored, resulting in pMA_{33} (74% conversion after 24 hrs) with $M_{n,\,SEC}$ = 4,000 g mol^{-1} and $Đ$ = 1.08 (**Table 5-1, Entry 2, Figure 5-3 b**). Apart from MA, the efficiency of Cyrene as solvent for the synthesis of polymethacrylates was explored. In this context, the polymerization of methyl methacrylate (MMA) was conducted under similar conditions with methyl α- bromo phenylacetate as initiator, yielding $pMMA_{50}$ (95% after 18 hrs) with $M_{n,\,SEC}$ = 6,000 g mol^{-1} and $Đ$ = 1.12 (**Table 5-1, Entry 3, Figure 5-2 & 5-3c**). Therefore, based on these initial experiments it was anticipated that Cyrene could be efficiently employed as an alternative, biodegradable solvent for the Cu(0) wire-RDRP of both MA and MMA.

Table 5-1. ^{1}H NMR and SEC analysis for the Cu(0) wire mediated RDRP of MA and MMA using Cyrene as solvent. Inert conditions were applied.

Entry[a]	Monomer /Initiator	Time (h)	Monomer Conv. [b] (%)	$M_{n,\,theor.}$ (g mol^{-1})	$M_{n,\,SEC}$[c]	$Đ$
1	MA/EBiB	18	90	4400	4800	1.08
2	MA/dodecyl-BiB	24	75	4000	5600	1.23
3	MMA/MBPA	18	95	6400	7200	1.11

[a] In all polymerizations, the volume ratio of monomer to solvent was maintained at 1: 1.
[b] Conversion was calculated *via* ^{1}NMR in $CDCl_3$.
[c] Determined by $CHCl_3$ SEC analysis and expressed as molecular weight relative to pMMA narrow molecular weight standards.

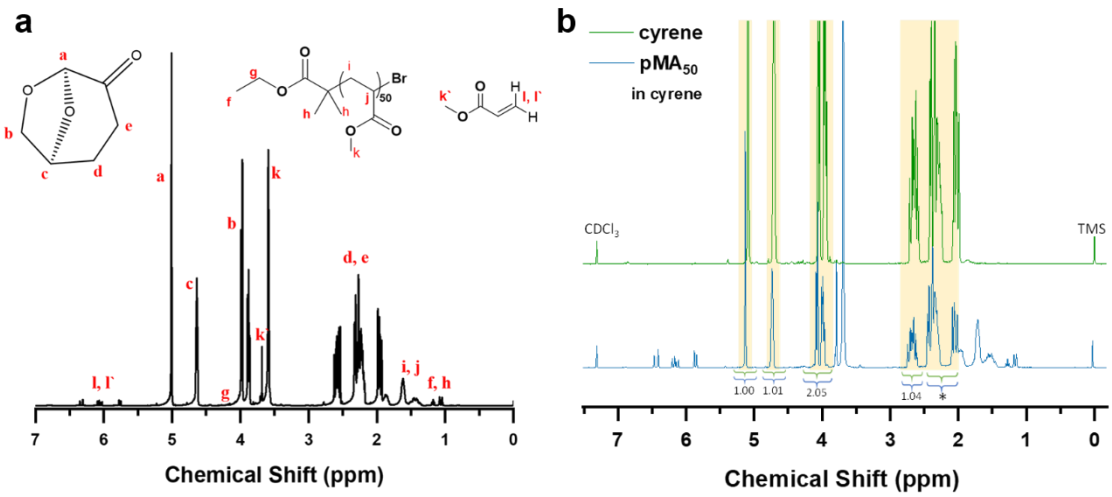

Figure 5-1. a) ^{1}H NMR for Cu(0) wire-mediated RDRP of MA using EBiB as initiator and Cyrene as solvent under N_2. Conditions: [M]: [I]: [Cu(II)Br_2]: [Me_6Tren] = 50: 1: 0.05: 0.18, V_{Cyrene} = 50 % v/v with respect to monomer. Conversion was determined by comparing the integrals of monomeric vinyl protons (l, l`) to polymer signals (k). **b)** ^{1}H NMR spectra of Cyrene and pMA_{50} (in Cyrene) showing no evidence of side reactions or degradation of the solvent.[23] Integration values at: 5.10 ppm (1.00), 4.71 ppm (1.01), ~3.96 – 4.06 ppm (2.05), ~2.63 ppm (1.04), ~2.35 ppm and ~2.03 ppm (* overlaid with polymer peaks).

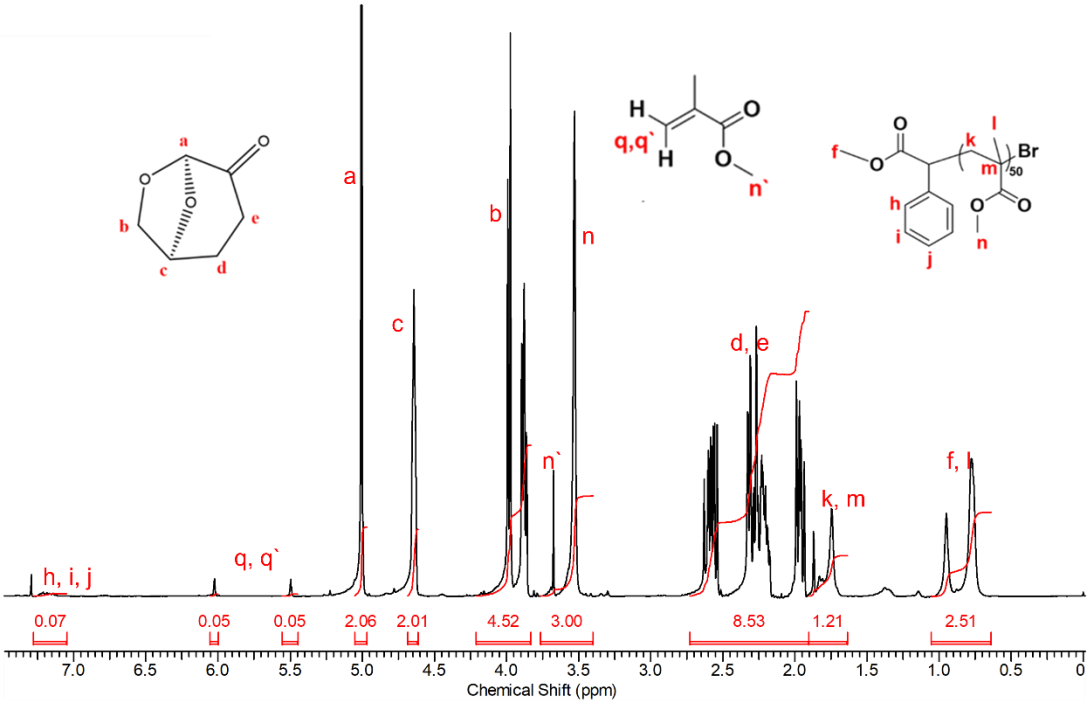

Figure 5-2. ^{1}H NMR for Cu(0) wire mediated RDRP of MMA using MBPA as initiator and Cyrene as solvent under N_2. Conditions: [M]: [I]: [Cu(II)Br_2]: [Me_6Tren] = 50: 1: 0.05: 0.18, V_{Cyrene} = 50 % v/v with respect to monomer. Conversion was determined by comparing the integrals of monomeric vinyl protons (q, q`) to polymer signals (n).

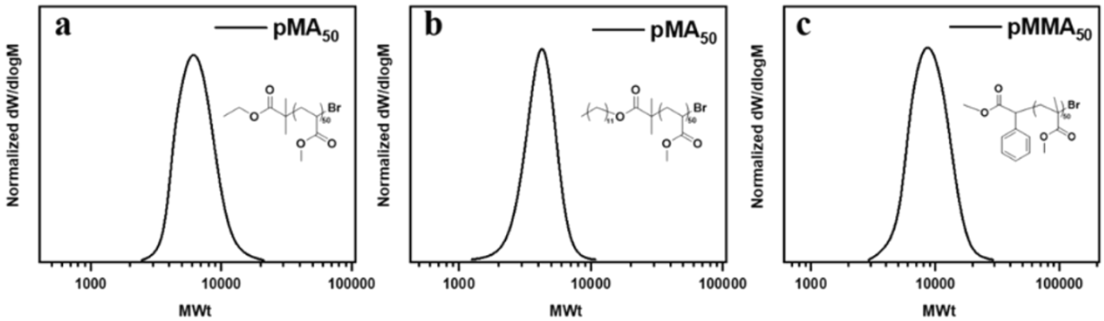

Figure 5-3. $CHCl_3$-SEC derived molecular weight distributions showing the evolution of MWts for (a) pMA_{50} using EBiB as initiator, (b) pMA_{50} using dodecyl-BiB as initiator and (c) $pMMA_{50}$ using MBPA as initiator. Conditions: [M]: [I]: [Cu(II)Br_2]: [Me_6Tren] = 50: 1: 0.05: 0.18, V_{Cyrene} = 50 % v/v with respect to monomer. Reagents were deoxygenated.

Some of previous work in the Haddleton group has focused on the Cu-RDRP of various monomers without any type of deoxygenation.[39-42] Therefore, a variety of hydrophobic monomers including MA, MMA, *tert*-butyl acrylate (*t*BA), benzyl acrylate (BzA), trifluoroethyl acrylate (TFEA) and styrene (St),were polymerized *via* Cu(0)-RDRP *by omitting deoxygenation*, thus rendering this approach more user-friendly. Cu(0)-RDRP of MA over 3 h resulted in 90% monomer conversion with $M_{n,SEC}$ = 4,800 g mol^{-1} and $Đ$ = 1.08. The time needed for the other monomers varied from 20 to 45 hours all leading to high conversions, good control over the M_n and relatively low dispersities (**Table 5-2, Figure 5-4**, ^{1}H NMR spectra are given in section *5.4.4 Supplementary Figures and Tables*, **Figures 5-10** to **5-15**). These results are similar to the $M_{n,SEC}$, dispersity and conversion observed for the non-deoxygenated Cu(0) wire-RDRP of MA in commonly used organic solvents, as described by Liarou *et al.*. For example the polymerization of MA in DMSO resulted in pMA with 96% monomer conversion to polymer after 4 hours, narrow dispersity ($Đ$ = 1.07) and good agreement between theoretical ($M_{n,\ theor.}$ = 4,300) and experimental molecular weight ($M_{n,\ SEC}$ = 5,200).[39] It is noteworthy that following the polymerization of *t*BA the formation of a biphasic system was observed, with a top polymer-rich phase and a bottom solvent-rich layer containing the majority of the catalyst and residual monomer (3%).

Table 5-2. ^{1}H NMR and SEC analysis for the Cu(0) wire mediated RDRP without deoxygenation of various hydrophobic monomers using Cyrene as solvent.

Entry[a]	Time (h)	Monomer Conv.[b] (%)	$M_{n,\ theor.}$ (g mol^{-1})	$M_{n,\ SEC}$[c]	$Đ$
p(MA)$_{50}$	3	90	4400	4800	1.08
p(MMA)$_{50}$	20	75	4000	5600	1.23
p(*t*BA)$_{50}$	20	97	6400	7200	1.11
p(St)$_{50}$	36	98	7300	7000	1.37
p(BzA)$_{50}$	24	88	7300	6000	1.18
p(TFEA)$_{50}$	45	94	7400	4500	1.11

[a] In all polymerizations, the volume ratio of monomer to solvent was maintained 1: 1.
[b] Conversion was calculated *via* ^{1}NMR in $CDCl_3$.
[c] Determined by $CHCl_3$ SEC analysis and expressed as molecular weight relative to pMMA narrow molecular weight standards.

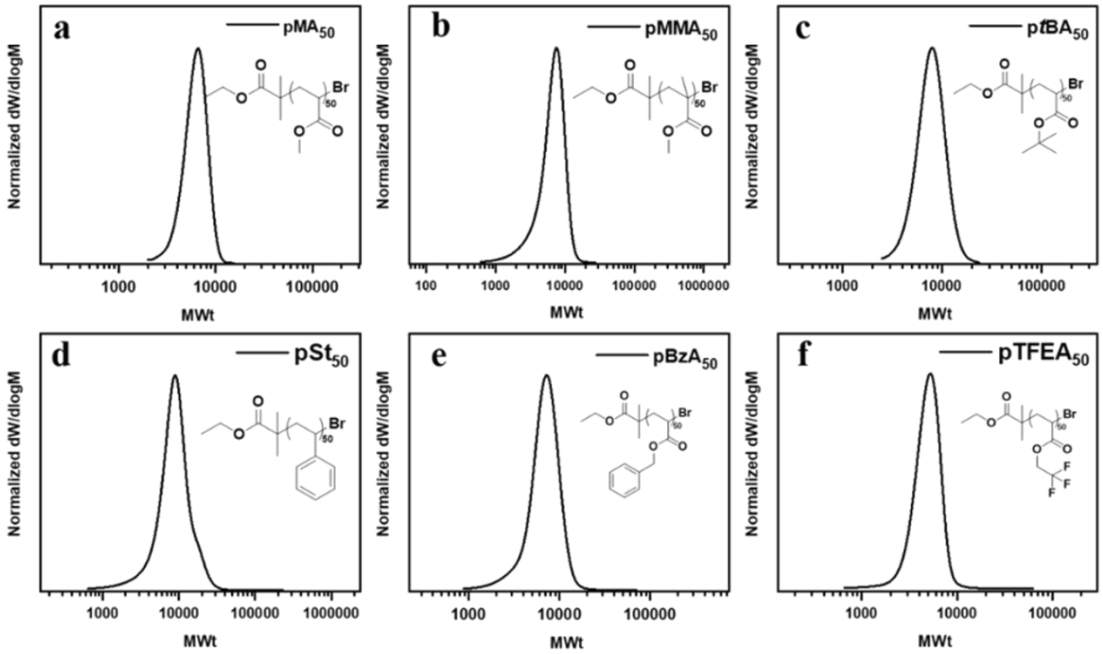

Figure 5-4. $CHCl_3$-SEC derived molecular weight distributions showing the evolution of MWts for (a) pMA_{50}, (b) $pMMA_{50}$, (c) p*t*BA, (d) pSt_{50}, (e) pBzA and (f) pTFEA synthesized by Cu(0) wire mediated RDRP in Cyrene. Conditions: [M]: [EBiB]: [Cu(II)Br_2]: [Me_6Tren] = 50: 1: 0.05: 0.18, V_{Cyrene} = 50 % v/v with respect to monomer. No deoxygenation of reagents.

Subsequently, the ability to achieve a range of molecular weights in Cyrene as solvent and in the presence of air/oxygen was investigated. By targeting DP_n values from 5 to 800, polymers with molecular weights from 700 to 28,000 g mol^{-1} with narrow dispersities were obtained (**Table 5-3, Figure 5-5**). When low DPs were targeted (higher [EBiB]) (**Table 5-3, Entries 1-4**) high conversion of MA and very good agreement between theoretical and experimental M_n values was observed. However, moving to higher DP_n values with lower [EBiB], and thus lower concentration of propagating chains led to an increase of the polymerization times, while lower yields and loss of initiator efficiency (I_{eff}) was also seen (**Tables 5-3**, **Entries 5-7** and **Table 5-6, Figures 5-15** to **5-21** in section *5.4.4*). The higher molar masses required prolonged reaction times leading the polymerization to be more susceptible to side reactions. It has also been reported that the initiator participates in the O_2-consumption mechanism,[39] therefore low [EBiB] could affect the rate of O_2-consumption and subsequently result in loss of I_{eff} and chain termination.

Table 5-3. ^{1}H NMR and SEC analysis for the Cu(0) wire-mediated RDRP of various DPs of pMA in Cyrene, without deoxygenation.

Entry[a]	DP_n	Time (h)	Mon. Conv.[b] (%)	$M_{n,\,theor.}$ (g mol^{-1})	$M_{n,\,SEC}$[c]	Đ
1	5	3	99	630	700	1.12
2	10	3	>99	1100	1000	1.11
3	20	3	>99	1900	2000	1.12
4	50	3	90	4100	4800	1.08
5	100	24	86	7600	11600	1.09
6	200	44	88	15000	19100	1.08
7	800	96	43	29800	27800	1.10

[a] In all polymerizations the volume ratio of monomer to solvent was maintained at 1: 1.
[b] Conversion was calculated *via* ^{1}H NMR in $CDCl_3$.
[c] Determined by $CHCl_3$ SEC analysis and expressed as molecular weight relative to pMMA narrow molecular weight standards.

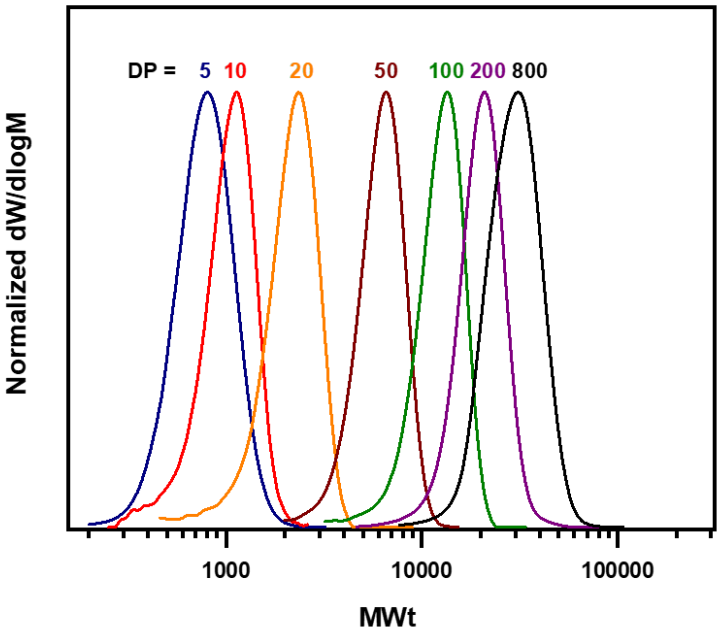

Figure 5-5. $CHCl_3$-SEC derived molecular weight distributions showing the evolution of MWts for various DP_n values (5, 10, 20, 50, 100, 200, 800) of pMA synthesized by Cu(0) wire-mediated RDRP in Cyrene without deoxygenation. Conditions: [EBiB]: [Cu(II)Br_2]: [Me_6Tren] = 1: 0.05: 0.18, V_{Cyrene} = 50 % v/v with respect to monomer.

In order to verify the ω-Br functionality of the obtained polymers, matrix assisted laser desorption/ionization time-of- flight mass spectroscopy (MALDI-ToF-MS) was employed for pMA_{20}.[43, 44] A single peak distribution corresponding to bromine-capped polymer chains was found, indicating the retention of the ω-end (**Figure 5-6**) with a calculated mass for bromine terminated polymer with $DP_n = 25$ of 2369.9 Da and an observed mass = 2370.2 Da with the associated isotopic pattern expected for incorporation of bromine, confirming the structure as shown in **Figure 5-6**. This led us to proceed to the synthesis of AB and ABA block copolymers consisting of methyl and ethyl acrylate (A= MA, B= EA) (**Table 5-4, Figure 5-7**) *via* sequential monomer addition, thus verifying that the end-group fidelity could be attained not only in the case of the pMA_{10} macroinitiator, but also for the pMA_{10}-*b*-pEA_{10} diblock, leading to a well-defined triblock copolymer synthesized in the presence of oxygen.

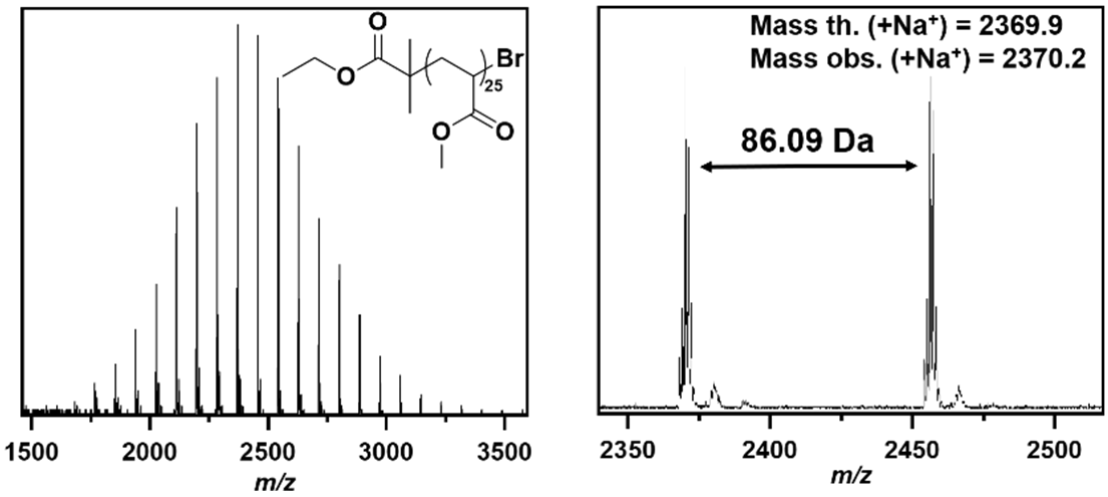

Figure 5-6. MALDI-ToF-MS spectra for the –Br terminated pMA_{25}.

Table 5-4. ^{1}H NMR and SEC analysis for the *in-situ* chain extensions through Cu(0) wire mediated RDRP without any type of deoxygenation.

Polymer [a]	Time (h)	Mon. Conv. [b] (%)	$M_{n,\,theor.}$ (g mol^{-1})	$M_{n,\,SEC}$ [c]	Đ
pMA_{10}	3	95	1000	1200	1.11
pMA_{10}-*b*-pEA_{10}	15	95	2000	2300	1.12
pMA_{10}-*b*-pEA_{10}-*b*-pMA_{10}	overnight	75	2600	3500	1.21

[a] In all polymerizations, the volume ratio of monomer to solvent was maintained 1: 1.
[b] Conversion was calculated *via* ^{1}NMR in $CDCl_3$.
[c] Determined by $CHCl_3$ SEC analysis and expressed as molecular weight relative to pMMA narrow molecular weight standards.

Apart from the facile removal of Cu(0) *via* simply removing the stirrer bar with the wrapped copper wire, we were also interested in exploring the limits of this chemistry by lowering the [Cu(II)Br_2]. Consequently, polymerization of MA (targeted DP_n = 50) was conducted by varying the amount of Cu(II)Br_2. Starting from 0.05 equivalents of Cu(II)Br_2 and reducing its amount by half, we were able to limit the catalyst content to 7.8 x 10^{-4} eq., which is 64-fold lower than the 0.05 eq. of Cu(II)Br_2 previously used. All polymerizations were carried out at ambient temperature for 3 hrs, achieving monomer conversions from 92 to 97 %. By comparing the SEC results from these polymerizations (**Table 5-5, Figure 5-8**), slightly higher molecular weights and dispersities were observed with decreasing [Cu(II)Br_2]. It might have been expected that by changing the [Me_6Tren]: [Cu(II)Br_2] ratio, the equilibrium between dormant and active species is affected and this is depicted in the molecular characteristics *i.e.* M_n and $Đ$.

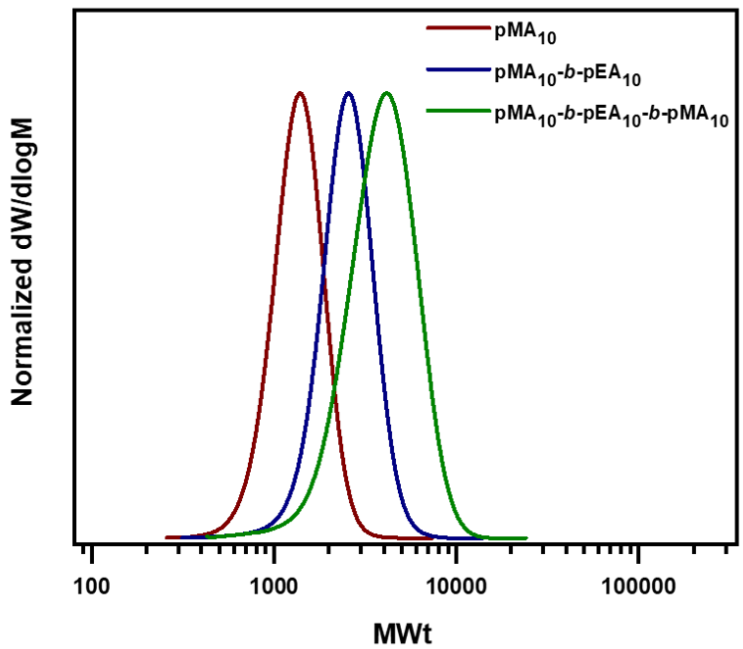

Figure 5-7. $CHCl_3$-SEC derived molecular weight distributions showing the evolution of MWts of pMA_{10} (red), pMA_{10}-*b*-pEA_{10} (blue) and pMA_{10}-*b*-pEA_{10}-*b*-pMA_{10} (green) synthesized by Cu(0) wire-mediated RDRP in Cyrene without any type of deoxygenation.

Table 5- 5. ^{1}H NMR and SEC analysis for pMA_{50} synthesized by Cu(0) wire mediated-RDRP in Cyrene without any type of deoxygenation using various [Cu(II)Br_2].

Cu(II)Br_2 (eq.)[a]	Time (hrs)	Mon. Conv.(%)[b]	$M_{n,\ theor.}$ (g mol^{-1})	$M_{n,\ NMR}$[b]	$M_{n,\ SEC}$[c]	Đ
0.00078	3	97	4400	4900	5600	1.20
0.00156	3	94	4200	5500	5600	1.20
0.00312	3	92	4200	4800	5500	1.20
0.00625	3	94	4200	4800	5600	1.15
0.0125	3	92	4200	4500	5100	1.12
0.025	3	92	4200	4600	4800	1.10
0.05	3	97	4400	4800	4800	1.08

[a] In all polymerizations, the volume ratio of monomer to solvent was maintained at 1: 1.
[b] Conversion was calculated *via* ^{1}NMR in $CDCl_3$.
[c] Determined by $CHCl_3$ SEC analysis and expressed as molecular weight relative to pMMA narrow molecular weight standards.

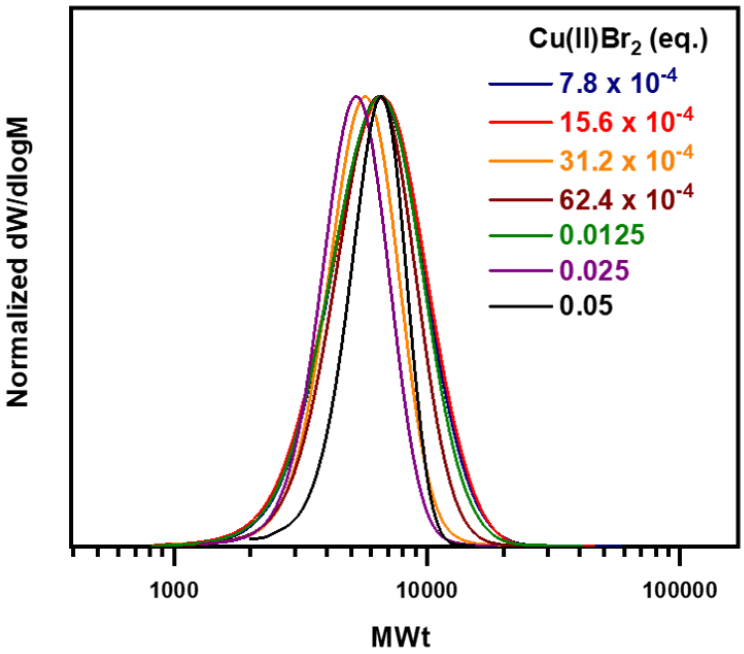

Figure 5-8. $CHCl_3$-SEC derived molecular weight distributions showing the evolution of MWts of pMA_{50} synthesized by Cu(0) wire-mediated RDRP in Cyrene without any type of deoxygenation with various [Cu(II)Br_2].

Finally, the oxygen consumption profile for polymerization of pMA in Cyrene was monitored by use of an oxygen concentration probe. As shown in **Figure 5-9**, in the absence of headspace, full oxygen consumption takes place within the first 5 minutes of the reaction (2 mL total reaction volume), while even when 0.5 mL of

headspace is present, the oxygen consumption lasts for 24 minutes. This observation comes in agreement with previous work by Liarou *et al*., and verifies the importance of headspace, which is highlighted in smaller scale reactions (2 mL total reaction volume). As has previously been reported, [39] all the reagents of the polymerization (Cu(0)-wire, initiator, Cu(II)Br_2/Me_6Tren) contribute to oxygen consumption, and synergistically lead to full consumption of dissolved oxygen, which occurs within the first minutes of the reaction (in the absence of headspace). It is noted that the [O_2] at t=0 in the reaction mixture containing Cyrene was <6 mg L^{-1}, while in the case of DMSO it was >8 mg L^{-1}.

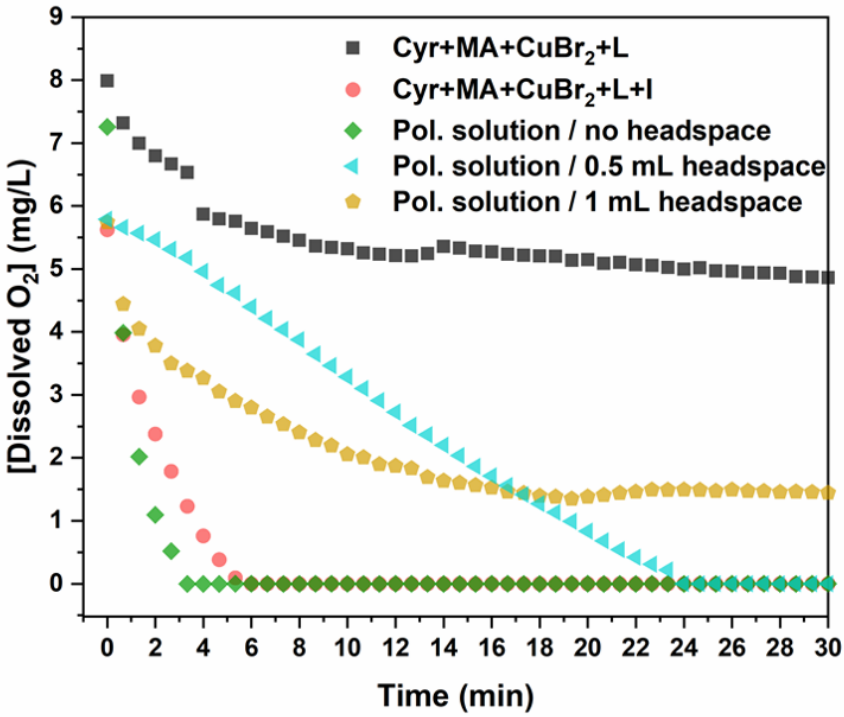

Figure 5-9. Graphical illustration of the dissolved oxygen consumption during Cu(0) wire mediated RDRP of MA, effect of headspace and role of the polymerization components. The first two measurements (black square ■ and pink circle ●) were run without the use of Cu(0) wire.

5.3 Conclusions

In summary, in this chapter the use of Cyrene, which derives from renewable resources, as an alternative dipolar aprotic solvent for the Cu(0) wire-mediated RDRP of various hydrophobic monomers is reported. Polymerization proceeded successfully under both deoxygenated and non-deoxygenated conditions, allowing production of polymers with high end-group fidelity at high conversions, allowing for sequential monomer addition for the synthesis of di- and tri- block copolymers. Even with very low [Cu(II)Br_2] (as low as 7.8 x 10^{-4} eq.) the obtained pMAs exhibited controlled macromolecular characteristics. Cyrene offers a valuable biorenewable alternative to harsh aprotic polar solvents which are increasingly seen as unattractive.

5.4 Experimental section

5.4.1 Materials

All materials were purchased from Sigma-Aldrich or Cornellius (benzyl acrylate) and were used as received unless otherwise stated. Cu(0) wire (gauge 0.25 mm) was purchased from Comax Engineered wires and purified by immersion in concentrated 37% HCl for 12 minutes, subsequently washed with deionized water and acetone and dried with compressed air prior to use. Tris-(2-(dimethylamino)ethyl)amine (Me_6Tren) was prepared according to the literature and stored in fridge.[45]

5.4.2 Instrumentation and Characterization techniques

Proton Nuclear Magnetic Resonance (^{1}H NMR)

^{1}H NMR spectra were recorded on Bruker DPX-300 spectrometers in deuterated chloroform ($CDCl_3$) obtained from Sigma-Aldrich. Chemical shifts are given in ppm downfield from the internal standard tetramethylsilane. Monomer conversions were determined *via* ^{1}H NMR spectroscopy by comparing the integrals of monomeric vinyl protons to polymer signals.

Size Exclusion Chromatography (SEC)

SEC was carried out using an Agilent Infinity II 1260 MDS instrument equipped with differential refractive index (DRI), viscometry (VS), dual angle light scatter (LS) and multiple wavelength UV detectors. The system was equipped with 2 x PLgel Mixed C columns (300 x 7.5 mm) and a PLgel 5 µm guard column. The eluent was $CHCl_3$ run at 1 ml/min at 30 ^{o}C. Poly(methyl methacrylate) standards (Agilent EasiVials) were used to create a 3rd order calibration between 1,020,000 – 1,840 g mol^{-1}. Analyte samples were filtered through 0.22 µm pore size GVHP filters before injection. Respectively, experimental molar mass ($M_{n,SEC}$) and dispersity ($Đ$) values of synthesized polymers were determined by conventional calibration using Agilent GPC/SEC software.

Matrix-assisted laser desorption/ionization time-of-flight

The measurements were conducted using a Bruker Daltonics Ultraflex II MALDI-ToF mass spectrometer, equipped with a nitrogen laser delivering 2 ns laser pulses at 337 nm with positive ion ToF detection performed using an accelerating voltage of 25 kV. Solutions in tetrahydrofuran (THF) (50 μL) of trans-2-[3-(4-tert-butylphenyl)-2-methyl-2-propyldene] malononitrile (DCTB) as a matrix (saturated solution), sodium iodide as the cationization agent (1.0 mg mL^{-1}) and sample (1.0 mg mL^{-1}) were mixed, and 0.7 μL of the mixture was applied to the target plate. Spectra were recorded in reflectron mode calibrated with poly(ethylene glycol) monomethyl ether (PEGMe) 1900 Da.

Oxygen Probe; Pocket Oxygen Meter - FireStingGO2 (from Pyro Science):

For the determination of dissolved oxygen concentration and the *in-situ* monitoring of O_2-consumption, the solvent resistant oxygen probe OXSOLV was immersed in septum-sealed polymerization reactions. The starting point of the measurements (t=0) was determined as the time that the initiator was added. Upon completion of the measurement, the oxygen probe was cleaned with acetone-methanol-H_2O-acetone and was left to dry (excess of acetone was removed by careful wiping with soft tissue). The analysis of the data was conducted with the FireStingGO2 Manager software.

5.4.3 Experimental procedures

Synthesis of tris-(2-(dimethylamino)ethyl)amine (Me_6Tren)

Tris-(2-aminoethyl)amine (50 mL, 0.33 mol) was added dropwise over a period of 1 hour to a mixture of formic acid (320 mL, 8.15 mol) and formaldehyde (270.9 mL, 3.64 mol) with vigorous stirring and using a large ice bath to cool the reaction mixture. The reaction was stirred for 12 hours at 120 ºC under reflux. After leaving to cool, the volatile fractions were removed under reduced pressure and a saturated sodium hydroxide solution was used to adjust the mixture to approximately pH 10. The oil layer was extracted into chloroform and dried with magnesium sulfate (~ 20 g). the solvent was then removed *in vacuo* to yield a yellow oil. The oil was distilled under reduced pressure to give a colorless liquid and stored in the fridge ((57 g). ^{1}H NMR ($CDCl_3$, 400 MHz, **Figure 5-22**), δ (ppm): 2.50 and 2.27 (t, 12 H, $(CH_3)_2NC\boldsymbol{H}_2C\boldsymbol{H}_2NR$), 2.12 (s, 18 H, $(C\boldsymbol{H}_3)_2NR$).

Typical procedure for Cu(0) wire mediated RDRP of MA or MMA under inert conditions

A glass vial with total volume capacity of 20 mL was charged with $Cu(II)Br_2$ (0.05 eq.) and Cyrene (4 mL). Me_6Tren (0.18 eq.) was added through a microliter syringe and the solution was sonicated until total dissolution of $Cu(II)Br_2$ (~10-15 mins). Subsequently, monomer (MA or MMA) (4 mL, 50 eq.), initiator (EBiB or DBiB or MBPA) (1 eq.) and pre-activated Cu(0) wire (5 cm) wrapped around a stirring bar were added to the vial and the vial sealed with a septum and wrapped with foil. Then, the mixture was deoxygenated under N_2 bubbling for 15 minutes. The polymerization was left to commence at ambient temperature.

Typical procedure for Cu(0) wire mediated RDRP of (meth)acrylates and styrene with targeted DP_n = 50, without external deoxygenation

$Cu(II)Br_2$ (0.05 eq.) Cyrene(1 mL) and Me_6Tren (0.18 eq.) were added to a 2 mL glass vial and the solution was sonicated until total dissolution of $Cu(II)Br_2$ (~10-15 mins). Subsequently, monomer (1 mL, 50 eq.), EBiB (1 eq.) and pre-activated Cu(0)wire (5 cm) wrapped around a stirring bar were added to the vial and the vial sealed with a septum. The polymerization was left to commence at ambient temperature. Following

the polymerization reaction, samples were taken and passed through a short column of neutral alumina to remove dissolved copper salts prior to analysis by ^{1}H NMR in $CDCl_3$ and SEC in $CHCl_3$.

Purification: Cyrene, residual monomer and copper salts were removed by precipitation (x 3) in cold MeOH-H_2O mixtures. Subsequently, the polymer redissolved in THF and $MgSO_4$ was added. After filtration, the solvent was removed by rotary evaporator under reduced pressure. The polymer was dried in vacuum oven at 40 ºC for 24 hrs before ^{1}H NMR analysis.

Monomers used: methyl acrylate (MA), methyl methacrylate (MMA), *tert*-butyl acrylate (*t*-BA), styrene, benzyl acrylate (BzA) and trifluoroethyl acrylate (TFEA).

Typical procedure for in situ chain extensions

Initially, pMA with targeted DP_n =10 was synthesized following the typical procedure for the homopolymerization of MA described above. After 3 hrs, an aliquot (~ 100 µL) was taken for ^{1}H NMR and SEC analysis. Upon reaching 95% conversion, 900 µL of the polymerization solution was withdrawn with a 1 mL polypropene (PP) syringe, without opening the vial, and the solution of Cyrene and EA (targeted DP_n for the pEA block = 10, with 50 % v/v Cyrene) were added in the pMA-Br macroinitiator solution. The polymerization was left to commence and upon reaching 95 % conversion, 900 µL of the pMA-pEA solution was withdrawn. For the formation of the third block, a solution of Cyrene and MA (targeted DP_n for the pMA block = 10, with 50 % v/v Cyrene) was added in the pMA-pEA solution.

5.4.4 Supplementary Figures and Tables

Cu(0) wire mediated RDRP of MA in Cyrene without any type of deoxygenation. Targeted DP_n = 50

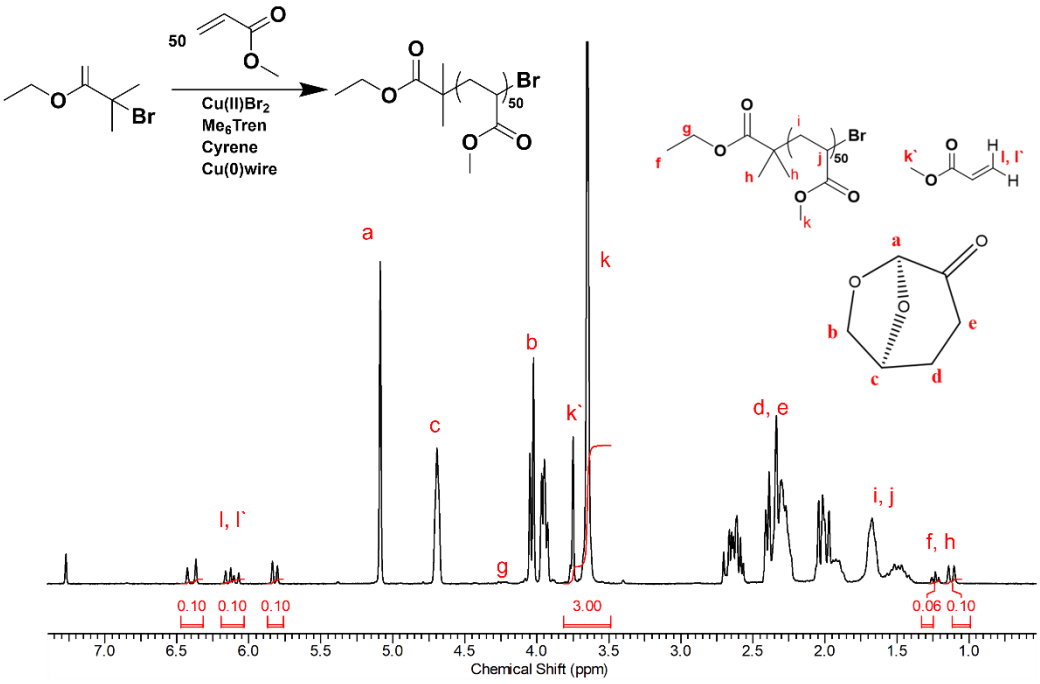

Figure 5-10. Reaction scheme and ^{1}H NMR for Cu(0) wire mediated RDRP of MA using EBiB as initiator and Cyrene as solvent. Conditions: [M]: [I]: [Cu(II)Br_2]: [Me_6Tren] = 50: 1: 0.05: 0.18, V_{Cyrene} = 50 % v/v with respect to monomer, no deoxygenation of reagents. Conversion was determined by comparing the integrals of monomeric vinyl protons (l, l`) to polymer signals (k).

Cu(0) wire mediated RDRP of MMA in Cyrene without any type of deoxygenation. Targeted DP_n = 50

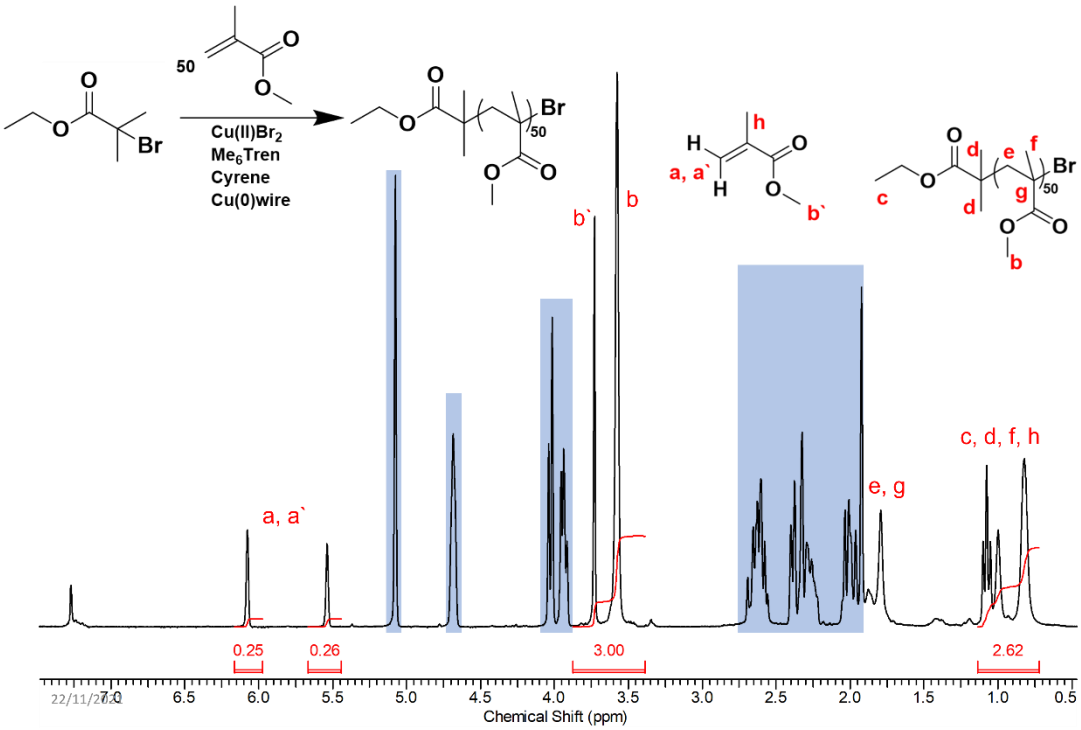

Figure 5-11. Reaction scheme and ^{1}H NMR for Cu(0) wire mediated RDRP of MMA using EBiB as initiator and Cyrene as solvent. Conditions: [M]: [I]: [Cu(II)Br_2]: [Me_6Tren] = 50: 1: 0.05: 0.18, V_{Cyrene} = 50 % v/v with respect to monomer, no deoxygenation of reagents. Conversion was determined by comparing the integrals of monomeric vinyl protons (a, a`) to polymer signals (b). The peaks covered in the blue area correspond to cyrene.

Cu(0) wire mediated RDRP of tert-BA in Cyrene without any type of deoxygenation. Targeted DP_n = 50

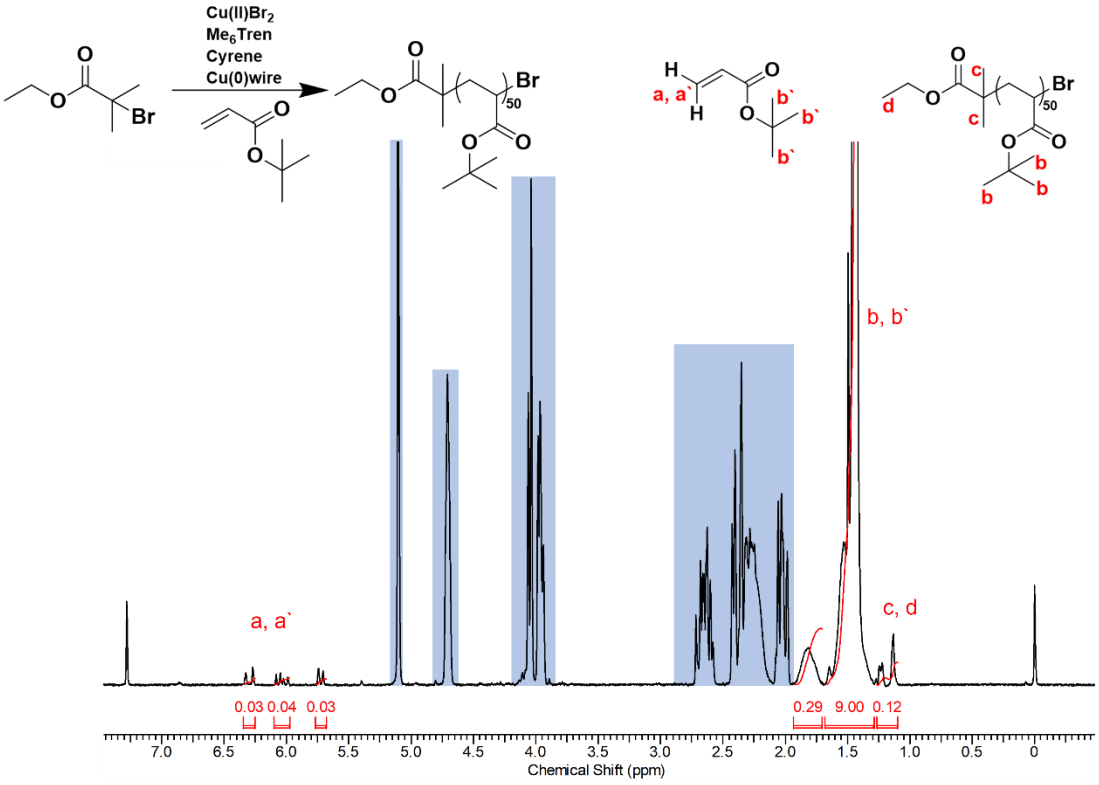

Figure 5-12. Reaction scheme and ^{1}H NMR for Cu(0) wire mediated RDRP of *t*BA using EBiB as initiator and Cyrene as solvent. Conditions: [M]: [I]: [Cu(II)Br_2]: [Me_6Tren] = 50: 1: 0.05: 0.18, V_{Cyrene} = 50 % v/v with respect to monomer, no deoxygenation of reagents. Conversion was determined by comparing the integrals of monomeric vinyl protons (a, a`) to polymer signals (b). The peaks covered in the blue area correspond to cyrene.

Cu(0) wire mediated RDRP of styrene in Cyrene without any type of deoxygenation. Targeted DP_n = 50

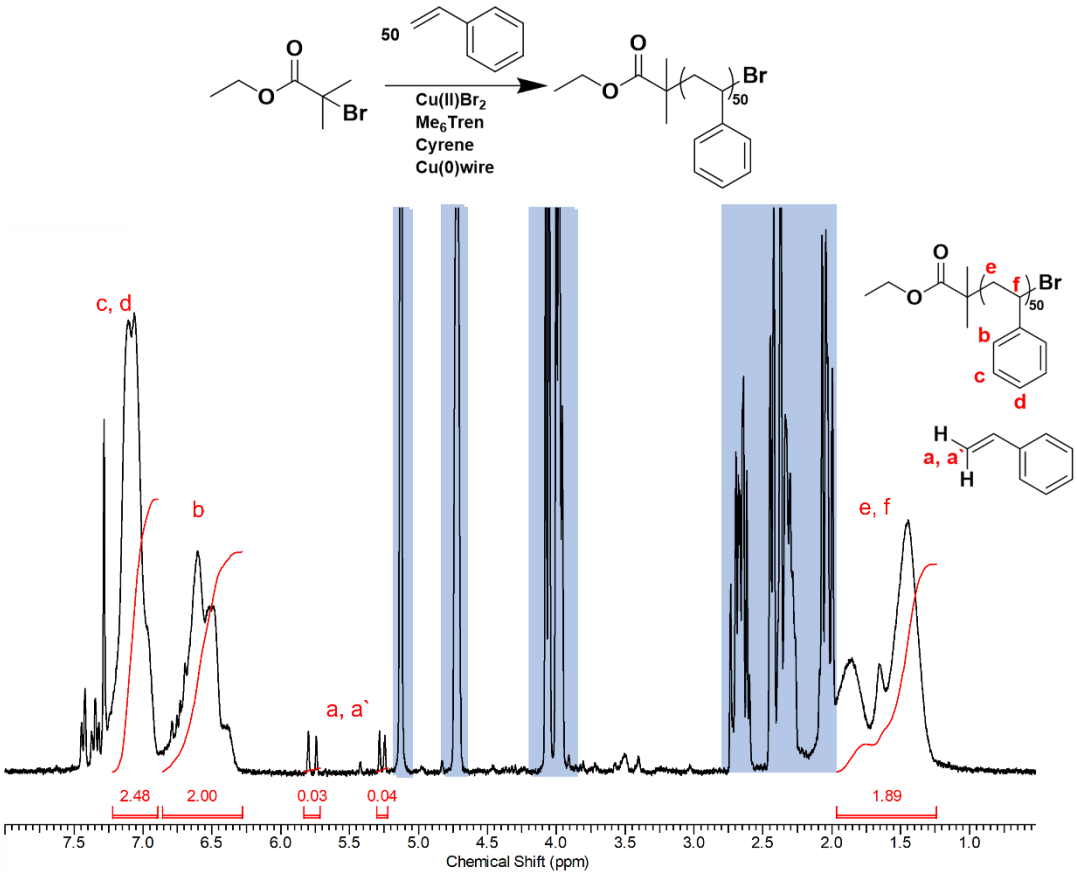

Figure 5-13. Reaction scheme and ^{1}H NMR for Cu(0) wire mediated RDRP of styrene using EBiB as initiator and Cyrene as solvent. Conditions: [M]: [I]: [Cu(II)Br_2]: [Me_6Tren] = 50: 1: 0.05: 0.18, V_{Cyrene} = 50 % v/v with respect to monomer, no deoxygenation of reagents. Conversion was determined by comparing the integrals of monomeric vinyl protons (a, a`) to polymer signals (b). The peaks covered in the blue area correspond to cyrene.

Cu(0) wire mediated RDRP of BzA in Cyrene without any type of deoxygenation. Targeted DP_n = 50

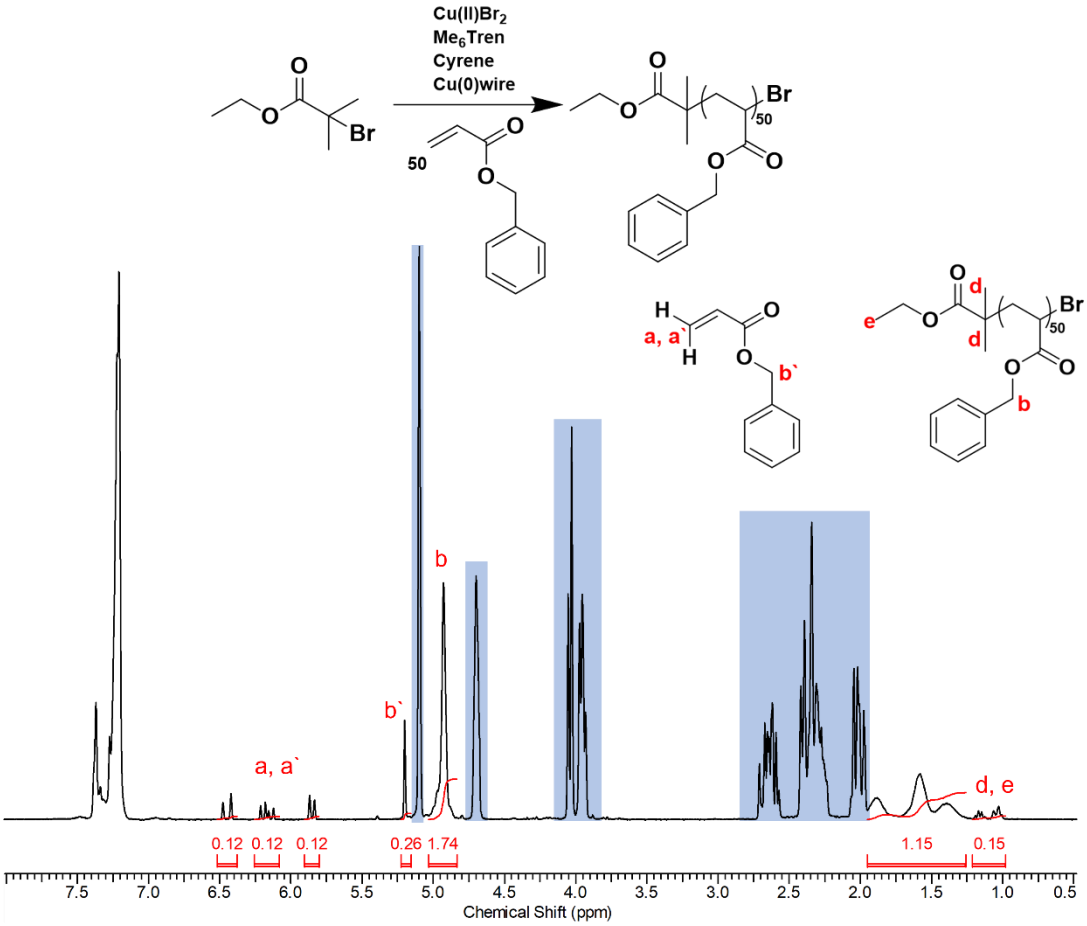

Figure 5-14. Reaction scheme and ^{1}H NMR for Cu(0) wire mediated RDRP of BzA using EBiB as initiator and Cyrene as solvent. Conditions: [M]: [I]: [Cu(II)Br_2]: [Me_6Tren] = 50: 1: 0.05: 0.18, V_{Cyrene} = 50 % v/v with respect to monomer, no deoxygenation of reagents. Conversion was determined by comparing the integrals of monomeric vinyl protons (a, a`) to polymer signals (b). The peaks covered in the blue area correspond to cyrene.

Cu(0) wire mediated RDRP of TFEA in Cyrene without any type of deoxygenation. Targeted DP_n = 50

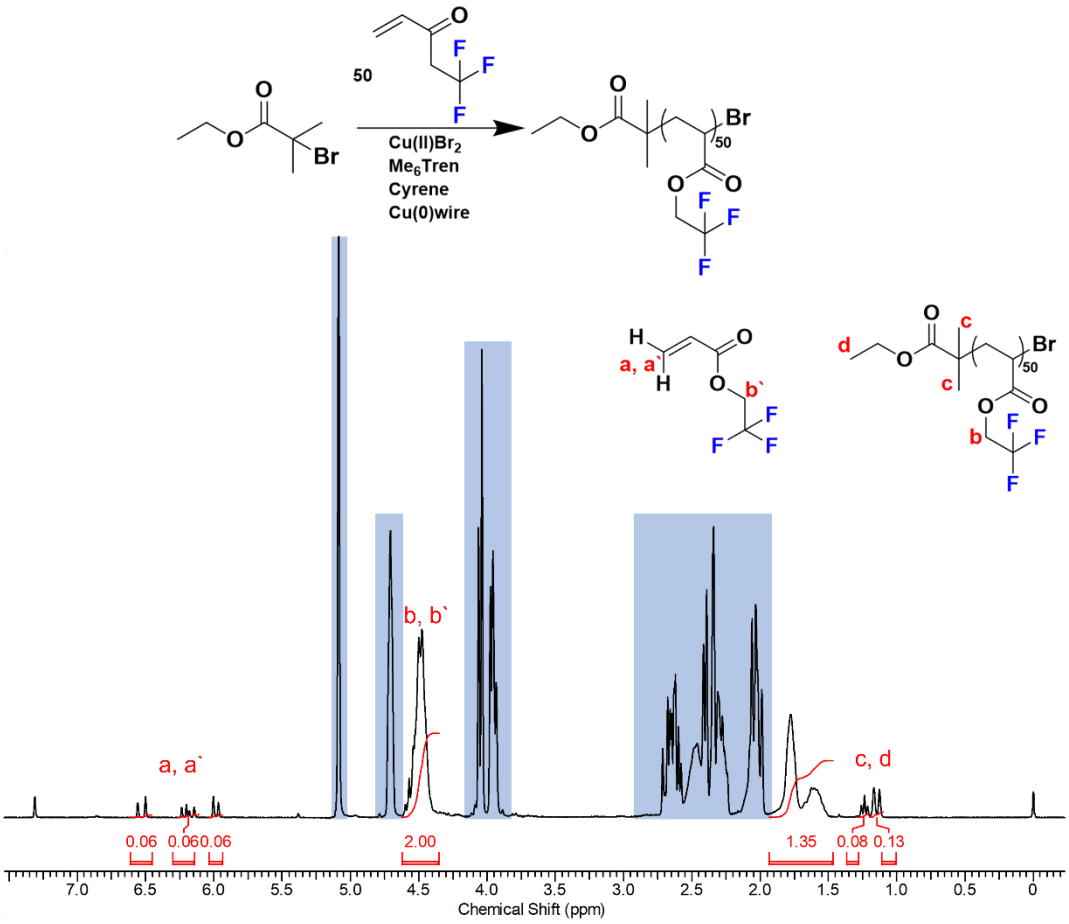

Figure 5-15. Reaction scheme and ^{1}H NMR for Cu(0) wire mediated RDRP of TFEA using EBiB as initiator and Cyrene as solvent. Conditions: [M]: [I]: [Cu(II)Br_2]: [Me_6Tren] = 50: 1: 0.05: 0.18, V_{Cyrene} = 50 % v/v with respect to monomer, no deoxygenation of reagents. Conversion was determined by comparing the integrals of monomeric vinyl protons (a, a`) to polymer signals (b). The peaks covered in the blue area correspond to cyrene.

Table 5-6. ^{1}H NMR analysis of the purified polymers obtained from Cu(0)wire-mediated RDRP of MA without deoxygenation.

Targeted Polymer	Conversion (%)	$M_{n,\,th.}$ (g mol^{-1})	$M_{n,\,NMR.}$ (g mol^{-1})	I_{eff} [b] (%)
pMA$_5$	99	630	710	89
pMA$_{10}$	>99	1100	1200	92
pMA$_{20}$	>99	1900	2300	83
pMA$_{50}$	90	4100	5100	80
pMA$_{100}$	86	7600	10300	74
pMA$_{200}$[a]	88	15000	-	-
pMA$_{800}$[a]	43	29800	-	-

[a] The initiator efficiency for the polymerizations of MA with targeted DP_n = 200 and 800 are not reported due to the low intensity of the peaks that correspond to initiator.
[b] $I_{eff} = (1 - ((M_{n,\,NMR} - M_{n,\,th.}) / M_{n,\,NMR})) \times 100$

Cu(0) wire mediated RDRP of MA in Cyrene. Targeted DP_n = 5

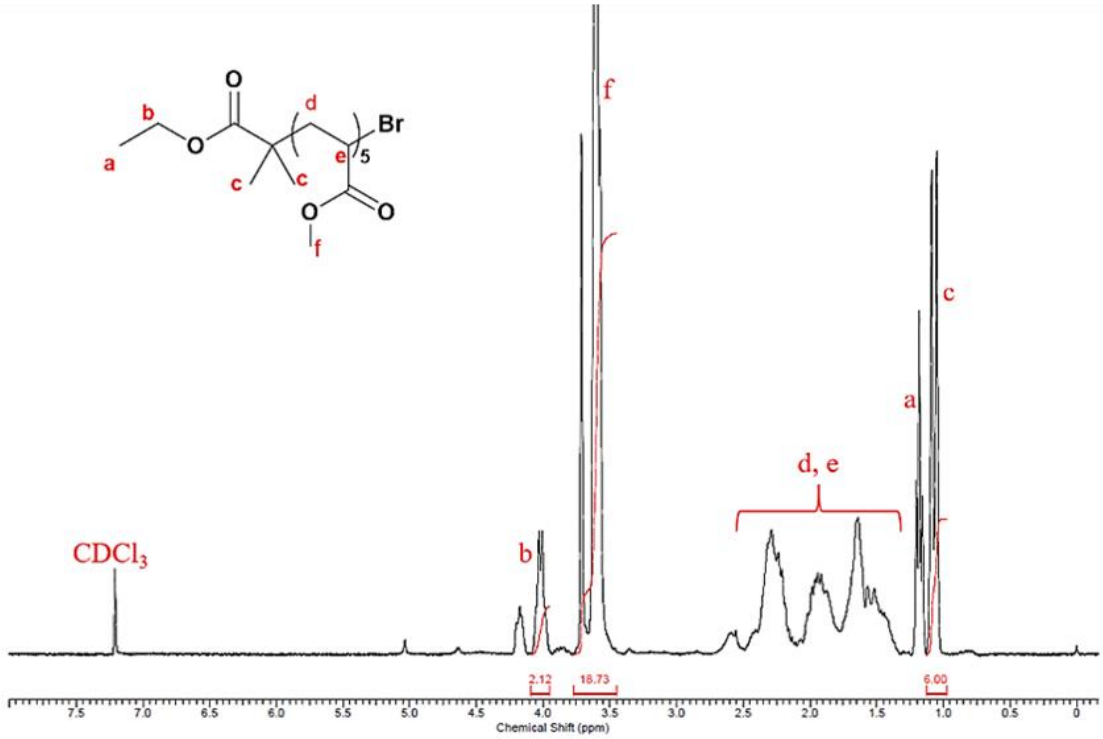

Figure 5-16. ^{1}H NMR for Cu(0) wire-mediated RDRP of MA using EBiB as initiator and Cyrene as solvent under N_2. Conditions: [M]: [I]: [Cu(II)Br$_2$]: [Me$_6$Tren] = 5: 1: 0.05: 0.18, V_{Cyrene} = 50 % v/v with respect to monomer. Spectrum was collected after the purification of the polymer for the determination of I_{eff} and the $M_{n,\,NMR}$.

Cu(0) wire mediated RDRP of MA in Cyrene. Targeted DP_n = 10

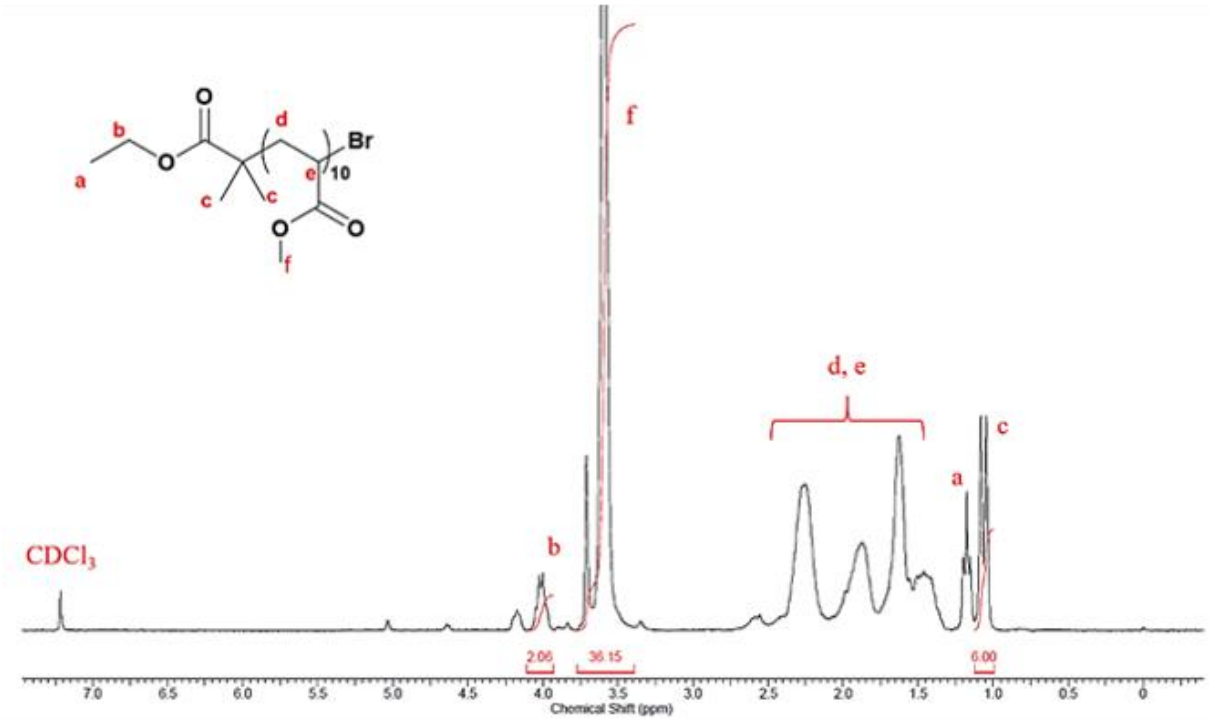

Figure 5- 17. ^{1}H NMR for Cu(0) wire-mediated RDRP of MA using EBiB as initiator and Cyrene as solvent under N_2. Conditions: [M]: [I]: [Cu(II)Br_2]: [Me_6Tren] = 10: 1: 0.05: 0.18, V_{Cyrene} = 50 % v/v with respect to monomer. Spectrum was collected after the purification of the polymer for the determination of I_{eff} and the $M_{n,\,NMR}$.

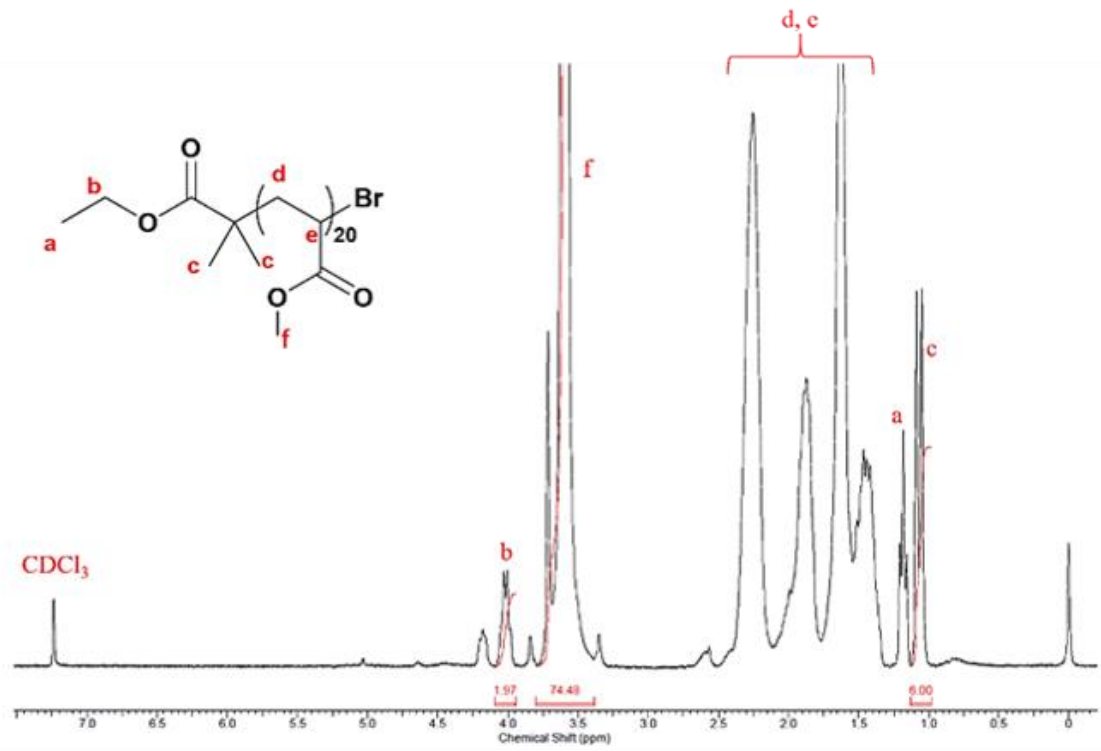

Figure 5-18. ^{1}H NMR for Cu(0) wire-mediated RDRP of MA using EBiB as initiator and Cyrene as solvent under N_2. Conditions: [M]: [I]: [Cu(II)Br_2]: [Me_6Tren] = 20: 1: 0.05: 0.18, V_{Cyrene} = 50 % v/v with respect to monomer. Spectrum was collected after the purification of the polymer for the determination of I_{eff} and the $M_{n,\,NMR}$.

Cu(0) wire mediated RDRP of MA in Cyrene. Targeted DP_n = 50

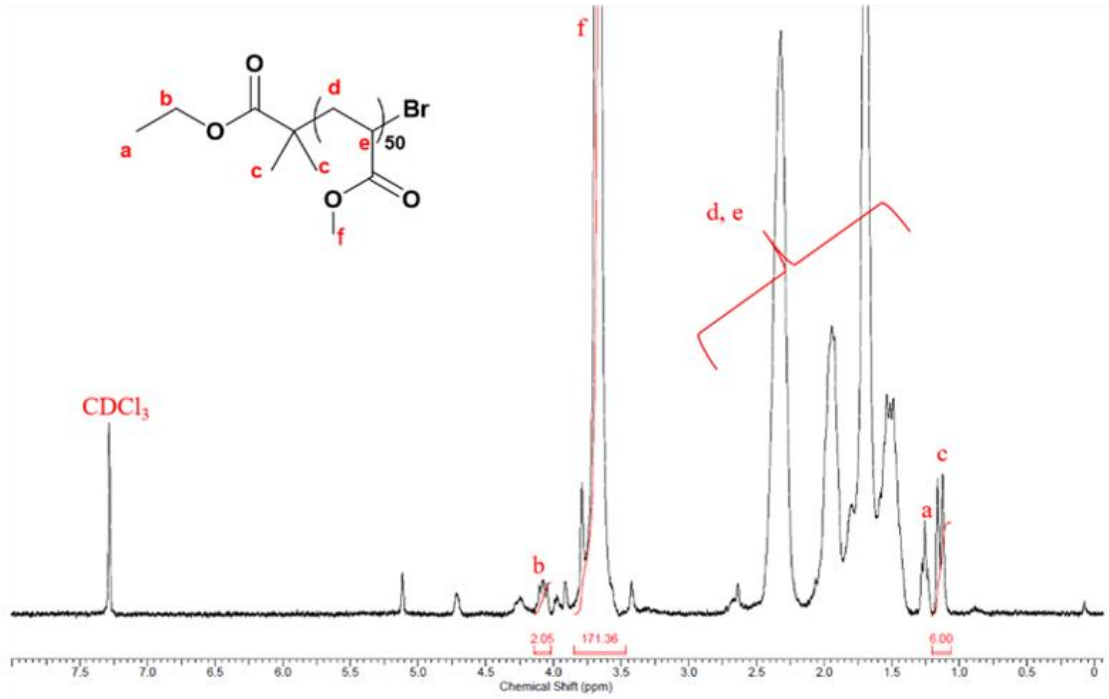

Figure 5-19. ^{1}H NMR for Cu(0) wire-mediated RDRP of MA using EBiB as initiator and Cyrene as solvent under N_2. Conditions: [M]: [I]: [Cu(II)Br_2]: [Me_6Tren] = 50: 1: 0.05: 0.18, V_{Cyrene} = 50 % v/v with respect to monomer. Spectrum was collected after the purification of the polymer for the determination of I_{eff} and the $M_{n,\,NMR}$.

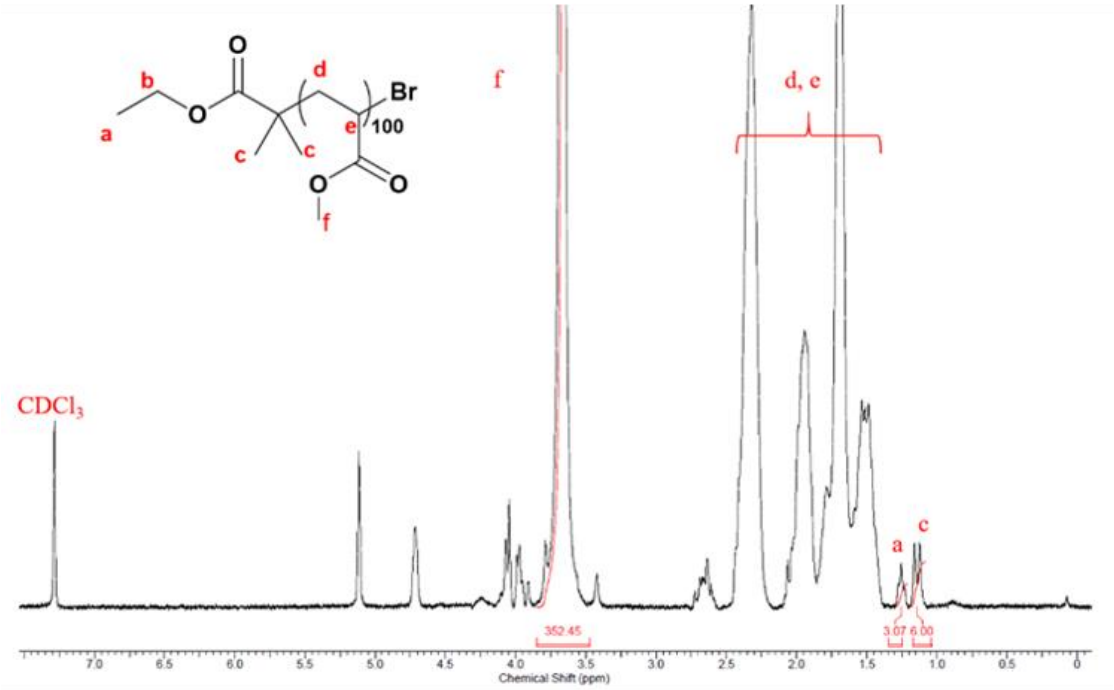

Figure 5-20. ^{1}H NMR for Cu(0) wire-mediated RDRP of MA using EBiB as initiator and Cyrene as solvent under N_2. Conditions: [M]: [I]: [Cu(II)Br_2]: [Me_6Tren] = 100: 1: 0.05: 0.18, V_{Cyrene} = 50 % v/v with respect to monomer. Spectrum was collected after the purification of the polymer for the determination of I_{eff} and the $M_{n,\,NMR}$.

Cu(0) wire mediated RDRP of MA in Cyrene. Targeted DP_n = 200

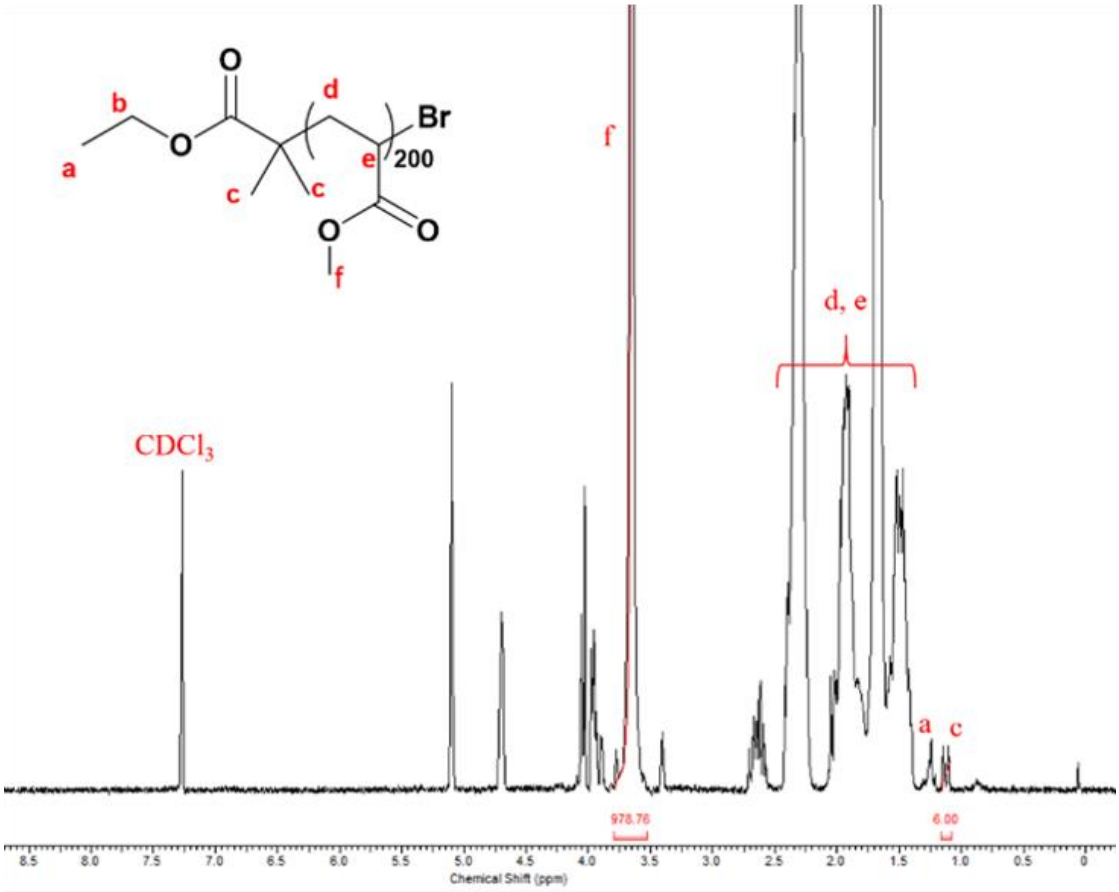

Figure 5-21. ^{1}H NMR for Cu(0) wire-mediated RDRP of MA using EBiB as initiator and Cyrene as solvent under N_2. Conditions: [M]: [I]: [Cu(II)Br_2]: [Me_6Tren] = 200: 1: 0.05: 0.18, V_{Cyrene} = 50 % v/v with respect to monomer.

Cu(0) wire mediated RDRP of MA in Cyrene. Targeted DP_n = 800

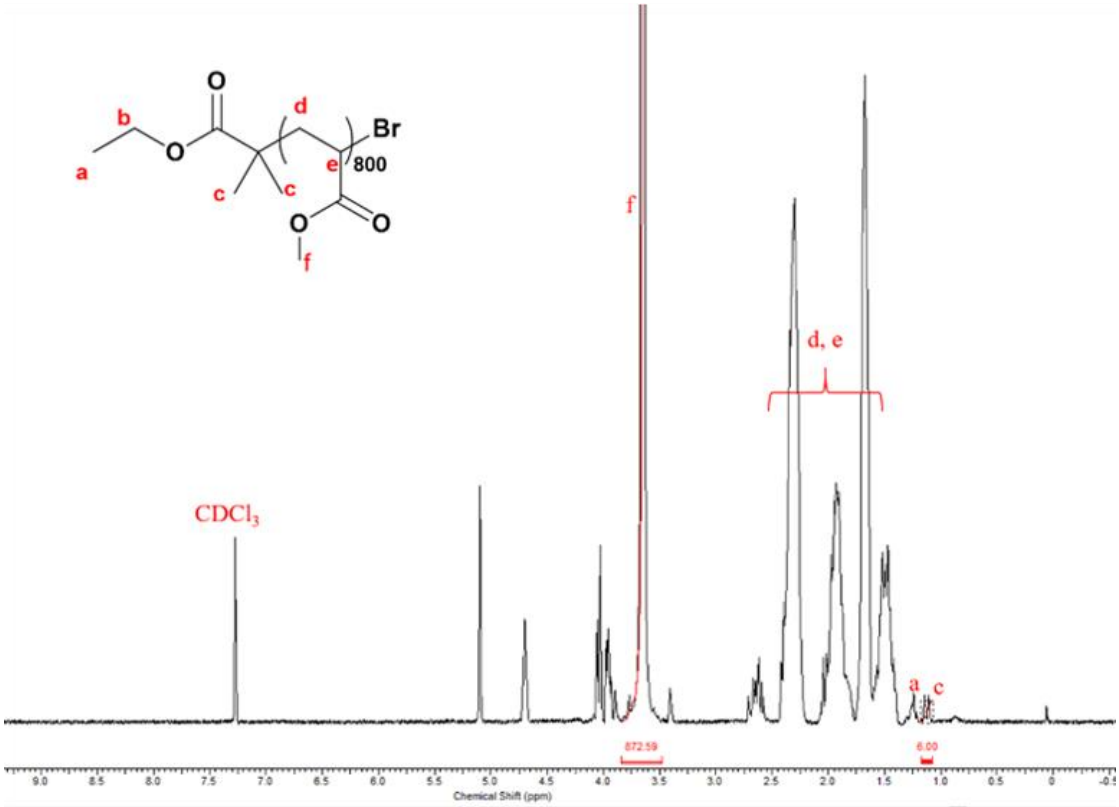

Figure 5-22. ^{1}H NMR for Cu(0) wire-mediated RDRP of MA using EBiB as initiator and Cyrene as solvent under N_2. Conditions: [M]: [I]: [Cu(II)Br_2]: [Me_6Tren] = 800: 1: 0.05: 0.18, V_{Cyrene} = 50 % v/v with respect to monomer.

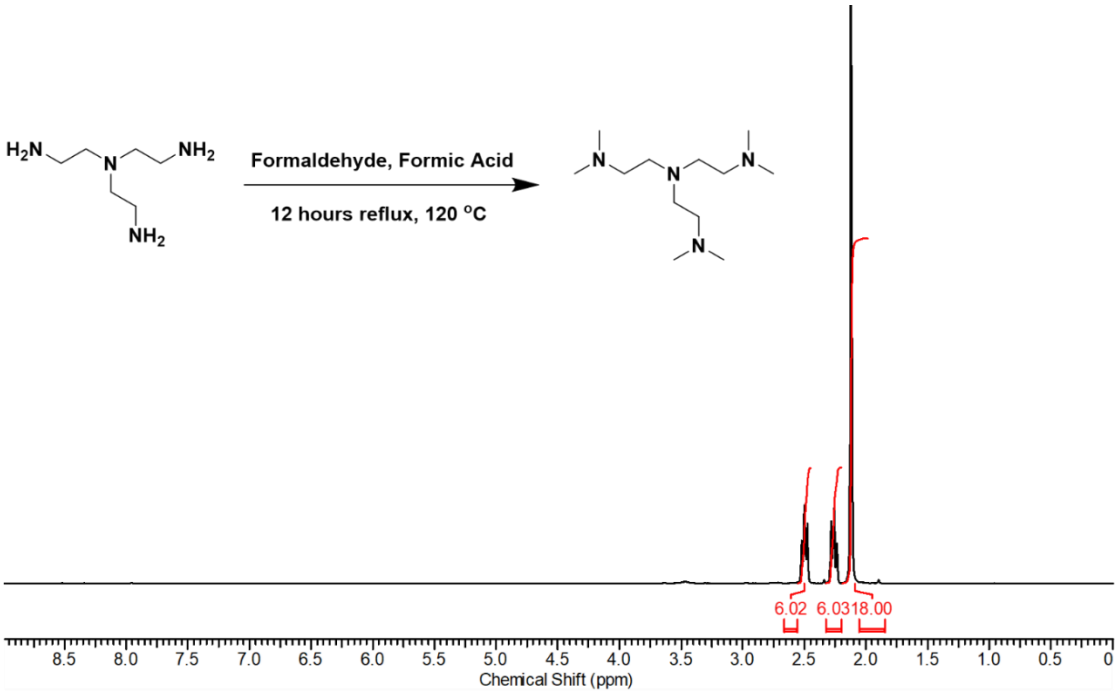

Figure 5-23. Reaction scheme for the synthesis of Me$_6$Tren and ^{1}H NMR spectrum of the pure product. 400 MHz, δ (ppm): 2.50 and 2.27 (t, 12 H, J = 2 Hz, $(CH_3)_2NC\boldsymbol{H}_2C\boldsymbol{H}_2NR$), 2.12 (s, 18 H, $(C\boldsymbol{H}_3)_2NR$).

5.5 References

1. Kato, M.; Kamigaito, M.; Sawamoto, M.; Higashimura, T., Polymerization of Methyl Methacrylate with the Carbon Tetrachloride/Dichlorotris-(Triphenylphosphine)Ruthenium(II)/Methylaluminum Bis(2,6-Di-Tert-Butylphenoxide) Initiating System: Possibility of Living Radical Polymerization. *Macromolecules* **1995,** *28* (5), 1721-1723.

2. Wang, J.-S.; Matyjaszewski, K., Controlled/"Living" Radical Polymerization. Atom Transfer Radical Polymerization in the Presence of Transition-Metal Complexes. *J. Am. Chem. Soc.* **1995,** *117* (20), 5614-5615.

3. Percec, V.; Guliashvili, T.; Ladislaw, J. S.; Wistrand, A.; Stjerndahl, A.; Sienkowska, M. J.; Monteiro, M. J.; Sahoo, S., Ultrafast Synthesis of Ultrahigh Molar Mass Polymers by Metal-Catalyzed Living Radical Polymerization of Acrylates, Methacrylates, and Vinyl Chloride Mediated by Set at 25 °C. *J. Am. Chem. Soc.* **2006,** *128* (43), 14156-14165.

4. Chiefari, J.; Chong, Y. K.; Ercole, F.; Krstina, J.; Jeffery, J.; Le, T. P. T.; Mayadunne, R. T. A.; Meijs, G. F.; Moad, C. L.; Moad, G.; Rizzardo, E.; Thang, S. H., Living Free-Radical Polymerization by Reversible Addition−Fragmentation Chain Transfer: The RAFT Process. *Macromolecules* **1998,** *31* (16), 5559-5562.

5. Hawker, C. J.; Bosman, A. W.; Harth, E., New Polymer Synthesis by Nitroxide Mediated Living Radical Polymerizations. *Chem. Rev.* **2001,** *101* (12), 3661-3688.

6. Aksakal, S.; Liu, R.; Aksakal, R.; Becer, C. R., Nitroxide-Mediated Polymerisation of Thioacrylates and Their Transformation into Poly(Acrylamide)S. *Polym. Chem.* **2020,** *11* (5), 982-989.

7. Theodorou, A.; Liarou, E.; Haddleton, D. M.; Stavrakaki, I. G.; Skordalidis, P.; Whitfield, R.; Anastasaki, A.; Velonia, K., Protein-Polymer Bioconjugates Via a Versatile Oxygen Tolerant Photoinduced Controlled Radical Polymerization Approach. *Nat. Commun.* **2020,** *11* (1), 1486.

8. Hancox, E.; Liarou, E.; Town, J. S.; Jones, G. R.; Layton, S. A.; Huband, S.; Greenall, M. J.; Topham, P. D.; Haddleton, D. M., Microphase Separation of Highly Amphiphilic, Low N Polymers by Photoinduced Copper-Mediated Polymerization, Achieving Sub-2 nm Domains at Half-Pitch. *Polym. Chem.* **2019,** *10* (46), 6254-6259.

9. Nguyen, N. H.; Leng, X.; Sun, H.-J.; Percec, V., Single-Electron Transfer-Living Radical Polymerization of Oligo(Ethylene Oxide) Methyl Ether Methacrylate in the Absence and Presence of Air. *J. Polym. Sci., Part A: Polym. Chem.* **2013,** *51* (15), 3110-3122.

10. Nguyen, N. H.; Rosen, B. M.; Percec, V., SET-LRP of N,N-Dimethylacrylamide and of N-Isopropylacrylamide at 25 °C in Protic and in Dipolar Aprotic Solvents. *J. Polym. Sci., Part A: Polym. Chem.* **2010,** *48* (8), 1752-1763.

11. Zhang, Q.; Li, Z.; Wilson, P.; Haddleton, D. M., Copper-Mediated Controlled Radical Polymerization under Biological Conditions: Set-Lrp in Blood Serum. *Chem. Commun.* **2013,** *49* (59), 6608-6610.

12. Jessop, P. G., Searching for Green Solvents. *Green Chemistry* **2011,** *13* (6), 1391-1398.

13. Prat, D.; Hayler, J.; Wells, A., A Survey of Solvent Selection Guides. *Green Chemistry* **2014,** *16* (10), 4546-4551.

14. Pena-Pereira, F.; Kloskowski, A.; Namieśnik, J., Perspectives on the Replacement of Harmful Organic Solvents in Analytical Methodologies: A Framework toward the Implementation of a Generation of Eco-Friendly Alternatives. *Green Chemistry* **2015,** *17* (7), 3687-3705.

15. Camp, J. E., Bio-Available Solvent Cyrene: Synthesis, Derivatization, and Applications. *ChemSusChem* **2018,** *11* (18), 3048-3055.

16. Kudo, S.; Zhou, Z.; Norinaga, K.; Hayashi, J.-i., Efficient Levoglucosenone Production by Catalytic Pyrolysis of Cellulose Mixed with Ionic Liquid. *Green Chemistry* **2011,** *13* (11), 3306-3311.

17. Zhang, J.; White, G. B.; Ryan, M. D.; Hunt, A. J.; Katz, M. J., Dihydrolevoglucosenone (Cyrene) as a Green Alternative to N,N-Dimethylformamide (DMF) in MOF Synthesis. *ACS Sustainable Chemistry & Engineering* **2016,** *4* (12), 7186-7192.

18. Camp, J. E.; Nyamini, S. B.; Scott, F. J., Cyrene™ Is a Green Alternative to DMSO as a Solvent for Antibacterial Drug Discovery against ESKAPE Pathogens. *RSC Med. Chem.* **2020,** *11* (1), 111-117.

19. Salavagione, H. J.; Sherwood, J.; De bruyn, M.; Budarin, V. L.; Ellis, G. J.; Clark, J. H.; Shuttleworth, P. S., Identification of High Performance Solvents for the Sustainable Processing of Graphene. *Green Chemistry* **2017,** *19* (11), 2550-2560.

20. Sherwood, J.; De bruyn, M.; Constantinou, A.; Moity, L.; McElroy, C. R.; Farmer, T. J.; Duncan, T.; Raverty, W.; Hunt, A. J.; Clark, J. H., Dihydrolevoglucosenone (Cyrene) as a Bio-Based Alternative for Dipolar Aprotic Solvents. *Chem. Commun.* **2014,** *50* (68), 9650-9652.

21. Shafizadeh, F.; Furneaux, R. H.; Stevenson, T. T., Some Reactions of Levoglucosenone. *Carbohydr. Res.* **1979,** *71* (1), 169-191.

22. Private communication with Circa Group on July 22nd, **2020**

23. Wilson, K. L.; Kennedy, A. R.; Murray, J.; Greatrex, B.; Jamieson, C.; Watson, A. J. B., Scope and Limitations of a DMF Bio-Alternative within Sonogashira Cross-Coupling and Cacchi-Type Annulation. *Beilstein J. Org. Chem.* **2016,** *12*, 2005-2011.

24. Mistry, L.; Mapesa, K.; Bousfield, T. W.; Camp, J. E., Synthesis of Ureas in the Bio-Alternative Solvent Cyrene. *Green Chemistry* **2017,** *19* (9), 2123-2128.

25. Bryan, M. C.; Diorazio, L.; Fei, Z.; Fraunhoffer, K.; Hayler, J.; Hickey, M.; Hughes, S.; McLaws, M.; Richardson, P.; Roiban, G.-D.; Schober, M.; Smith, A. G.; Steven, A.; White, T.; Wuyts, S.; Yin, J., Green Chemistry

Articles of Interest to the Pharmaceutical Industry. *Organic Process Research & Development* **2018,** *22* (6), 667-680.

26. Wilson, K. L.; Murray, J.; Jamieson, C.; Watson, A. J. B., Cyrene as a Bio-Based Solvent for HATU Mediated Amide Coupling. *Organic & Biomolecular Chemistry* **2018,** *16* (16), 2851-2854.

27. Krishna, S. H.; McClelland, D. J.; Rashke, Q. A.; Dumesic, J. A.; Huber, G. W., Hydrogenation of Levoglucosenone to Renewable Chemicals. *Green Chemistry* **2017,** *19* (5), 1278-1285.

28. Kelly, C. M., Noga, D. E., Sidenstick, J. E., Ben-Asher, L. Kondo, A, *US Pat.*, 20150299393A1, **2015**.

29. Marino, T.; Galiano, F.; Molino, A.; Figoli, A., New Frontiers in Sustainable Membrane Preparation: Cyrene™ as Green Bioderived Solvent. *J. Membr. Sci.* **2019,** *580*, 224-234.

30. Zhao, D.; Kim, J. F.; Ignacz, G.; Pogany, P.; Lee, Y. M.; Szekely, G., Bio-Inspired Robust Membranes Nanoengineered from Interpenetrating Polymer Networks of Polybenzimidazole/Polydopamine. *ACS Nano* **2019,** *13* (1), 125-133.

31. Ray, P.; Hughes, T.; Smith, C.; Hibbert, M.; Saito, K.; Simon, G. P., Development of Bio-Acrylic Polymers from Cyrene™: Transforming a Green Solvent to a Green Polymer. *Polym. Chem.* **2019,** *10* (24), 3334-3341.

32. Horn, M.; Matyjaszewski, K., Solvent Effects on the Activation Rate Constant in Atom Transfer Radical Polymerization. *Macromolecules* **2013,** *46* (9), 3350-3357.

33. Harrisson, S.; Mackenzie, S. R.; Haddleton, D. M., Pulsed Laser Polymerization in an Ionic Liquid: Strong Solvent Effects on Propagation and Termination of Methyl Methacrylate. *Macromolecules* **2003,** *36* (14), 5072-5075.

34. Liarou, E.; Staniforth, M.; Town, J. S.; Marathianos, A.; Grypioti, M.; Li, Y.; Chang, Y.; Efstathiou, S.; Hancox, E.; Wemyss, A. M.; Wilson, P.; Jones, B. A.; Aljuaid, M.; Stavros, V. G.; Haddleton, D. M., UV Irradiation of Cu-Based Complexes with Aliphatic Amine Ligands as Used in Living Radical Polymerization. *Eur. Polym. J.* **2020,** *123*, 109388.

35. Bertrand, O.; Wilson, P.; Burns, J. A.; Bell, G. A.; Haddleton, D. M., Cu(0)-Mediated Living Radical Polymerisation in Dimethyl Lactamide (DML); an Unusual Green Solvent with Limited Environmental Impact. *Polym. Chem.* **2015,** *6* (48), 8319-8324.

36. Carmichael, A. J.; Haddleton, D. M.; Bon, S. A. F.; Seddon, K. R., Copper(I) Mediated Living Radical Polymerisation in an Ionic Liquid. *Chem. Comm.* **2000,** (14), 1237-1238.

37. Zerk, T. J.; Bernhardt, P. V., Solvent Dependent Anion Dissociation Limits Copper(I) Catalysed Atom Transfer Reactions. *Dalton Trans.* **2013,** *42* (32), 11683-11694.

38. Whitfield, R.; Anastasaki, A.; Nikolaou, V.; Jones, G. R.; Engelis, N. G.; Discekici, E. H.; Fleischmann, C.; Willenbacher, J.; Hawker, C. J.; Haddleton,

D. M., Universal Conditions for the Controlled Polymerization of Acrylates, Methacrylates, and Styrene Via Cu(0)-RDRP. *Journal of the American Chemical Society* **2017,** *139* (2), 1003-1010.

39. Liarou, E.; Whitfield, R.; Anastasaki, A.; Engelis, N. G.; Jones, G. R.; Velonia, K.; Haddleton, D. M., Copper-Mediated Polymerization without External Deoxygenation or Oxygen Scavengers. *Angew. Chem. Int. Ed.* **2018,** *57* (29), 8998-9002.

40. Liarou, E.; Anastasaki, A.; Whitfield, R.; Iacono, C. E.; Patias, G.; Engelis, N. G.; Marathianos, A.; Jones, G. R.; Haddleton, D. M., Ultra-Low Volume Oxygen Tolerant Photoinduced Cu-RDRP. *Polym. Chem.* **2019,** *10* (8), 963-971.

41. Marathianos, A.; Liarou, E.; Anastasaki, A.; Whitfield, R.; Laurel, M.; Wemyss, A. M.; Haddleton, D. M., Photo-Induced Copper-RDRP in Continuous Flow without External Deoxygenation. *Polym. Chem.* **2019,** *10* (32), 4402-4406.

42. Liarou, E.; Han, Y.; Sanchez, A. M.; Walker, M.; Haddleton, D. M., Rapidly Self-Deoxygenating Controlled Radical Polymerization in Water Via in Situ Disproportionation of Cu(I). *Chem. Sci.* **2020,** *11* (20), 5257-5266.

43. Town, J. S.; Jones, G. R.; Haddleton, D. M., MALDI-LID-ToF/ToF Analysis of Statistical and Diblock Polyacrylate Copolymers. *Polymer Chemistry* **2018,** *9* (37), 4631-4641.

44. Town, J. S.; Jones, G. R.; Hancox, E.; Shegiwal, A.; Haddleton, D. M., Tandem Mass Spectrometry for Polymeric Structure Analysis: A Comparison of Two Common MALDI–ToF/ToF Techniques. *Macromol. Rapid Commun.* **2019,** *40* (13), 1900088.

45. Ciampolini, M.; Nardi, N., Five-Coordinated High-Spin Complexes of Bivalent Cobalt, Nickel, Andcopper with Tris(2-Dimethylaminoethyl)Amine. *Inorganic Chemistry* **1966,** *5* (1), 41-44.

Chapter 6: *Summary and Outlook*

The main focus of this work was to explore the potential of improving the accessibility of transition metal-mediated polymerizations and render them more environmentally and industrially friendly processes.

Although Controlled Radical Polymerizations are powerful tools for the synthesis of a plethora of materials with diverse properties and architectures,[1-4] there are still many challenges to address. New methodologies or enhancements to existing ones need to be developed for the introduction of sustainable materials in order to reduce the ecosystem toxicity and the environmental concern regarding the use of these materials. The majority of the work described in this thesis was focused on exploiting current radical polymerization techniques for the development of methodologies with a potential application in industry. In order to achieve that, a fundamental study was carried out (*Chapter 2*) to gain more knowledge on how the stabilization of a water-borne polymer colloid occurs in a surfactant-free system. CCTP is a versatile technique, which can be applied directly in water, requires significantly low amounts of a Co catalyst and results in macromonomers with controlled molecular weight. Macromonomers synthesized through CCTP were used in this study and in combination with emulsion polymerization, a better understanding on the stabilization process was obtained. It was also demonstrated that the particle size of the latex particles could be predetermined by adjusting the stabilizer to monomer ratio.

CCTP macromonomers are an efficient alternative for the preparation of polymeric materials with high colloidal stability.[5-10] RAFT-mediated surfactant-free emulsion polymerization has progressed significantly over the last two decades with highly promising applications.[11-15] However, most RAFT agents are not commercially available and their synthesis may be challenging. Most importantly, such reagents are malodorous and their use results in colored products (pink or yellow), which can be removed through chemical modification of the end group, thus posing some limitations in several applications, like personal care products. Based on the findings of the work described in *Chapter 2*, future work on the synthesis of macromonomers

through Co-mediated polymerization could expand the pool of types of stabilizers used, in a purely environmentally friendly approach.

In the past few years, sustainability and efficacy of the polymeric materials have been the main focus of both academic and industrial researchers. In the field of agrochemicals, industries are interested in polymer microencapsulation technology due to the choices it offers,[16, 17] regarding the deposition of an active ingredient (AI) in a crop and more specifically, the release of the AI when exposed to a particular trigger. Delayed release of the AI would prolong its effectiveness, which allows for less precisely timed application. In the same context as in *Chapter 2*, but in a more industrially relevant approach, the application of amphiphilic statistical macromonomers obtained through CCTP were used in a two step process in *Chapter 3*. In a simple process, amphiphilic macromonomers were used to successfully disperse an insecticide (CYNT) in aqueous media, resulting in stable AI dispersions. Following this, feeding of a monomer mixture (MMA : BA =10 : 1) directly in these dispersions led to polymer coated CYNT particles, as confirmed by HPLC and SEM. Besides the low amounts of Co catalyst that are required for the synthesis of the macromonomers, with this process low amounts of macromonomers are used. Although the CYNT content can be as high as 30 w/w % in these dispersions, when polymerizations in higher solids content were attempted (50 w/w %) the mixture was solidified, setting some limitations of this approach. Nevertheless, this could be further studied, as well as the behavior of the macromonomers as dispersants in an industrial scale.

This project allows for improvement regarding the release profile of the coated particles. It was shown that the extraction of CYNT from the aqueous formulation to organic media could be monitored by changing the volume of the aqueous phase. However, further studies are required in order to better understand the process of release in an actual crop application. Upon application of the formulation in a plant field and after water evaporation a film could be formed on the plant, consisting of the dispersed AI particles and polymer particles. For this reason, it is important for this chemistry to be applied with the use of biodegradable polymers or materials that derive from biorenewable resources.

As previously discussed, this work was focused on improving the accessibility of current polymerization techniques with a potential application in industry. In this concept, an academically well-established living radical polymerization method, namely photo-induced Cu-RDRP was performed in a continuous flow process (*Chapter 4)*. Continuous flow reactions are a very efficient alternative for batch reactions, providing high reproducibility, consistency, low-cost and multi-scale polymerizations.

In this chapter, an already reported system for its ability to prepare polymeric materials in continuous flow reactions,[18, 19] was demonstrated in an oxygen tolerant approach, thus providing a simple platform for multi-scale polymerizations in a facile and consistent manner. Hence, by avoiding stringent anaerobic conditions that are usually required for a flow-setup, well-defined polyacrylates were synthesized verifying the robustness of the photo-induced Cu-RDRP process. This was further corroborated by the synthesis of sophisticated architectures (8-arm star homopolymer), as well as hydrophobic and hydrophilic polymers through a user-friendly setup. Despite the high end-group fidelity of the obtained polymers, as was demonstrated through post polymerization modification, further studies on the ability of the system to perform block copolymerization is required.

Moreover, the continuous flow photo-induced Cu-RDRP process in aqueous media still remains a challenge. The use of alkali metal halide salts could increase the control of the Cu-RDRP process by effectively increasing the concentration of deactivating species without disturbing the equilibrium between active and dormant species.[20-22] This could be an interesting approach to achieve successful polymerizations in aqueous media, however other parameters should also be considered, *i.e.* the choice of the tubing. For instance, tubing made of perfluoroalkoxy alkane (PFA) or fluorinated ethylene propylene (FEP) has high oxygen permeability, while Halar and Tefzel (tetrafluoroethylene) exhibit higher oxygen barrier properties.[23]

Finally, this approach could enable the introduction of a living radical polymerization process, as well as the concept of the continuous flow chemistry in undergraduate laboratories or in any educational institution without access to specialist equipment for deoxygenation.

In *Chapter 5*, the potential of cyrene, a biorenewable and biodegradable compound, to be used as solvent in Cu-RDRP was investigated. For this purpose several acrylates (as well as MMA and styrene) were polymerized through the oxygen tolerant approach of Cu(0) wire-mediated RDRP. The polymers exhibited macromolecular characteristics similar to those obtained in solvents commonly used in the literature.[24, 25] The successful Cu(0)-mediated polymerization reaction in cyrene (even at very low catalyst loadings) makes this technique further accessible for applications where harsh aprotic polar solvents are increasingly seen as undesirable reagents.

Despite the advantages that cyrene offers, its use in the field of polymer science as solvent or even as monomer precursor is limited or overlooked. Due to its green and sustainable character, cyrene has a potential use as solvent in organic synthesis,[26] as well as in chain-growth and step-growth polymerization reactions. Cyrene was found to be a suitable solvent for ROMP,[27, 28] as well as the preparation of polyamidoimides[29] and polyurethanes.[30] The price of cyrene currently is relatively high (£182/L), however it is expected that the availability of cyrene will increase, which should reduce its cost and enlarge its popularity as a green medium for polymer synthesis.

6.1 References

1. Kato, M.; Kamigaito, M.; Sawamoto, M.; Higashimura, T., Polymerization of Methyl Methacrylate with the Carbon Tetrachloride/Dichlorotris-(Triphenylphosphine)Ruthenium(II)/Methylaluminum Bis(2,6-Di-Tert-Butylphenoxide) Initiating System: Possibility of Living Radical Polymerization. *Macromolecules* **1995,** *28* (5), 1721-1723.

2. Wang, J.-S.; Matyjaszewski, K., Controlled/"Living" Radical Polymerization. Atom Transfer Radical Polymerization in the Presence of Transition-Metal Complexes. *J. Am. Chem. Soc.* **1995,** *117* (20), 5614-5615.

3. Chiefari, J.; Chong, Y. K.; Ercole, F.; Krstina, J.; Jeffery, J.; Le, T. P. T.; Mayadunne, R. T. A.; Meijs, G. F.; Moad, C. L.; Moad, G.; Rizzardo, E.; Thang, S. H., Living Free-Radical Polymerization by Reversible Addition−Fragmentation Chain Transfer: The RAFT Process. *Macromolecules* **1998,** *31* (16), 5559-5562.

4. Hawker, C. J.; Bosman, A. W.; Harth, E., New Polymer Synthesis by Nitroxide Mediated Living Radical Polymerizations. *Chem. Rev.* **2001,** *101* (12), 3661-3688.

5. Engelis, N. G.; Anastasaki, A.; Nurumbetov, G.; Truong, N. P.; Nikolaou, V.; Shegiwal, A.; Whittaker, M. R.; Davis, T. P.; Haddleton, D. M., Sequence-Controlled Methacrylic Multiblock Copolymers Via Sulfur-Free RAFT Emulsion Polymerization. *Nature Chemistry* **2017,** *9* (2), 171-178.

6. Schreur-Piet, I.; Heuts, J. P. A., In Situ Stabilizer Formation from Methacrylic Acid Macromonomers in Emulsion Polymerization. *Polymer Chemistry* **2017,** *8* (43), 6654-6664.

7. Engelis, N. G.; Anastasaki, A.; Whitfield, R.; Jones, G. R.; Liarou, E.; Nikolaou, V.; Nurumbetov, G.; Haddleton, D. M., Sequence-Controlled Methacrylic Multiblock Copolymers: Expanding the Scope of Sulfur-Free RAFT. *Macromolecules* **2018,** *51* (2), 336-342.

8. Schreur-Piet, I.; van Herk, A. M.; Laven, J.; Heuts, J. P. A., Synthesis and Rheological Characterization of Latexes Stabilized by Methacrylic Acid Containing Macromonomers. *Industrial & Engineering Chemistry Research* **2019,** *58* (46), 21105-21117.

9. Shegiwal, A.; Wemyss, A. M.; Liarou, E.; Town, J.; Patias, G.; Atkins, C. J.; Marathianos, A.; Lester, D. W.; Efstathiou, S.; Haddleton, D. M., Polymerisable Surfactants for Polymethacrylates Using Catalytic Chain Transfer Polymerisation (CCTP) Combined with Sulfur Free-Raft in Emulsion Polymerisation. *Eur. Polym. J.* **2020,** *125*, 109491.

10. Marathianos, A.; Wemyss, A. M.; Liarou, E.; Jones, J. R.; Shegiwal, A.; Town, J. S.; Lester, D. W.; Li, Y.; Haddleton, D. M., Controlling the Particle Size in Surfactant-Free Latexes from ω-Propenyl Oligomers Obtained through Catalytic Chain Transfer Polymerization. *ACS Appl. Polym. Mater.* **2021,** *3* (6), 3185-3196.

11. Li, Y.; Armes, S. P., Raft Synthesis of Sterically Stabilized Methacrylic Nanolatexes and Vesicles by Aqueous Dispersion Polymerization. *Angewandte Chemie International Edition* **2010,** *49* (24), 4042-4046.

12. Charleux, B.; Delaittre, G.; Rieger, J.; D'Agosto, F., Polymerization-Induced Self-Assembly: From Soluble Macromolecules to Block Copolymer Nano-Objects in One Step. *Macromolecules* **2012,** *45* (17), 6753-6765.

13. Velasquez, E.; Rieger, J.; Stoffelbach, F.; D'Agosto, F.; Lansalot, M.; Dufils, P.-E.; Vinas, J., Surfactant-Free Poly(Vinylidene Chloride) Latexes Via One-Pot RAFT-Mediated Aqueous Polymerization. *Polymer* **2016,** *106*, 275-284.

14. Lesage de la Haye, J.; Martin-Fabiani, I.; Schulz, M.; Keddie, J. L.; D'Agosto, F.; Lansalot, M., Hydrophilic Macroraft-Mediated Emulsion Polymerization: Synthesis of Latexes for Cross-Linked and Surfactant-Free Films. *Macromolecules* **2017,** *50* (23), 9315-9328.

15. Martín-Fabiani, I.; Lesage de la Haye, J.; Schulz, M.; Liu, Y.; Lee, M.; Duffy, B.; D'Agosto, F.; Lansalot, M.; Keddie, J. L., Enhanced Water Barrier Properties of Surfactant-Free Polymer Films Obtained by Macroraft-Mediated Emulsion Polymerization. *ACS Applied Materials & Interfaces* **2018,** *10* (13), 11221-11232.

16. Green, J. M.; Beestman, G. B., Recently Patented and Commercialized Formulation and Adjuvant Technology. *Crop Protection* **2007,** *26* (3), 320-327.

17. Rai, M. K.; Asthana, P.; Singh, S. K.; Jaiswal, V. S.; Jaiswal, U., The Encapsulation Technology in Fruit Plants—a Review. *Biotechnology Advances* **2009,** *27* (6), 671-679.

18. Wenn, B.; Martens, A. C.; Chuang, Y. M.; Gruber, J.; Junkers, T., Efficient Multiblock Star Polymer Synthesis from Photo-Induced Copper-Mediated Polymerization with up to 21 Arms. *Polymer Chemistry* **2016,** *7* (15), 2720-2727.

19. Vrijsen, J. H.; Osiro Medeiros, C.; Gruber, J.; Junkers, T., Continuous Flow Synthesis of Core Cross-Linked Star Polymers Via Photo-Induced Copper Mediated Polymerization. *Polymer Chemistry* **2019,** *10* (13), 1591-1598.

20. Raus, V.; Kostka, L., Optimizing the Cu-Rdrp of N-(2-Hydroxypropyl) Methacrylamide toward Biomedical Applications. *Polymer Chemistry* **2019,** *10* (5), 564-568.

21. Page, Z. A.; Bou Zerdan, R.; Gutekunst, W. R.; Anastasaki, A.; Seo, S.; McGrath, A. J.; Lunn, D. J.; Clark, P. G.; Hawker, C. J., A Di-Tert-Butyl Acrylate Monomer for Controlled Radical Photopolymerization. *Journal of Polymer Science Part A: Polymer Chemistry* **2017,** *55* (5), 801-807.

22. Cabannes-Boué, B.; Yang, Q.; Lalevée, J.; Morlet-Savary, F.; Poly, J., Investigation into the Mechanism of Photo-Mediated RAFT Polymerization Involving the Reversible Photolysis of the Chain-Transfer Agent. *Polymer Chemistry* **2017,** *8* (11), 1760-1770.

23. Melker, A.; Fors, B. P.; Hawker, C. J.; Poelma, J. E., Continuous Flow Synthesis of Poly(Methyl Methacrylate) Via a Light-Mediated Controlled

Radical Polymerization. *Journal of Polymer Science Part A: Polymer Chemistry* **2015,** *53* (23), 2693-2698.

24. Liarou, E.; Whitfield, R.; Anastasaki, A.; Engelis, N. G.; Jones, G. R.; Velonia, K.; Haddleton, D. M., Copper-Mediated Polymerization without External Deoxygenation or Oxygen Scavengers. *Angew. Chem. Int. Ed.* **2018,** *57* (29), 8998-9002.

25. Whitfield, R.; Anastasaki, A.; Nikolaou, V.; Jones, G. R.; Engelis, N. G.; Discekici, E. H.; Fleischmann, C.; Willenbacher, J.; Hawker, C. J.; Haddleton, D. M., Universal Conditions for the Controlled Polymerization of Acrylates, Methacrylates, and Styrene Via Cu(0)-RDRP. *Journal of the American Chemical Society* **2017,** *139* (2), 1003-1010.

26. Kong, D.; Dolzhenko, A. V., Cyrene: A Bio-Based Sustainable Solvent for Organic Synthesis. *Sustainable Chemistry and Pharmacy* **2022,** *25*, 100591.

27. Debsharma, T.; Schmidt, B.; Laschewsky, A.; Schlaad, H., Ring-Opening Metathesis Polymerization of Unsaturated Carbohydrate Derivatives: Levoglucosenyl Alkyl Ethers. *Macromolecules* **2021,** *54* (6), 2720-2728.

28. Fadlallah, S.; Peru, A. A. M.; Longé, L.; Allais, F., Chemo-Enzymatic Synthesis of a Levoglucosenone-Derived Bi-Functional Monomer and Its Ring-Opening Metathesis Polymerization in the Green Solvent Cyrene™. *Polymer Chemistry* **2020,** *11* (47), 7471-7475.

29. Weidmann, U. WO 2017/050541 Al, **2017**.

30. Germán, L.; Cuevas, J. M.; Cobos, R.; Pérez-Alvarez, L.; Vilas-Vilela, J. L., Green Alternative Cosolvents to N-Methyl-2-Pyrrolidone in Water Polyurethane Dispersions. *RSC Advances* **2021,** *11* (31), 19070-19075.